FORD GT 40

SAE Papers

Table of Contents

The Ford GT Sports Car

R. C. Lunn
Ford Motor Co.

Painting by Peter Helck, AUTOMOBILE QUARTERLY, Spring, 1964

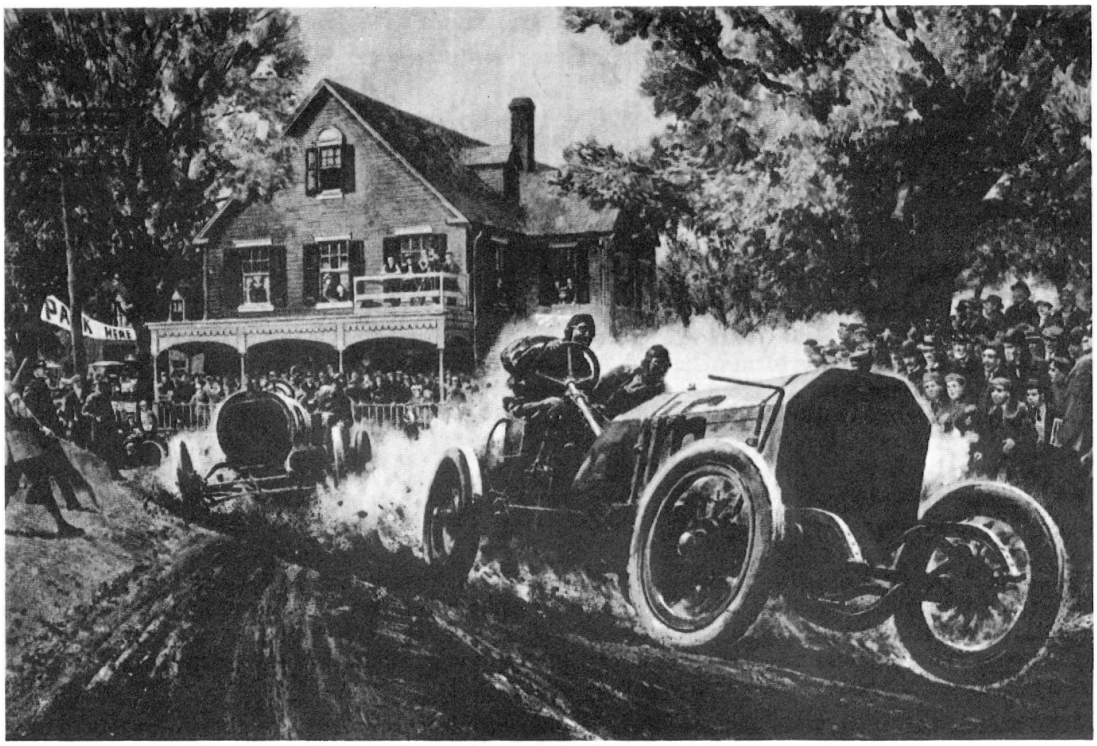

INTRODUCTION

The origin of automobile racing cannot be established easily, but it can be assumed that it all started with the build of the second car. In studying the history of racing, it becomes apparent that the emotions that generate the desire to invent and create are synonymous with the desire to demonstrate the results of creative efforts in open competition. Conversely, the desire to win also has generated technical advances which have contributed to, and accelerated the evolution of the present-day passenger vehicle.

Although modern industrial methods have devised other systems for developing products, racing still provides a unique opportunity for the exploration of new ideas and materials. To keep abreast of competition and meet a racing schedule necessitates quick model turnover, and, because this type of work is executed by small groups, the individuals involved develop a wide versatility of skills and experience relating to total vehicle concept and development.

The major advantages of the racing program can, therefore, be summarized as follows:

- The main line product benefits from the development and usage of new ideas and materials.
- The engineers are afforded a wide range of experience in a concentrated time period.
- An excellent promotional medium is provided by demonstrating products in open competition.

It was with this foregoing basic philosophy that Ford Motor Company, in 1962, re-entered racing in the fields of stock, drag, and rallies and made plans for participation with Ford power at Indianapolis. Early in 1963, the decision was made to extend Ford's participation in competition to the highly sophisticated form of road racing known as GT sports. This arena of racing had been dominated by European manufacturers whose vehicles, over decades, had reached an extremely high state of technical development. Such famous marques as Bentley, Talbot, Lagonda, Aston Martin, Mercedes and Ferrari had figured prominently in the sport, while American efforts were left largely to individual enthusiasts.

The decision to enter this highly developed form of racing was influenced not only by the technical challenge involved but also by the fact that the cars had to be road-legal and raced mostly on commercial highways, such as the Le Mans circuit in France. Consequently, GT sports vehicles are closely allied to normal passenger vehicles and encounter all the problems of highway driving including handling, driver environment, braking, stability and safety. The main difference, however, is that under racing conditions these problems are accentuated, thus providing an excellent development ground for new techniques and innovations.

In the early stages of the program, consideration was given to acquiring an established builder of GT cars, but it was finally decided to create a unique Ford vehicle to challenge the established European supremacy in this form of racing. This paper, therefore, has been prepared to provide the automotive profession with an account of the conception of the Ford GT and its evolution leading to the victory at Le Mans in 1966.

THE TECHNICAL CHALLENGE

Like most product programs, the design and performance objectives for the Ford GT project were largely established by the status of the leading competition. It was evident, from an analysis of competitors in 1963, that top speeds in excess of 200 mph, average laps of more than 130 mph, and durability to sustain an average of more than 120 mph for 24 hours would be necessary to compete successfully at Le Mans in the ensuing years.

The racing objectives were also established. They required the cars to be potential winners in the long-distance races such as Daytona, Sebring, Spa, Nurburg Ring, Targa Florio, as well as Le Mans, and to be capable of winning the FIA World Championship for this type of vehicle. Added to these targets was the timing objective that required the cars to be racing within one year of starting the program.

Attempting to meet these objectives was a scintillating technical challenge, particularly starting from scratch; whereas, competition had reached its sophisticated product level after nearly 40 years of evolutionary development. It was therefore considered necessary to pursue a highly analytical approach to the design in its concept stage rather than rely on evolutionary development.

The magnitude of the engineering problems involved may better be appreciated by a look at the conditions that exist on a race track such as Le Mans. Figure 1 shows this famous circuit, which is made up of conventional roads that are closed to commercial traffic only for the race in June and a short practice session in April. The cars travel clockwise on this 8.3-mile track and encounter road conditions which test every aspect of a car's capabilities. In the 1966 event, speeds ranged from 215 mph on the main straight to 35 mph on the slowest corner, incurring severe braking, acceleration

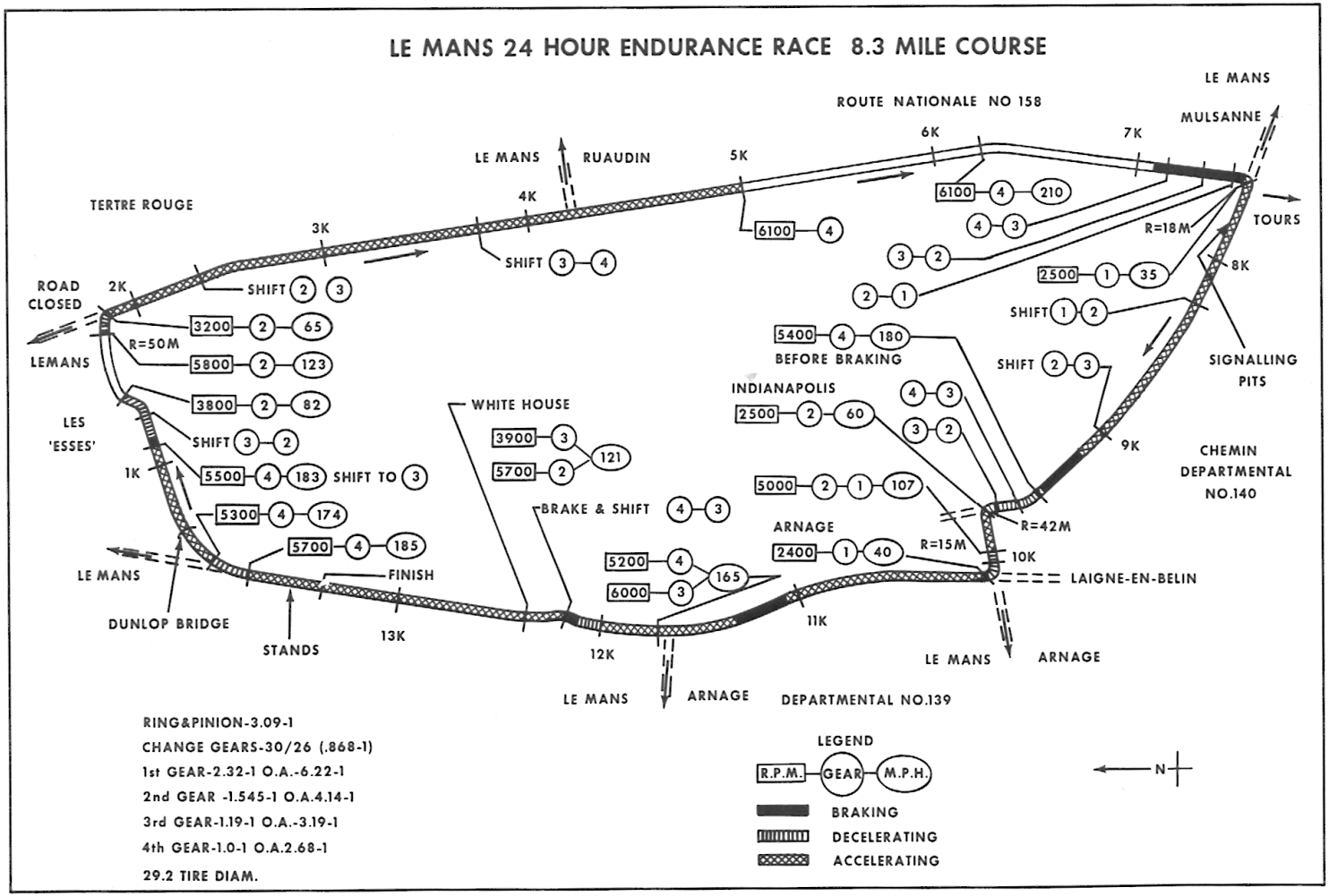
LE MANS 24 HOUR ENDURANCE RACE 8.3 MILE COURSE
LE MANS
ROUTE NATIONALE NO 158
MULSANNE
6K
7K
LE MANS
RUAUDIN
5K
4K
TERTRE ROUGE
3K
6100 4 210
4 3
R=18M
TOURS
6100 4
3 2
2500 1 35
2 1
8K
2K
SHIFT 2 3
SHIFT 3 4
ROAD CLOSED
SHIFT 1 2
3200 2 65
5400 4 180
BEFORE BRAKING
R=50M
SHIFT 2 3
SIGNALLING PITS
5800 2 123
LEMANS
INDIANAPOLIS
3800 2 82
WHITE HOUSE
4 3
2500 2 60
LES 'ESSES'
3900 3
121
3 2
SHIFT 3 2
5700 2
9K
CHEMIN DEPARTMENTAL NO.140
1K
5500 4 183 SHIFT TO 3
5000 2 1 107
BRAKE & SHIFT 4 3
R=42M
5300 4 174
ARNAGE
R=15M
2400 1 40
10K
5700 4 185
5200 4
165
6000 3
LAIGNE-EN-BELIN
LE MANS
FINISH
11K
DUNLOP BRIDGE
STANDS
13K
12K
LE MANS
ARNAGE
LE MANS
ARNAGE
DEPARTMENTAL NO.139
RING&PINION-3.09-1
CHANGE GEARS-30/26 (.868-1)
1st GEAR-2.32-1 O.A.-6.22-1
2nd GEAR -1.545-1 O.A.4.14-1
3rd GEAR-1.19-1 O.A.-3.19-1
4th GEAR-1.0-1 O.A.2.68-1
29.2 TIRE DIAM.
LEGEND
R.P.M. GEAR M.P.H.
N
BRAKING
DECELERATING
ACCELERATING

Figure 1

and constant shifting up and down through the gears. Other corners had to be negotiated at speeds up to 175 mph, and there was full power application for the major part of the circuit. The 24-hour duration of the race, with its night-day aspect and varied weather conditions, necessitates a fully-equipped road vehicle in every sense. For reference against the original objectives, the 1966 event was won at an average speed of 126 mph, despite considerable rain, and a new lap record was set at 142 mph.

VEHICLE CONFIGURATION AND PACKAGE

In 1962, a group from Ford Product Research and Styling areas had designed, constructed, and developed the Mustang I sports car (SAE Paper No. 611F). These same personnel were then assigned to the GT program, and the information which evolved from the Mustang I study served as a starting datum for concept work on the GT sports car.

The initial problem was to select a vehicle configuration which was likely to meet the performance objectives and could be packaged within the FIA rule limitations. The Mustang I exercise had clearly shown the advantages of using a midship engine configuration to attain a low, sleek vehicle silhouette. This arrangement also offered excellent weight distribution characteristics and had been well-proven in other spheres of racing, such as Formula I. It was therefore decided to pursue this same configuration for the GT car.

Initial package studies showed that the essential components could be installed in a vehicle silhouette of 156 inches long, 40 inches high (hence the name GT 40), and 95-inch wheelbase, and still meet the FIA requirements. The

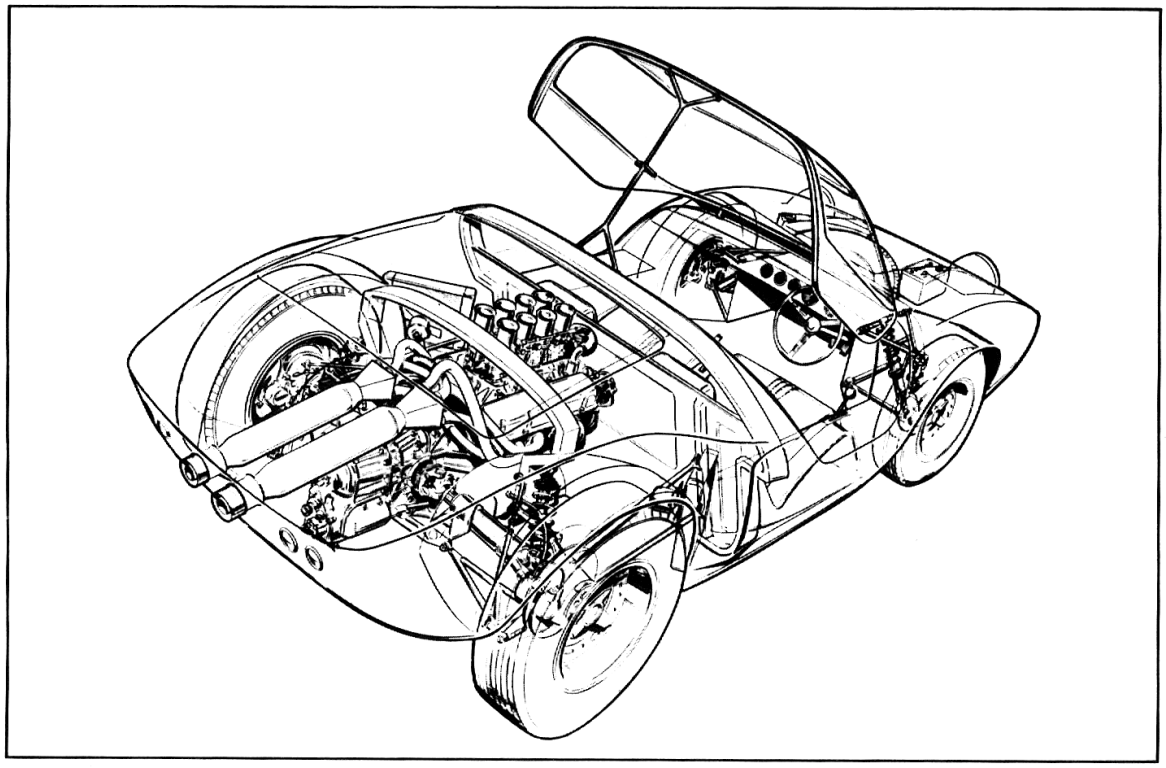

Figure 2 – Original Concept Sketch of GT 40

over-all arrangement included a forward-hinged canopy top; twin radiators located behind the seats with side-ducting; the 256 CID V-8 engine developed for Indianapolis; cross-over tuned exhausts; forward-located spare wheel, oil tank and battery; fixed seats and movable controls; side-sill gas tanks; and, because no suitable transaxle existed within the Company, a proprietary vendor-developed unit was selected. The original sketch showing this combination of ingredients is shown in Figure 2.

Concurrently with package development, a full-size clay was constructed for over-all shape appraisal. The essential requirement was to encompass the basic mechanical ingredients and meet the FIA rule limitations. With these exceptions, however, the choice of shape was largely determined by what seemed right at that time as there was no previous knowledge of road car forms developed for speeds in excess of 200 mph. The result of this original shape study is shown in Figure 3.

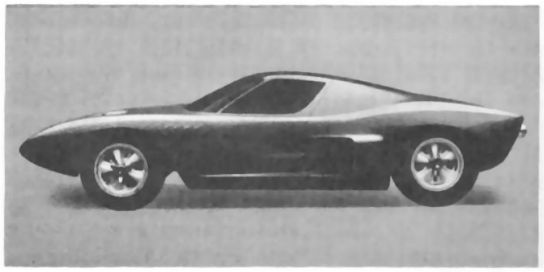

Figure 3 – First Concept Clay Model of GT 40

Subsequent analysis of side radiators showed heat dissipation to be marginal, and a forward-located unit was therefore adopted. The hinged canopy was also dropped in favor of two separate doors in order to clearly meet the FIA rule requirements.

Having arrived at a basic configuration and initial shape, an analysis program was then planned for the following areas:

- Aerodynamics
- Engine
- Transaxle — Driveshafts
- Body
- Suspension — Steering — Brakes — Wheels
- Interior — Driver Environment
- Fuel System

AERODYNAMICS

It was evident from the outset of the project that aerodynamics would play a major part in the program. With the exception of land-speed record cars, no vehicle had been developed to travel at speeds in excess of 200 mph on normal highways. The speeds involved were greater than the take-off speed of most aircraft, but, conversely, the main problem was to keep the vehicle on the ground.

Following initial package and shape studies, a 3/8 aerodynamic model was constructed, and a series of tests were carried out at the University of Maryland wind tunnel (Figure 4). Early tests showed that, although

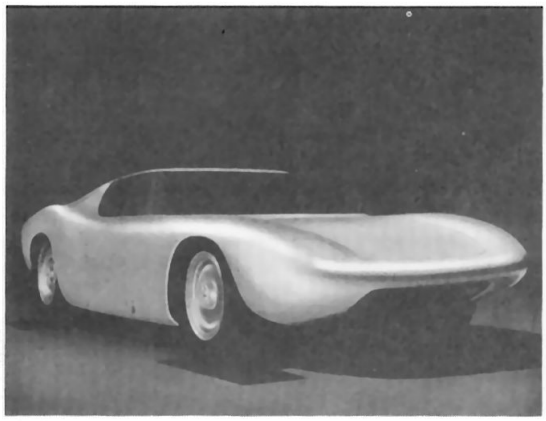

Figure 4 – 3/8 Model in Maryland Wind Tunnel

the drag factor was satisfactory, the lift at 200 mph was over half the weight of the vehicle. Subsequent tests with variations of nose height showed the low nose to have some advantage, but lifts were still totally unacceptable. The major improvement came with the addition of "spoilers" under the front end which not only reduced the lift to an acceptable standard, but, quite surprisingly, also reduced drag. A selective summary of these early test figures is shown in Figure 5. It should be remembered that these tests were conducted with a 3/8 model with equivalent speed readings of 125 mph. Results, therefore, had to be extrapolated to 200 mph, and ground effects could not be recorded.

TABLE OF LIFTS AND DRAGS IN POUNDS

Configuration	Front End Low-Positioned Spoiler	Drag	Lift Front Axle	Lift Rear Axle	15° Yaw Drag	15° Yaw Lift Front Axle	15° Yaw Lift Rear Axle
Basic Car	None	503	528	168	590	768	384
High Nose Shape	None	519	540	108	614	844	362
Low Nose Shape	None	507	445	199	596	704	422
Low Nose Shape	3.50 deep Flat Faired	488	236	272	591	309	343

Figure 5

Shown in Figure 6 are the total drag and rolling resistance curves plotted against available horsepower. This shows that the car should reach approximately 210 mph. In actual fact, the original GT 40's could only reach 197 mph in still air, although they did exceed 200 mph when passing other cars. The reason for this discrepancy was established when the actual prototype was tested in a full-size wind tunnel. It was found that 76 of the 350 horsepower available were being absorbed in internal ducting such as radiators, brake ducts, engine air, and interior ventilation; whereas, only 30 hp had been allowed for these items in the original calculations. Another item which did not show up in these early wind tunnel tests was the aerostability problem, which will be discussed later in the paper.

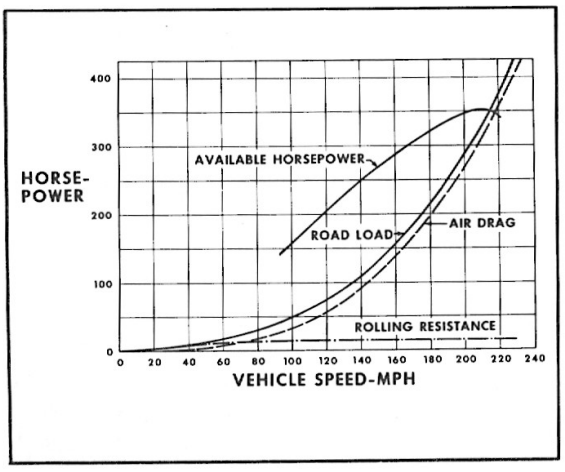

Figure 6

ENGINE

As previously mentioned, the engine selected for the GT 40 was the 4.2 liter (256 CID) unit that had been developed by Ford Motor Company for the 1963 Indianapolis Race. It was derived from the 289 Fairlane engine but included the use of aluminum block and heads, and a dry sump oil system, but, unlike the present Ford double overhead cam Indianapolis engine, still retained push rods. To adapt these units for road racing required detuning to run on commercial pump fuel; addition of full-sized alternator and starter systems; changes to the scavenge system for greater variations of speed and cornering; providing an induction system with greater flexibility for road use in adverse climatic conditions; and general detail changes to suit the package installation. These engines gave approximately 350 hp in their detuned state for long-distance races.

TRANSAXLE

The vendor-developed transaxle was packaged into the concept despite its disadvantage of having only four speeds and non-synchromesh engagement. This unit had been used previously on lightweight vehicles in sprint events, but analysis showed that it should be capable of handling the GT 40 power requirements. In addition, it was the only commercially-available unit that would meet the timing objectives.

Figure 7 shows the engine and transaxle combination, and Figure 8 shows the unit being installed in the vehicle with the cross-over-tuned exhaust system.

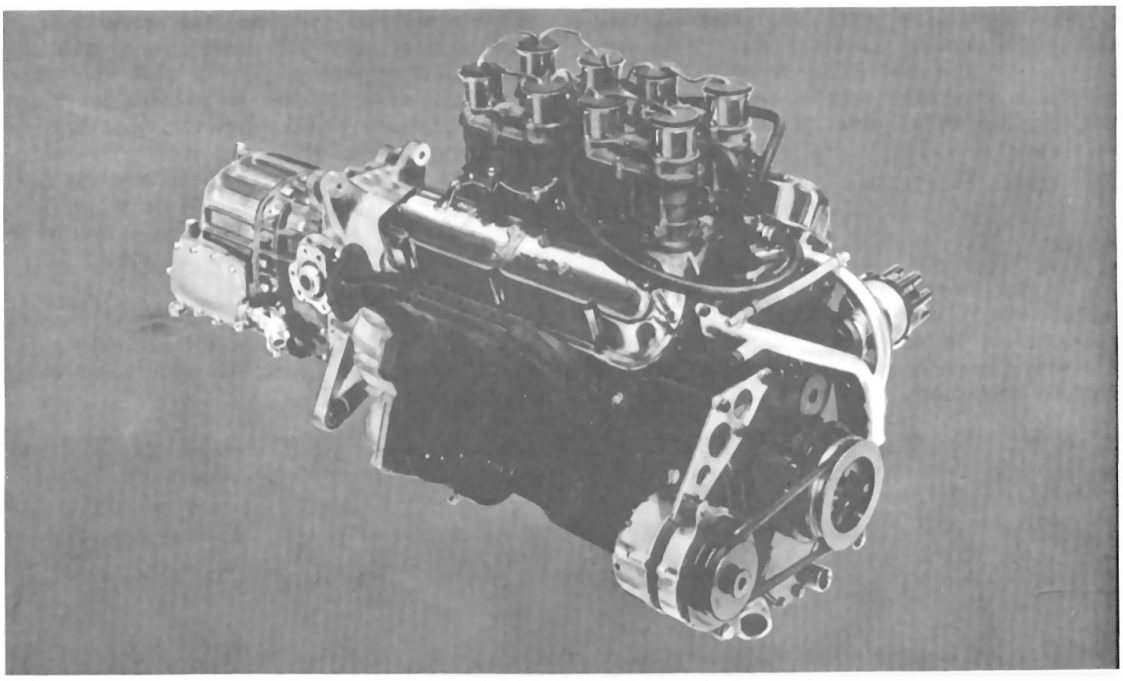

Figure 7 – 256 CID Engine and vendor-developed Transaxle – the Power Train Used in the Original GT 40's

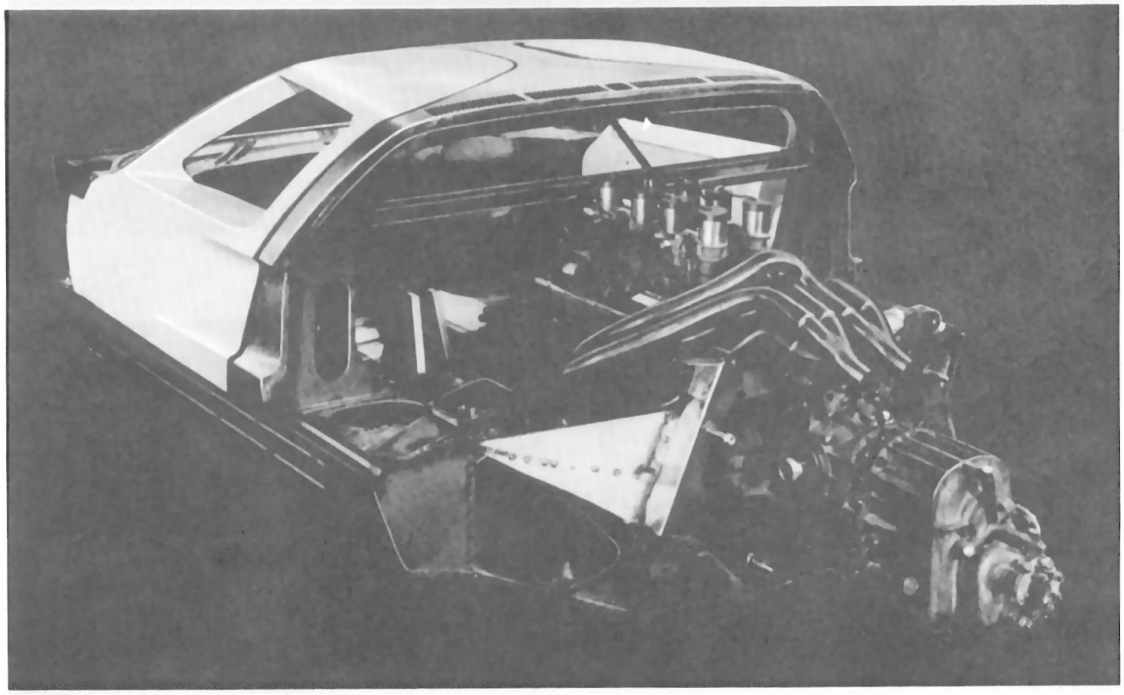

Figure 8 – Installation of 256 Engine Showing Tuned Exhaust System

The driveshafts were originally planned with single Cardan universal joints at the outboard end and pot joints inboard. Rubber couplings were later selected for the inboard end, mainly in an attempt to dampen out harshness and improve general driveline durability.

BODY

It was elected to use a thin sheet steel (.024"-.028") construction to avoid lengthy development of exotic lightweight materials. The strength-carrying structure consisted of a unitized underbody with torque box side sills to house the fuel cells, two main bulkheads, a roof section, and end structures to pick up suspension mountings. Front and rear substructures were attached to provide for body support, spare wheel, radiator, and battery mounting, and to give supports for the quick-lift jacks. The doors were cut extensively into the roof to provide reasonable entry and exit and, together with end sections and rocker panels, were made of hand-laminated fiberglass materials.

Great care was taken to design all fittings flush with the body panels, including the glass sections which were installed by adhesive techniques.

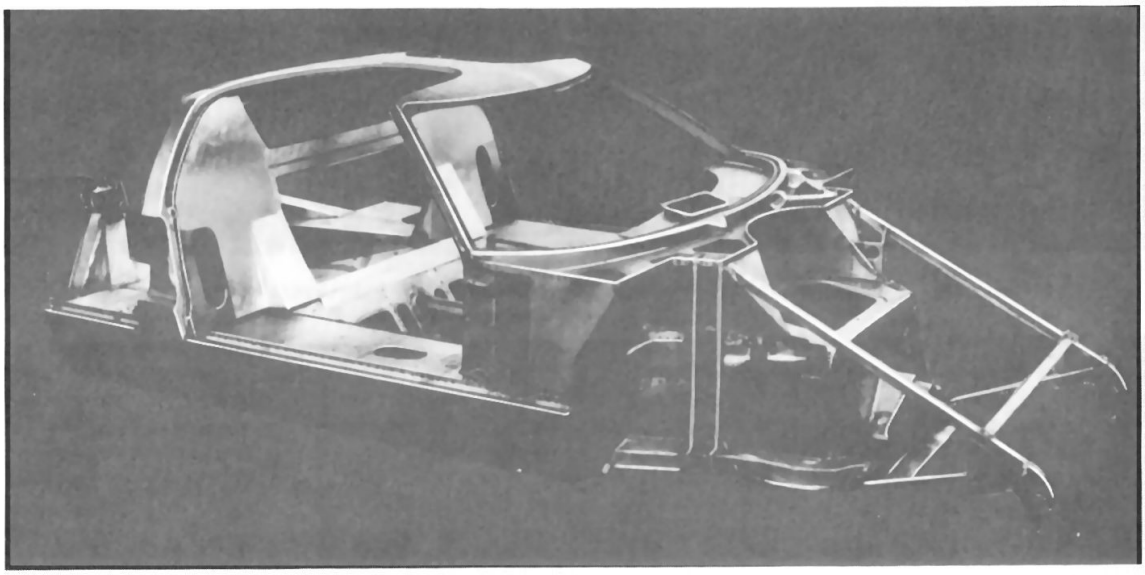

Figure 9

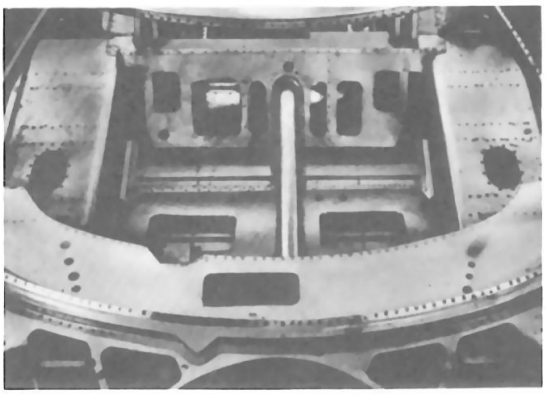

Figure 10

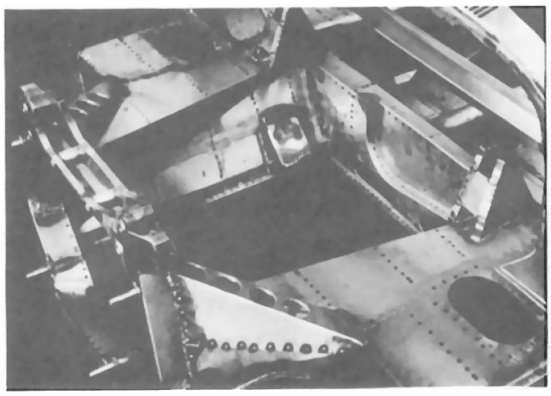

Figure 11

The use of steel sheet for the structure allowed normal methods of welding and brazing in the fabrication. Projection welding was used extensively because of the many blind sections in the structural members. The resulting structure provided an extremely strong unit, giving over 10,000 ft./lb. per degree in torsional rigidity. Figures 9 through 14 show the body structure in the process of fabrication and assembly.

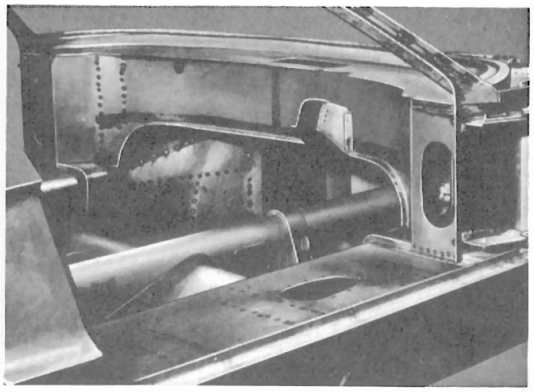

Figure 12

SUSPENSION, STEERING, BRAKES, AND WHEELS

A number of factors governed design of the suspension units. The package size imposed space limitations; the lightweight structure required spreading the attachment points to minimize point loadings; the high-speed aerodynamic tests indicated the desired use of "anti" features; the units required adjustability to suit the varying circuits; and the resulting balance of compromise still had to provide for excellent road-handling characteristics.

The front suspension was designed as a double "A" frame, with the cast magnesium upright supporting the live wheel spindle and

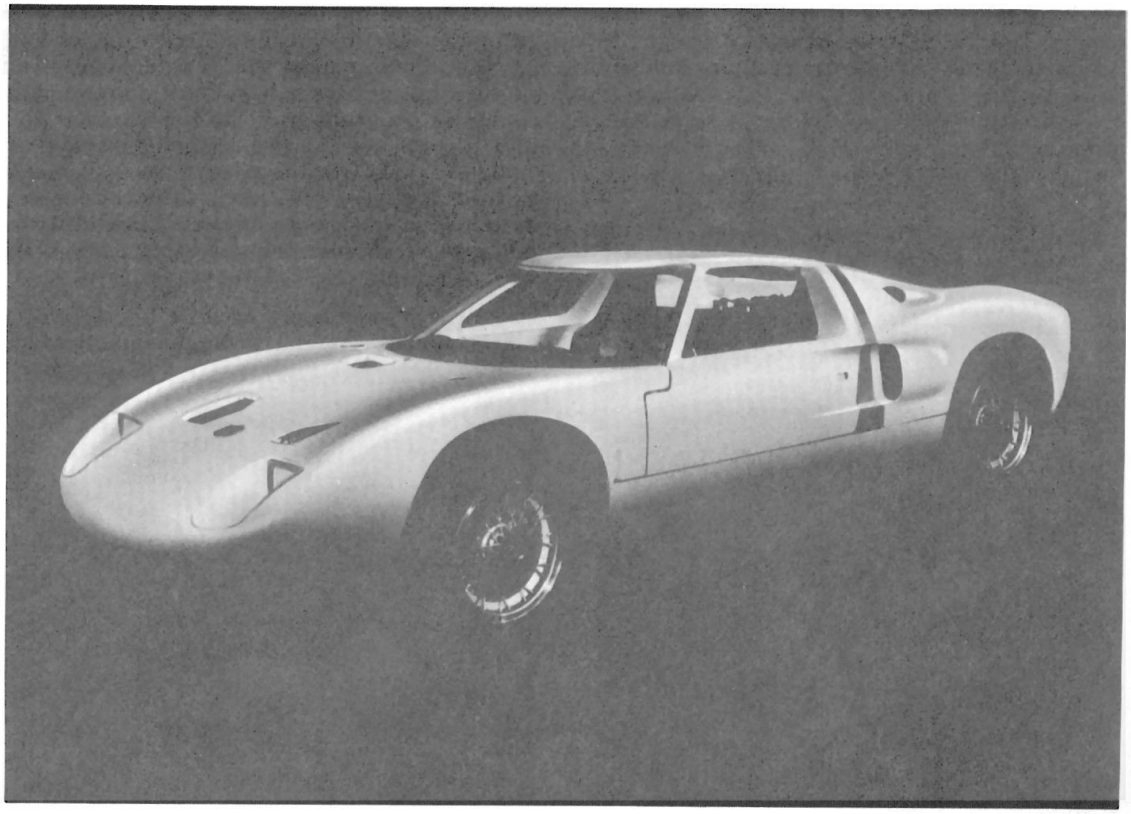

Figure 13

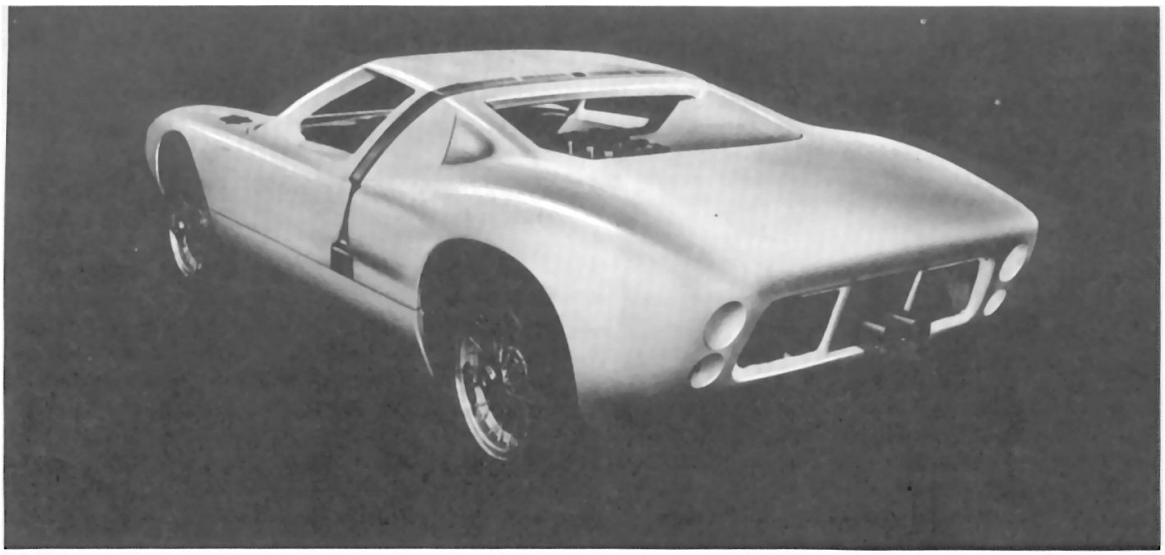

Figure 14

the Girling aluminum brake caliper. The foot well and the position of the spare wheel necessitated an unusually short top arm. The support axes of the "A" frames were arranged to provide an anti-dive feature of approximately 30 per cent.

The rear suspension used double-trailing links from the main bulkhead and transverse links comprising a top strut and an inverted lower "A" frame. The angling of the "A" frames to the magnesium upright casting, combined with the arrangement of linkage geometry, provided anti-lift and anti-squat features of approximately 30 per cent.

These multi-link suspensions presented a problem in establishing wheel geometry. Extensive use of the computer was required with so many links moving in different planes and on canted axes. Once the basic configuration of suspension linkage had been established, a computer program was formulated that took into account all the factors involved. Curves could then be plotted in a matter of a few hours to meet a given condition — a process which speeded up the design period and aided the balance of compromise involved.

A rack and pinion was selected for the steering system, mainly because it was particularly suitable for the package conditions involved. The rack had a ratio of 16:1 which

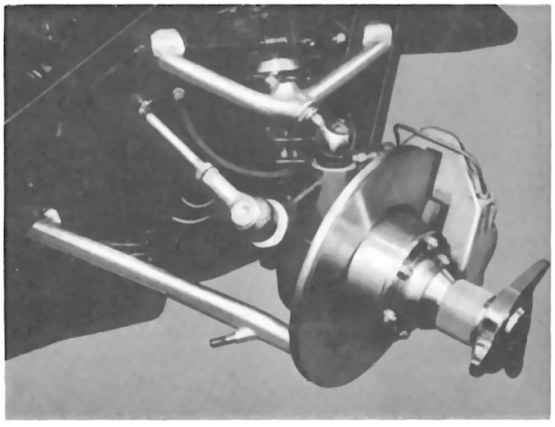

Figure 15 — Front Suspension and Steering Assembly

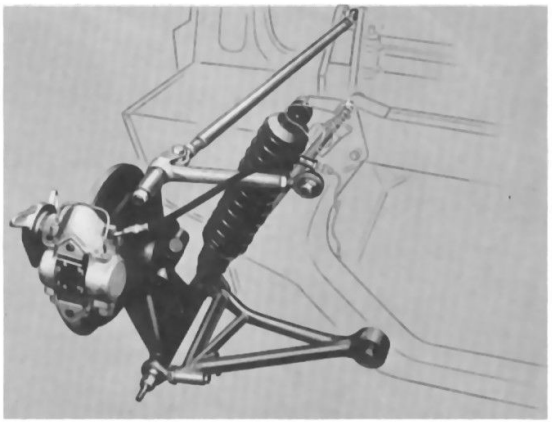

Figure 16 — Rear Suspension Assembly

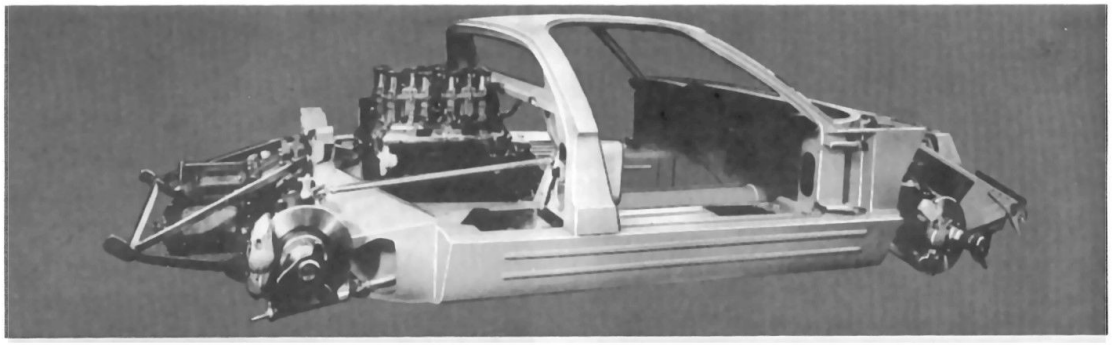

Figure 17 – Basic Structure with Suspensions and Engine Installed

in turn gave an over-all ratio of 2-1/4 turns of the steering wheel from lock-to-lock.

Girling CR and BR racing calipers were used front and rear, respectively, with solid cast iron discs, which were 11-1/2 x 1/2-inch thick. A dual master cylinder was employed for separate front and rear systems which incorporated a balance mechanism for adjustment of braking distribution.

Cast magnesium wheels were originally specified, but development problems precluded their use on the first cars. Prototypes were therefore fitted with wire wheels with alloy rims of 15-inch diameter with a 6-1/2-inch wide front rim and an 8-inch wide rear rim.

Figures 15 and 16 show the front and rear suspension units, and Figure 17 shows these units in an over-all context with the chassis.

INTERIOR – DRIVER ENVIRONMENT

Driver environment was a major consideration as long-distance races require maximum driver concentration for periods of up to four hours. An interior buck was constructed as a physical aid in developing seating conditions and to determine optimum positioning of instrumentation and controls.

The fixed-seat, movable-pedal concept was carried over from the Mustang I project. This arrangement offered structural advantages and provided snug support around the driver to help prevent fatigue from high-speed cornering effects. A nylon netting was used for the basic support medium and was covered with a pad containing ventilation holes to help evaporate driver perspiration. The pedals were mounted on a cast alloy member which could be adjusted for variation in driver size (Figure 18).

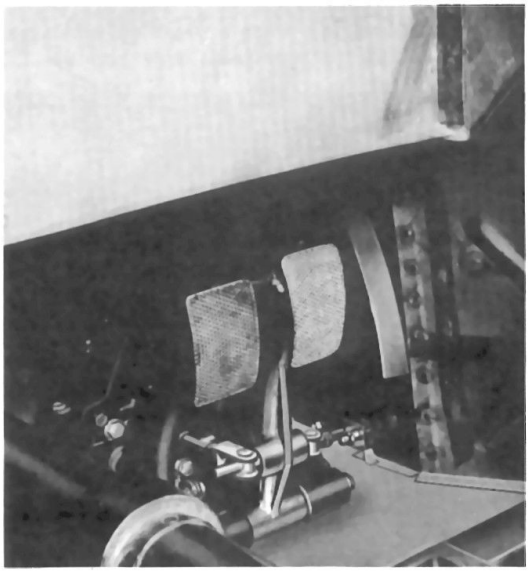

Figure 18 – Adjustable Pedal Mechanism

Instruments were positioned so that their faces pointed directly at the driver in order to minimize distortions and reflections. All switches and controls were located and formed so that they could be reached easily and recognized visually or by touch. Flow-through ventilation was provided, together with full protection from adverse weather conditions.

The general arrangement of the interior is shown in Figure 19.

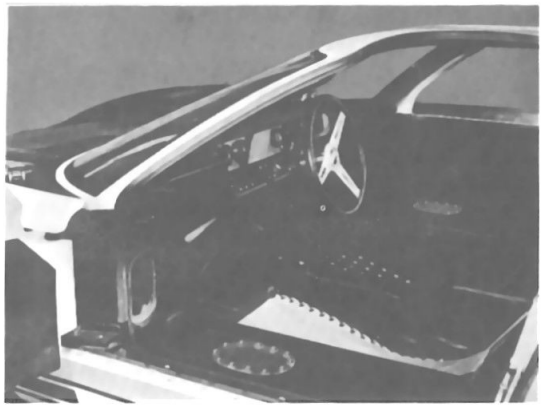

Figure 19 — Interior Showing Fixed Seat Arrangement. Passenger Seat Trim Removed to Show Nylon Net Support.

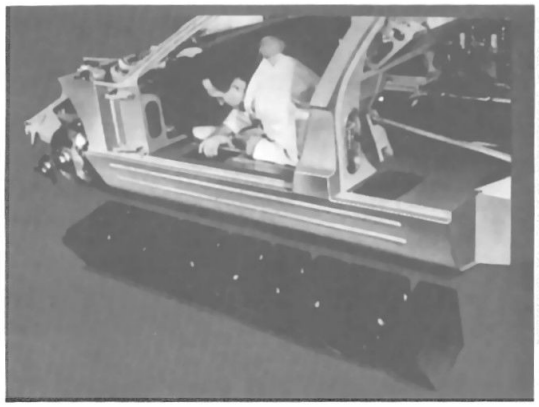

Figure 20 — Structure Being Prepared for Fuel Cell Installation

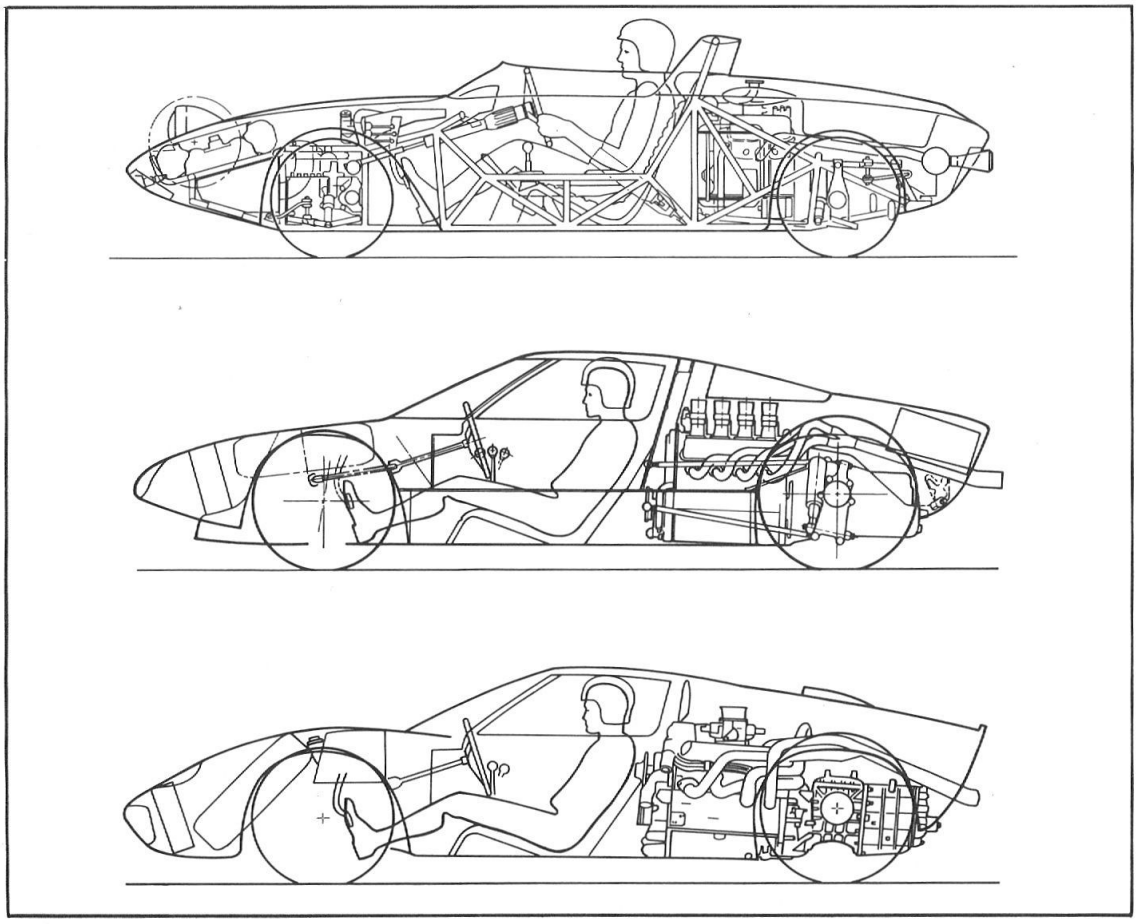

Figure 21 — Outline Packages Showing Evolution of GT 40 from the Mustang I. The Later Development of the MK II Package is Shown for Reference

FUEL SYSTEM

To contain the allowable 42 gallons of fuel in this small package, provide for rapid filling, devise a means of picking up the fuel, and provide adequate driver safety was a study within itself. The arrangement selected was two separate tank systems in the side sills, each with its own filler cap and fuel pickup box. These separate systems were designed with individual electric pumps feeding a common supply pipe to the carburetors. Provision was also made in one tank for a reserve pickup unit. The steel shell of the tanks was, of course, part of the main structure. In these were fitted neoprene bags to aid in crash safety. Baffling was attained by means of a plate supported from the top inspection cover. A fuel cell is shown prior to assembly, in Figure 20.

The findings and effects of each of the specialized studies were continuously reflected in the package layout and full-size clay model. The evolution of the package can be seen in Figure 21, which shows the Mustang I as a datum, the GT 40 package, and the later MK II layout is shown for reference.

PROTOTYPE BUILD

The design and analytical studies were completed during the summer of 1963, together with a clay model reflecting the package changes (Figure 22). The problem was then how and where to execute the final design build and development.

It was finally decided to execute this phase of the program in Europe, since many of the proprietary components were readily available in this area, as were experienced craftsmen in this field of racing. An arrangement was made with the Lola Company to use their resources and facility for one year, as they already had some experience in GT sports cars with a midship engine configuration. In forming this alliance, we were also able to use one of the Lola prototypes for the installation and development of the Ford suspension and driveline components.

In September of 1963, the center of activity was therefore moved from Dearborn to England, together with a nucleus of Ford engineers, car layouts, power pack components, and full-size models.

Component testing was completed by the end of November, 1963, and the remainder of that winter was spent in detailing and procuring items for the first prototype builds. The first GT 40 car was completed on April 1, 1964, some eleven months after putting pencil to paper in Dearborn. This car is shown in Figures 23 and 24. A second vehicle was completed ten days later, and hectic preparations were made to get both vehicles to the Le Mans practice on April 16. Bad weather conditions in England prevented any serious testing and the cars had an aggregate of only four hours running time with no high-speed experience before being shipped to France. The first day of practice also proved to be rain drenched and after very few laps, the first car was totally wrecked on the Mulsanne Straight when it left the road at over 150 mph. The second vehicle also experienced trouble and suffered a minor collision. Luckily, both drivers were unharmed,

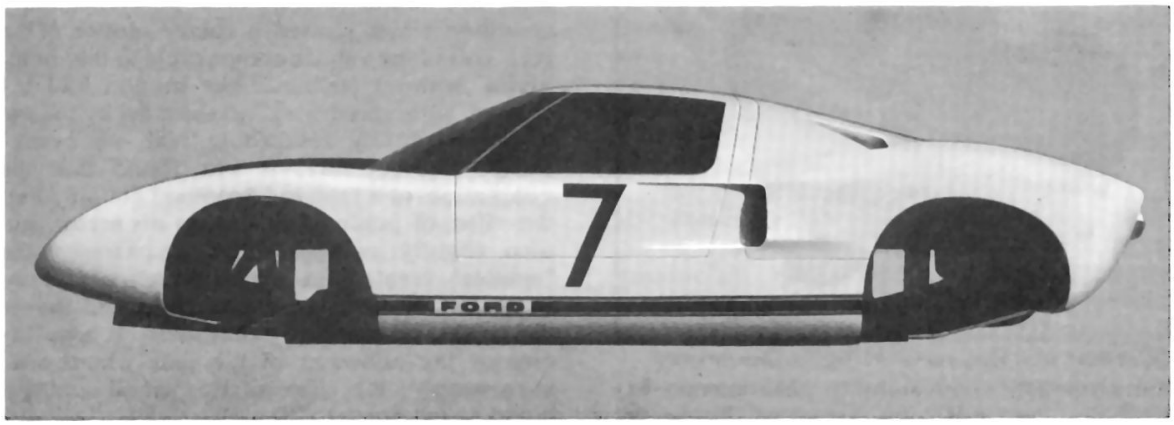

Figure 22 – Developed Model of Original GT 40

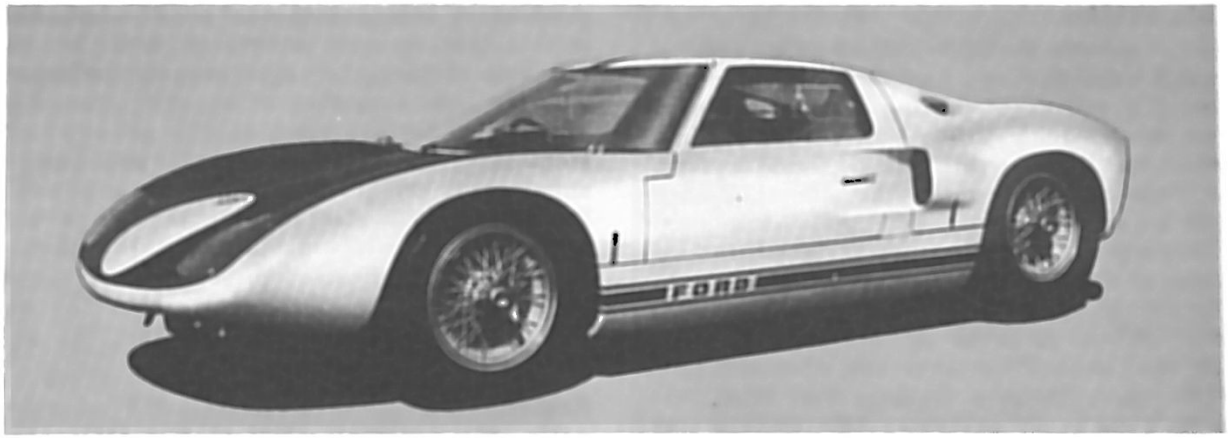

Figure 23 – Original GT 40 Prototype

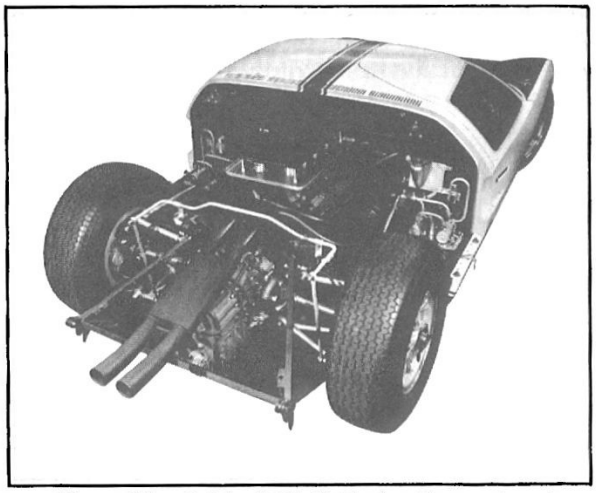

Figure 24 – Original GT 40 Engine Compartment

but obviously some stability phenomenon existed that had not been apparent during the design analytical phase. The problem and the solution were found within one week after returning to England, where further testing was carried out at the MIRA proving ground. The fault was found to have been an aerostability condition which caused a rotary motion of the rear end of the vehicle comparable to that of an arrow without feathers. The motion had increased with speed and, accentuated by the wet track, eventually resulted in rear end breakaway. Subsequently, it was found that the adaptation of a rear end "spoiler" not only had the effect of putting feathers on an arrow, but also slightly reduced drag. Apparently, the "spoiler" creates an airtail which artificially increases the vehicle's aspect ratio and moves the center of pressure rearwards. It also increases the adhesion of the rear wheels and, surprisingly, the effect of this small addition could be felt down to 70 mph.

Figure 25 – Prototype at Nurburg Ring 1964 with "Duck-Tail Spoiler" Added to Rear End

The second car from the Le Mans practice was modified by the addition of the "spoiler" (Figure 25) and was rebuilt in readiness for the GT 40's first race outing at Nurburg Ring on May 31, 1964. The car performed most favorably in practice and qualified second only to the fastest Ferrari. It also ran second in this 1000 Kilometer race in the early hours but retired after 2-1/2 hours. The reason for the retirement was a suspension bracket failure because of an incorrect welding process, but when the vehicle was examined, there were several other areas showing distress and near failure. The outing was, therefore, most successful as a development exercise, and the lessons learned were quickly incorporated in the three vehicles being built for the Le Mans race in mid-June, 1964. These vehicles were completed and weighed in at Le Mans scrutineering at 1960 pounds, less driver and fuel.

In practice, the cars qualified second, fourth, and ninth. During the race, one car held the lead for the early hours before retiring with a transmission failure. The second car retired after five hours with a broken fuel line, and the third car retired after 13-1/2 hours with transaxle problems but not before establishing an all-time lap record.

Every attempt was made to correct the transaxle problems within the limited time available before the next race at Rheims, France, on July 5, 1964. Again, the cars led the race in the early hours, set new lap records, but all retired with transaxle failures. In addition, the nature of this circuit showed insufficient cooling of the brake discs which remained red hot during the entire time the cars were running.

The GT 40's first season of racing in 1964, therefore, showed seven starts in major events with no finishes. The cars had demonstrated that they met the performance objectives but failed badly on durability aspects. The winter of 1964 was devoted to detail preparation of the cars for the 1965 season and at this stage, the responsibility for racing the vehicles was given to the Shelby-American racing team. Twenty-one modifications were executed on the transaxles, the rubber driveshafts were replaced with Dana couplings, and the decision was made to install standard 289 C.I.D. cast iron engines, using wet sump lubrication. The original cast wheels were also installed and increased to 8-inch front and 9-1/2-inch rear rims. Two of these cars made their first appearance in the 1965 season at the Daytona 2000 Kilometer Race on February 28, 1965. They finished first and third in this event, setting an average speed record of 99.9 mph for the distance in 12 hours and 20 minutes (Figure 26). Two vehicles also were entered in the Sebring Race in March, 1965, and finished second over-all and first in class, once more demonstrating that a fair degree of durability had been attained. These cars were raced by the Company once more in 1965 at Le Mans, but without success.

The decision was then made to manufacture 50 of these cars in order to qualify them for the production sports car category. These cars were completed in the 1965 period after detailed changes and the adoption of the 5-speed ZF transaxle. These GT 40's were sold to the public and, in the hands of private race teams and individuals, won the World Championship for production sports cars in 1966.

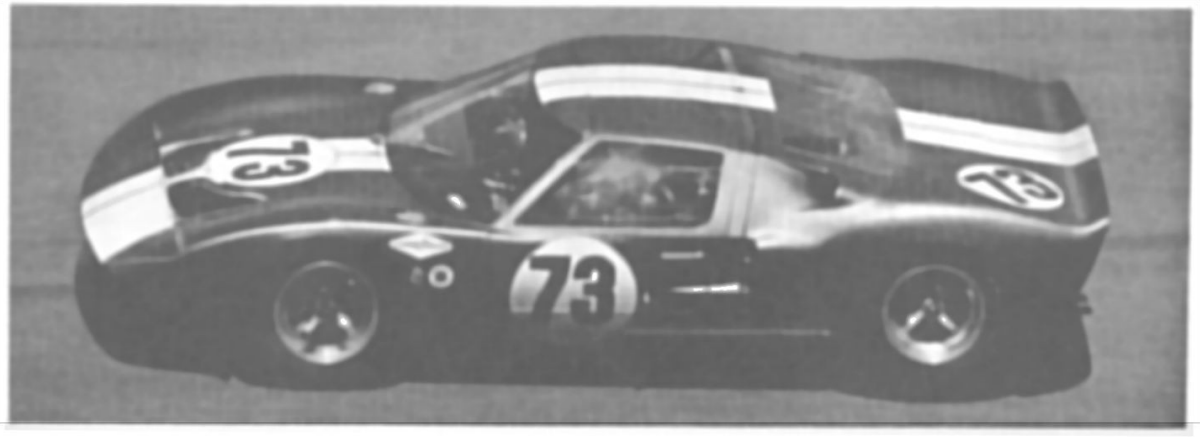

Figure 26 — GT 40's First Win at Daytona 1965

MARK II PROGRAM

In the fall of 1964, the engineering team relocated in Dearborn and started operations at Kar-Kraft, a Ford contracted facility. This team continued engineering on the GT 40 and also started a new experimental vehicle project.

The 1964 season had shown the prototype GT 40's were currently competitive on performance factors but lacked durability. Although work was progressing on correcting durability problems, it was obvious that the GT 40 performance, in the fast-moving racing field, would soon be outmoded. The problem was, therefore, how to get an improved power-to-weight factor and at the same time achieve a high durability level. The alternatives were to generate more power from the 289 C.I.D. series engine or adapt the 427 C.I.D. engine which had been developed for stock car racing. This latter approach would also involve the development of a unique transaxle to handle the higher power. The other indeterminates were whether the additional weight (some 250 pounds) for the larger engine and heavier transaxle and driveline would unduly deteriorate handling and accentuate braking problems. It was decided, however, to explore this approach by constructing a test vehicle and physically evaluating its performance. The program was initiated in the winter of 1964 and was designated the MK II project. At the outset, it should be emphasized that the exercise was intended to generate information for a future model, and there was no intention of racing the car.

Package studies showed the 427 C.I.D. engine could be accommodated in the GT 40 basic structure by modifying the seating position and rear bulkhead members (Figures 27 and 28). The basic suspension units were unchanged, but provision was made for 8-inch wide cast magnesium front wheels and 9-1/2-inch rear wheels. Housing of the wider spare wheel necessitated revising its position, and the new front end arrangement made provision for a remote engine oil tank on the bulkhead and a larger radiator (Figure 29).

A major problem was to generate a transaxle unit which would handle the 427 C.I.D. power and the extra weight of the vehicle. For expediency the gear cluster from the conventional 427 C.I.D. driveline was used but with completely new housings and axle unit. This approach resulted in a heavier and less efficient arrangement than a direct transfer box, but had the advantage of using developed components. The housings were designed in magnesium, and a pair of quick-change gears

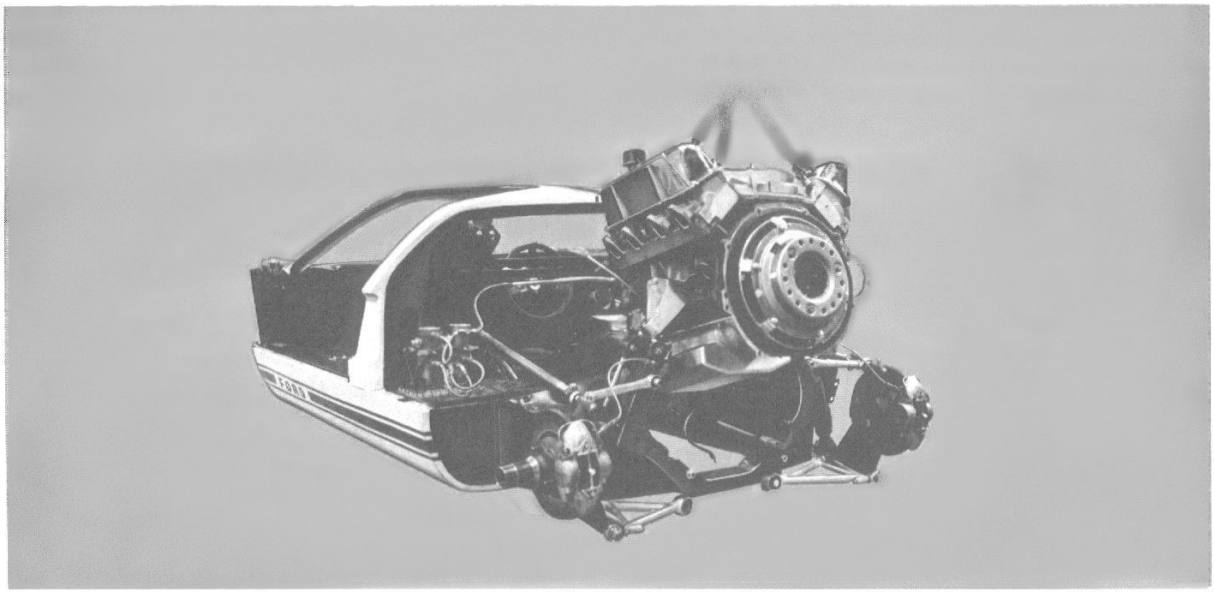

Figure 27 — Installation of 427 Engine in MK II Chassis

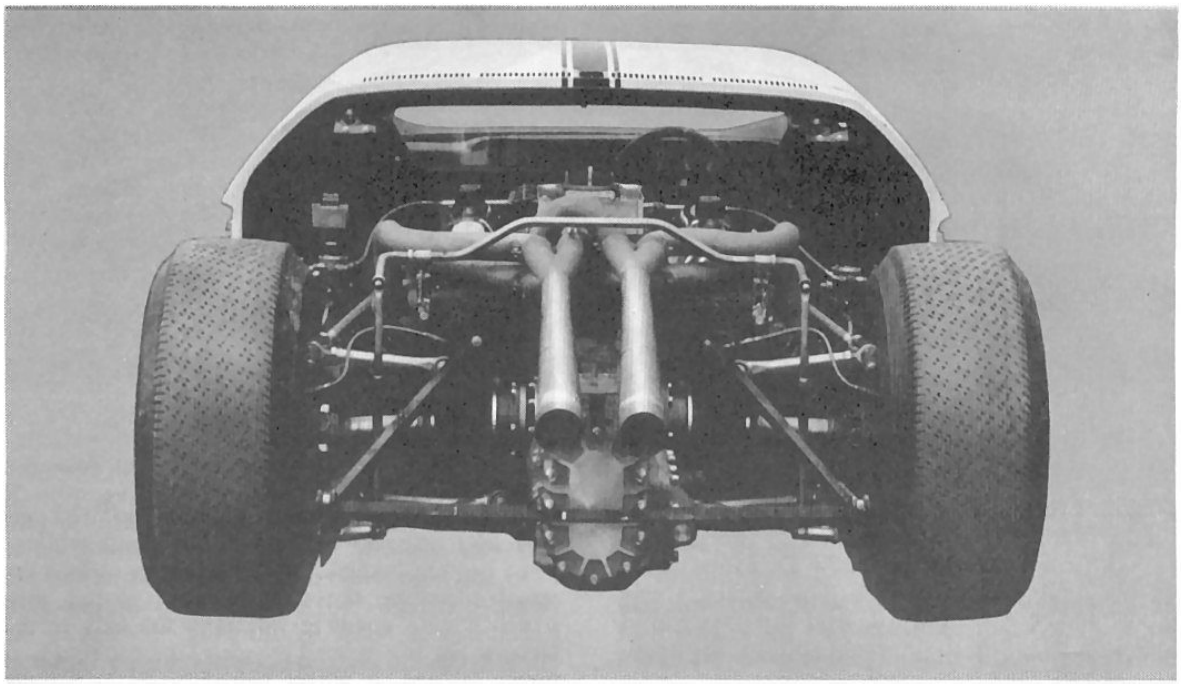

Figure 28 – Original MK II Engine Compartment

transmitted the power to the pinion shaft. The resulting over-all package from these changes required new front and rear structures and body shells.

The first experimental MK II vehicle was completed during April, 1965, and was evaluated on the 5-mile oval at Ford's Michigan Proving Ground (Figure 30). After only a few hours of tailoring, the car lapped this circuit at an average speed of 201-1/2 mph and exceeded 210 mph on the straight-away. Subsequent testing on road circuits showed that handling had deteriorated only slightly. From the results of these tests, it was calculated that this vehicle should be capable of lapping the Le Mans circuit in 3 min. 30 sec. to 3 min. 35 sec. without exceeding 6200 rpm. If these

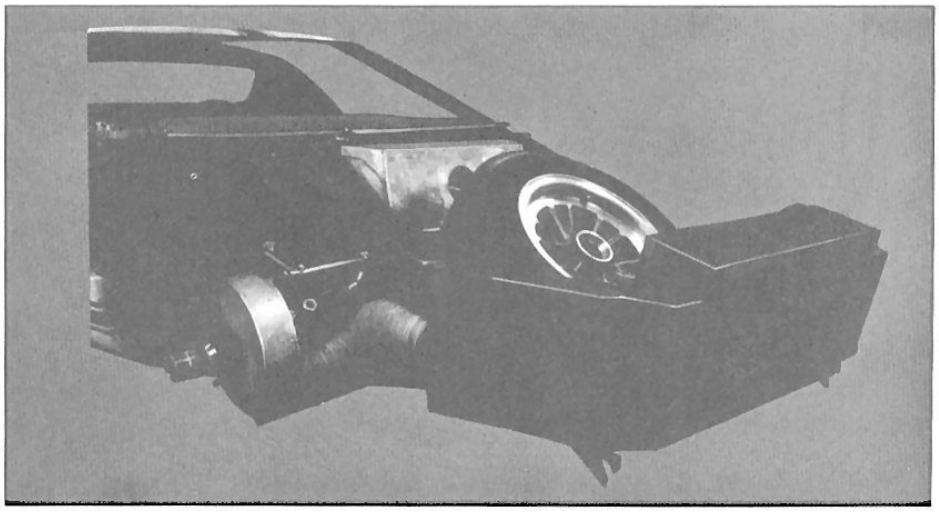

Figure 29 – Original MK II Front End Arrangement

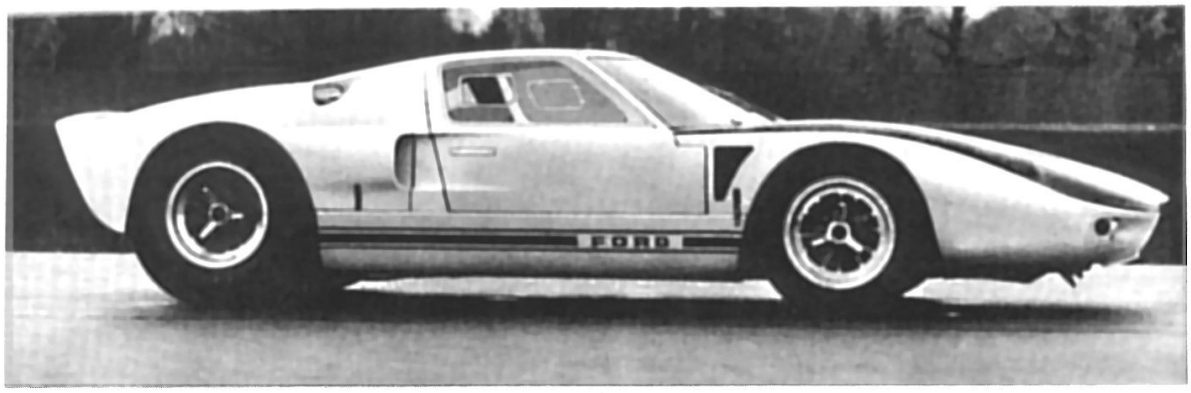

Figure 30 — Original MK II Prototype with Long Nose Configuration

lap times could be realized at this relatively low engine rpm, the car would obviously have high potential to win at Le Mans. The decision was made, therefore, to attempt to run two of these experimental cars in the 1965 Le Mans event as an exploratory exercise. This decision was made at the end of April, and the cars would therefore be going to the event without the benefit of the practice week-end.

In the ensuing five weeks, the first car underwent initial testing and rebuild, and a second car was hurriedly constructed. The second car actually arrived at Le Mans without even having turned a wheel. Having missed the April practice, the first evening of pre-race practice was spent in tailoring the cars to the circuit. On the second evening, the car that had never turned a wheel before arriving at the

Figure 31 — Two Original MK II Cars at Le Mans 1965

track set an all-time record lap of 3 min. 33 sec. — an average of 141 mph.

One car qualified first, and when the race started on Saturday, both cars went out ahead of the field and comfortably lapped at 3 min. 40 sec. without exceeding 6000 rpm (Figure 31). Unfortunately, hurried preparation resulted in the cars being retired after two and seven hours, respectively, with non-fundamental driveline problems. One car had a speck of sand in the clutch slave cylinder which caused the piston to stick and generate heat at the throw-out bearing. The heat, in turn, softened an oil retaining ring in the axle ultimately resulting in loss of oil. The second car broke a gear which had been incorrectly drilled. The cars, however, achieved their purpose of establishing the capability of the engine-driveline combination. The potential indicated in this initial experimental outing resulted in the 1966 program being based on the MK II vehicle.

The following chart shows the MK II power-to-weight factor compared to the original GT 40 and the production version. Vehicle weights are quoted, less fuel and driver.

	Vehicle Weight	HP	HP/Lb.
MK II	2400 Lbs.	485	.202
Production GT 40	2150 Lbs.	385	.179
Original GT 40 Prototype	1960 Lbs.	350	.179

In preparation for 1966, a concentrated vehicle development program was planned using the Daytona, Sebring, and Riverside tracks. In addition, specialized component developments were initiated on items such as engine (SAE Papers No. 670066, 670067) ignition and electrical system (SAE Paper No. 670068), transaxle (SAE Paper No. 670069), driveshafts and brakes (SAE Paper No. 670070). Although some fundamental changes emerged from this development program, the main emphasis was on refinement to establish durability rather than improve performance. The final engine-driveline arrangement is shown in Figure 32.

A major contribution to speeding up development was originated by the Ford engine and transmission engineers. They evolved a dynamometer which could run the engine and

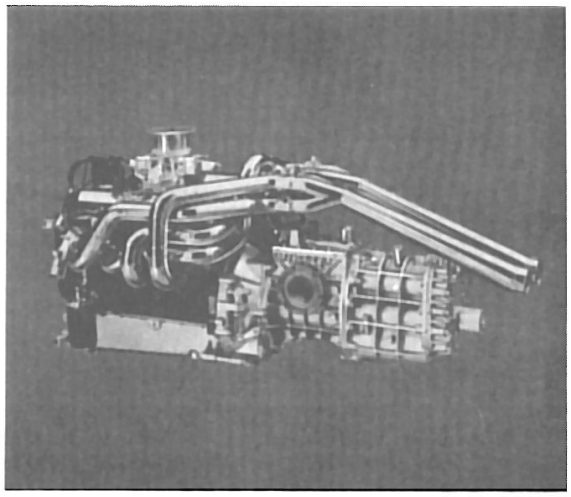

Figure 32 — Developed Engine and Driveline Assembly

driveline units under simulated road conditions that had been recorded on tape in an instrumented vehicle (SAE Paper No. 670071). This device allowed component testing to proceed independently of vehicle availability and climatic conditions.

Major changes that resulted from testing and development included:

- New shorter nose configuration to save weight and improve aerodynamics.
- Addition of external rear brake scoops.
- Higher efficiency radiators.
- Strengthened chassis brackets for durability.
- Live rear hubs for improved durability.
- Internal scavenge pump to minimize vulnerability and save weight.
- Generally improved ducting to radiators, carburetors and brakes.
- Crossover fuel system with a single filler neck.
- Ventilated brake discs to improve durability.
- Quick-change brake disc design to facilitate changes during pit stops.

All of these changes were incorporated in the vehicles that made their first appearance at the Daytona 24-Hour Race on February 5-6,

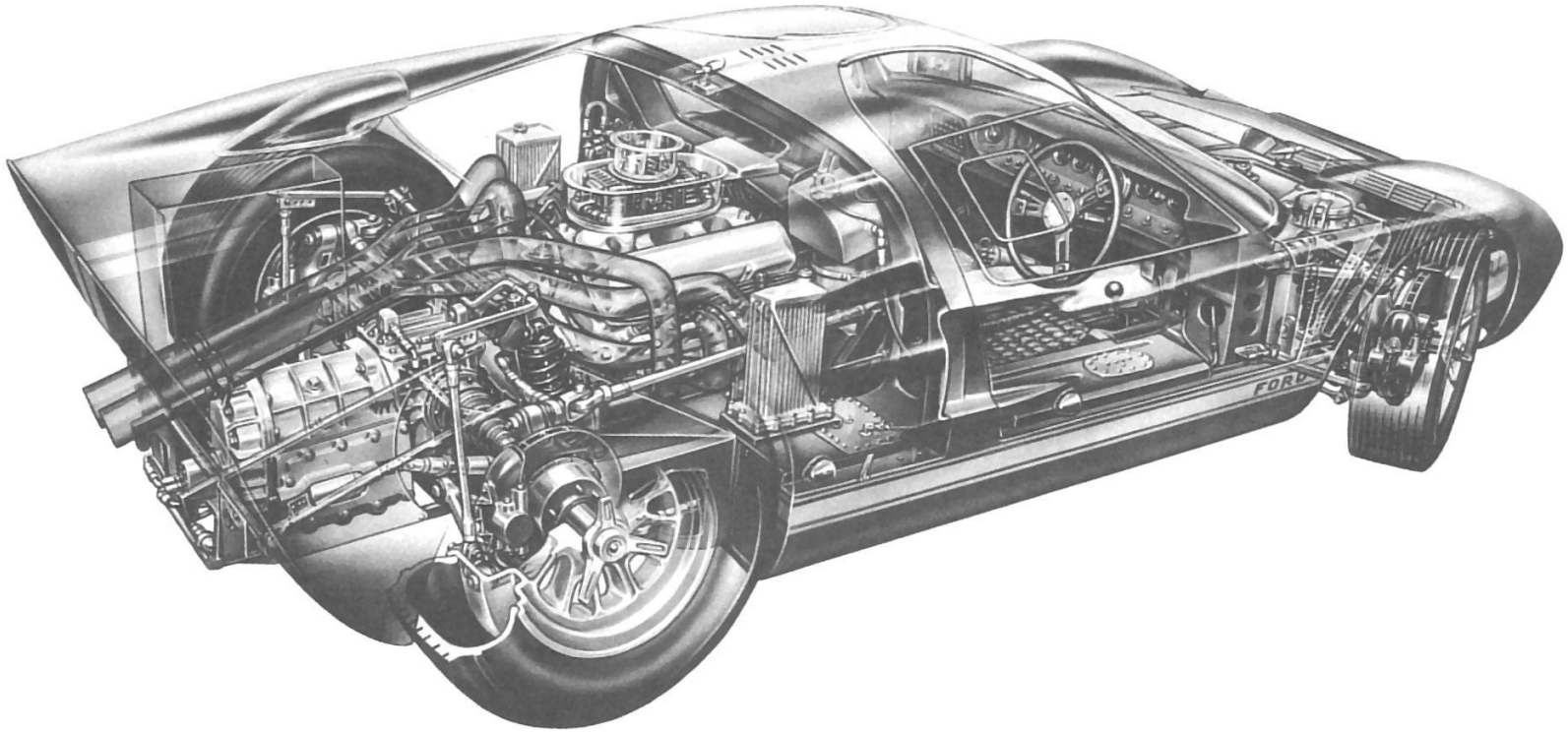

Figure 33 — Final Layout of Components for the MK II

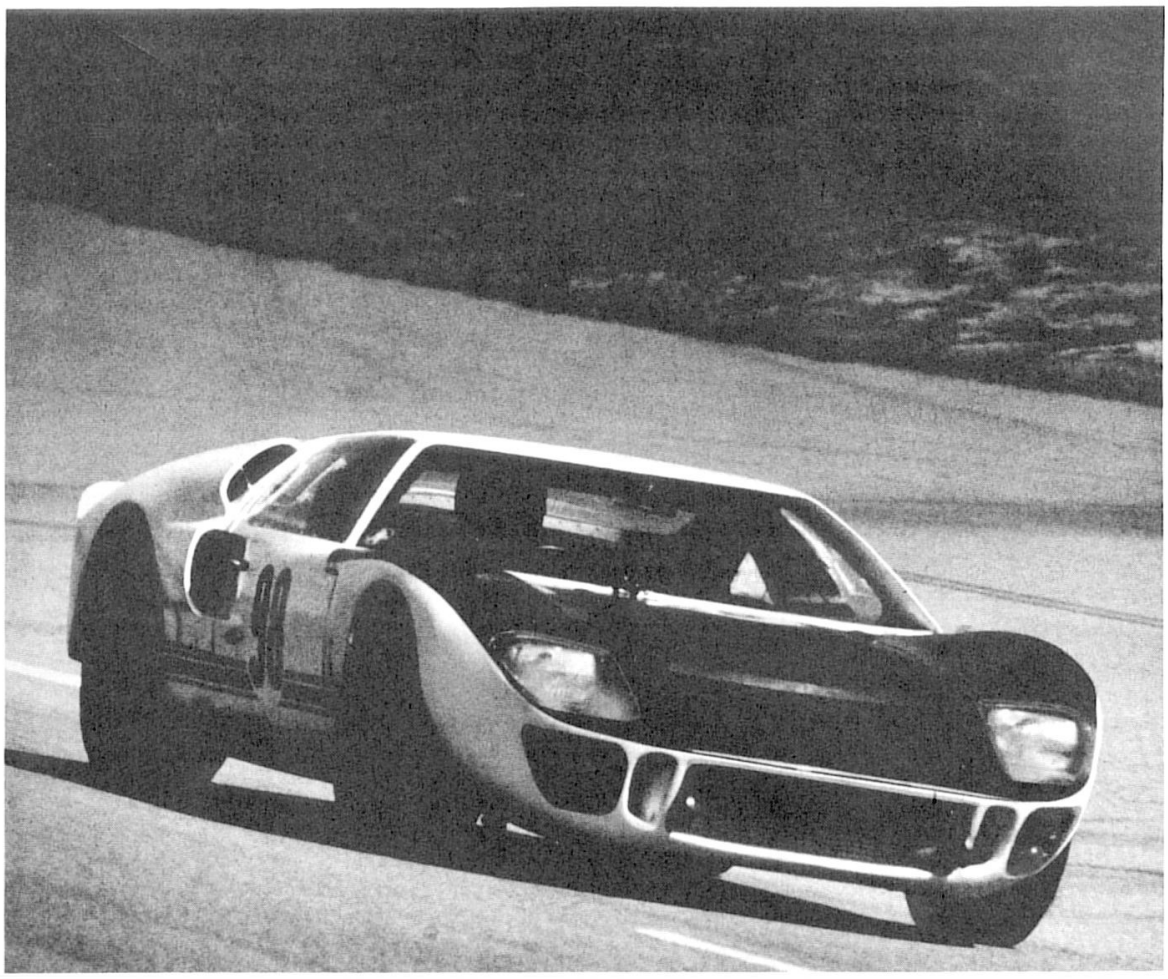

Figure 34 — Winning MK II at Daytona 1966

1966 (Figure 33). The MK II cars virtually led the race all the way, finishing first, second, and third for their first victory (Figure 34). It is interesting to note that in 1965 when this race was approximately at the half-way point, the winning GT 40 averaged 99.9 mph. In 1966, the event was of 24 hours duration and the winning average was 109 mph. This indicates the fast-moving nature of this field of competition.

The second race in 1966 was the Sebring event, where MK II's finished first and second, setting new distance and lap records, and a GT 40 finished third over-all. The car that finished first was an open version of the MK II with an aluminum underbody that was designated the XI (Figure 35).

One car was entered in the Spa 1000 Kilometer Race and finished second.

After attending the practice session in April, eight cars were prepared for the Le Mans event that took place on June 18-19, 1966. MK II's qualified in the first four places and set a new lap record of 3 min. 31 sec. or 142 mph. The race took place in cloudy weather with intermittent showers during the 24 hours. MK II's finished first, second, and third and, despite the weather conditions, established a new record for the 24 hours of 126 mph (previous best was 122 mph on a dry track), (Figure 36).

As a result of winning Daytona, Sebring, Le Mans, and finishing second at Spa, the MK II also won the World Championship for prototype cars in 1966, thereby meeting the original objectives set forth in 1963.

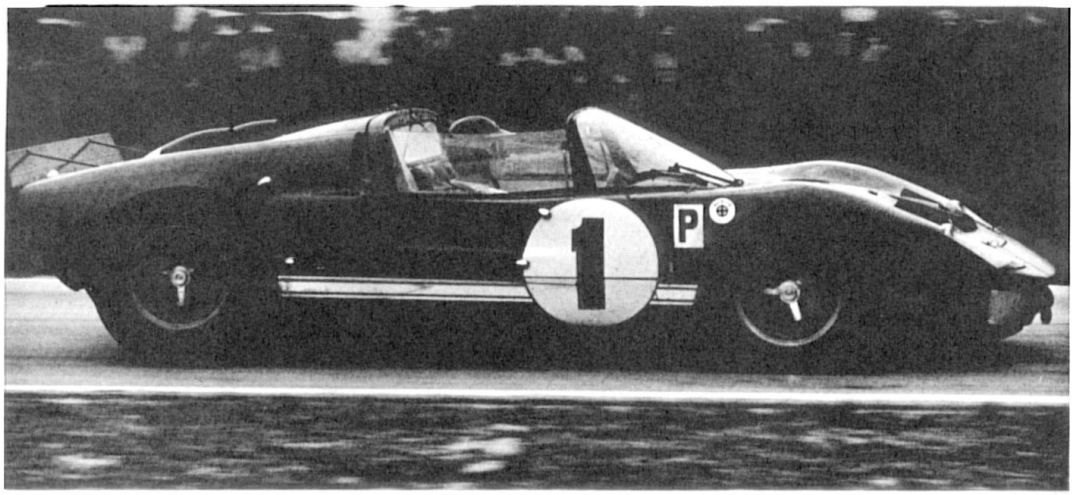

Figure 35 – XI Car Winning Sebring 1966

Figure 36 – The Three MK II's Taking Checkered Flag at Le Mans 1966

SUMMARY

It required three years, new technology, facilities and financial backing to take the Ford GT from the drawing board to the checkered flag at Le Mans. But above all, it required personal effort, ingenuity, skill, incentive and courage on the part of individuals to bring the project to fruition. The racing achievements will undoubtedly become a notation in the record book, but the contributions to automotive technology should provide a lasting satisfaction to all those who participated in the program.

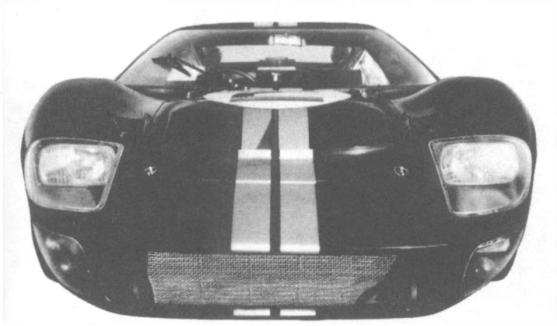

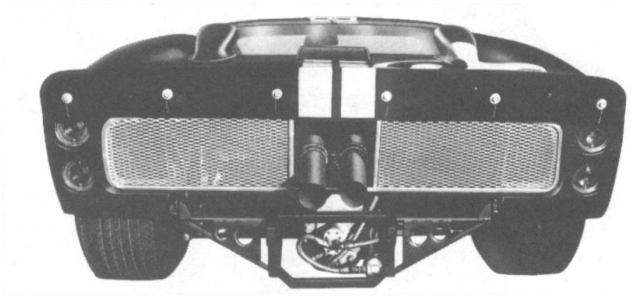

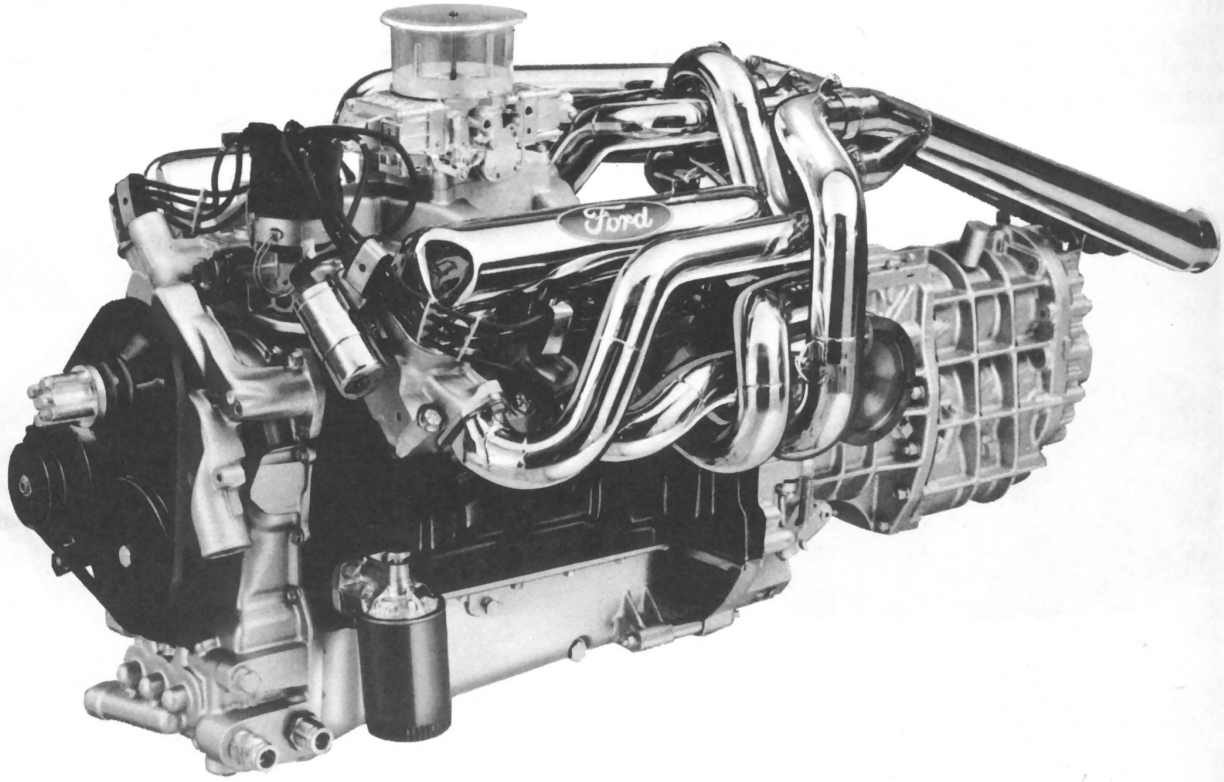
Ford

Mark II–427 GT Engine

Joseph F. Macura and Jonathan Bowers
Ford Motor Co.

INTRODUCTION

The Mark II Ford 427 cubic inch displacement GT engine used in the 1966 Le Mans race was a modified version of the 1966 High-Performance production 427. (Figure 1) Major changes from the standard version included the use of aluminum cylinder heads, "dry-sump" lubrication system, new carburetor, aluminum water pump, transistorized ignition, special flywheel, an aluminum front cover, and a magnesium oil pan.

These changes, along with various design refinements, were made to meet particular demands imposed by vehicle design, race regulations, endurance requirements, and vehicle performance characteristics.

Valuable background experience in developing engines for GT use had been accumulated since the fall of 1963 when the 255 cubic inch, pushrod "Indianapolis" engine was selected for the 1964 Le Mans race. This engine (Figure 2) was installed in a newly developed GT vehicle which was entered in the Nurburgring 1000 KM race in May, 1964, in order to test the vehicle and engine combination under actual racing conditions. Suspension problems forced the vehicle to retire in the fifteenth lap.

In June, three of the new GT vehicles powered by the 255 "Indianapolis" engine competed in the Le Mans race. One of the vehicles set a new lap record but various vehicle

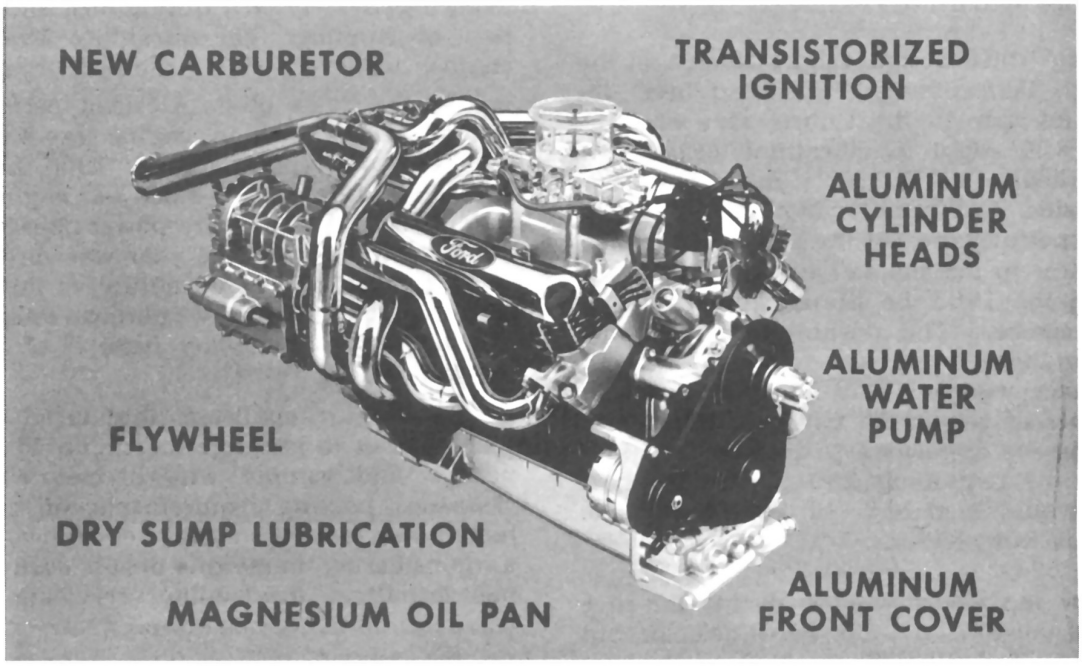

Figure 1

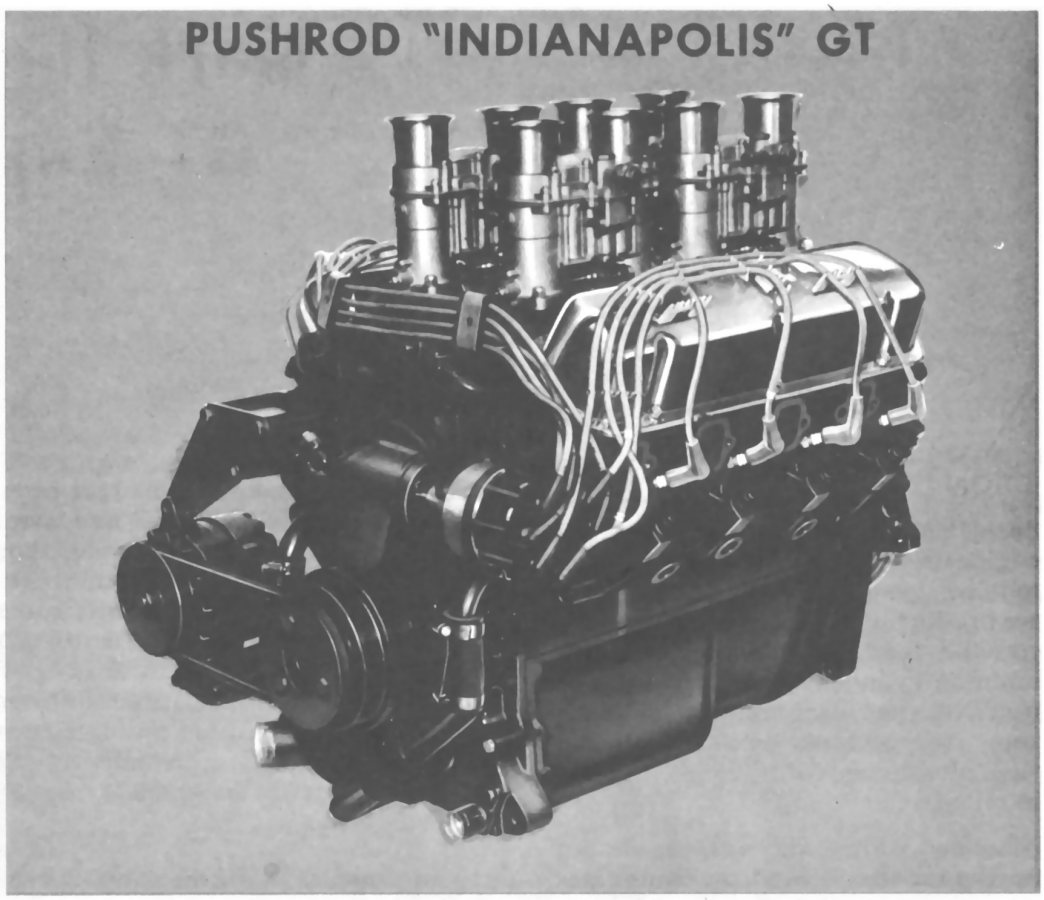

Figure 2

mechanical problems led to the retirement of all three entries by the fifteenth hour.

During 1964 a lightweight version of the 427 High-Performance engine had been developed for use in the Cobra. One of these engines, with slight modifications, (Figure 3) was installed in a GT vehicle undergoing tests at Riverside, California, early in 1965. The excellent performance of the vehicle prompted the decision to use the 427 cu. in. lightweight engine in the 1965 Le Mans race, primarily as a pacesetter. The durability level of the engine for this type of race was unknown, but performance was such that the vehicles would be capable of setting an unusually fast pace. By forcing the opposition to run beyond their capacity, the remaining 289 cu. in. powered vehicles would then have an excellent chance to finish in lead positions.

A new lap record was set during the race by one of the 427 cu. in. powered vehicles, but the strategy ended at that point, as all of the Ford entries retired early due to mechanical problems. The 427 cu. in. engines had performed extremely well during their short duration of running. The durability level of the engine, however, still remained unanswered.

On the basis of its excellent performance in '65, the 427 cu. in. engine was selected as the main powerplant for the 1966 Le Mans race. The 427 cu. in. stock car engine could readily meet the 450 horsepower objective. Our major effort during the year was directed toward improving the durability of the engine. To meet this objective, we planned to capitalize on the proven durability features of the production engine.

The major challenge that faced our engineers was to package the engine in the new vehicle and comply with necessary ground clearance, cooling requirements, oil capacity, intake and exhaust system clearance, as well as considering numerous details such as hot-fuel handling, driveability, servicing, maintenance, and instrumentation.

As with all of our high-performance and competition engine work, one of the most

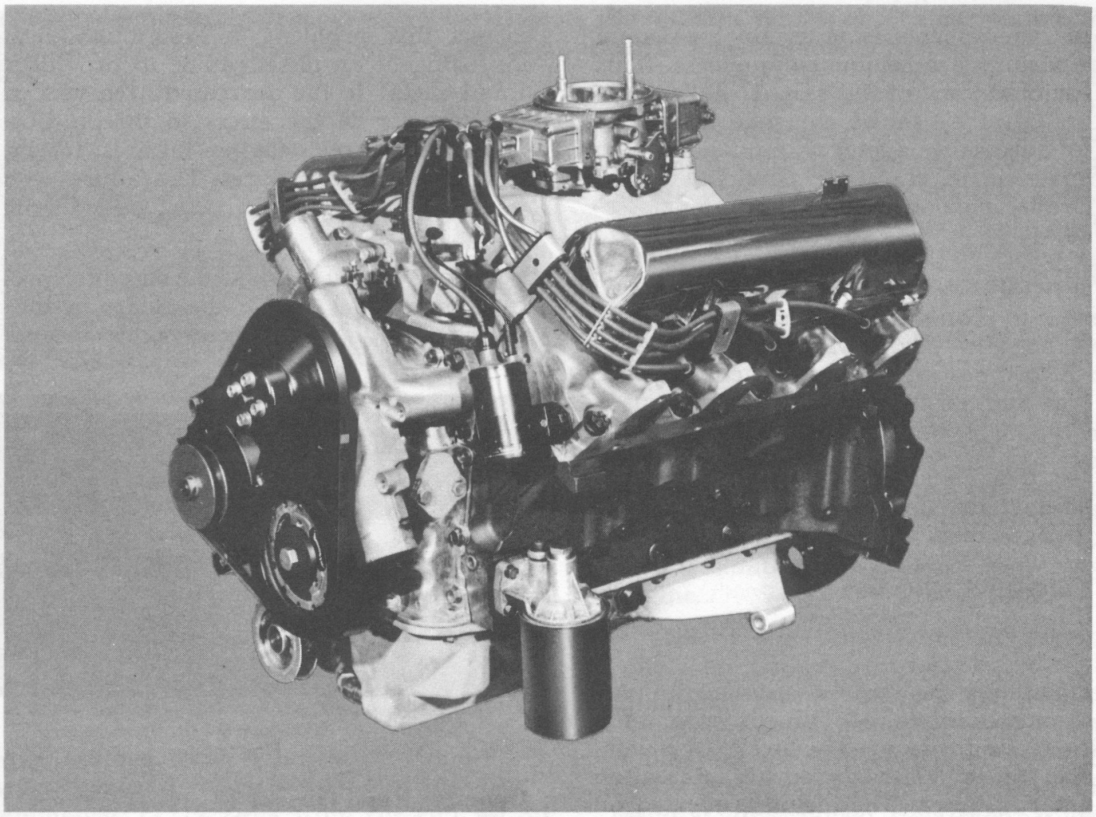

Figure 3

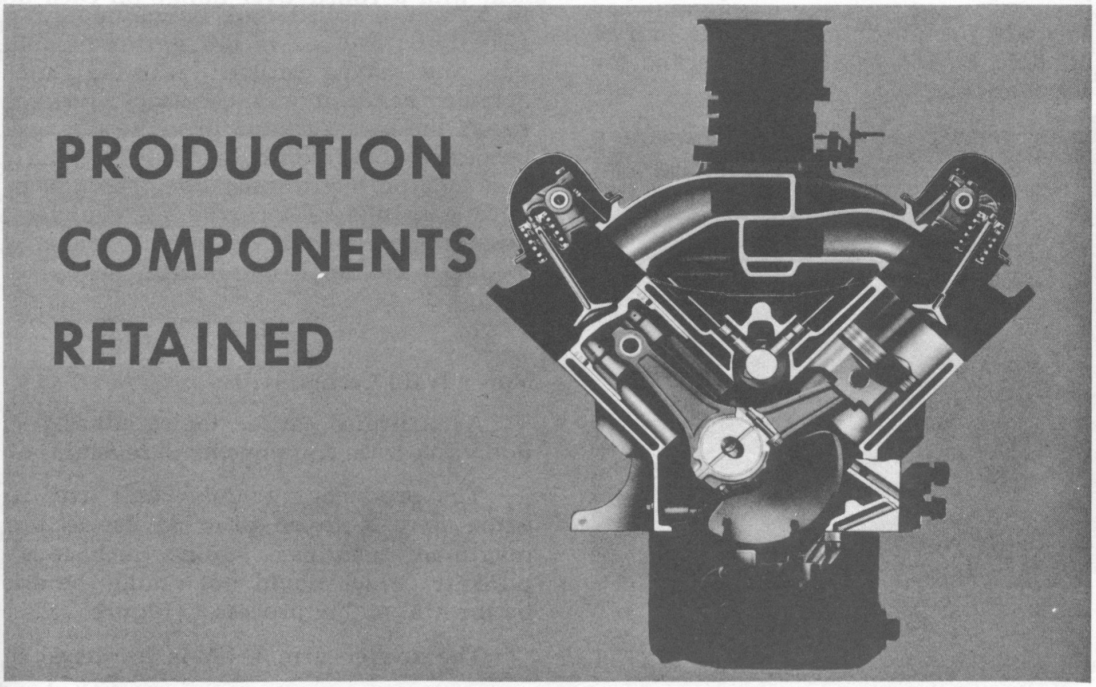

Figure 4

stringent requirements is to retain maximum use of existing production components. This cross-sectional view of the MK II 427 cu. in. engine (Figure 4) shows to some extent the degree of success we achieved, having retained the cylinder block, camshaft, crankshaft, connecting rods, pistons, valve train, and intake manifold.

DESCRIPTION

In order to promote a better understanding of the total engine engineering effort, the description of component and system changes is divided into four groups: detail modifications, unique components designed primarily to affect weight savings, a review of those parts that were changed for durability reasons, and the unique designs dictated by vehicle requirements.

DETAIL MODIFICATIONS

Piston

The standard production piston is an aluminum extrusion which affords maximum strength-to-weight ratio. The thread-type surface finish on the skirt is used for lubrication and scuff resistance. The piston is located on center, since "cold-start piston slap" is of no concern. The pin bores are honed for optimum geometry and piston-to-piston compatibility. Two slots are provided in the upper half of each pin hole at 45° from the centerline for added lubrication.

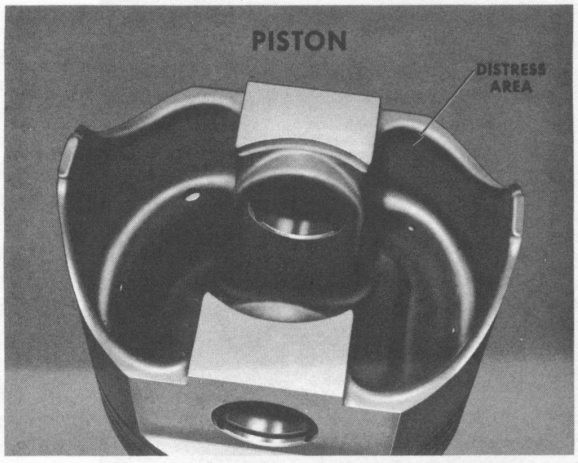

Figure 5

A number of incidents of skirt cracking at the large radius in the slipper occurred during dynamometer testing. (Figure 5) In order to correct this problem, a design modification, consisting of an offset radius to provide additional metal in the distressed area was made. The transfer of the stress to the pin boss resulted in chaotic engine failures instead of spasmodic piston failures. The failures were the result of the piston pin being pulled from the piston.

It was decided to use the standard production piston and polish the skirts in the distressed area to provide an extra measure of insurance.

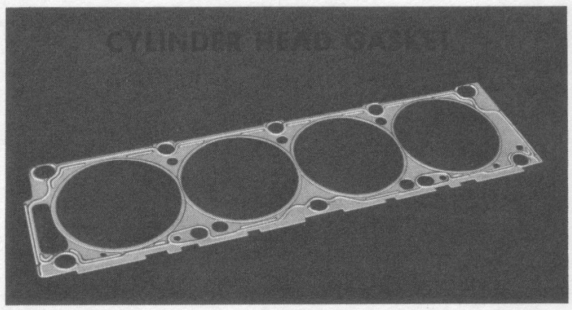

Figure 6

Cylinder Head Gasket

The standard production cylinder head gasket is a stainless-steel beaded design, .016 thick, with a rolled-over flange on each bore. (Figure 6) The use of this gasket did not present any sealing problem with the aluminum cylinder head. It was necessary, however, to revise the bolt torquing procedure in order to prevent cracks in the cylinder head at the center bolt hole on the exhaust side. The new procedure consisted of torquing all cylinder head bolts in the conventional manner, but at 20 ft.-lb. intervals until the maximum value was obtained.

Valve Train Components

As indicated earlier, the standard production valve train components were retained.

The production nodular cast iron rocker arms were X-rayed prior to use to provide maximum insurance against inclusions and porosity, which could not readily be detected by the Magnaflux process. (Figure 7)

The rocker arm shaft is hardened in the rocker arm bearing area and is held in place by slotted malleable iron supports bolted to the cylinder head.

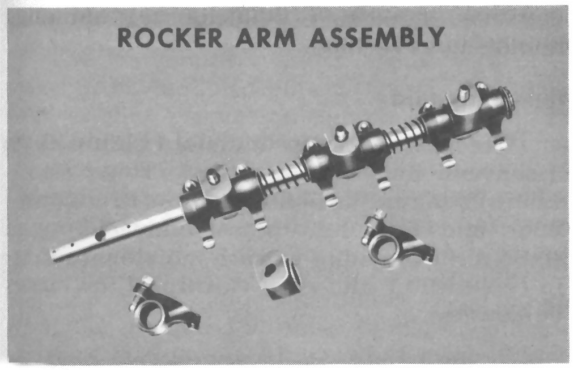

Figure 7

The pushrod is comprised of an electric-weld tubing with a ball bearing welded to the tappet end and a stamped case-hardened cup welded to the opposite end. One isolated push-rod failure was experienced during the course of vehicle tests and was attributed to an improperly heat-treated socket. To guard against further incidents of this nature, all pushrods were quality inspected.

Throughout the program, spasmodic valve spring failures were experienced. The failures always occurred in the lower closed coil approximately 1-1/2 coils from the end. In an effort to reduce the mechanical friction thought to be the source of failure, the production springs were cadmium-plated to provide a form of lubricant on each coil. Since this did not reduce the number of failures, the plating operation was discontinued.

When time literally ran out and no further changes could be incorporated to alleviate the problem, a concerted effort was made to train the pit crews in the art of changing valve springs with a minimum amount of time. Fortunately, no valve spring failures, which affected vehicle performance, were experienced during the race.

Crankshaft

A forged steel crankshaft with cross-drilled oil passages feeding the connecting rod bearings is standard on the 427 cu. in. production engine.

All of the "bobweight" is counterbalanced within the crankshaft counterweights. External counterbalancing has been avoided because of the excessive edge-loading it imposes on the front and rear main bearings. Main bearings are of the steel-backed over-plated copper-lead lining construction. The number three main bearing absorbs the crankshaft thrust loads.

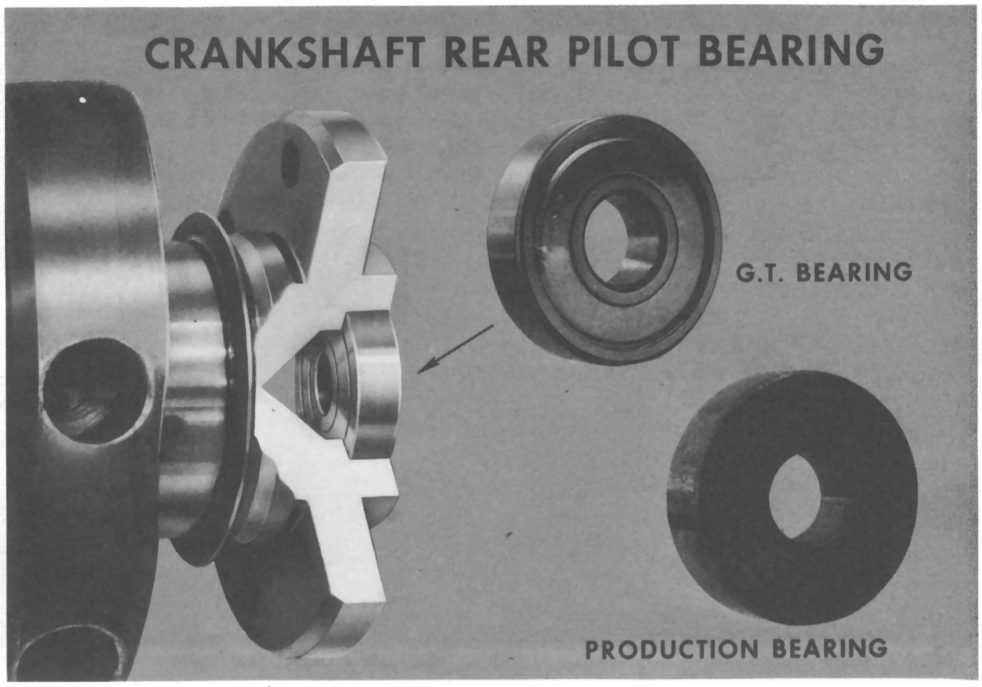

Figure 8

This crankshaft was used in the GT application with only one modification, the sintered-bronze clutch pilot bearing was replaced with a double-row sealed-ball bearing. (Figure 8) Early vehicle tests indicated a need for a sealed bearing to prevent the high-temperature resistant grease from leaking onto the flywheel face of the clutch, thus avoiding a slipping condition.

UNIQUE COMPONENTS FOR WEIGHT SAVINGS

The reduction of weight was based on the use of aluminum and magnesium castings, wherever feasible. The first 1965 experimental engines weighed 555 pounds. These engines were built with aluminum cylinder heads, water pump housing, crankshaft damper hub and a magnesium intake manifold. A twenty-five pound weight penalty was imposed on the 1966 engines through the requirement for an internal "dry-sump" lubrication system and a decision to use the standard production aluminum intake manifold. The magnesium manifold was discarded because of difficulty in obtaining homogenous castings.

Intake Manifold

The cast aluminum manifold (Figure 9) is a conventional "over-and-under" single four-venturi design. The optimum runner configurations and sizes had been obtained through static airflow studies of each individual runner in conjunction with each element of the induction system.

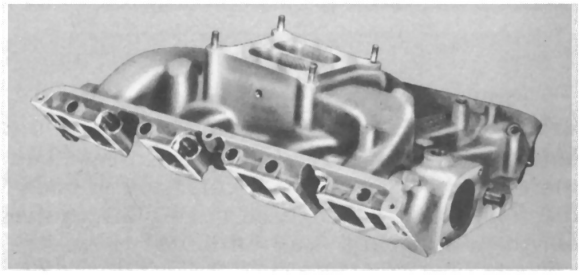

Figure 9

(Further information regarding the induction system is contained in Mr. A. O. Rominsky's paper No. 670067 on MK II — 427 Engine Induction System.)

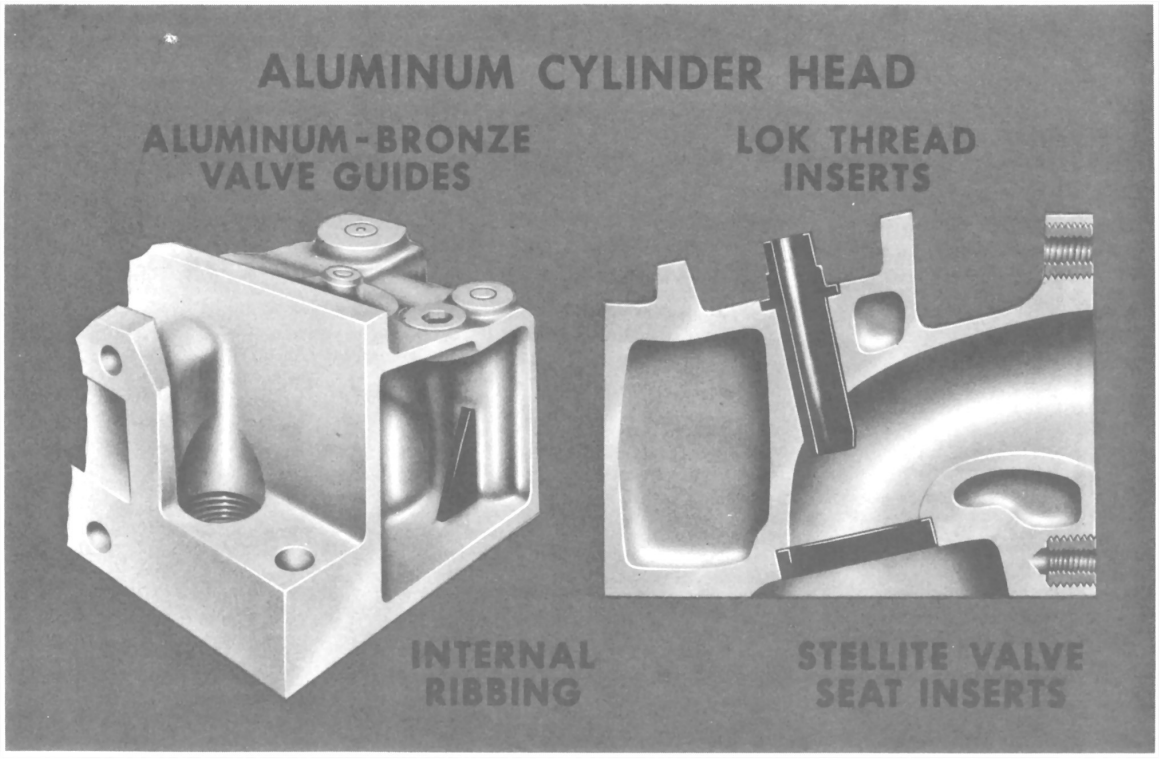

Figure 10

Cylinder Head

The aluminum cylinder heads were produced from modified plastic patterns obtained from existing production equipment. The heads contain internal ribbing and heavier sections consistent with design practices for aluminum. (Figure 10) Aluminum-bronze valve guides and stellite valve seat inserts were incorporated.

During the early stages of the experimental build program, .050" was added to the intake manifold mounting surfaces to eliminate head cracking during assembly torquing. Steel "Lok Thread" inserts were used in the exhaust header mounting holes to prevent mutilation of the threads during the installation of the exhaust headers in the vehicle.

Crankshaft Vibration Damper

The production crankshaft vibration damper consists of an alloy iron inertia ring mounted to an iron hub casting with an elastomer sleeve. The inertia member has sufficient mass to cope with the torsional amplitudes and frequencies induced by high rpm. The damper was redesigned (Figure 11) to incorporate a cast aluminum hub in order to reduce engine weight while retaining the same inertia member. The damper contains holes for the insertion of weights during mass balancing of the engine assembly.

Figure 11

Water Pump

The water pump housing was cast in aluminum, utilizing the existing production equipment for the cast iron housing. (Figure 12) Because of the high water temperatures experienced during a test trip where the ambient temperatures were 90°F, a larger impeller was used to increase the capacity of the pump. Subsequent wind tunnel tests were conducted to finalize the pump capacity.

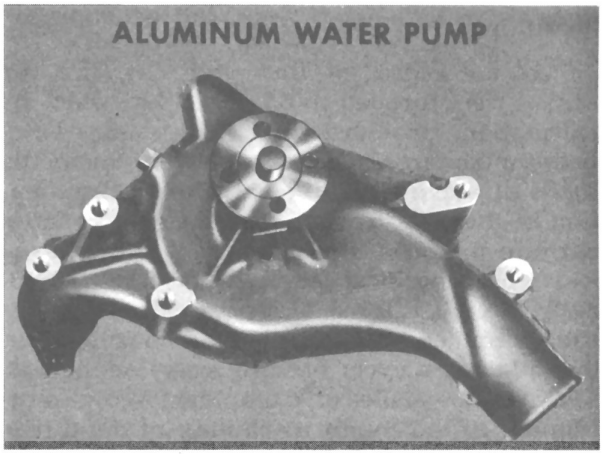

Figure 12

REVISED COMPONENTS FOR DURABILITY

As indicated earlier, the primary objective was to meet durability requirements. In line with this, the following production components were revised to achieve the objective.

Connecting Rod

The forged steel connecting rod is the type currently being used in the production engine. (Figure 13) The cap is located with respect to the rod half by two steel dowels which are contained in counter-bores at the parting line. The cap-screw has a 12-point head, washer face and undercut shank. The thread is a "tri-

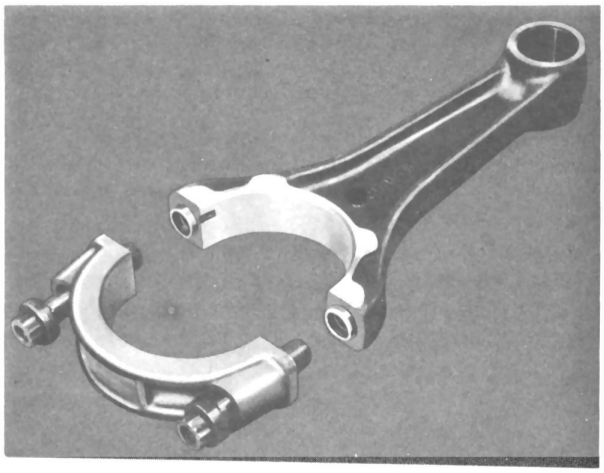

Figure 13

lobe" interference fit type designed to spread the load more uniformly along its full length. The cap screw is prelubricated with a graphite compound during assembly to minimize the high friction torque inherent in the interference fit thread.

At the outset of this program, the cap screws were torqued to 55-60 ft. lbs., which by calculation, provided sufficient clamping force between the cap and rod to withstand the inertia loads at maximum anticipated rpm. Examination of the rods from two engines, which failed early in the program indicated that the failure was due to bending fatigue of the bolt. Insufficient clamping force between the cap and the rod permitted movement at the parting line, thus placing a cyclic bending stress on the bolt. The lack of sufficient clamping force was attributed to the rough machining of the thread in the rod bolt hole. Some of the fixed torque load was expended in overcoming the additional friction caused by the poorly threaded hole. For the race, the connecting rod bolt holes were specially processed to improve the quality of the thread and the cap screws were installed by loading to a predetermined stretch.

Piston Rings

The first and second compression rings are the same as those used in the production engine. They are 1/16 thick, barrel-faced and chrome plated. The top ring is cast of high-tensile ductile iron and the second ring is standard piston ring iron.

In the early stages of the program, the production oil control ring expander was used.

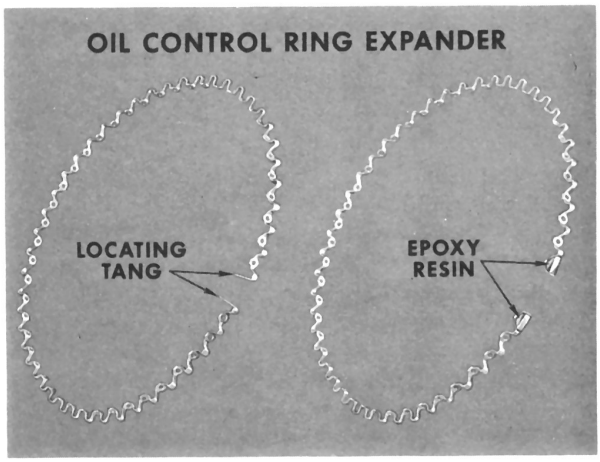

Figure 14

This expander had a locating tang at each end which was inserted into a hole in the piston oil ring groove. Several instances of broken tangs resulted from inherent loading. To eliminate this problem, the expander was redesigned to remove the tangs, and a standard butt-joint was used in conjunction with epoxy resin filled ends. (Figure 14)

Piston Pin

Production piston pins were used. However, production tolerances were such that the end play could vary between 0.000" to .024". During the test program, several piston pin retainers failed, which was attributed to the severe pounding of the piston pin against the retainer. The piston pins were then select-fitted to obtain 0.001/.005 end play. This did not resolve the problem. An analysis of subsequent failures indicated that those piston and connecting rod assemblies which were at or near the low limit were failing. This was attributed to negative end-play due to the bending of the piston pin boss of the piston. The end play was revised to .005/.010", and no further retainer failures were experienced. (Figure 15)

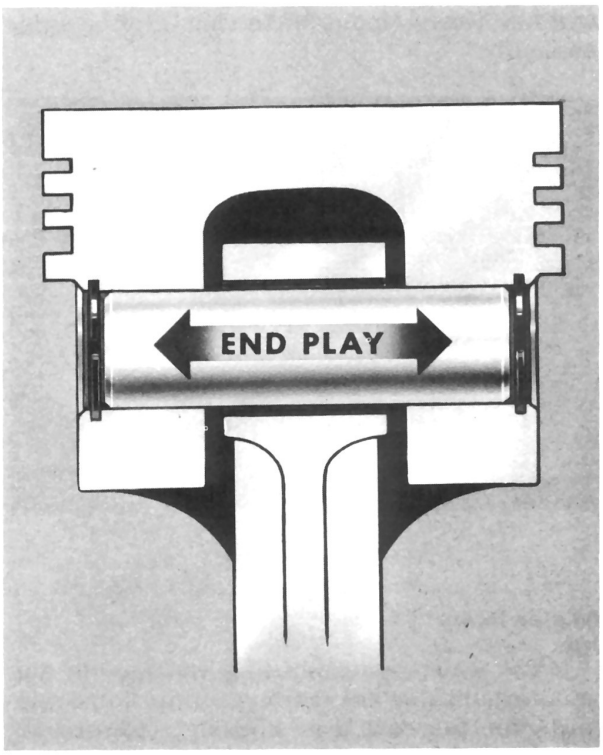

Figure 15

Valves

Intake and exhaust valves are of similar construction to those used in the production engine, except for smaller head diameters necessitated by the use of valve seat inserts in the aluminum cylinder heads. The lightweight valves have hollow stems which are flash-chrome-plated for scuff resistance. The 1.625 diameter exhaust valve is sodium cooled and is made from a 21-4N material with a hardened Silicrome #1 stem tip. The 2.06 diameter intake valve is made from Silicrome X-B material.

To improve durability, both valves were designed with tulip heads having a divergent cross section for constant stress. The stem blends into the head at a slight angle to eliminate the possibility of the diameter in the transition area being less than the stem diameter. (Figure 16)

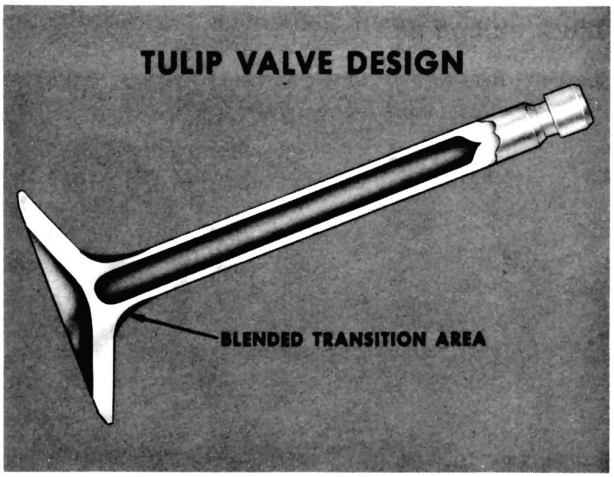

Figure 16

Valve Stem Seal

The production teflon valve stem seal, (Figure 17) which is pressed onto the upper end of the valve guide, was used. Several seals disintegrated during sustained high rpm operation. One seal failure almost resulted in an engine failure during testing at Daytona. Examination of the engine disclosed that the metal band of the failed valve stem seal had migrated to the lubrication system scavenge pump, causing it to seize. The failures were attributed to insufficient valve stem-to-seal clearance. This clearance was increased, and no further failures were experienced.

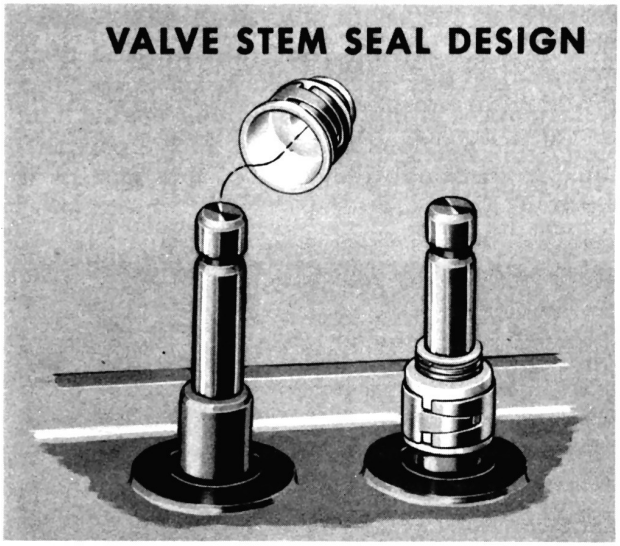

Figure 17

Rear Oil Seal

Early in the program, the engines were built with the conventional rope-type rear oil seal used in passenger car engines. This seal rides on a knurled journal behind an oil slinger machined into the crankshaft. A clutch slipping problem due to a leaky rear oil seal, was experienced during tests at Daytona. The rope seal was replaced by a two-piece rubber compound lip seal designed to fit into the existing groove. The knurl on the crankshaft journal was polished prior to the installation of the seal to prevent possible tearing of the lip. (Figure 18) No rear seal leaks were found after oil leak checks of the engines from races and dynamometer durability testing.

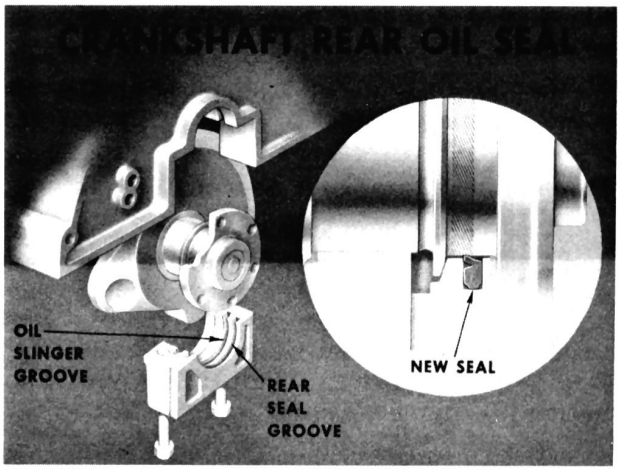

Figure 18

Electrical System

The Ford breakerless transistorized ignition system was used because of its excellent performance in the Indianapolis engine and during the previous two years in GT competition. A schematic diagram of this system is shown in Figure 19.

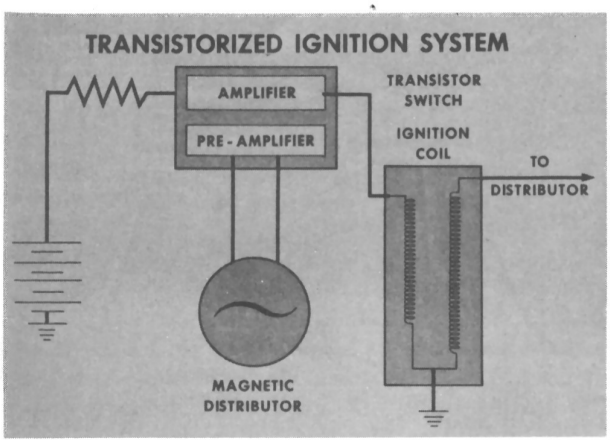

Figure 19

This system employs a variable reluctance for achieving voltage control in the triggering of the main ignition circuit. A concentric permanent magnet and coil, in conjunction with a tooth rotor, varies the reluctance of the magnetic circuit as it rotates. The proper voltage waveform is achieved to trigger the main ignition circuit. The main circuit is fully transistorized for compactness and high reliability. This circuit permits a spark coil to deliver an almost constant voltage throughout the entire high speed range.

UNIQUE COMPONENTS DUE TO VEHICLE REQUIREMENTS

The design of the vehicle dictated special requirements for the engine, clutch, lubrication system, and the cooling system.

Flywheel and Ring Gear Assembly

A new flywheel was designed to accommodate the double-disc clutch. It was machined from a steel casting with the standard production ring gear press-fitted to the flywheel and welded securely. Holes were drilled in the front side of the flywheel as required, for mass balancing the engine assembly. (Figure 20)

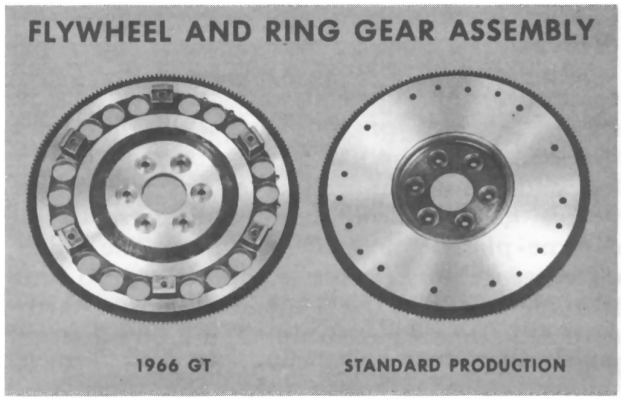

Figure 20

Front Cover

The sand cast aluminum front cover extends below the bottom of the cylinder block to accommodate the oil scavenge pump system. (Figure 21) It was extended as much as competition rules for ground clearance would permit. The front cover is sealed to the crankshaft in the conventional manner and a single gasket is provided to seal the cover to the cylinder block and oil pan.

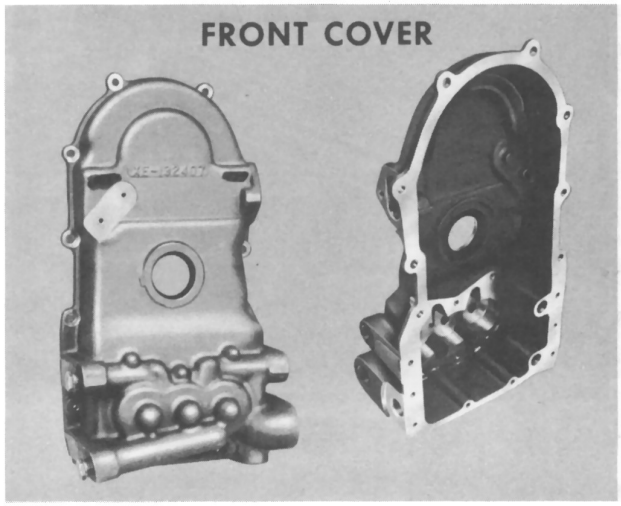

Figure 21

Oil Pan

The sand cast magnesium oil pan extends from the front cover to the rear of the cylinder block. (Figure 22) Provision is made on the inside of the oil pan for the installation of front and rear oil scavenge pickups. Drilled passages in the pan leading to the oil pick-ups, exit at the front of the pan and match the scavenge pump inlet holes in the front cover. The oil pan

Further information regarding the ignition system is contained in Mr. R. C. Hogle's paper No. 670068 on MK II — 427 Ignition and Electrical System.

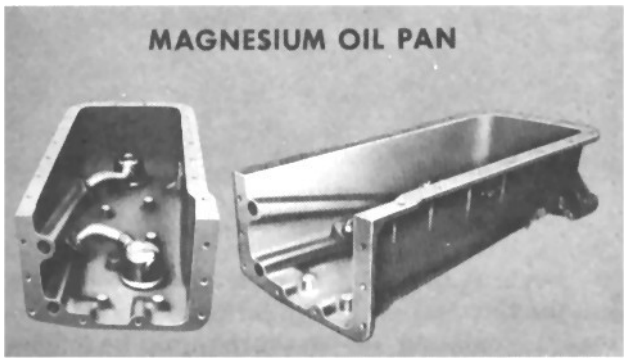
MAGNESIUM OIL PAN

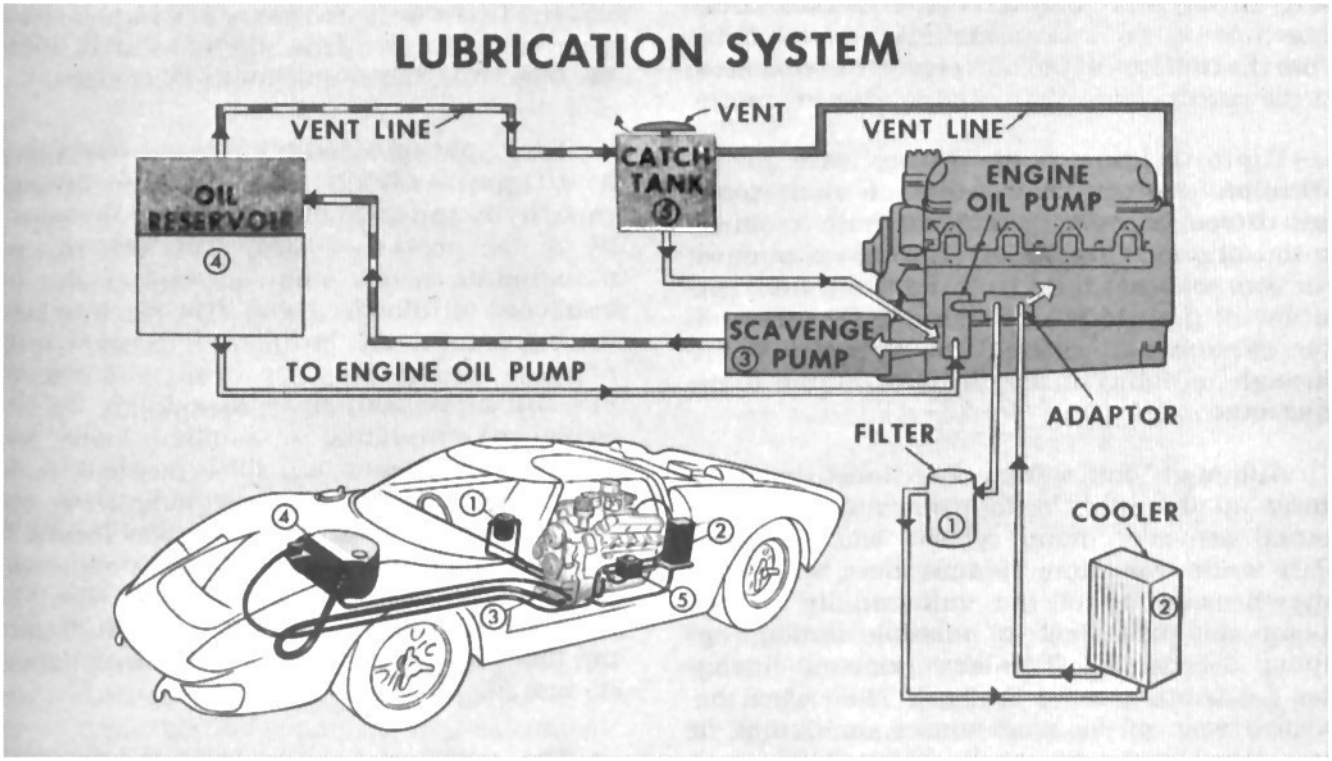
LUBRICATION SYSTEM
VENT LINE
VENT
VENT LINE
CATCH TANK ⑤
OIL RESERVOIR ④
ENGINE OIL PUMP
SCAVENGE ③ PUMP
TO ENGINE OIL PUMP
ADAPTOR
FILTER
COOLER
①
②
③
④
⑤

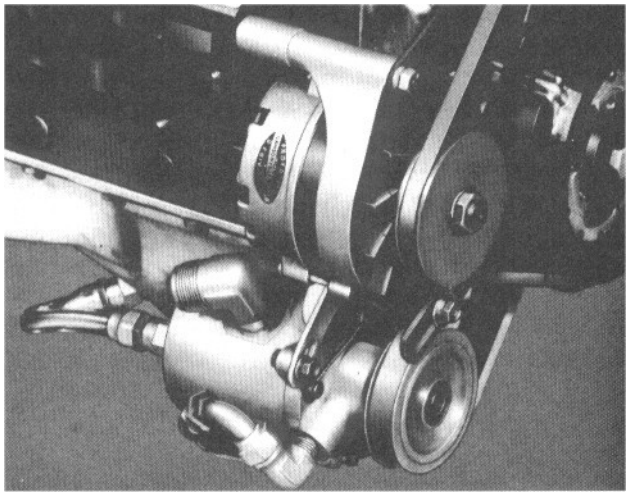

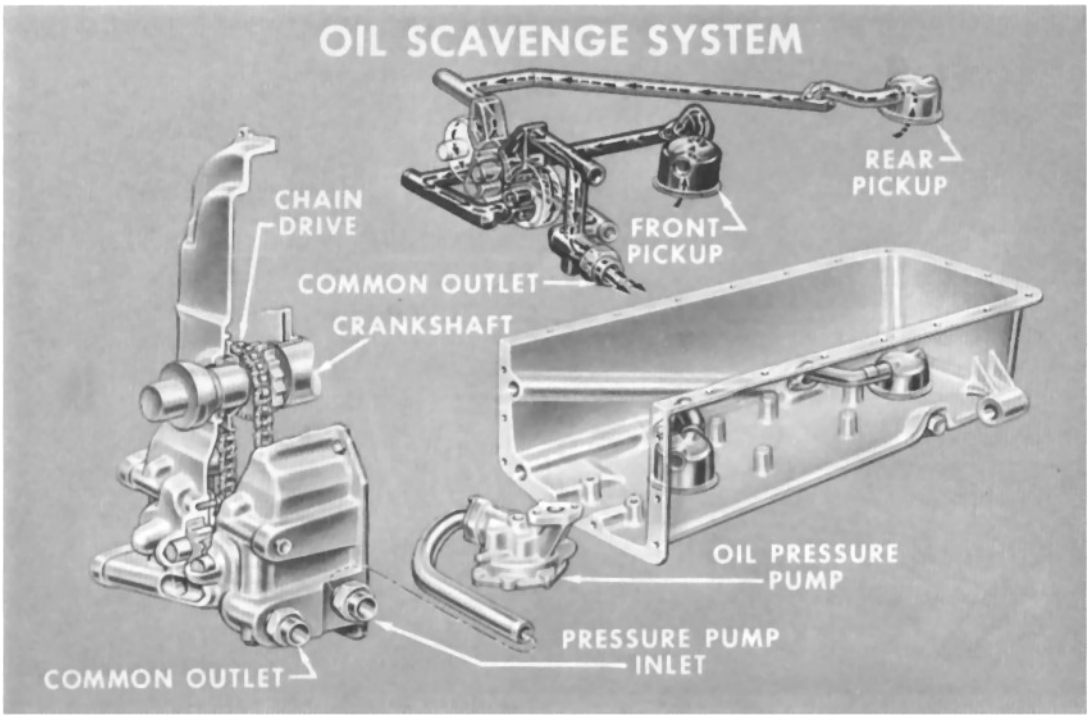
OIL SCAVENGE SYSTEM
REAR PICKUP
CHAIN DRIVE
FRONT PICKUP
COMMON OUTLET
CRANKSHAFT
OIL PRESSURE PUMP
PRESSURE PUMP INLET
COMMON OUTLET

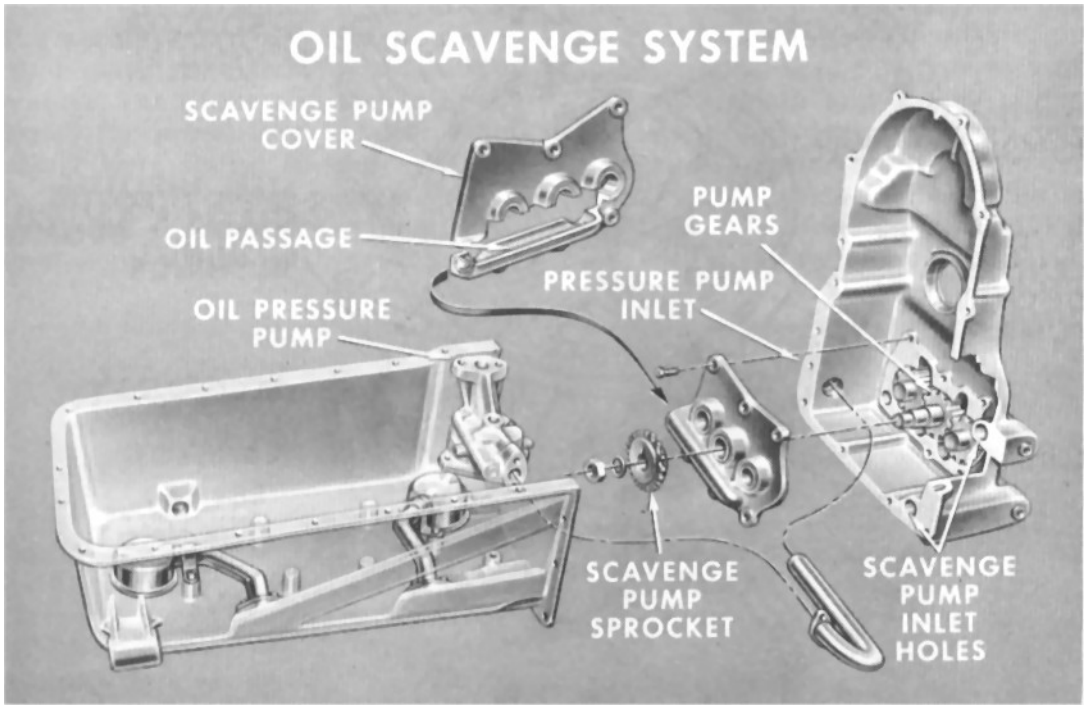
OIL SCAVENGE SYSTEM
SCAVENGE PUMP COVER
OIL PASSAGE
PUMP GEARS
PRESSURE PUMP INLET
OIL PRESSURE PUMP
SCAVENGE PUMP SPROCKET
SCAVENGE PUMP INLET HOLES

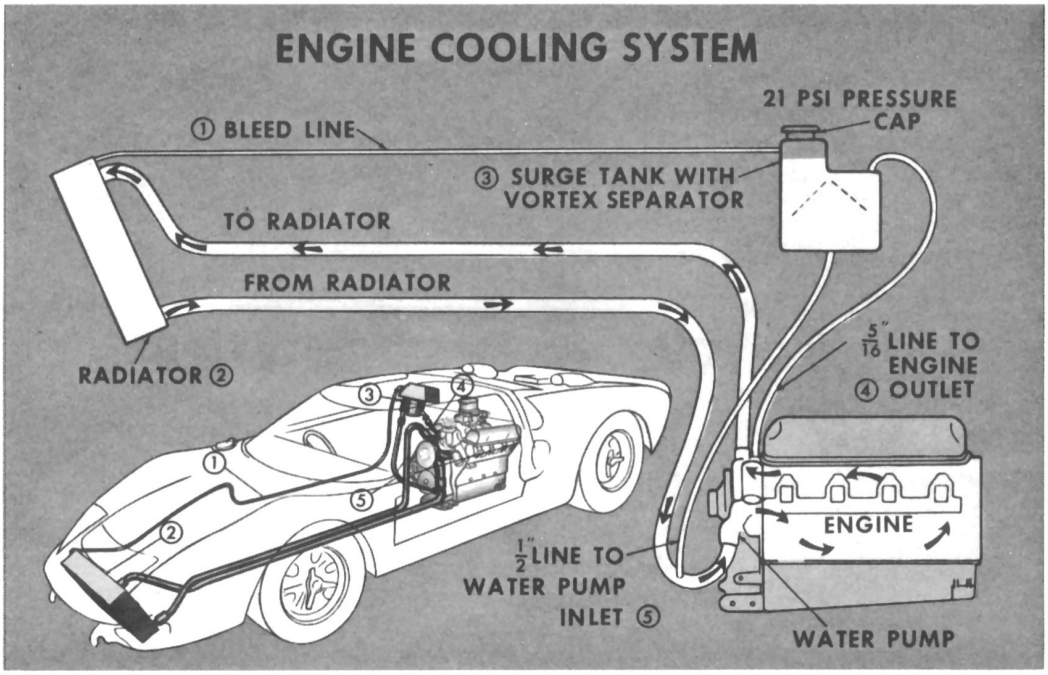

Figure 27

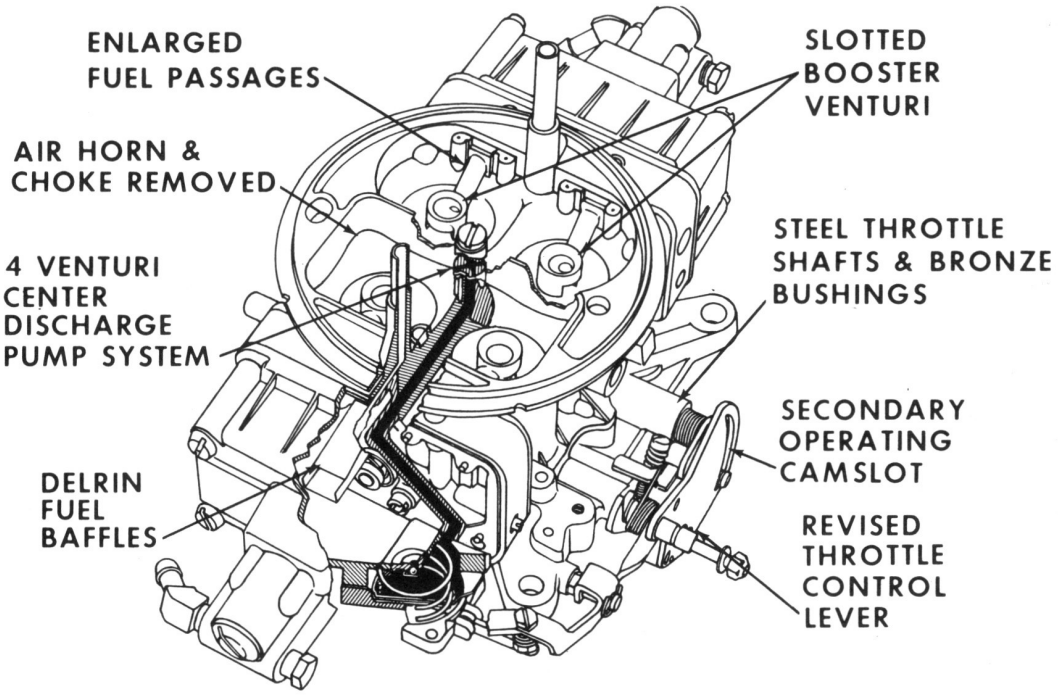

Figure 28

Cooling System

A diagrammatic sketch of the vehicle cooling system is shown in Figure 27. The production engine series-flow cooling system was retained.

The following modifications to the cooling system were adopted in order to stabilize the water temperatures at an acceptable level based on vehicle and wind tunnel tests:

- Larger surge tank equipped with a vortex separator to allow for expansion and deaeration of the water.
- Increasing the size of the line from the engine water outlet to the surge tank to obtain

acceptable de-aeration with minimum loss of cooling capacity.

- Increasing the size of the line from the surge tank to the pump inlet to insure positive pressure at the pump inlet regardless of pressure losses in coolant system.
- Installation of a 20 psi pressure cap on the surge tank to raise the air-to-boil temperatures of the system.
- Increasing the water pump capacity by installing a larger impeller.

Carburetor

Several modifications were made to the production 780 cfm carburetor to improve its operation in the GT car. (Figure 28) These modifications included the use of mechanically operated secondary throttles instead of vacuum operated secondaries to give the driver full throttle control. Steel throttle shafts and bronze bushings were added for durability and safety. A center-discharge accelerator pump was added to deliver an equal amount of fuel to each of the four venturi during acceleration. Delrin baffles were installed in the fuel bowls to eliminate spill-over on extreme acceleration. and deceleration. The choke and the air horn were eliminated for unrestricted air flow. The booster venturi were slotted to improve fuel distribution. The fuel discharge passages were enlarged to meet fuel requirements at high rpm, and the throttle control lever was revised to accommodate the special throttle linkage required for the installation.

Fuel System

Figure 29 shows the complete fuel system in the vehicle. Three electric fuel pumps are used in this installation. Two of these pumps are connected in parallel and are used at all times unless the engine runs out of fuel. In such an emergency, the driver switches over to the third fuel pump. This enables the driver to return to the pit for refueling.

At the outset of the program, the standard production mechanical fuel pump was used in conjunction with one emergency electric pump. During vehicle testing, some mechanical fuel pump arm failures were experienced when running on the electric pump. Unloading of the arm caused a non-follow condition because of lack of fuel pressure. The mechanical fuel pump was then replaced by two electric pumps.

Exhaust System

Figure 30 shows the fabricated tubular header system that was designed to fit the vehicle installation. The 427 cu. in. engine has been quite responsive to this type of header system. The 32" length and 2-1/4" diameter of the headers, required to obtain optimum power at high rpm, were determined from dynamometer tests. Severe bends in the tubing appeared to have no effect on tuning as long as cross-sectional areas were maintained.

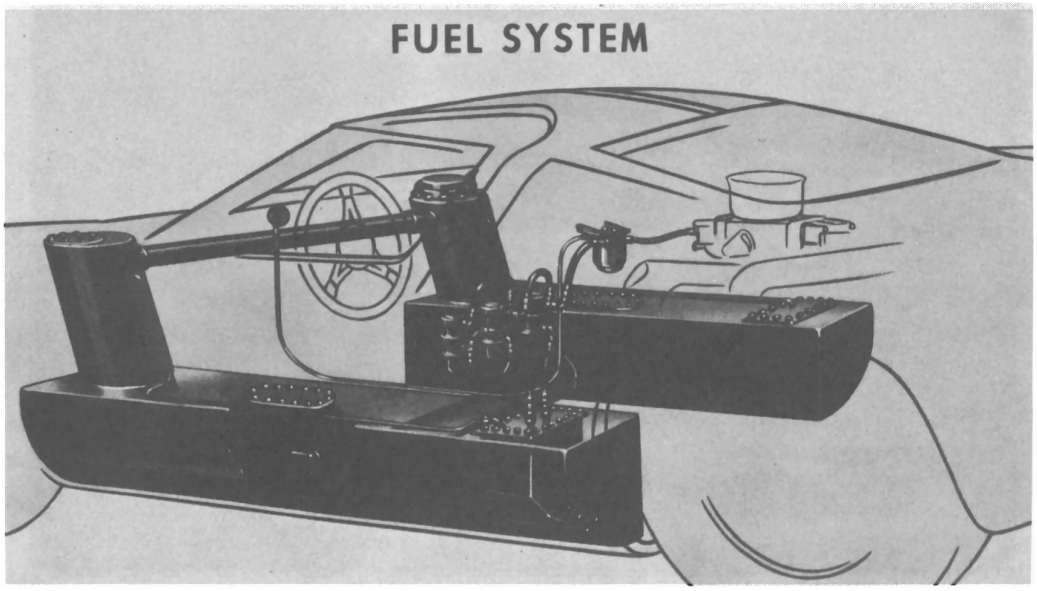

Figure 29

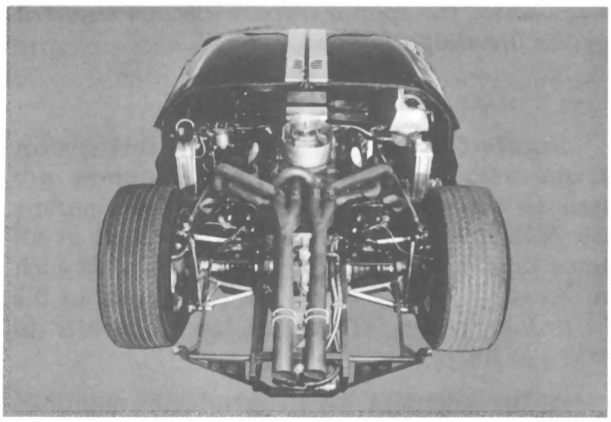

Figure 30

DYNAMOMETER TESTING

Dynamometer testing was predicated on the fact that while performance was important, durability was the prime consideration. With this in mind, it was decided to subject all new designs, revisions, etc., to two types of dynamometer durability testing. The first test was one which had been devised for checking the durability of the 427 cu. in. engine used in stock car racing. It consisted of cycling the engine between 6000 and 7000 rpm at wide-open-throttle for a period of six hours.

Upon the successful completion of this test, an exact duplicate of the engine was built and installed in a specially designed dynamometer setup. (Figure 31) This test simulated the actual running conditions prevailing during one lap of the Le Mans race with the driving pattern for the circuit duplicated relative to length of time in each gear, maximum rpm, etc.

The entire powertrain was cradled between two electric dynamometers which were coupled to the output shafts of the transaxle. The throttle, clutch mechanism, and gear shift selector were actuated by an air-valve solenoid system controlled electronically at a master panel.

Because of the limitation of the dynamometer equipment, some compromises were made. The final cycle was considered to be one which would test the durability of the powertrain to a degree equivalent to that anticipated in the race.

The duration of the test was established at 48 hours to provide a maximum safety factor.

(Further information regarding this installation is contained in the SAE paper No. 670071 "Laboratory Simulation — Mark II GT Powertrain".)

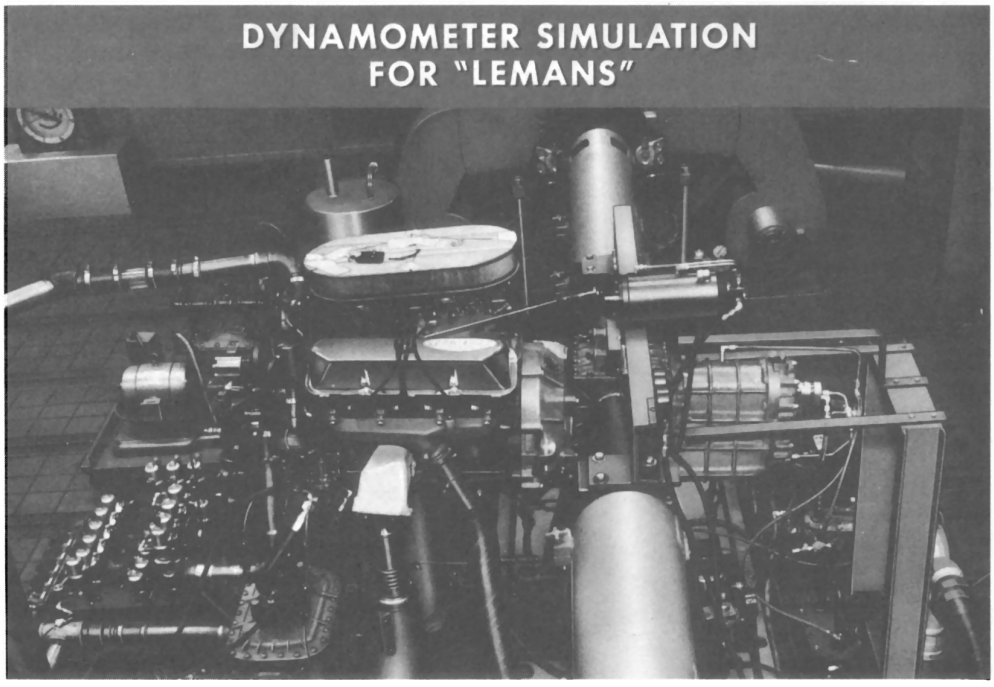

Figure 31

Each engine is given a four-hour dynamometer break-in and power run. An average of four hours of vehicle "shakedown" are required after engine installation in the vehicle. Five to nine hours of pre-race practice can be accumulated on each engine. This could result in considerable amount of running time prior to the race.

The simulation test was used extensively during the program. It proved to be an excellent instrument in exposing weaknesses of various components which were then redesigned and retested. The process was repeated as often as required on test engines until the durability objective of 48 hours was attained. It is interesting to note that the last experimental engine, which successfully completed the test, was compared with the engine from the winning car at Le Mans with respect to wear rate of the various components, general condition of the engine, etc., and no appreciable differences were found.

The performance phase of the dynamometer development of this engine was concentrated on obtaining 450 horsepower at 6200 rpm with a 10.5:1 compression ratio. Achieving this objective presented no problem. The 427 cu. in. push rod engine used in stock car competition had been refined to such an extent that it was capable of producing 525 h.p. at 6400 rpm with a 12.0:1 compression ratio.

Figure 32 shows the actual performance of the early GT engines using a moderate camshaft and having a 10.5:1 compression ratio compared to a representative production engine having a 12.0:1 compression ratio.

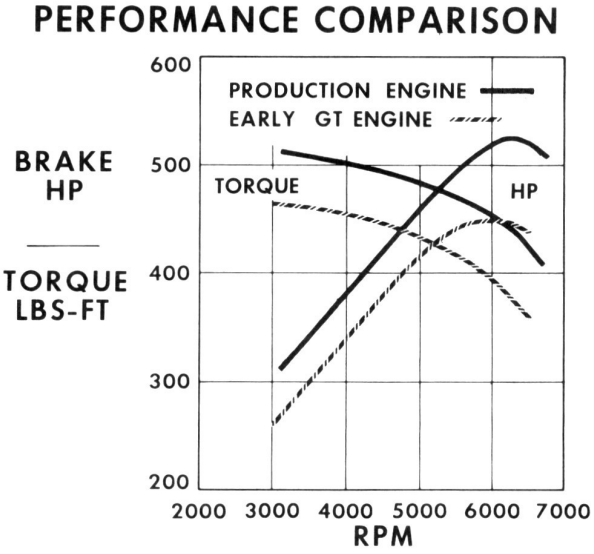

Figure 32

Detail refinements to the engine during the year resulted in progressive improvements in engine performance. Figure 33 shows four power curves for the GT engine, indicating the progress. The average power of all the engines used at Le Mans was 485 h.p. at 6400 rpm which easily surpassed our original objective. Except for the pre-Daytona engines, all of these runs were made with the same camshaft used in stock car competition.

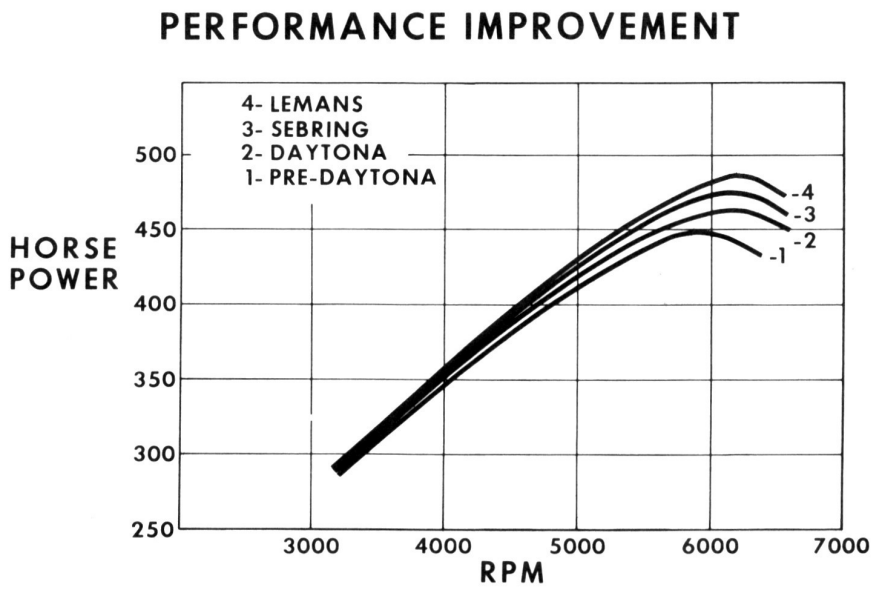

Figure 33

TRACK TESTING

Daytona International Speedway

This track was selected for testing because the maximum engine rpm obtainable on the back stretch could approach those expected on the Mulsanne Straight at Le Mans.

In order to evaluate the engine durability for a 24 hour period of continuous running, tests were conducted in August and December of 1965. The results of these tests revealed problems previously mentioned concerning the pushrod, piston skirts, valve springs, rear oil seals and valve stem seals.

Five cars were entered in the Daytona Continental with as many "fixes" as possible. The results of this race provided confirmation of soundness of these changes.

Sebring

A test was conducted in March at the track. Because of the many gear shift changes required to complete one circuit of this track, the associated high rpm would further evaluate the effectiveness of the "fixes" previously introduced in the Daytona Race.

The internal dry sump scavenge system was introduced in the Sebring Race because of its successful performance on dynamometer tests. No problems were experienced with this system during the race.

However, as previously mentioned, it was during this race that the serious shortcoming in connecting rod bolt fatigue life was revealed.

Riverside International Speedway

This track was used intermittently throughout the program primarily to "shakedown" the vehicle prior to a race or test.

Le Mans

At the practice in April, the vehicles were instrumented to record engine data. The results confirmed the accuracy of the theoretical data used to set up the Le Mans cycle on the dynamometer.

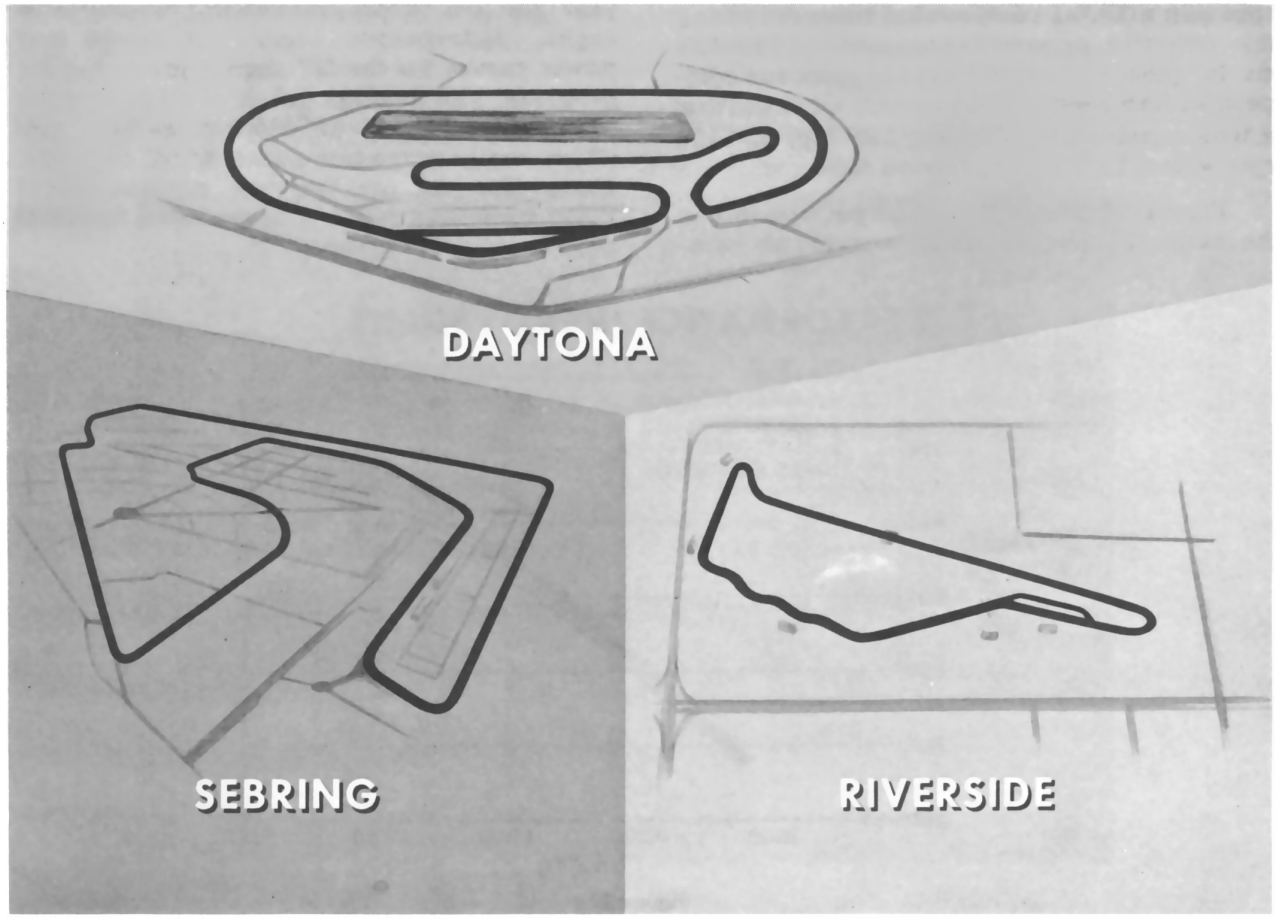

SUMMARY

The result of the 1966 Le Mans race speaks for itself in attesting to the success of the 427 cu. in. GT engine. This race is recognized to be the supreme test of durability in racing circles. To achieve our objective with an inexpensive, basically-production engine, equipped with a single four-venturi carburetor is a measure of the degree of engineering technology and manufacturing quality embodied in our production engines.

Because we were working with production designs, many of the engineering changes and design refinements necessary to achieve per-design refinements necessary to achieve performance or durability objectives can be incorporated directly into standard production engines. Accelerated schedules, common to projects of this nature, frequently lead to the development of more efficient techniques and methods, which then become a new standard for future production applications.

SPECIFICATIONS

ENGINE

Type	90° V-8 OHV
Bore	4.2346
Stroke	3.784
Displacement	427
BHP at Engine RPM	485 at 6200-6400
Torque at Engine RPM	474.5 at 3200-3600
Compression Ratio	10.5:1
Fuel System	Carburetion
Number Carburetors	One – 4V
Oil System	Dry Sump
Oil Pressure	80-84 PSI
Dry Weight (Less Air Cleaner, Clutch Assy., Exhaust Manifold)	580#
Firing Order	1-5-4-2-6-3-7-8
Ignition	Breakerless Transistorized
Maximum Spark Advance	38° at 4000
Alternator Rating	52 Amps.

PISTON AND PIN

Piston to Bore (Skirt)	.006-.007
Skirt Taper	.001
Top of Piston to Top of Block	.018
Piston Pin Material	SAE 5015 Steel
Piston Pin Clearance – (Piston)	.0007-.0009
Piston Pin Clearance – (Rod)	.0003-.0005
Piston Pin End Play	.005-.012
Piston Pin Offset	None
Piston Pin Diameter	.9751

PISTON RINGS

	TOP	SECOND	OIL CONTROL
Width	.062	.062	.125
End Gaps	.028	.028	.032
Groove Clearance	.0027	.0027	Snug in Groove

CONNECTING RODS

Material	SAE 1041 Steel
Length Center to Center	6.488
Weight	806 Grams
Clearance (Journal)	.002-.003
End Play (Two Rods)	.018-.028

CRANKSHAFT

Material	SAE 1046 Steel
Main Bearing Clearance	.002-.0031
End Play	.004-.008
Main Bearing Diameter	2.7488
Crankpin Journal Diameter	2.4384

CYLINDER BLOCK

Cylinder Bore Diameter (Range)	4.2328-4.2364
Thrust Bearing Face Runout	.001
Camshaft Bearing Clearance	.001-.003

CYLINDER HEAD

Volume CC with Valves & Spark Plug in Place	91
Valve Seat Material	High Cobalt Alloy Steel
Valve Seat Fit	.002-.004 Shrink Fit
Valve Guide Material	Aluminum Bronze SAE 68A
Valve Guide Fit	.0025-.0035 Press Fit

SCAVENGE OIL PUMP

Chain Drive	Single Strand Roller
Pitch	.375
Drive Ratio to Crankshaft	1/1

DISTRIBUTOR

Backlash	.002-.010
End Play	.004-.020
Initial Timing	8° at 700 RPM

SPECIFICATIONS – Continued

VALVE SYSTEM

	INTAKE	EXHAUST
Valves Per Cylinder	1	1
Gage Diameter	2.060	1.625
Lash (Hot)	.025-.027	.025-.027
Seat Width	.03	.055
Seat Angle	30°	45°
Stem Clearance	.001-.0024	
Camshaft Timing		
Opening at .100 Valve Lift	8°30' ATC	39°30' BBC
Closing at .100 Valve Lift	36°30' ABC	11°30' BTC
Duration	324°	
Overlap Theo.	96°	
Camshaft Drive Mechanism	Silent Chain	
Chain Pitch	.500	
Valve Lift – Zero Lash	.527	
Valve Spring Load	Valve Open	Valve Closed
Outer – Lbs with Damper	80-90	255-280
Rocker Arm Ratio	1.76:1	
Rocker Arm to R/A Shaft Clearance	.0015-.003	

UNIQUE BOLT TORQUE

Bolt and nut installation torque specifications with lubricated threads (preservative oil acceptable) except as noted by * or # or %.

	OPERATION	THD SIZE	INSTALLATION TORQUE
Bolt	– Oil Pan	5/16-18	20 Ft. Lb.
Bolt	– Rocker Arm Cover to Cylinder Head	5/16-18	10-12 Ft. Lb.
%Bolt	– Pressure Plate to Flywheel	5/16-18	15-20 Ft. Lb.
Stud	– Carburetor to Intake Manifold	5/16-18	Drive to Limit of Threads
Bolt	– Distributor Hold-Down Clamp	5/16-18	5-8 Ft. Lb.
%Nut	– Carburetor Mounting	5/16-24	120-156 In. Lb.
Cross Bolt	– Main Bearing Cap	3/8-16	38-42 Ft. Lb.
Bolt	– Intake Manifold	3/8-16	32-35 Ft. Lb.
Bolt	– Exhaust Manifold to Cylinder Head	3/8-16	12-18 Ft. Lb.
Bolt	– Flywheel to Crankshaft	7/16-20	75-85 Ft. Lb.
Bolt	– Main Bearing Cap	1/2-13	95-105 Ft. Lb.
Bolt	– Cylinder Head	1/2-13	100 Ft. Lb. (Cold)**
Plug	– Oil Pan Drain – Safety Wired	1/2-20	15-20 Ft. Lb.
Bolt	– Crank Damper to Crankshaft	5/8-18	70-90 Ft. Lb.
Oil Filter	– Oil Filter	3/4-16	95-105 Ft. Lb.
Screw	– (Attach Timing Pointer to Front Cover)	10-24	2-4 Ft. Lb.
*Spark Plug		18 MM	15-25 Ft. Lb.
#Bolt	– Connecting Rod	7/16-20	.0055-.006 Elongation
Bolt	– Cam Sprocket to Camshaft	7/16-14	40-45 Ft. Lb.

*Use Graphite on Threads
#Moly Kote on Threads and Under Bolt Head
%Dry
**No Hot Torque Required

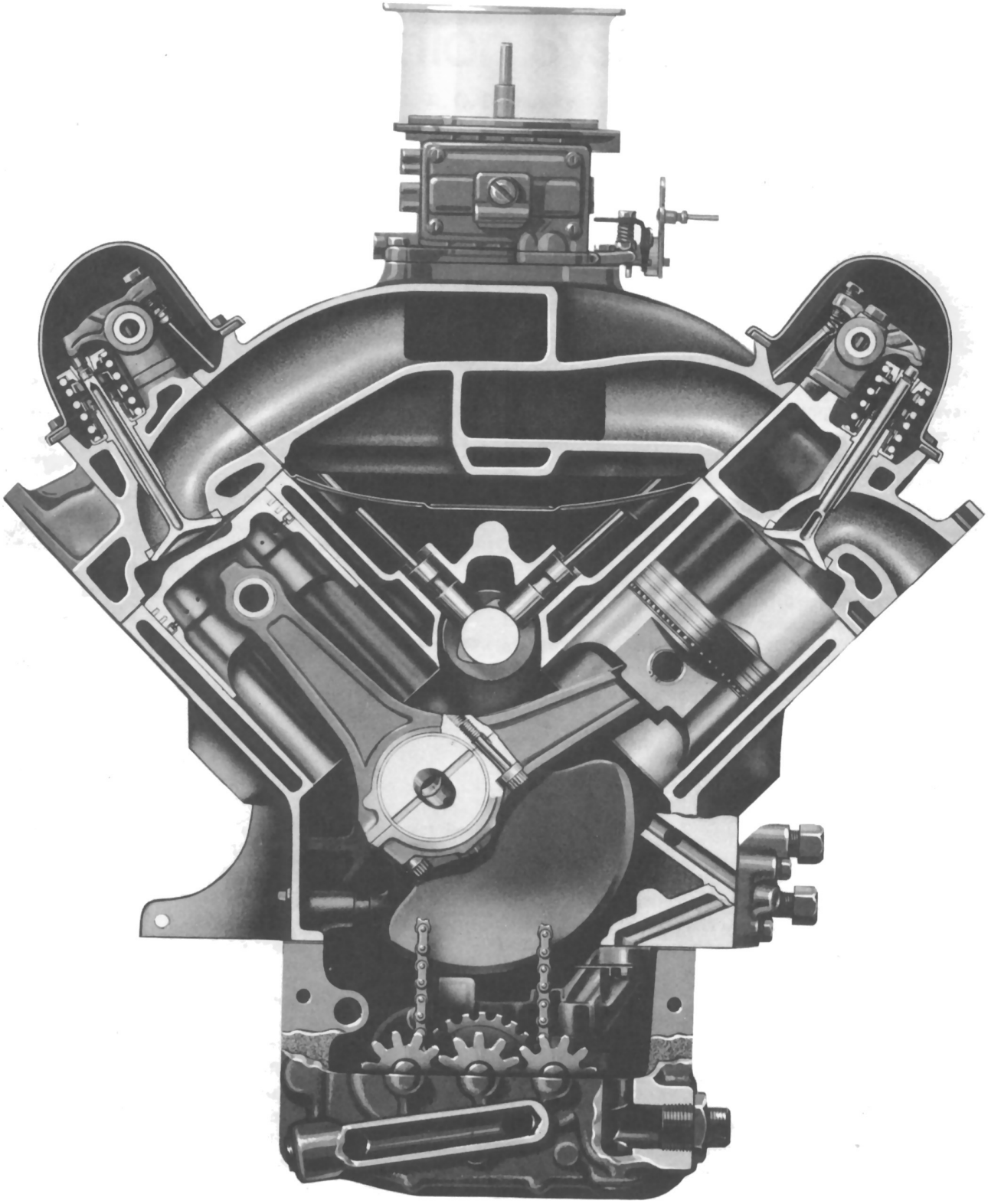

Page 46 Left Blank

Mark II–427 GT Engine Induction System

A. O. Rominsky
Engine and Foundry Div.
Ford Motor Co.

ABSTRACT

Among the factors attributable to Ford's success at Le Mans, France in 1966 is the high efficiency air induction system of the 427 GT engine. Contrary to the basic design parameters of passenger car engine induction systems, which consider part-throttle transitions and fuel economy, induction systems for high speed, high-output competitive engines are quite the opposite. These engines demand maximum airflow capacity, and equal balance of air/fuel mixture to each cylinder to insure high efficiency throughout the engine speed range under full-throttle conditions.

Recognition of this need, its resolution, and the application of resultant techniques to the Ford 427 engine since its inception in 1963, are the basis for this paper. The GT induction system is the product of a new development technique that involved the extended use of an induction flowstand, as well as extensive studies of various types of manifolds and cylinder heads. During the course of this work, successive improvements in modeling and pattern making have combined to refine the art to a high degree of sophistication.

FACTORS ATTRIBUTABLE to Ford's success at Le Mans, France in 1966 are many. The factor we would like to single out for discussion is the high efficiency air induction system of the 427 GT engine.

Contrary to the basic design parameters of passenger car engine induction systems, which consider part-throttle transitions and fuel economy, induction systems for high speed, high-output competitive engines are quite the opposite. These engines demand maximum airflow capacity, and equal balance of air/fuel mixture to each cylinder to insure high efficiency throughout the engine speed range under full-throttle conditions.

Recognition of this need, its resolution, and the application of resultant techniques to the Ford 427 engine since its inception in 1963, are the basis for this paper.

INDUCTION SYSTEM FLOWSTAND

The development of the 427 induction systems was dependent upon the use of an airflow measuring device which had been used predominately for research purposes by the automotive industry for many years. The instrument measures steady-state airflow through complete induction systems or individual components under a regulated pressure drop (Fig. 1). Air is drawn through the component being evaluated by a constant-speed, constant-flow vacuum pump. The air flows through the components, an orifice tank, and a system of control valves before exhausting to atmosphere. A manometer is used to measure pressure drops, and a calibrated inclinometer measures steady-state airflow in cubic feet per minute.

By selecting various orifice combinations, airflow can be controlled from 1 - 1140 cfm with approximately 0.1-10 in. Hg pressure drop across the component being evaluated for airflow.

For our purpose, induction system airflow evaluations are measured at a pressure drop of 5 in. Hg. This value established a baseline for comparison of all flowstand development and has no significance with regard to pressure drops in an engine.

EARLY INDUCTION SYSTEM DEVELOPMENT

Based on the premise that a downward-flow intake manifold and large intake ports were required to produce increased performance, a high-riser intake manifold and cylinder head

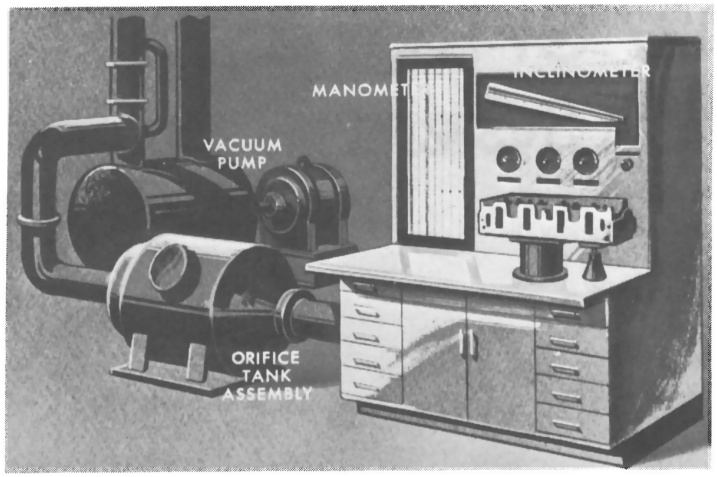

Fig. 1 - Induction system flowstand

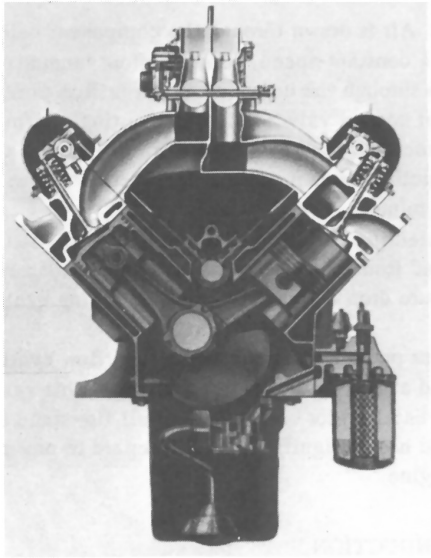

Fig. 2 - High-riser induction system, 427 engine

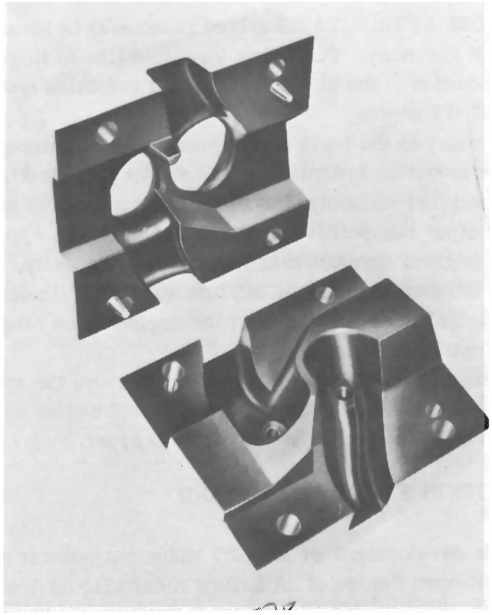

Fig. 3 - Plastic cylinder head flowbox

design was introduced with the 427 engine in 1963 (Fig. 2). At that time, special consideration was given to breaking away from the traditional method of designing cylinder heads and intake manifolds. Normally, drafting layouts were made which stressed constant or gradually changing areas throughout the intake manifold runners, and smooth diverging cross-sectional areas from the intake port entrance to the port throat. Manifold design variations, generated by this method, would not guarantee a significant performance improvement after new manifold castings were made, machined, and tested on an engine.

In analyzing this problem, it was thought that the ports and runners of the intake manifold and the cylinder head could possibly be utilized as development tools to achieve maximum induction system airflow and efficiency in a more reliable and less time-consuming fashion. To implement the approach, the induction system flowstand was brought into use as a development tool.

CYLINDER HEAD - To study the airflow characteristics in the intake and exhaust ports of the high-riser cylinder head, a plastic cylinder head flowbox was constructed which contained an intake port, exhaust port, and a combustion chamber built from drafting outlines (Fig. 3). This flowbox was made in two pieces and split along the normal parting lines to enable making internal revisions with clay or by grinding. The flowbox was mounted to the induction system test stand on a flanged cylindrical tube of the same ID as the actual cylinder bore (Fig. 4). Clay was used at the air entrance to the flowbox to provide a smooth, nonturbulent airflow into the system.

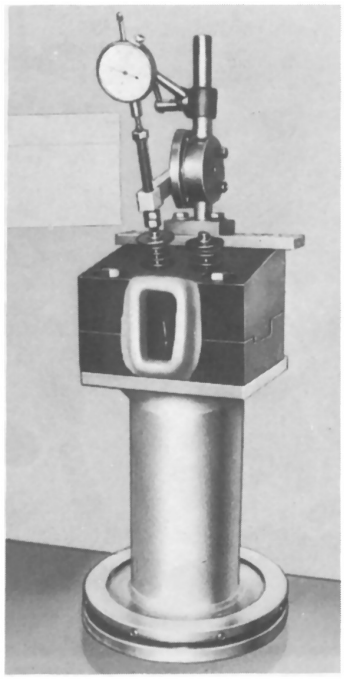

Fig. 4 - Cylinder head flowbox mounted on flowstand, intake port

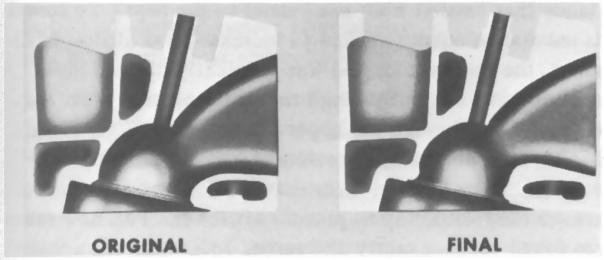

Fig. 5 - Cylinder head intake port modifications

A dial indicator and adjusting screw were installed above the intake valve to accurately control the valve at various opening positions. This enabled plotting the airflow curve throughout the valve opening and closing cycle for any camshaft.

Clay modifications to the intake port floor and throat effected an airflow improvement (Fig. 5). The port floor was raised, or humped, in the path of the airstream where the air turns from the port into the throat. This redirected the air to the roof of the port near the throat and resulted in an appreciable increase in airflow.

The throat and seat of the intake port were found to be critical at high air velocities. Various valve seat angles and throat diameters built into the port throat area resulted in minor airflow improvements. The addition of a venturi-type ring adjacent to the valve seat increased the airflow substantially.

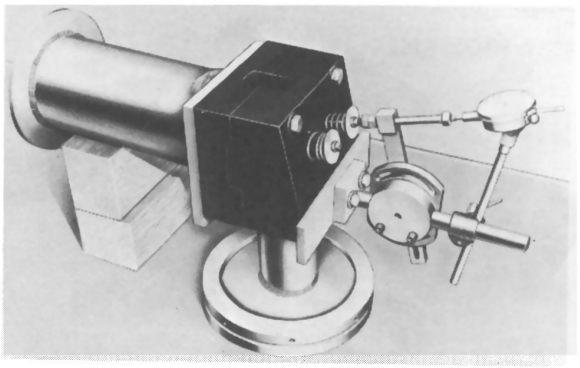

Fig. 6 - Cylinder head flowbox mounted on flowstand, exhaust port

Fig. 7 - Rubber core of high-riser cylinder head contours

The exhaust port was investigated in a similar manner. The cylinder head flowbox was remounted on the flowstand (Fig. 6) with the exhaust port held against a tube mounted on the inlet of the flowstand. The cylindrical bore tube remained mounted on the flowbox to direct the air through the combustion chamber and out the exhaust port, similar to the piston moving upward on the exhaust stroke in a running engine. The exhaust port floor was modified in conjunction with minor revisions to the port roof. Modification to the combustion chamber afforded little improvement in airflow; therefore, it was left unchanged.

Having completed development of the entire flowbox, a rubber compound was poured into the cylinder head flowbox and allowed to harden. This hardened core was used for dimensioning the port contour. A layout was made to determine the external shape of the cylinder head (Fig. 7). When these new cylinder heads were cast, machined, and checked, airflow capacity was slightly less than the flowbox model. This loss was due to the drafting limitations in transferring the rubber core contours to the layouts.

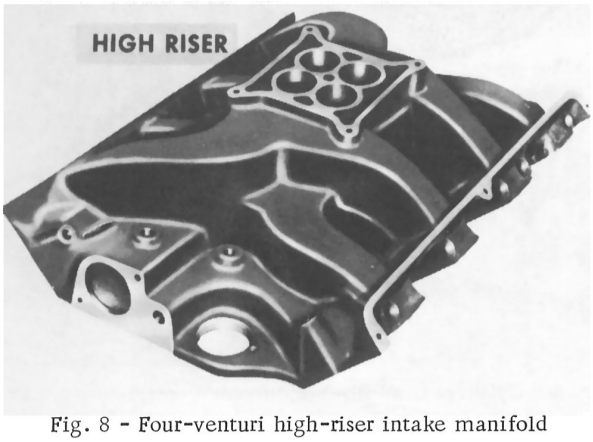

Fig. 8 - Four-venturi high-riser intake manifold

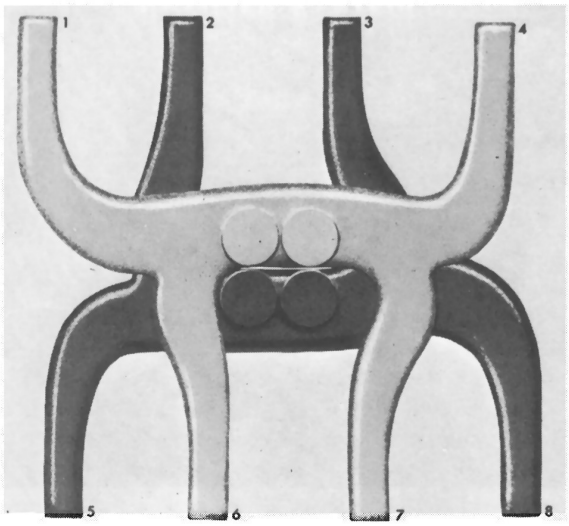

Fig. 9 - Four-venturi high-riser intake manifold runner system

INTAKE MANIFOLD - Our attention was then turned from the cylinder head to the intake manifold. It was required that the manifold be a four-venturi over-and-under design which is used extensively on passenger car engines (Fig. 8). It consists of two dependent sets of intake manifold runners which are connected to their respective plenum chambers (Fig. 9). One set of runners is at intake port level, and the other slightly above this level. This arrangement is necessary, since each set of runners feeds cylinders on both banks of the engine and must therefore cross each other.

This four-venturi manifold design separates the successive firing pulses by alternating the engine firing order from one runner system to the other. Therefore, each cylinder draws from separate runner systems of the manifold.

The cylinder head flowbox was placed on the flowstand in the intake port flow position, and the manifold was attached. Each runner of the intake manifold was checked separately to measure the cubic feet per minute of airflow at various intake valve openings ranging from 0.050 - 0.500 in. (Fig. 10). The test results indicated the degree of unbalance that existed from one runner to the next. To correct this unbalance condition, and to increase total airflow in all runners, the intake manifold was physically divided into three sections; one cut through the lower plenum area, and the second cut through the upper plenum area (Figs. 11 and 12). To determine if the sectioning had any effect on airflow, the intake manifold was reassembled and all seams were covered with clay to prevent air leaks. The flow values were found to be exactly the same, indicating that the amount of area lost by cutting had no effect on overall airflow.

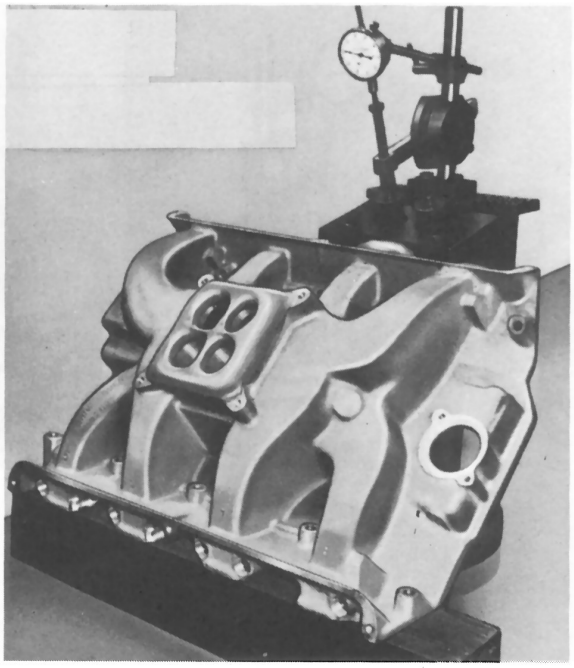

Fig. 10 - High-riser cylinder head and intake manifold mounted on flowstand

It was now possible to open the manifold and to make various contour changes in the manifold runners by adding clay to the passages or by grinding away metal. It was found that the airflow of each runner could be increased and that the runners could be balanced to flow equal amounts of air.

Wood pattern equipment was then made to simulate the cavities in the developed manifold. From these patterns, changes were made in the casting equipment, new castings were produced and machined, and rechecked on the airflow stand.

As was the case with the cylinder head castings, flowstand results indicated a slight loss of airflow as compared to the sectioned manifold (Fig. 13). This was attributed to the fact that an absolute duplication of the clayed or ground contours in the sectioned manifold was difficult to transfer to wood patterns. However, airflow of this modified induction system, as compared to the original cylinder head and manifold, showed a marked increase.

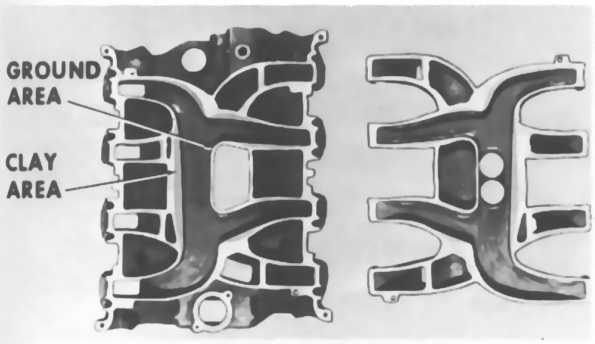

Fig. 11 - High-riser intake manifold sectioned through lower plenum

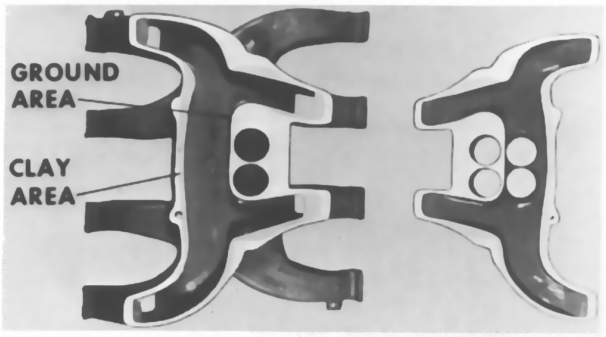

Fig. 12 - High-riser intake manifold sectioned through upper plenum

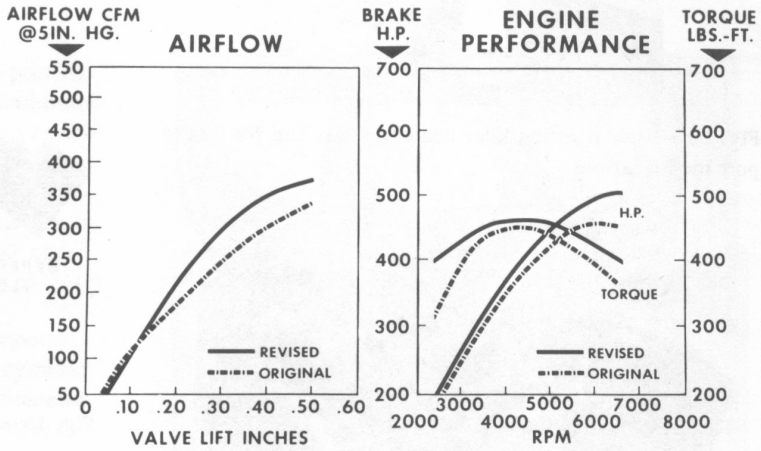

Fig. 13 - Induction system comparisons, high-riser intake manifold and cylinder head

Later airflow studies confirmed that some contours in a manifold runner can be so critical that the addition, movement, or removal of 0.010 in. clay thickness in an area can change the airflow by 5%.

The revised cylinder head, coupled with the new intake manifold, was installed on a dynamometer engine to measure the actual variation in performance attributed to the design changes. The results indicated an increase in horsepower.

MEDIUM RISER INDUCTION SYSTEM DEVELOPMENT

Further development of the intake port and manifold design clearly indicated that the high-riser concept alone was not essential to increased performance (Fig. 14). Induction airflow studies verified that reducing the cylinder head intake port closure, and lowering the intake manifold carburetor mounting pad to facilitate engine packaging and manufacturing did not affect engine output. This engine-induction system combination became known as the medium-riser engine.

CYLINDER HEAD - Using the cast iron high-riser cylinder head as a flowbox, the intake port roof line was reshaped by adding clay, and the port opening was reduced 1/2 in. with-

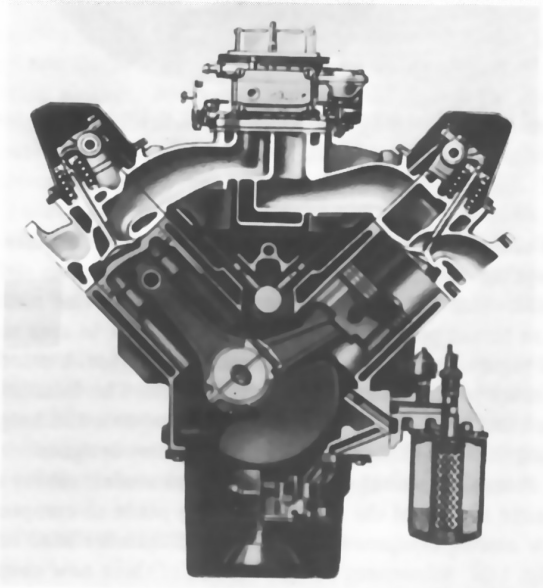

Fig. 14 - Medium-riser induction system, 427 engine

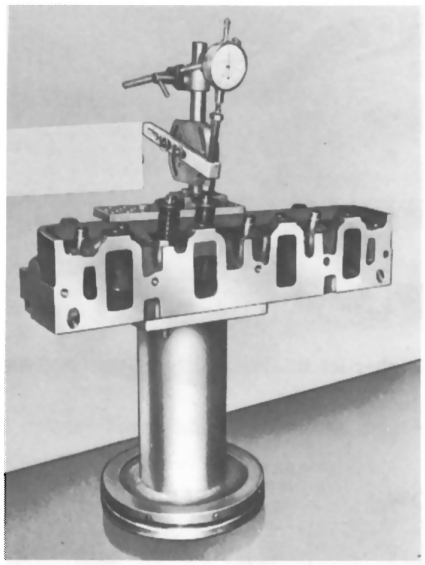

Fig. 15 - High-riser cylinder head on flowstand for intake port modifications

Fig. 16 - Rubber core of medium-riser cylinder head contours

out sacrifice of airflow (Fig. 15). All attempts to raise or lower the floor line at the port entrance resulted in airflow losses. This 1/2 in. reduction in the port roof line resulted in an intake port entrance which was smaller in area than the regular passenger car version of this engine, but it flowed as much air as the high-riser intake port. The exhaust port remained unchanged, since it was not increased in height when the high-riser cylinder head was first designed.

From the redeveloped cylinder head model, rubber and plastic models of the intake port were made to complete new casting equipment for the revised cylinder head castings (Fig. 16). Subsequent airflow checks of these new castings revealed the exact flow curve exhibited by the high-riser cylinder head.

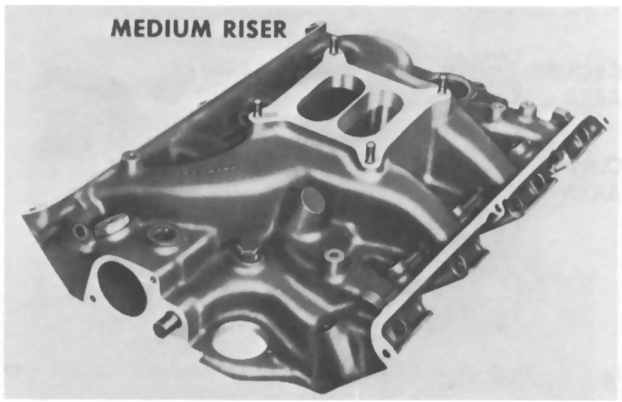

Fig. 17 - Four-venturi medium-riser intake manifold

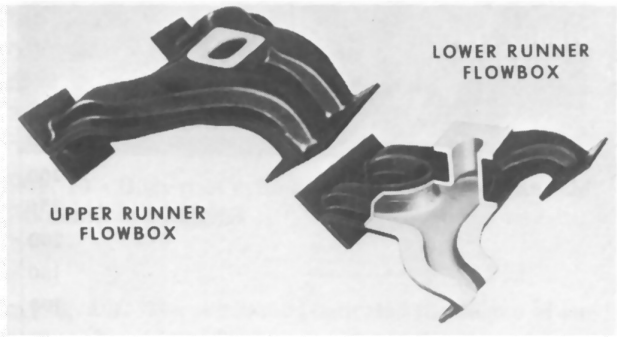

Fig. 18 - Fiberglass flowboxes of manifold runner system

FOUR-VENTURI MEDIUM-RISER MANIFOLD - The program to design and develop a new, lower four-venturi intake manifold to mate with the medium-riser cylinder head provided the opportunity to advance the technique. A design layout was first generated which defined the cylinder head port locations, the new carburetor pad location, the existing pushrod locations, and the manifold runners (Fig. 17). It was required that the runners be similar in design but lower in silhouette than those developed for the high-riser manifold.

Wood runner coresticks were made, and two fiberglass flowboxes were made from the wood coresticks, one flowbox for the upper manifold runner, and the other for the lower runner system (Fig. 18). These fiberglass flowboxes were then ground and clayed in the same manner as the sectioned casting of the high-riser manifold to obtain maximum airflow and balance between all cylinders. Once airflow comparable to the high-riser manifold was obtained, a plastic epoxy resin was poured into the flowboxes and, upon hardening, the plastic coresticks were removed (Fig. 19). To compensate for casting shrinkage, the plastic coresticks were sectioned at constant cross-sectional areas so as not to affect the final airflow capacity. Actual casting corebox equipment could now be made directly from the plastic coresticks, assuring exact duplication in the manifold casting.

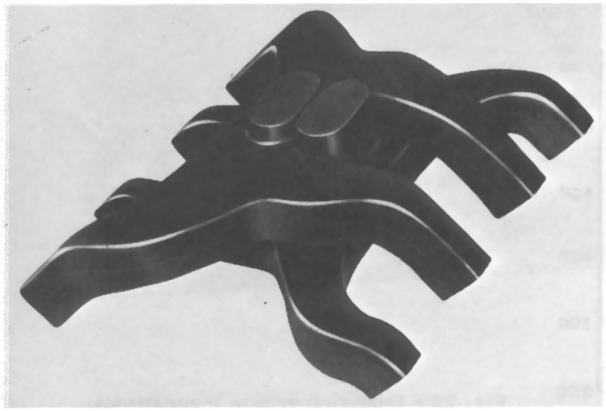

Fig. 19 - Plastic coresticks of upper and lower manifold runner system

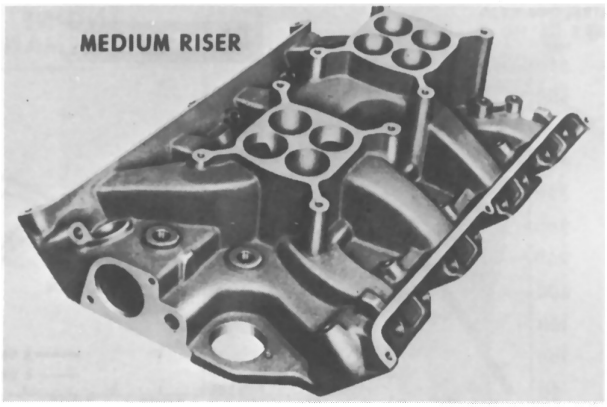

Fig. 20 - Dual four-venturi medium-riser intake manifold

To complete the design, a layout was made to provide normal metal thickness around the coresticks, to determine attaching locations of external components, and to provide machining dimensions. The finished intake manifold was rechecked on the flowstand. Airflow was almost identical to the original fiberglass flowboxes. The runner coreboxes were made directly from the plastic coresticks, and near-perfect duplication of the runner shape and airflow capacity was realized.

The success of this advancement in port and runner development technique was proved when the new cylinder head and intake manifold were installed on a dynamometer engine which had been "baselined" with the high-riser induction system. The new medium-riser engine power curve was within 1 hp of the high-riser system, which was well within limits of our objective.

EIGHT-VENTURI MEDIUM-RISER MANIFOLD - Following the same procedures used to develop the four-venturi manifold, a new dual four-venturi intake manifold was developed (Fig. 20). The manifold runners were essentially the same as the four-venturi intake manifold and were divided into an upper and lower system to even out firing pulses.

The four riser bores for the front carburetor were located as far forward on the manifold as possible without interfering with the distributor. In order to position these bores as close to the center of the front four runners as possible, the carburetors were rotated 180 deg, positioning the secondary venturies forward and the primaries to the rear of the manifold. The rear four riser bores were also located as far forward as possible to orient them near the center of the rear four manifold runners, thus allowing minimum clearance between carburetors.

This riser bore and manifold runner configuration shortened the runner lengths considerably and provided an almost straight-line airflow path (Fig. 21). One primary and one secondary carburetor venturi were now located diagonally opposite each other, feeding one cylinder on each bank. Cylinders 1 and 6, 2 and 5, 3 and 8, and 4 and 7 each used a different pair of carburetor venturies.

This type of straight-flow design also minimized fuel

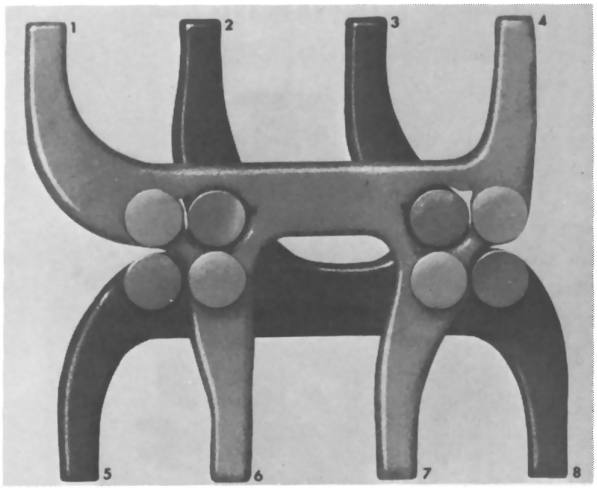

Fig. 21 - Dual four-venturi medium-riser intake manifold runner system, SOHC engine

distribution problems. The fuel distribution was further improved and the airflow increased by the incorporation of balancing passages and a plenum located between the front and rear carburetor riser bores. This permitted each runner to receive an additional boost of air/fuel mixture from the carburetor located on the opposite end of the manifold. Vertical vanes were oriented around the riser bore pillars to aid in directing the mixture from the riser bore through the plenum and to the runners. These vanes were also necessary to obtain balance between runners with maximum possible flow.

The resulting airflow figures of the new dual four-venturi intake manifold and cylinder head combination indicated a substantial increase in breathing capacity as compared with the single four-venturi manifold (Fig. 22). Corresponding improvements were experienced in performance.

GT INDUCTION SYSTEM

The medium-riser induction system was adapted to the Ford GT engine. The four-venturi intake manifold design

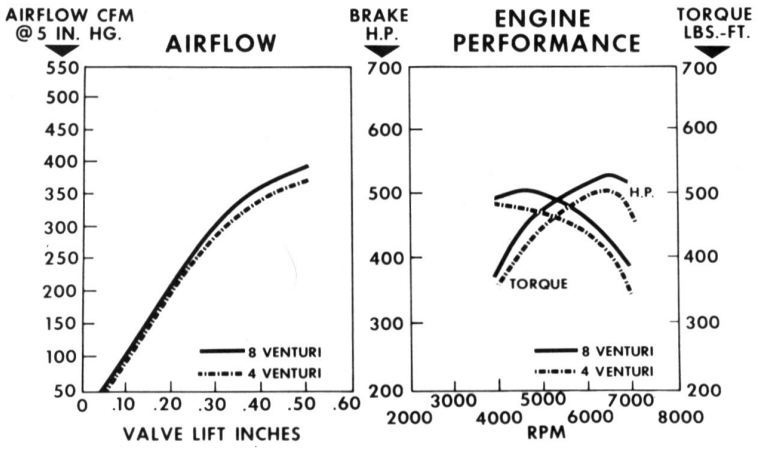

Fig. 22 - Induction system comparisons, medium-riser cylinder and intake manifold

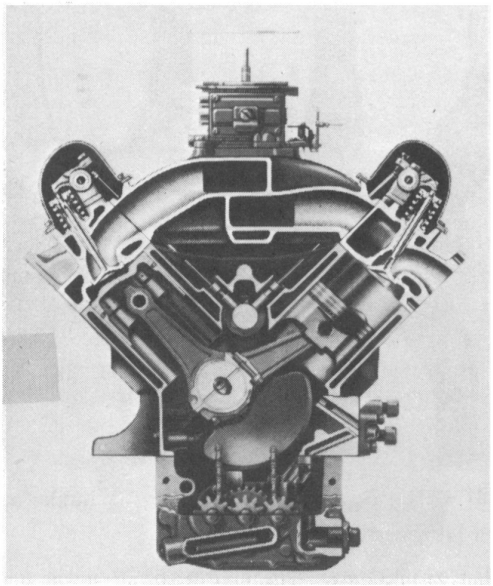

Fig. 23 - Medium-riser induction system, 427 GT engine

was adopted in its entirety, but the cylinder head design was slightly modified to enable the heads to be cast in aluminum rather than cast iron for reasons of weight reduction (Fig. 23).

In conjunction with the material change, valve seat inserts and valve guides were incorporated in the cylinder head. To provide clearance between intake and exhaust seat inserts and retain a common valve centerline, the valve head diameters were reduced from 2.19 to 2.09 in. for the intake valve, and from 1.72 to 1.65 in. for the exhaust valve. The intake valve seat inserts maintained the same venturi configuration as the iron cylinder head, even though the throat diameter was reduced by 0.100 in.

Airflow checks of the intake and exhaust ports of the aluminum cylinder head showed a slight reduction in airflow, which was also reflected as a slight loss in performance on the dynamometer (Fig. 24).

SOHC INDUCTION SYSTEM

Continuing demands for performance improvements led to another engine project -- the development of the 427

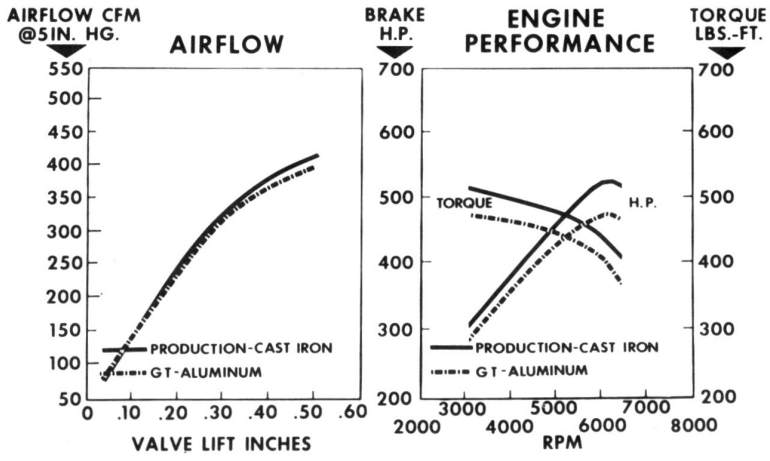

Fig. 24 - Induction system comparisons, GT cylinder head

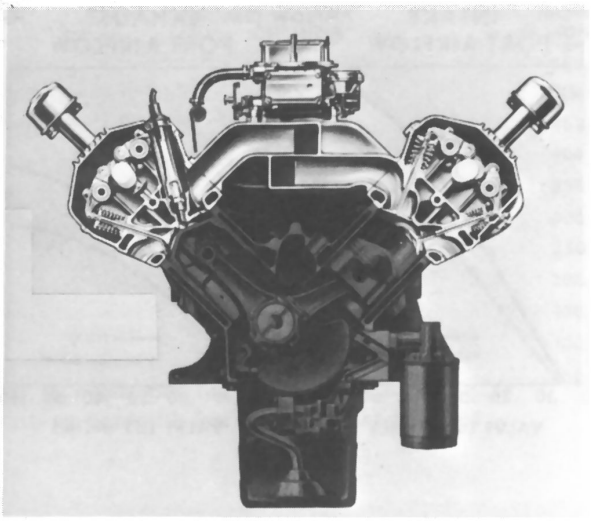

Fig. 25 - Induction system, 427 SOHC engine

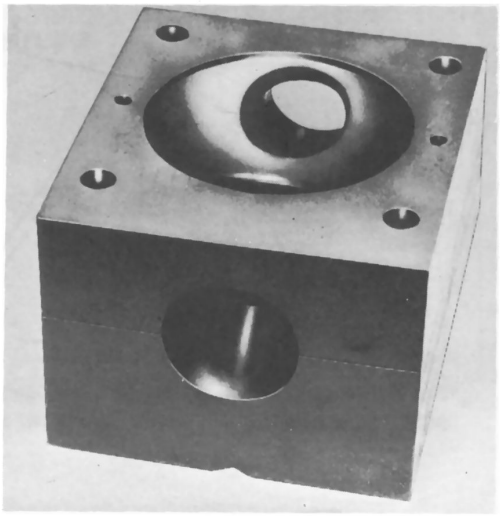

Fig. 27 - SOHC cylinder head flowbox

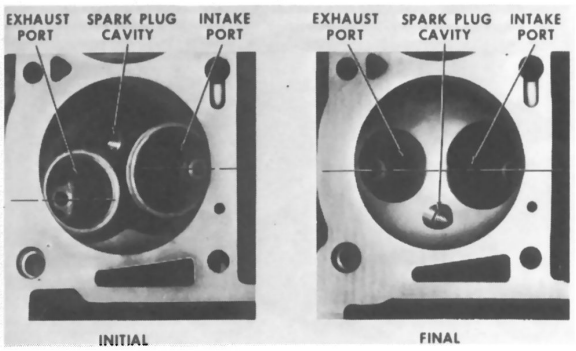

Fig. 26 - Combustion chamber designs, SOHC cylinder head

SOHC engine (Fig. 25). This engine was a natural evolutionary step from the proven concepts of the 256 DOHC engine and the 427 pushrod engine. To accommodate the new 427 SOHC engine, another induction system was developed.

CYLINDER HEAD - The initial cylinder head design used large intake and exhaust valves (Fig. 26). The exhaust valve was recessed and offset to one side of the combustion chamber to aid in more centrally locating the spark plug to provide equidistant flame travel. The intake valve was located on the combustion chamber centerline to provide the least valve shrouding possible for optimum breathing. The cast combustion chamber, which was a combination polyspherical-kidney shape, had to be qualified by machining for clearance between the piston and the chamber roof.

Airflow studies were conducted to establish baseline airflow data of this cylinder head design and to determine whether improvements could be realized through further contour development. Revisions in the combustion chamber were directed at modifying the exhaust valve cavity recess.

More gradual slopes improved airflow slightly. By gradually filling in the cavity and raising the exhaust valve toward a spherical roof line, a considerable increase in airflow was gained. Further chamber development evolved a fully machined hemispherical combustion chamber design. In this chamber design, the exhaust valve was now seated on the chamber roof but relocated directly on a transverse centerline opposite the intake valve in the chamber. This necessitated relocating the spark plug cavity to a location further from the geometric center of the chamber. It was felt that the increased airflow more than offset the less desirable spark plug location. Another advantage to the completely machined chamber was that the compression ratio could be closely governed.

Once the new combustion chamber was established, a plastic cylinder head flowbox was made to incorporate the new chamber exhaust port design along with the original intake port (Fig. 27). The intake port and exhaust port both had round cross sections from the port entrance to the valve seat for more efficient flow. Rectangular cross sections are used in pushrod engine port designs because of space limitations imposed by the pushrod location and valve positioning in the combustion chamber.

Modifications to intake port floor and roof resulted in airflow improvements (Fig. 28). A hump on the port floor above the port throat area redirected the air toward the roof of the port which utilized more of the effective throat curtain area and improved airflow efficiency. The roof of the intake port was moved outward by grinding directly above the throat area. The 30 deg intake valve seat was replaced by a radius to eliminate the sharp edges of an angular valve seat. Turbulence was thereby reduced in this area. Valve sealing was also improved by providing a positive-line contact on the valve seat.

Development of the exhaust port was accomplished in the same manner as development of the intake port. Exhaust port airflow responded to both a hump on the floor and a modified roof contour. The final design of the exhaust

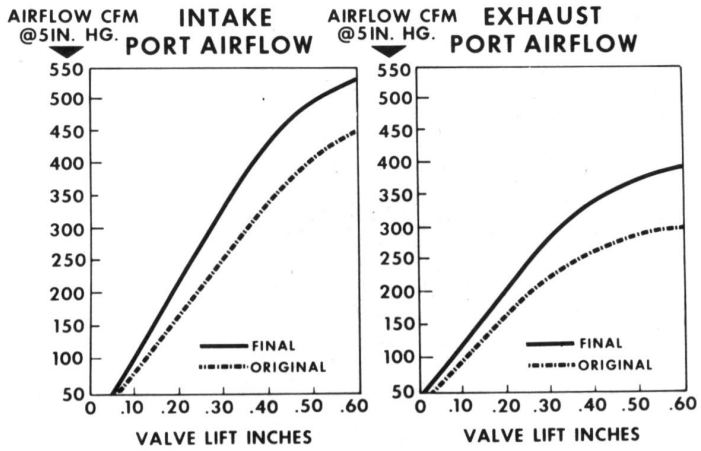

Fig. 29 - Induction system comparisons, 427 SOHC cylinder head

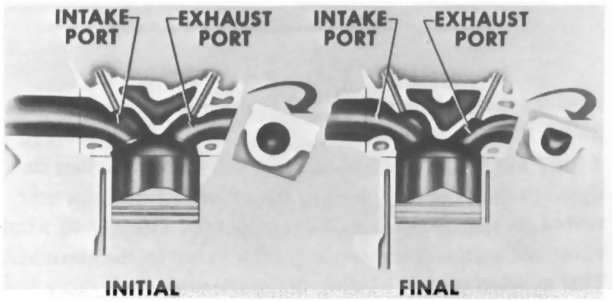

Fig. 28 - Port contour development, 427 SOHC cylinder head

port exit showed an airflow preference for a flat roof and rounded floor; whereas, maximum airflow is normally obtained using round cross sections. This design accommodates the radical change in direction from the top of the combustion chamber to the exhaust system. The rounded section at the bottom of the port exit was essential for good airflow when the valve was slightly off the seat and during the lower valve lift portion of the opening cycle. The flattened roof was necessary for maximum flow when the valve approached the wide-open position. The resulting design of the exhaust port exit of the cylinder head was a horizontal "D" shape.

The exhaust valve seat was changed from 45 to 30 deg, and the seat was modified from a 45 deg chamfer to a seat with a radius and throat similar to the intake side of the cylinder head.

The resulting airflow differential between the original cylinder head design and the airflow-developed final cylinder head is shown in Fig. 29.

FOUR-VENTURI INTAKE MANIFOLD - The four-venturi intake manifold runner and plenum designs followed those of the pushrod engine. The initial intake manifold design was accomplished without the benefit of airflow studies. Later manifold development, using fiberglass flowboxes patterned after the original manifold design, balanced the airflow of all the runners and increased the total airflow capability of the manifold. The manifold runners were rectangular

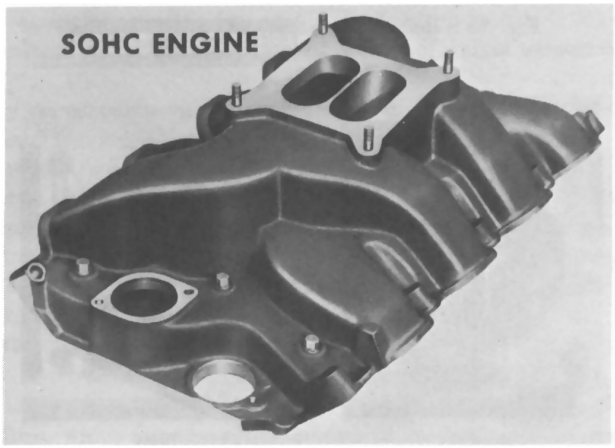

Fig. 30 - Four-venturi intake manifold, SOHC engine

in shape throughout most of the distance from the plenum to the cylinder head mounting face. At the mounting face, the cross section became circular to conform to the intake port shape. The four-venturi manifold design presently used on the single overhead cam engine utilizes circular sections throughout (Fig. 30).

Due to the high air velocities experienced in this four-venturi manifold design, fuel separation was found to be a problem. The four manifold outboard runners had a fairly direct path to the cylinders, while the other four runners had abrupt angles of more than 90 deg (Fig. 31). Airflow of all eight manifold runners had previously been balanced by contour development, but the engine experienced lean mixtures in the four cylinders fed by the inboard runners. As the air and fuel mixture descends from the carburetor through the riser bores and turns into the plenum, the velocities increase to the point where inertia drives the fuel particles to the ends of the manifold rather than to the inboard cylinders.

An airflow check, using the new cylinder head and four-venturi intake manifold combination showed an increase in

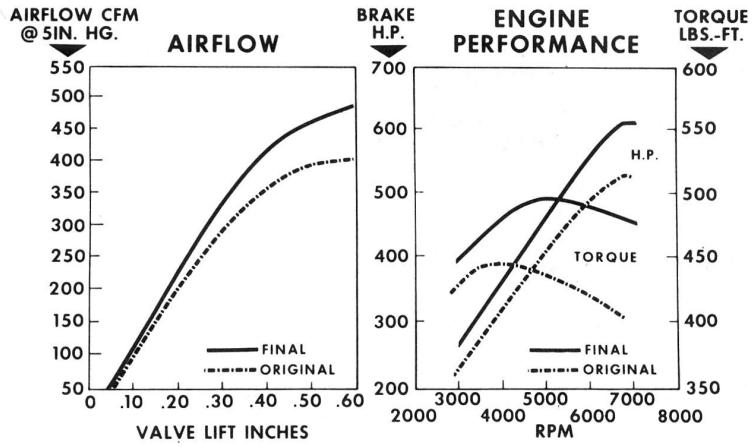

Fig. 32 - Induction system comparisons, SOHC cylinder head with four-venturi intake manifold

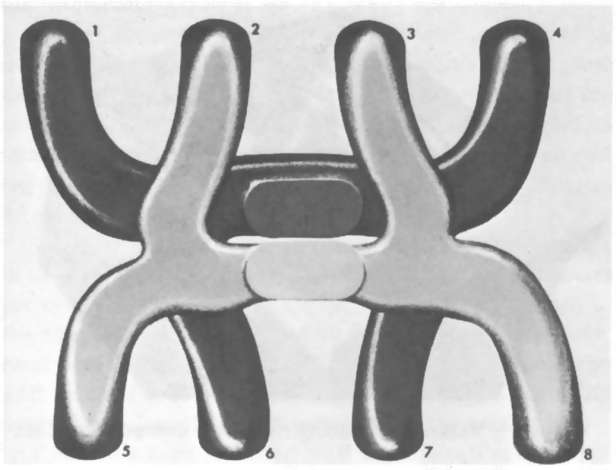

Fig. 31 - Four-venturi intake manifold runner system, SOHC engine

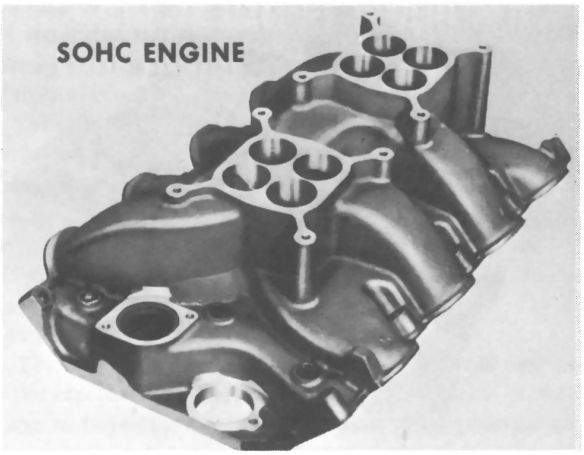

Fig. 33 - Dual four-venturi intake manifold, SOHC engine

airflow of 20% as compared with the original components. Dynamometer power curves also showed an increase of 20% in peak horsepower (Fig. 32).

EIGHT-VENTURI INTAKE MANIFOLD - A dual, four-venturi intake manifold was designed upon completion of the single four-venturi intake manifold development program (Fig. 33). The runner, plenum, balance passage and riser bore configuration were almost identical to the manifold designed for the pushrod engine. The intake runner cross section changed from rectangular to round near the runner exit to conform with the cylinder head port entrance design. All of the internal passages were also somewhat larger in cross section, primarily because of the increased flow requirement of the single overhead cam cylinder head port.

The airflow capacity curve for the dual four-venturi manifold showed gradual improvement, as compared with the single four-venturi manifold throughout the entire valve-opening cycle (Fig. 34). This indicated the potential performance advantage of the eight-venturi over the four-venturi engine package.

Induction system comparisons of the four-venturi versus eight-venturi intake manifolds conducted on a dynamometer engine showed an improvement in performance throughout the speed range of this multiple carburetion system. It is evident that an increase in airflow is inherent in this type of manifold design.

PRESENT INDUCTION SYSTEM DEVELOPMENT TECHNIQUES

The development technique for induction systems has evolved to the state currently being practiced. This technique has been simplified to the point where both design time and labor have been reduced appreciably, but most important was that the duplication accuracy has been improved significantly.

CYLINDER HEAD DEVELOPMENT - The next evolutionary step in the development of the cylinder head was concentrated mainly on the design of the intake port valve seat and throat. The objective was to improve design compatibility with manufacturing for the venturi throat, while main-

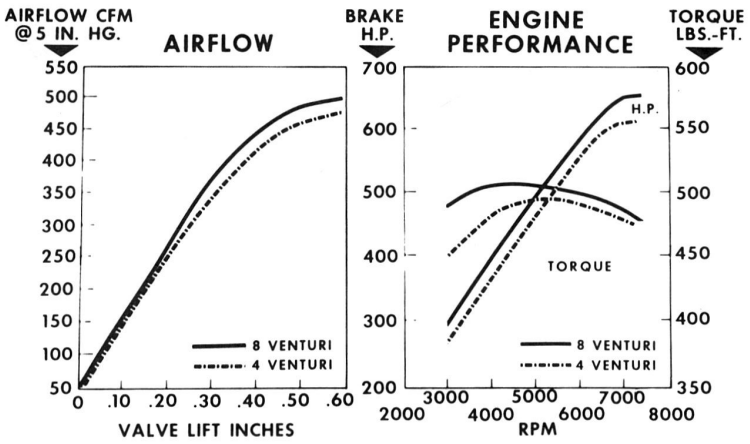

Fig. 34 - Induction system comparisons, SOHC engine

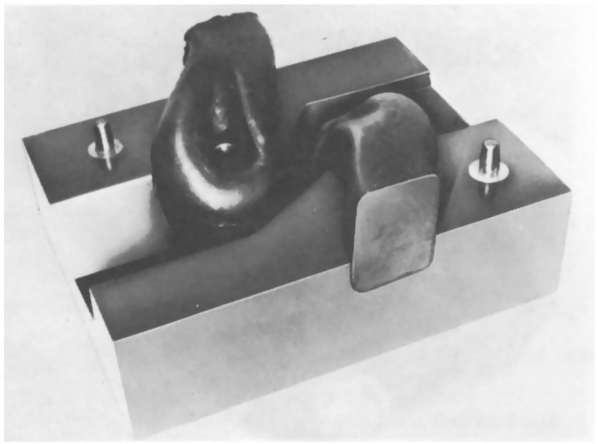

Fig. 35 - Cylinder head flowbox with rubber cores of intake and exhaust ports

Fig. 36 - Valve seat cutting tool with contour template

taining a high degree of airflow inherent in the present port design.

To facilitate cylinder head development, a rubber impression was made of the intake port, exhaust port and combustion chamber (Fig. 35). A plaster flowbox was made from this rubber impression which closely simulated the cast iron cylinder head. This plaster flowbox was easier to handle when removing material to make design changes.

Chamfers machined on the valve seats produced edges which had undesirable effects on airflow. As a result, a rounded-type of valve seat was considered. To make relatively accurate valve seat variations that would represent machined valve seats, a valve seat cutting tool was devised which used the valve guide as a pilot (Fig. 36). The opposite end of the tool contains a slot to hold the various valve seat contour templates and a large washer and nut to lock the templates in place. Rotating these templates in the plaster flowbox generated various valve seat shapes and contours. After each cut and flow test, the valve seat area was rebuilt with clay to its original state for additional evaluations. Determining a final valve seat radius presented a problem, since each radius seemed to complement only one valve position.

Before the final seat contour could be established, a throat diameter also had to be determined. Having arrived at the most desirable throat diameter, the final valve seat became a developed curve which favored the low valve lift positions near the combustion chamber end of the seat. The curve progressively rolled down to the throat area which added to airflow at the higher valve lift positions.

With the final seat contour and throat diameter established, the valve seat cutting tool was mounted on a comparator to multiply the image 20 times its size. This enabled the contour to be accurately scaled and the dimensions to be established for designing production cutting tools.

Airflow through the intake port of both the high-riser and medium-riser cylinder heads responded well through the valve-opening cycle from the time the valve left its seat to a 0.500 in. valve position. Airflow at an increased valve-opening position, such as 0.550 or 0.600 in. afforded no appreciable improvement in airflow. This discouraged

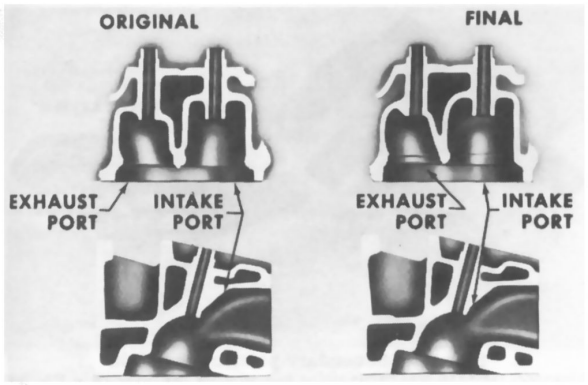

Fig. 37 - Cylinder head modifications

use of high lift camshafts to gain additional performance improvements.

Further development to improve port airflow resulted in moving the port side wall nearest to the combustion chamber center outward approximately 0.100 in. (Fig. 37). This increased the cross-sectional area at this point and caused the intake port to be receptive to increased valve lifts exceeding 0.600 in. which was beyond the valve lift contemplated for use on this engine.

The shifted side wall of the intake port created a problem in casting the water passage between the intake and exhaust ports. To enable adequate cooling between these ports, the exhaust port was modified by applying clay on the exhaust port side wall nearest the intake port to represent the shift required to reestablish the coolant passage. Since this resulted in a loss of exhaust port airflow, the port wall, roof and floor were modified until a combination was found that recovered the lost airflow.

The plaster flowbox was then used to make rubber impressions for engineering layouts. The rubber impression allows the port core to be easily sectioned in any area or plane for an actual view of that area. Laying the sectioned piece of rubber on a copying machine provides an immediate reproduction of the section being interpreted.

Simulating the rubber impression technique, a plastic core model is made in the plaster flowbox. This plastic core model is used as an aid in making the coreboxes for the cylinder head castings.

The correlation of cylinder heads cast, using this technique, closely duplicates the airflow capacity of the original plaster flowboxes.

INTAKE MANIFOLD DEVELOPMENT - The intake manifold design and development technique was also made more sophisticated and accurate. The initial steps for intake manifold development now consists of defining the locations of the cylinder head port, the carburetor pad, and the pushrod, in sketch form, since these elements run through the intake manifold. The sketch also roughly defines the flow path centerlines of the proposed manifold runners.

The next step is the fabrication of a cradle, which consists of two metal plates fastened together to form a 90 deg

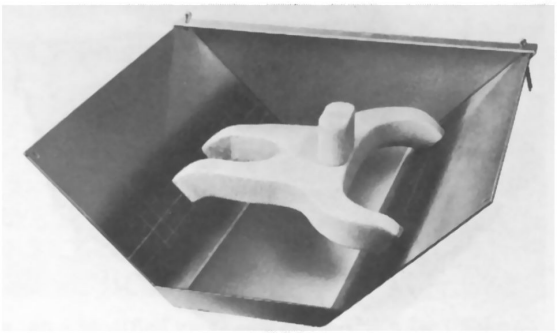

Fig. 38 - Styrofoam corestick model in cradle

wedge to simulate the cylinder head on the engine. Each plate has scribed layout lines which represent the cylinder head intake port openings. A third plate is then added across the top of the side plates at the height established for the carburetor mounting pad. This top plate has machined holes or slots which represent the riser bores.

Using the cradle and the locating sketches, a styrofoam model of the upper and lower manifold runner and plenum corestick is made (Fig. 38). The model is carefully formed to extend from the scribed cylinder head port openings on the cradle side plates, through the plenum, and to the top of the riser bores at the carburetor mounting pad in the top plate. Consideration is also given to provide adequate wall clearance between coresticks for casting.

The styrofoam corestick of the lower runner is then placed in the cradle. Screw holes are drilled through the side cradle plates to fasten the corestick in place. An approximate parting line is then established on the corestick, and metal shims are inserted in the styrofoam corestick at this point. Metal end-plates are then installed in the cradle and clay is applied to seal all joints. Next, a plaster mixture is poured into the cradle to the level of the shim stock parting line. Once the plaster hardens, the shim stock is removed from the styrofoam, and a parting agent is applied to all the exposed plaster surfaces (Fig. 39). Another plaster mixture is then poured into the cradle to the top of the riser bores and carburetor pad. When this has hardened, the plaster sections are opened and the styrofoam runner model is removed. The two plaster casts now form an intake manifold flowbox of the proposed lower runner section (Fig. 40). This sequence is repeated using the upper styrofoam runner core model. Both flowboxes are now ready for preliminary flowstand evaluation.

With one of the flowboxes attached to a cylinder head on the airflow test stand, individual runners are checked to determine airflow range and degree of unbalanced airflow.

The intake manifold runners are developed while mounted on a cylinder head to insure proper direction of airflow. The ultimate result is a complementary induction system (Fig. 41). Manifolds can be airflowed and developed independently. An appreciable drop in airflow, however,

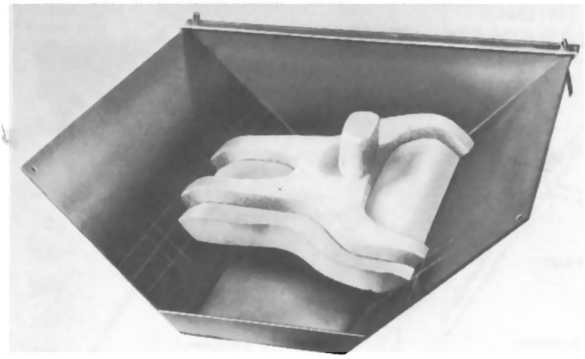

Fig. 39 - Lower plaster flowbox poured in cradle

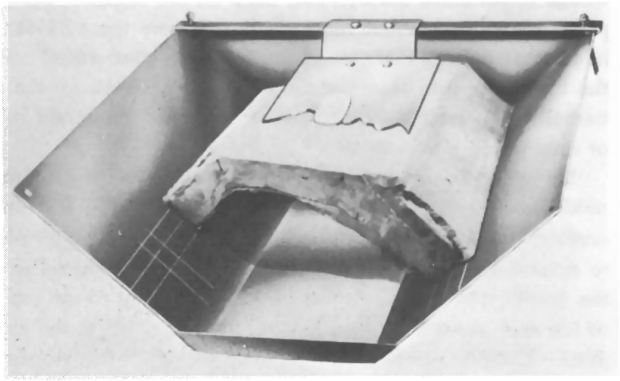

Fig. 40 - Upper plaster flowbox poured in cradle

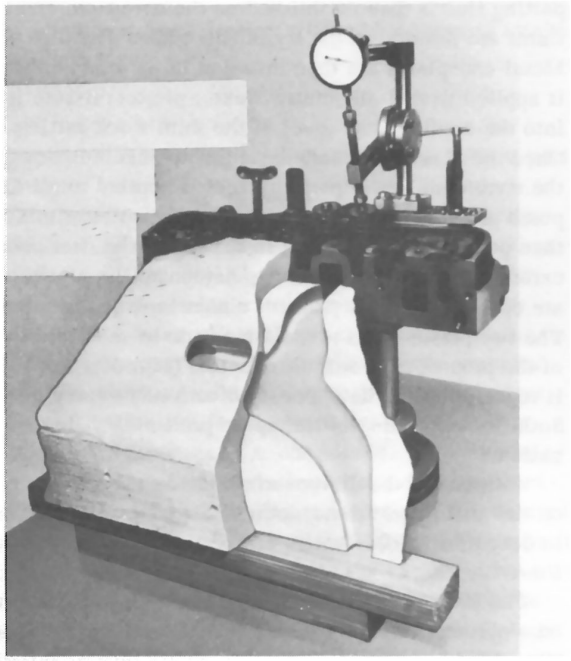

Fig. 41 - Plaster runner flowbox mounted to cylinder head on flowstand

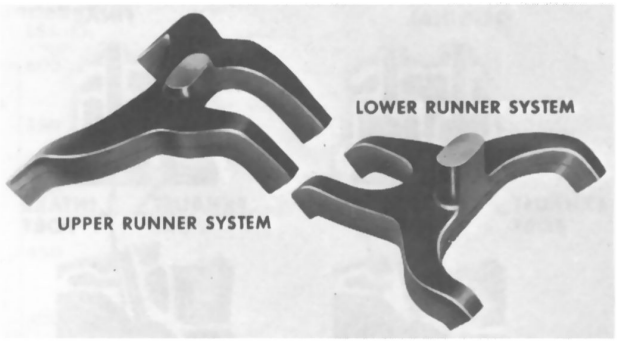

Fig. 42 - Secondary plastic coresticks

may result when coupled to a cylinder head. On occasion, port and manifold design limitations require that humps be added to the runner floor to improve airflow direction for increased efficiency.

Each runner of the plaster flowbox is then modified by grinding or adding clay to achieve maximum airflow and equal airflow between cylinders. Optimum plenum width and height must also be established to obtain increased flows. Particular attention must be taken to properly develop the areas where the runners connect to the plenum. Another critical area is the transition from the riser bores to the plenum. In most instances, a 1/2 in. radius produces the maximum airflow.

Once this stage of refinement is attained, additional clay is added to various areas in the manifold runners to determine if a reduction in size would maintain airflow volume while increasing flow velocity.

The next operation consists of pouring a plastic mixture into the plaster flowbox. After the plastic sets, the plaster flowboxes are parted and the plastic coresticks are removed. These coresticks are then nested into the metal cradle to determine if the proper metal thickness is still available between coresticks. Fiberglass flowboxes are then formed around these secondary plastic coresticks (Fig. 42). These flowboxes may contain slight modifications to the parting lines to facilitate casting. Once the fiberglass flowboxes are completed, they are rechecked for airflow and reworked, as necessary, to correct flows.

The primary plastic coresticks are then poured using the reworked fiberglass flowboxes (Fig. 43). These coresticks are used to construct the production casting equipment.

PORT AND RUNNER POLISHING - Another aspect of induction system development, which was investigated, was the polishing of ports and intake manifold runners. This tedious and time-consuming effort was found to be of no actual benefit to induction system airflow. Polishing has in some cases been found to be detrimental to airflow capacity. As mentioned earlier, some areas in the port and runner are so sensitive to variations in contour that the removal of the slightest amount of metal can redirect airflow and result in performance losses. In cases where polishing did have a beneficial effect, the port casting was found to be origin-

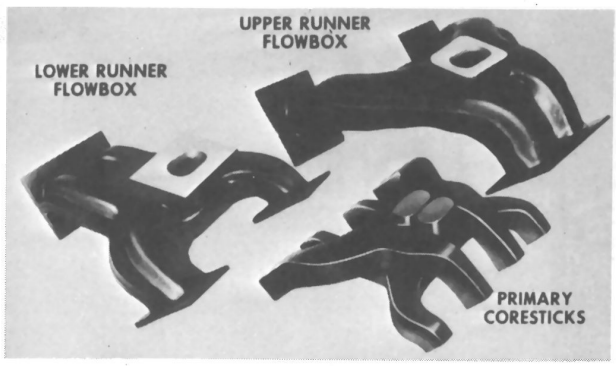

Fig. 43 - Fiberglass flowboxes with primary plastic coresticks

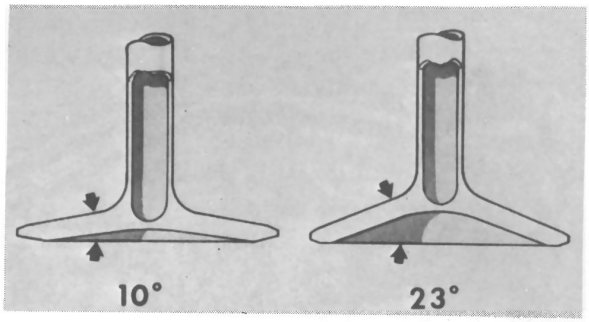

Fig. 45 - Modified valve underhead angle for improved durability

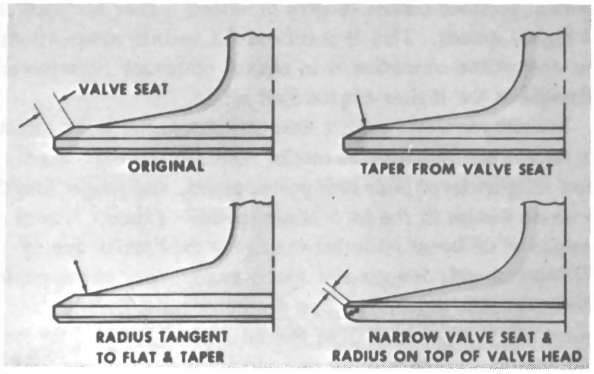

Fig. 44 - Intake valve designs

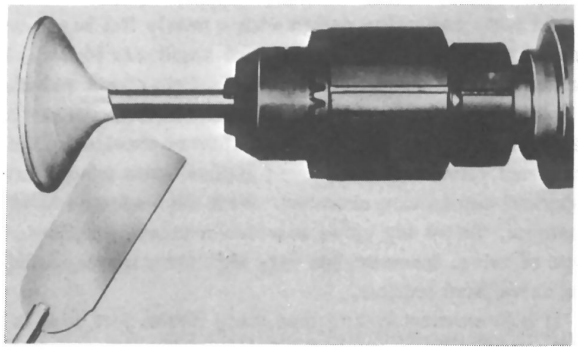

Fig. 46 - Valve head shaping

ally undersize, and the improvement was actually the result of correcting cross-sectional area. Of course, slight metal protrusions or casting fins which sometimes are the result of faulty cores should be removed by lightly grinding to eliminate the possibility of inducing turbulence.

VALVE DESIGN

Optimum valve design, to complement the intake port and exhaust port, is essential for maximum airflow. The valves initially used in the wedge combustion chamber of the 427 engine were similar in design to those found in a passenger car engine. The intake valve had a 30 deg valve seat angle and a 10 deg underhead angle, while the exhaust valve had a 45 deg valve seat angle and a 20 deg underhead angle. In the course of developing the intake and exhaust ports, various valve head configurations were evaluated (Fig. 44). Starting with the existing intake valve, several modifications were made. The underhead of the valve, adjacent to the seat, was first reworked to taper directly from the edge of the valve seat. Another modification was the addition of a slight radius, tangent to the flat and taper, before moving toward the stem at a 10 deg angle. Airflow favored the original valve design with the short flat.

Variations in valve seat angle had little effect on airflow in the various port and chamber configurations, although a 30 deg exhaust seat showed a definite improvement on the 427 single overhead cam engine. The valve seat width was then reduced, resulting in a definite increase in airflow. On the opposite side of the valve head, the radius replacing the chamfer had no effect on airflow.

The combination of the preceding data was the basis of the valve head design used on the early 427 cu in. engines (Fig. 45). The hollow stem of the valve was incorporated primarily as a means of reducing weight, thus increasing the valve toss or no-follow speed. The head was designed with a constant-stress head section for maximum head flexibility and minimum weight. Also, this valve was forged rather than cast for optimum strength and incorporated a swirl-polished underhead for removal of grind marks, as well as to provide turbulence-free airflow.

In later valve designs, the valve underhead angle was revised from 10 to 23 deg for durability at increased engine rpm. Studies indicated an airflow loss when using the 23 deg angle valve, but the airflow sacrifice was offset by increased valve durability and permitted higher engine speeds for longer periods of time. This valve design was used in the 427 GT engine and is currently being used in production.

Earlier airflow studies of the 23 versus 10 deg angle valves with the SOHC hemispherical combustion chamber design responded in the opposite manner. Increasing the angle on the intake valve progressively increased airflow. These results prompted a thorough investigation of valve head design.

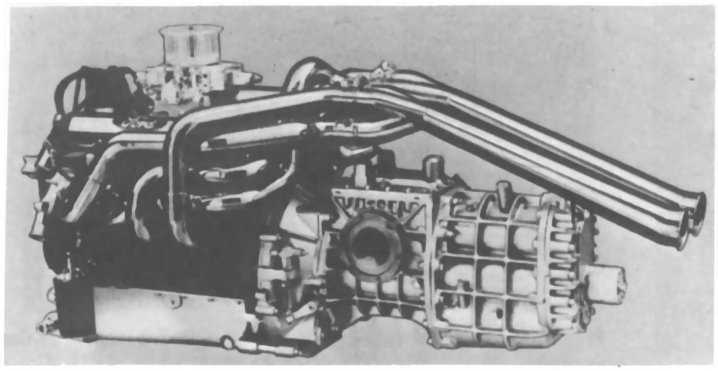

Fig. 47 - 427 GT engine

An early cast valve design with a nearly flat head was ground until the valve head-to-stem angle was 90 deg. This valve was then mounted in a motor-driven chuck and clay was added to or removed from the head to form various head shapes and angles (Fig. 46). As indicated previously, the increased valve angle improved airflow when using a hemispherical combustion chamber. With the wedge combustion chamber, the 90 deg valve provided maximum airflow. This type of valve, however, has very high stress levels through the valve head section.

It is interesting to note that many intake port designs will actually flow more air with the intake valve opened between 0.500 and 0.600 in. than a port with the valve removed. This is the type of complementary design desired for optimum airflow.

FUEL DISTRIBUTION

Fuel distribution was the only problem area encountered on engines equipped with four-venturi manifolds, which were developed using the airflow technique. This problem is caused by inadvertently designing fuel-separating features in the induction system even though the airflow is equally balanced throughout the manifold. The degree of unbalanced fuel distribution can be approximately determined in a running engine through the use of thermocoupled spark plugs, temperature-sensitive valve alloys, and exhaust gas analysis. In most instances, the problem can be minimized by making carburetor modifications in jetting, notching carburetor booster venturies to redirect fuel dispersions, or adding deflectors or pins. If the problem persists and cannot be alleviated by these means, a mechanical type of deflector can be introduced somewhere inside the manifold. Balance passages, notches and ribs may also be added.

INTAKE MANIFOLD AND EXHAUST MANIFOLD TUNING

Tuning an intake manifold consists of lengthening or shortening the intake manifold runners to vary the magnitude and rpm of the horsepower and torque peak (Fig. 47). Dynamometer development work demonstrated that the shortest possible runner lengths produced higher horsepower at higher speeds. This is practical for certain applications, but the prime objective is to obtain optimum horsepower throughout the higher engine rpm range.

Exhaust manifold tuning has, primarily, the same effect on engine performance as intake manifold tuning. Short pipe lengths favor high rpm power peaks, and longer lengths increase torque in the mid-range speeds. Exhaust system designs of different vehicles may vary drastically due to different chassis designs and space availability in the engine compartment. Optimum pipe diameter must first be established in order to realize the full benefit of exhaust system tuning. To determine the optimum pipe length for the exhaust system, pipes of an appropriate diameter are attached to an engine. While the engine is running in the rpm range in which the tuning is to be most effective, the true pipe length is determined. The pipes may be bent to fit the engine compartment, and all four pipes on one side of the engine must terminate in one plane. Severe bends in the tubing are permissible and have no effect on tuning, providing the proper cross-sectional areas are maintained. The pipes may then be connected to a common collector and then routed through a larger diameter pipe toward the rear or side of the vehicle to be expelled to atmosphere. The 427 cu in. engines have been responsive to the tuning of fabricated tubular header systems. The most successful systems produce higher horsepower throughout a wide speed range.

CONCLUSION

The GT induction system is the product of a new development technique that involved the extended use of an induction flowstand, as well as extensive studies of various types of manifolds and cylinder heads. During the course of this work, successive improvements in modeling and pattern making have combined to refine the art to a high degree of sophistication.

A large measure of credit for the development of tools and techniques, such as this, must be given to the challenge and impetus supplied by the Ford Motor Co.'s participation in the highly competitive sport of automobile racing.

Mark II-GT Ignition and Electrical System

Robert C. Hogle
Ford Motor Co.

There is no handbook of vehicle electrical system design or no secret formula which can serve as a guide in the development of electrical components for competitive events. The basic approach to the extent possible, therefore, was to use production components or components for which we had considerable background experience.

The design group assigned to the MK II project consisted of engineers with experience on components of their responsibility. The members of this group were asked to limit their considerations to failure mechanisms which were actually causing part failures, rather than to speculate on problems more imaginary than real. Failure analysis data were examined on components used in prior competitive events. Vibration was the major cause of failure; parts which were defective prior to installation or damaged at installation were a secondary cause of failure. Corrective design action was taken at the outset to eliminate these types of failures. Corrections were verified during dynamometer engine and driveline tests, as well as in vehicle durability tests.

The following excerpts, from the general regulations for the 24-hour race, have a bearing on electrical system performance and reliability.

- The vehicle must be equipped with a self-starter that may only be operated by the driver from his seat.
- The engine must be stopped during all pit stops.
- The starting motor, generator or battery may not be replaced as complete assemblies.

  Recharging of batteries by outside means is prohibited.
- The windshield wiper, self-starter, statutory lighting equipment and warning devices must be in working order throughout the race.
- Spare parts or tools must be on board the vehicle or in the working pit.
- The driver may not take spares or tools from the pit nor may these be brought to him.

From these few regulations, you can realize the importance of a reliable electrical system. Our total objective was to simply reduce the chance of electrical failure to an absolute minimum.

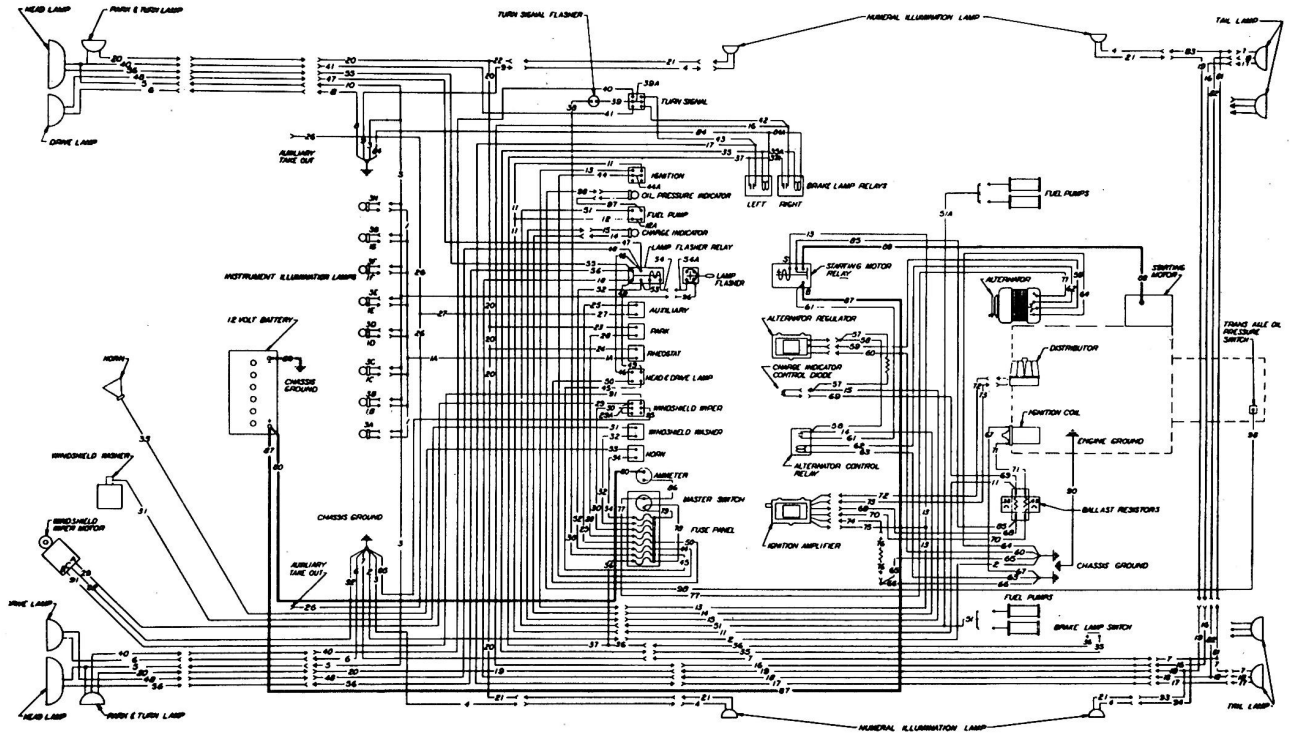

Figure 1 — Vehicle Circuit Diagram

WIRING SYSTEM

Wiring is a flexible component which is relatively easy to change and re-route. More often than not, it is kicked around until the last moment, which usually results in too many compromises for the best service.

The first task in developing an efficient wiring system is to determine the location of all electrical components with respect to their functional, environmental and servicing requirements. The engine electrical component locations were fixed by the basic engine design, and no changes could be made to the standard production locations and mountings. The transistorized ignition amplifier and voltage regulator were located behind the left seat, near the floor pan, adjacent to the alternator field relay. All control switches, fuses and lighting control relays were located on or behind the instrument panel.

A schematic diagram of the final vehicle wiring is shown in Figure 1. From the diagram you would think it was a fairly complex electrical system. A detailed review of the system, however, would show that it contains only the basic sub-systems found in any normal vehicle used on the public highways.

Figure 2 shows the physical components in their relative vehicle position. In spite of a relatively light electrical load in some of the circuits, the wire size chosen for the minimum acceptable tensile strength was #14 AWG with heavy-wall, chlorosulfonated polyethylene insulation, SAE Type HTS. This wire has a maximum service temperature of 275° F. and is the recommended SAE practice for heavy duty trucks. The insulation of this wire is thermo-setting and therefore, does not melt when subjected to the heat produced by an overloaded circuit. Adjacent wires in a harness using this insulation are not damaged when an overload occurs.

As a servicing convenience, electrical components were equipped with multiple disconnects wherever possible. Important polarity-sensitive components, such as the voltage regulator and ignition amplifier, could then be removed and replaced readily with no risk of hook-up error.

Determining a safe routing for wiring harness assemblies is an important consideration in maintaining the security of the wiring system. The shortest route results in significant weight savings and in the least voltage drop.

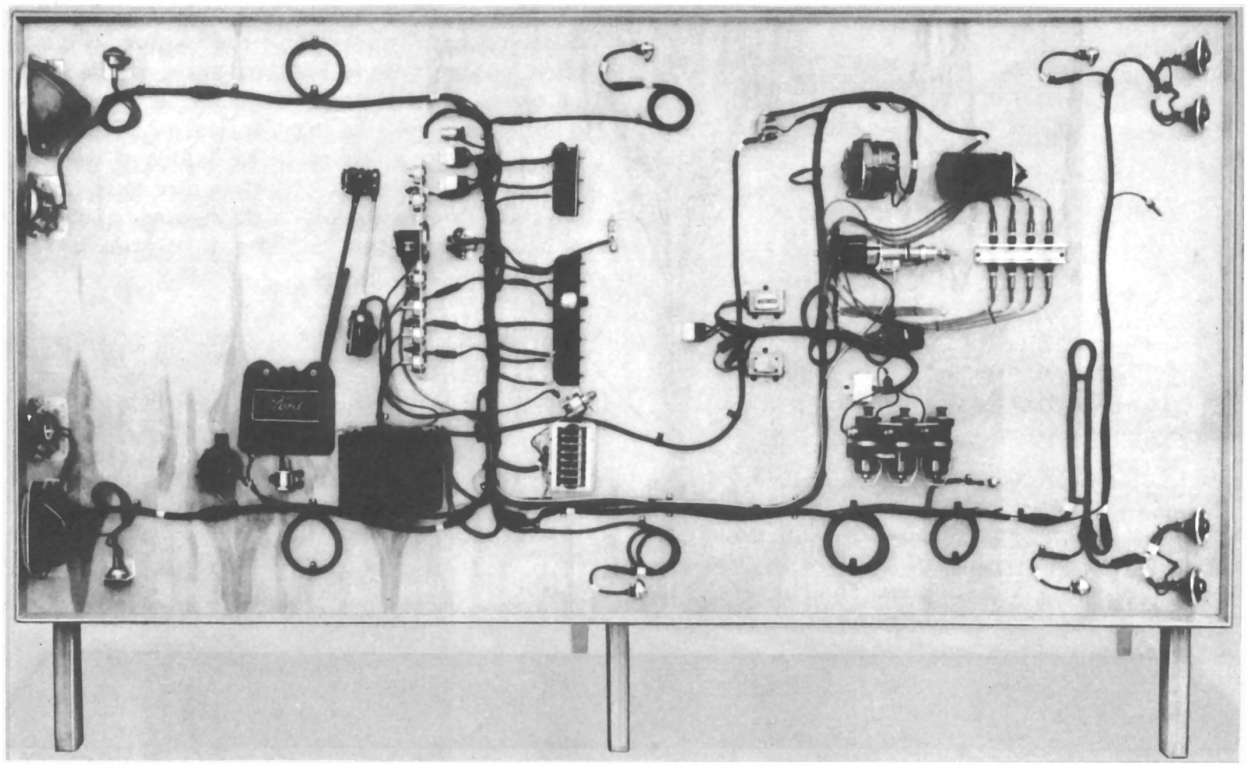

Figure 2 — Display Buck

Care must be taken to avoid congestion, damage by hot engine components, moving parts of the vehicle and other such potential trouble makers. Full utilization was made of the available protection afforded by existing channels in the vehicle structure.

Two harnesses, which take considerable abuse, are the front and rear body lighting harnesses. The front and rear body sections were made removable for ease of service; this required the use of high tensile strength harnesses with waterproof quick disconnects shown in Figure 3. The required tensile strength was obtained by extruding a neoprene jacket over the wiring harness. It is also required that these harnesses be provided with strain relief to prevent damage if the body sections were removed without first separating the disconnects manually.

All switches used were heavy truck or aircraft-types. A master disconnect switch in the primary circuit was used for safety purposes at pit stops and when the vehicle was being transported or stored.

GENERATING AND STARTING SYSTEM

Electrical loads for the MK II application were planned to be all continuous except the starting motor, horn, windshield washer and turn signals. Differences in day-night loads were not considered, since the entire race might be run under adverse weather conditions requiring lights and windshield wiper.

An alternator with a rating of 52 amperes was chosen; it exceeded the full-load requirements and no deficits had to be made up by the battery, except for pit stops.

The alternator and transistorized voltage regulator used were basically production units modified to withstand extreme vibration. The regulator incorporates 2 transistors, 3 diodes, several condensers and resistors and no moving parts whatsoever; the limiting factor in its application was that the ambient temperature must not exceed 200° F. The transistorized voltage regulator was a discrete component assembly in which all the components were locally potted to the circuit board.

Critical components, such as the alternator diodes, were selected for high reverse voltage and low-leakage characteristics. The rectifier

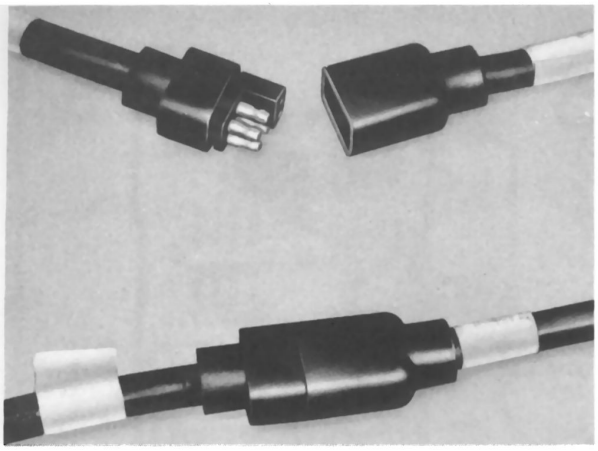

Figure 3 — Wiring Disconnects

assembly, shown in Figure 4, was potted to eliminate the possibility of relative motion between any of the components. The field coil was epoxied to the pole pieces to minimize the effect of vibration and rotational stresses.

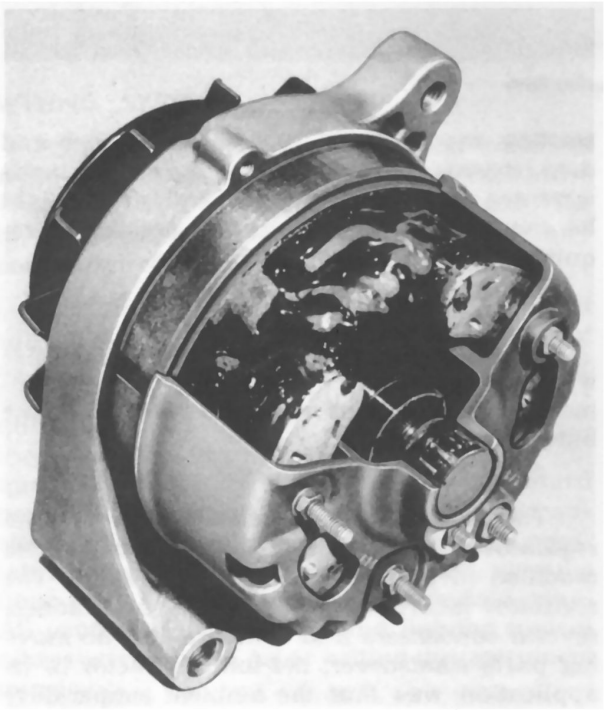

Figure 4 — Alternator

Figure 5 shows the 53-ampere hour SAE Group 2SMB battery with 9 plates per cell selected for this application. This is a standard multipiece battery sealed with hard epoxy in place of the normal soft asphalt seal. The plates are anchor-bonded to the bridges with an epoxy.

The starting motor has only one function to perform. It must crank the engine at a sufficiently high rpm to insure a start. In the interest of starting system reliability, it is essential to limit cranking to the shortest possible time. The starting motor must be matched with the battery and battery cables to insure high cranking rpm. The principle concern was, of course, to hot-crank a loaded engine, purge it, and accomplish a quick start.

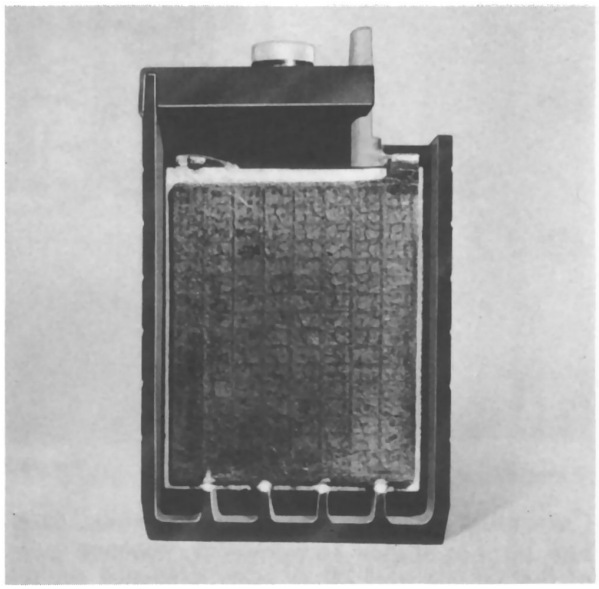

Figure 5 — Battery

The starting motor for this application was a 4.5" diameter, positive engagement production unit with minor modifications, as shown in Figure 6. The field coils, connecting links and brush shunts were bonded to the frame with silicone rubber. The actuating coil aluminum sleeve was replaced with brass to avoid possible fracture and interference with starter drive engagement.

ELECTRIC FUEL PUMPS

The electric fuel pumps shown in Figure 7, were production units mounted directly above the fuel tank to minimize the possibility of vapor lock. The inlet and outlet ports were enlarged to reduce flow losses.

Two pumps were used in the main fuel system with a third pump in reserve. The pumps were connected with common manifolds, and the selection of pumps was done electrically. No provisions for back flow is required, since each pump has two check valves preventing reverse flow in a non-operating pump.

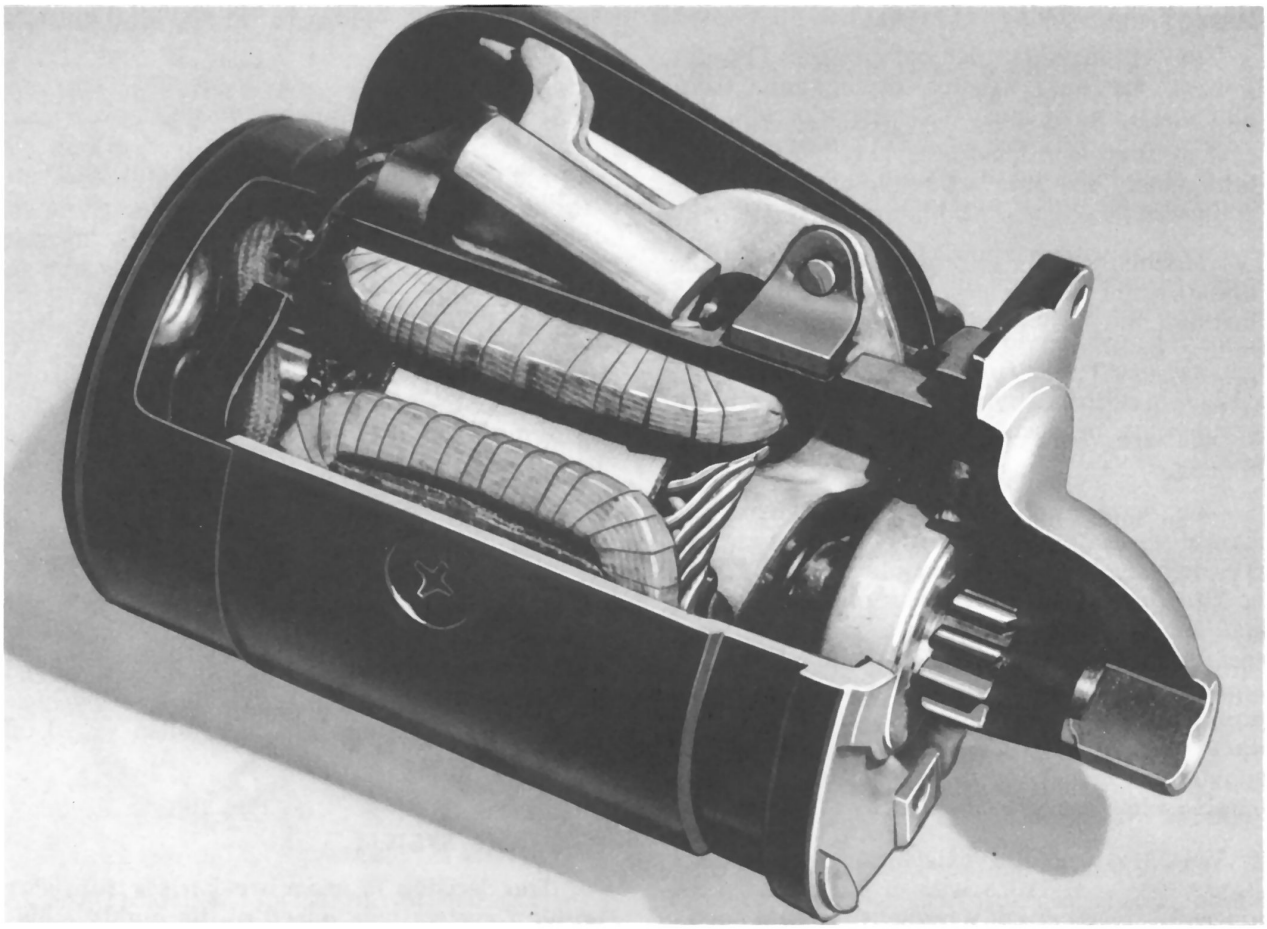

Figure 6 — Starting Motor

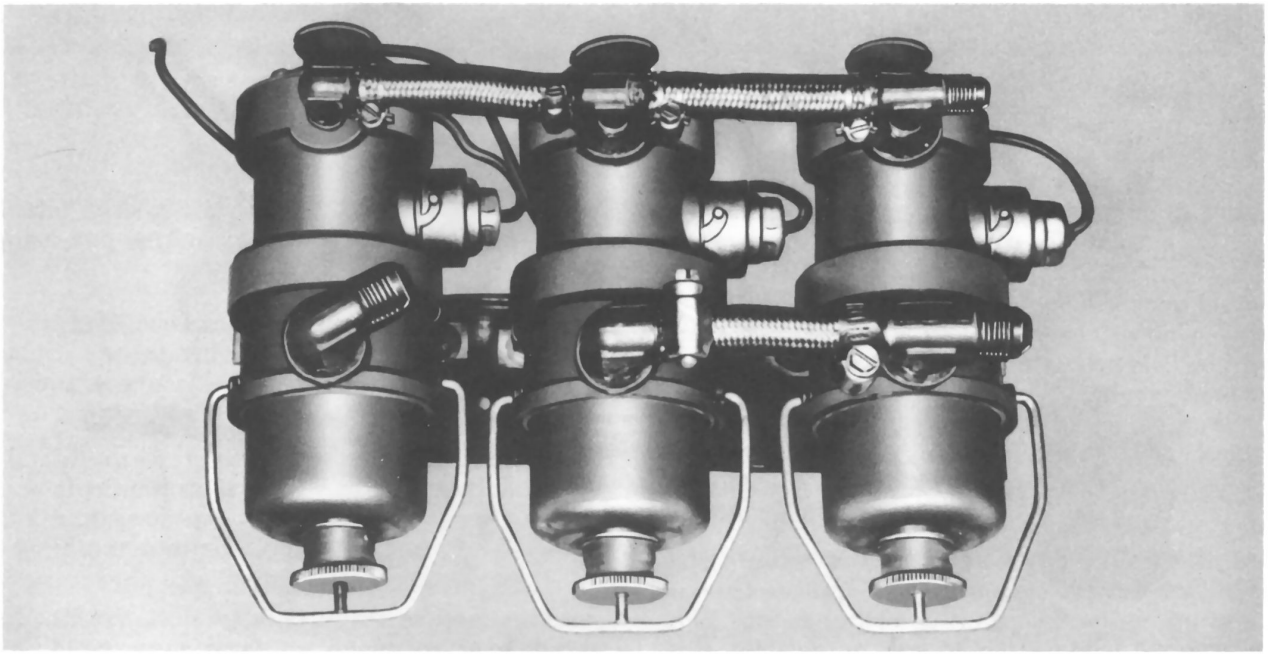

Figure 7 — Fuel Pumps

WINDSHIELD WIPER SYSTEM

The windshield wiper components (Figure 8) were modified to our specifications from units used on Boeing 707-type aircraft. The system used consisted of a D.C. motor, oscillating gear box and a flexible shaft, 15" long, connecting the motor and gear box.

Normal wiping speeds for aircraft applications are in the order of 240 wipes per minute through an angle of 60 degrees. The D.C. motor as applied to aircraft 28 volt systems operates at 11,000 rpm. Since the MK II has a 12 volt electrical system, the resulting wiping speeds were between 105 and 115 wipes per minute.

The wipe angle was increased from the normal aircraft application of 60 degrees to 110 degrees. The arm and blade were also a modification of equipment designed for aircraft use. The main portion of the arm was stainless steel tubing. A spring-loaded blade pressure adjustment was incorporated in the section that mounted to the gear box output shaft. The blade was an anti-windlift design modified to withstand vehicle design speeds, and was adjustable with respect to the arm.

Windlift was non-existent at any vehicle speed. Blade pressure was in the order of 30 ounces, which is slightly higher than that specified for passenger cars. The arm and blade assembly were given a black-mat finish to reduce glare.

LIGHTING SYSTEM

The head lamps used were high intensity, iodine-quartz units used on some European vehicles. These lamps have a single filament; no dimming is required since there is not oncoming traffic. The passing lamps, sometimes called driving lights, were also iodine-quartz. For nighttime operation, all four lamps are normally on, and the headlamps are turned off momentarily by means of a steering column-mounted flick switch, to signal a vehicle being overtaken. For daytime operation, the flick switch turns the driving lamps on to indicate a passing situation. All other lighting on the vehicle was of the normal incandescent-type, except for the heavy duty bulbs; these were developed jointly by the SAE and the industry for long-life heavy truck use. The most troublesome lights on the vehicle proved to be the side number identification and vehicle recognition lamps which were often wiped off on straw bales.

IGNITION SYSTEM

The decision to use a breakerless transistor ignition system was based on its highly satisfactory performance. This dates back to the

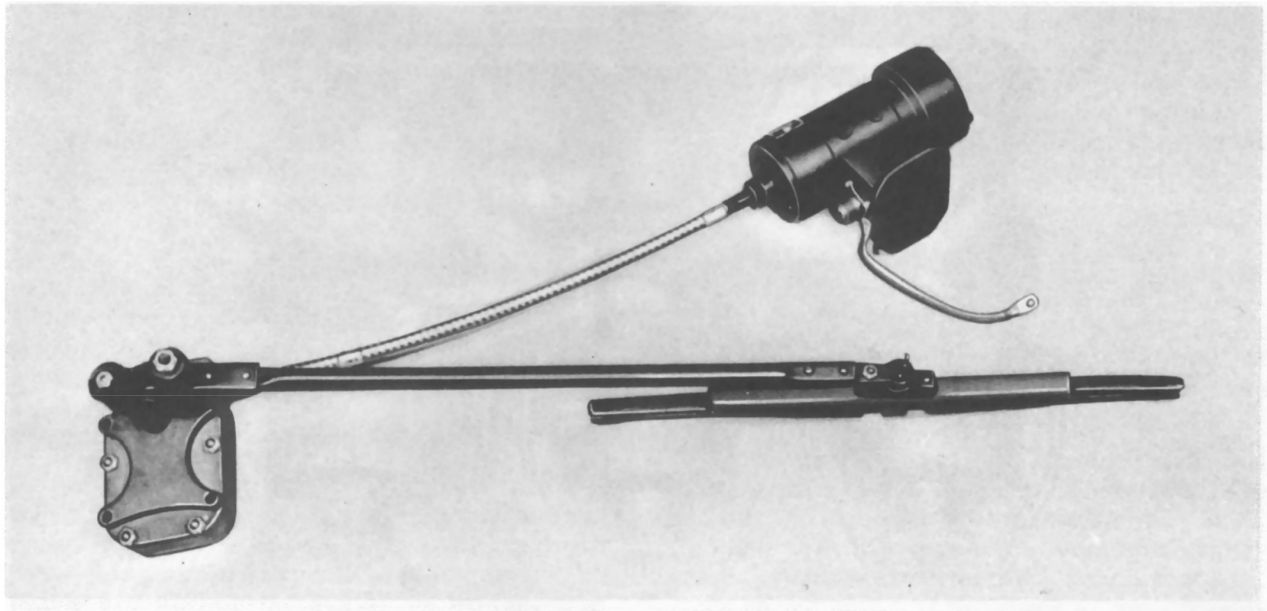

Figure 8 — Windshield Wiper

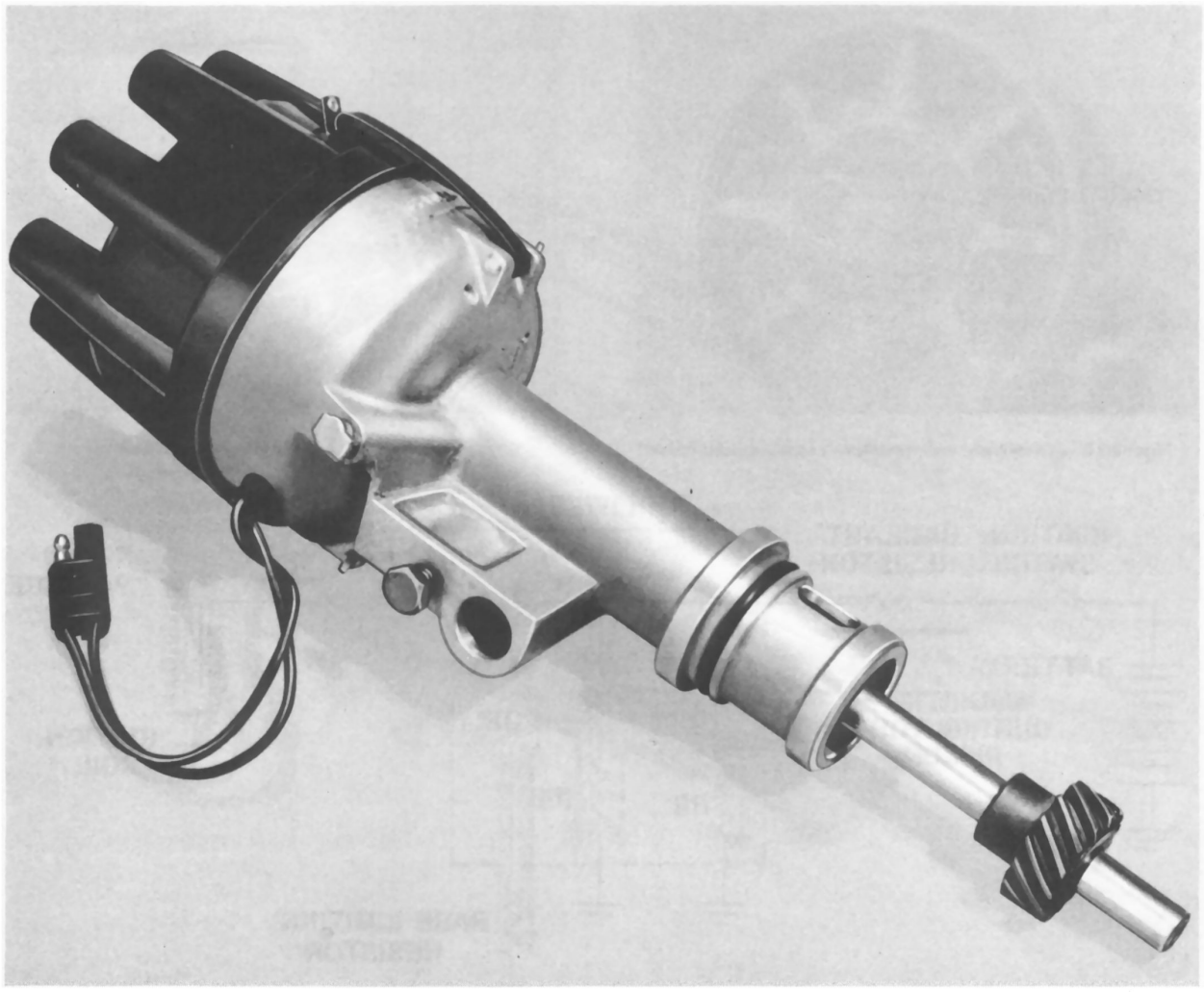

Figure 9 — Distributor Assembly

initial breakerless application on the 4.2 liter push rod engine used at Indianapolis in 1963.

There are two salient features of this system which are particularly advantageous for a racing engine:

1. Elimination of distributor contact bounce at high speeds which results in consistently high voltage to the spark plugs and no engine misfiring.

2. Elimination of distributor contact rubbing block wear resulting in no losses of engine timing.

These features enable the engine to finish the race in a "just-tuned" condition.

The breakerless ignition distributor incorporates a variable reluctance magnetic pickup in place of the breaker points. The distributors used on the Mark II and GT 40 are identical and differ from the original 4.2 liter application only in minor details. The principle change involves the addition of a centrifugal spark advance mechanism.

Figure 9 shows the distributor assembly incorporating a mechanical tachometer drive and the magnetic pickup. All other parts of this distributor are of a standard production design.

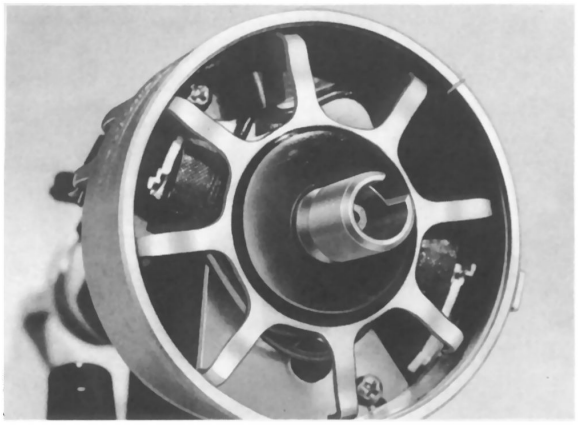

Figure 10 — Distributor Assembly — Less Cap and Rotor

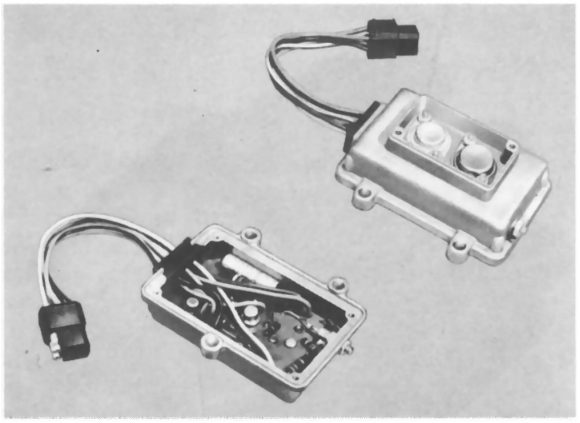

Figure 11 — Ignition Amplifier

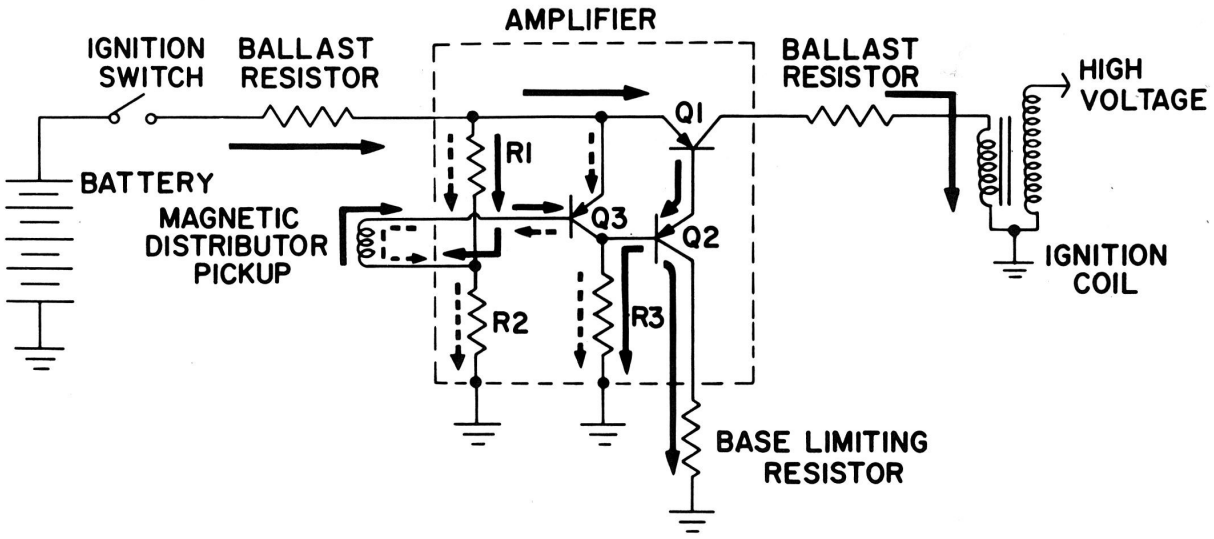

Figure 12 — Functional Circuit Diagram — Ignition Amplifier

Figure 10 shows the distributor with the cap and rotor removed. The eight-fingered metallic rotor and twin-coil stator form the key parts of the variable reluctance magnetic pickup. This arrangement produces eight pulses per revolution of the distributor shaft. The magnet is cast into the rotor assembly.

Figure 11 shows the electronic package, or amplifier. The heat sink housing is a modified production transistor regulator casting. The circuit utilizes discrete components interconnected on a printed circuit board. The power transistors are mounted directly to the heat sink and enclosed in the "dog house." The completed assembly is fully potted with epoxy resin to reduce the possibility of vibration damage and to improve the heat transfer characteristics of the internally mounted components.

Figure 12 is a functional schematic of the system.

The electrical signal from the magnetic distributor is referenced in the amplifier by the bias level set by resistors R1 and R2. This level is established so that with zero signal from the magnetic distributor, the input transistor (Q3) is turned ON, thereby clamping transistors Q2 and Q1 OFF. (The current flow is shown by the dotted line.) A negative signal from the distributor provides additional "ON" drive to Q3; however, since Q3 is fully saturated — that is, turned ON in its static state — this additional drive has no effect.

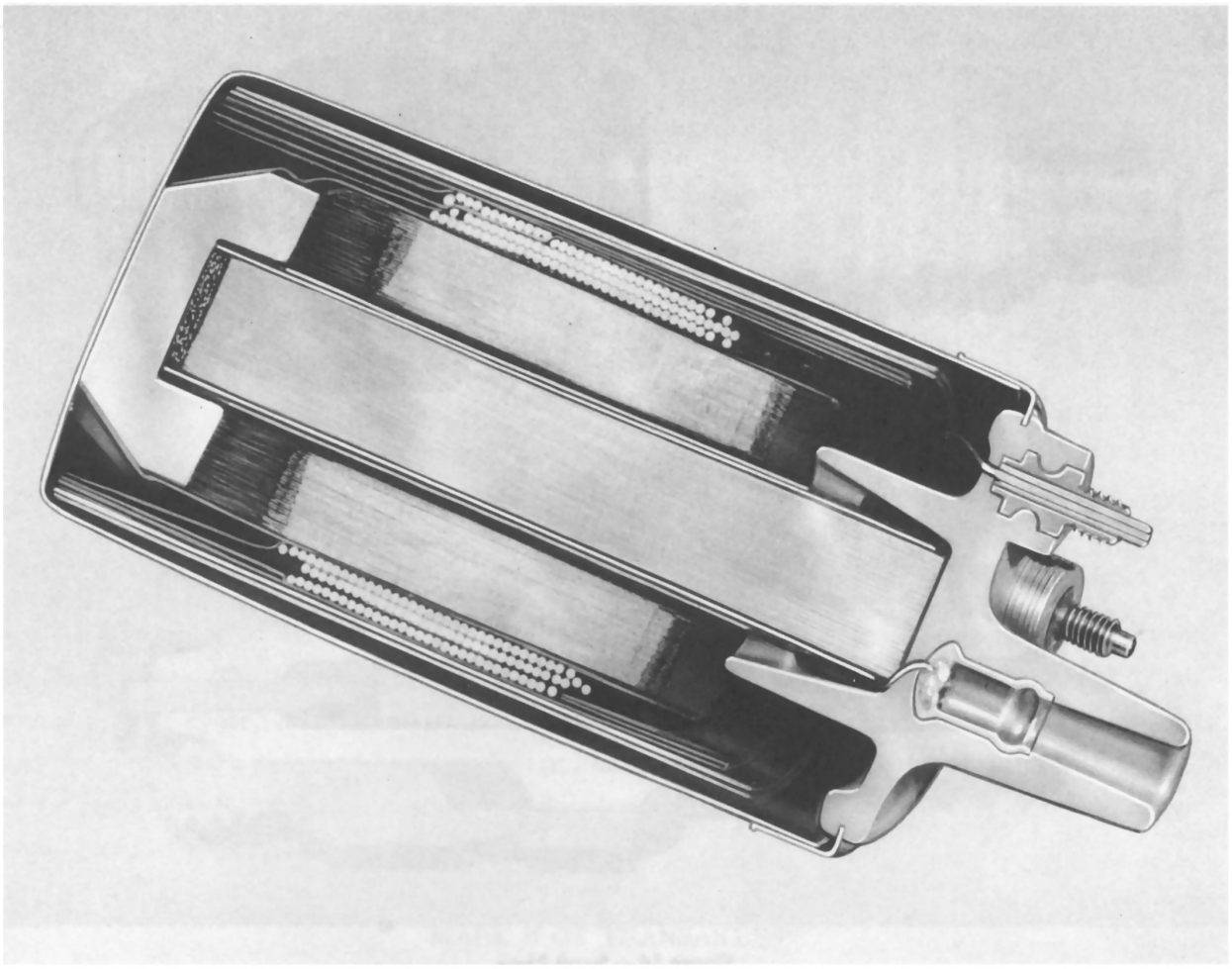

Figure 13 — Ignition Coil

When the positive output voltage from the distributor exceeds the bias level set by R1 and R2, the input transistor (Q3) turns "OFF"; this allows current to flow from the base of Q2 through resistor R3, thus turning Q2 "ON" and subsequently turning Q1 "ON." Current will now flow in the primary of the ignition coil. (The current flow when the amplifier is ON is shown by the solid line.)

The amplifier is turned "OFF," and high voltage is generated in the ignition coil by the rapidly collapsing magnetic field when the distributor output falls below the bias level set by R1 and R2.

The ignition coil, shown in Figure 13, is basically a production transistor unit. Like the amplifier, it has been fully potted with epoxy resin to guard against vibration damage and any loss in dielectric properties.

The high tension ignition wires from the distributor to the spark plugs and coil are special silicone rubber with a steel core. Silicone boots are fitted over the spark plugs, distributor and ignition coil terminals. The high temperature characteristics and increased flexibility of the silicone rubber, make this material especially desirable for the Mark II application.

The spark plugs, shown in Figure 14, were of the same design and construction as our standard gap automotive plugs except for the higher IMEP rating — cold heat range — required for use in a racing engine of this type.

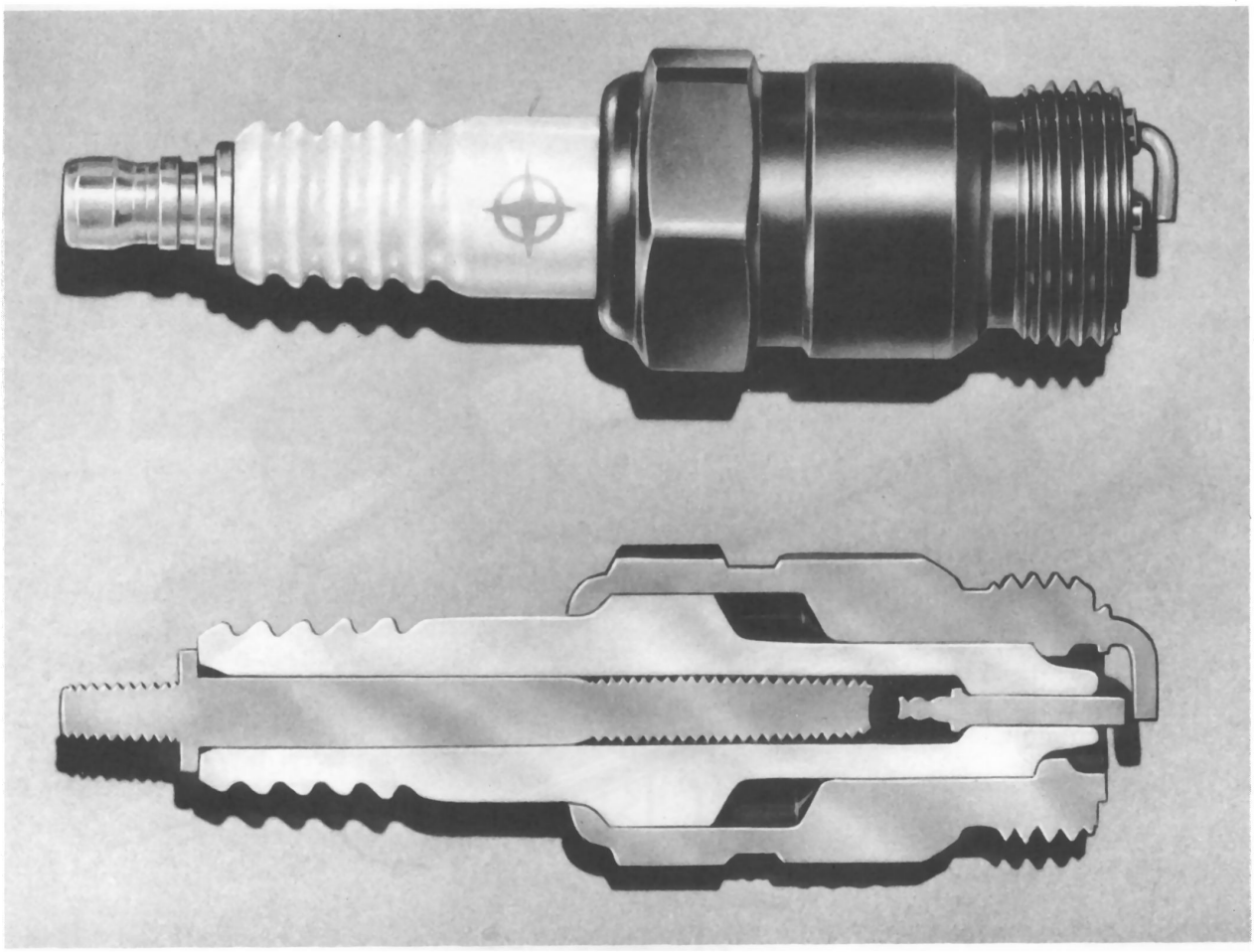

Figure 14 — Spark Plugs

Mark II-GT Transaxles

H. L. Gregorich and C. D. Jones
Ford Motor Co.

ABSTRACT

Mark II GT Transaxles

This paper provides a description of the Ford Mark II GT transaxle as used in the 1966 Le Mans race. The functional requirements, as established by a simulated Le Mans dynamometer test cycle, are summarized through integration of the engine torque and speed data and compared with gear and bearing design parameters to reflect their capacities in hours of Le Mans usage. The areas where the development work was particularly important are highlighted in the discussion.

MARK II GT TRANSAXLES*

While the specific subject of this paper, in a sense, did not exist as little as two years ago all of the mechanics for its functional needs were available. All of the mechanics, in fact, have been well developed for several years; the arrangement, however, is not in common use in this country and its application is treated as new. Interest in the subject is believed to stem, principally, from the demonstrated performance of the Mark II GT prototypes in the 1966 Le Mans Grand Prix race. Such interests most probably relate to the particular arrangement, mechanical action, functional capability and reliability, of the transaxle components, as well as the development work that brought them to their present state. This paper begins with a chronology of the subject's brief history. Following the chronology, a description and discussion of the particular type of transaxle used at Le Mans is given. The functional requirements for the transaxle, as established by a simulated Le Mans dynamom-

* The term transaxle is a contraction of the transmission and axle names into a single word. The precise subject refers to the transaxles which were in the 1966 Le Mans Mark II GT prototypes.

eter test cycle, are summarized through integration of the engine torque and speed data and compared with gear and bearing design parameters to reflect their capacities in hours of Le Mans usage. The discussion of development work is limited to those problems occurring within the transaxle; particularly those areas where the development work came to the rescue of the design concepts.

Chronology of the Transaxle

Following the 1964 Le Mans race, Ford Motor Company began the design of a heavier and more powerful experimental GT prototype car. The requirements of this new car excluded the use of any available proprietary transaxle; the contemplated use of a V-8 427 CID engine required heavier and stronger transmission and axle components than those that were currently packaged for race applications in either domestic or foreign cars.

In December of 1963, Ford had introduced a newly-developed four-speed manual transmission for the 427-4V passenger car applications. The ruggedness of these new four-speed transmissions led to their being considered for the GT transaxle application. By January 1965, a transaxle with conventional clutch, synchro-mesh four-speed transmission and axle with hypoid gearing and locking differential was being considered, at least as an alternate design.

In early 1965, prototype hardware for each of two transaxle designs was fabricated and assembled for vehicle evaluation. One of these designs featured a torque converter coupled to a two-speed transmission with Colotti-type gear engagement. The transmission was directly geared to the axle pinion gear shaft and powered the axles through a locking differential. The second design used the conventional clutch and four-speed transmission, with axle and locker components interchangeable with those of the first design.

Track performance of the initial experimental prototype vehicles was so satisfactory that two experimental cars were entered in the 1965 Le Mans Grand Prix race. Each of the GT vehicles was equipped with similar transaxle units; their design featured the conventional four-speed synchro-mesh transmission. Although the initial prototypes had low durability characteristics, Phil Hill, driving one of the Mark II cars, set a new lap record of 141.1 mph early in the race. This modest accomplishment undoubtedly created the incentive as well as established the objectives for the program.

Through mid-year of 1965, development work continued on the transaxles. By November 1965, several evaluation tests, including durability runs under race conditions, had permitted further evaluation of gear ratios and study of individual components for the need of modifications. Toward the close of 1965, two transaxle designs had been developed and were considered race-ready. One was the four-speed manual shift transaxle, and the other was a fully-automatic power shift transaxle.

The power shift transaxle axle was developed primarily for the J-Car, a prototype lighter than the Mark II's. Although the automatic-type transaxle was run at Daytona in a Mark II, the development work on the light car had not progressed sufficiently to be ready for the June 18, 1966 Le Mans race, so the unit did not receive further competitive evaluation.

The design with conventional clutch, transmission, etc., went on to make race history in the Mark II GT prototypes at the Daytona International, Sebring Grand Prix and Le Mans Grand Prix races and is, of course, the subject of this paper.

Transaxle Arrangement

The general arrangement of the transaxle is shown in Figure 1. In these sectional views, three principal construction areas may be identified.

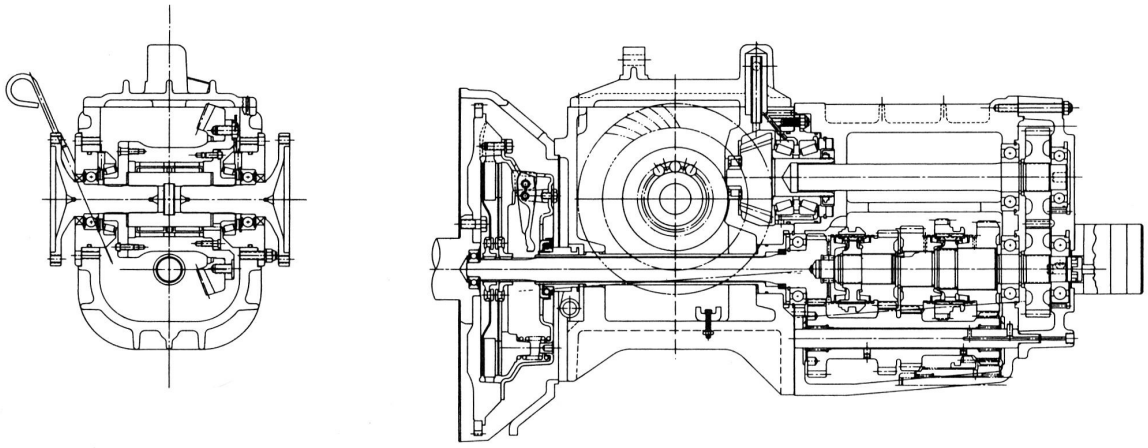

Figure 1

At the left side in the longitudinal section is the flywheel housing, which encloses a two-disc clutch, and provides support for the clutch actuating mechanism. This housing is mounted to the rear face of the engine block.

The differential housing is immediately behind the flywheel housing and is attached to it (a two-piece construction is used to provide flexibility in design without loss of too much rigidity). The differential section, in addition to encasing the locking differential and ring and pinion gears, provides support for the pinion bearings and differential side bearings. An access opening at the top of the case is provided with a cover with two integral mounting attachments to serve in conjunction with a supporting cross member as the rear mounts for the engine.

The transmission case, in turn, is mounted to the axle housing. This component, besides housing the transmission proper, has provisions for attaching, on the right, the shift mechanism and, at the rear, the transfer drive gear cover. A small gear pump, mounted on the rear face of the transfer drive cover and driven from the transmission, is used for maintaining flow of lubricants to and from an external cooler.

Structurally the flywheel housing, axle case and top cover provide support for the complete transaxle assembly, as well as carrying the reaction loads due to input shaft, and the axle shaft loads. All of the principal housings are of sand-cast magnesium alloy to minimize weight. Each of the cast housings was designed with sufficient wall strength and external ribbing so that no serious structural problems were experienced in the development tests. Problems related to deflections and interference fits did appear; discussions of such problems are included in the development discussion on the particular components affected.

The transaxle arrangement provides for power flow from the rear-mounted engine through a dual disc clutch to the transmission. From the transmission, power flows through a pair of transfer gears mounted at the rear of the transmission case, to the pinion gear, ring gear and locking differential. Stub shafts, splined to the locking differential, drive the rear wheels through Rzeppa-type jointed shafts.

Functional Requirements

The functional requirements of the transaxle and its components are, to a great extent, dictated by the engine torque characteristics, vehicle weight, weight distribution and wheel size. They are further established by the terrain and layout of the race course, and the anticipated vehicle speed and engine, as well as the number of laps to be completed.

For the Mark II GT transaxle application, the vehicle weight was 2850 lbs. (less the driver) with a weight distribution which provided sufficient traction to induce wheel-slip torques at 2500 ft. lbs. The engine of the Mark II developed up to 485 brake horsepower with available torque up to 460 ft. lbs. While the torque capacity and gear ratio requirements for the transaxle unit fall within or near the limits of those in use in current passenger cars, the high operating engine speed (up to 6800 rpm intermittently) requires special lubrication and cooling features to maintain satisfactory operating temperatures.

The layout and topography of the Le Mans race course requires vehicles with exceptional accelerating and braking characteristics, as well as high speed stability. The transaxle contributes to these requirements by its ability to respond quickly to any required gear change, either up or down shifts, and to retain gear engagement under all torque and speed conditions. Approximately 9000 gear shifts are required during the 24 hours of the race; many of the shifts, because of the high speed, require the synchronizers to perform three to four times the work required in conventional passenger car use. The anticipated transmission gear usage is itemized in Table 1; i. e., the approximate time spent in each gear whether in drive, coast or cruise operation. The vehicle is in the drive and cruise position 55% of the time. Except for cruise, this time is spent accelerating in the various transmission gear engagements. The coast time (amounting to 30%) is with the clutch engaged resulting in engine braking. The time spent in changing gears amounts to 15% of the total time or 3. 6 hours.

G.T. TRANSMISSION GEAR USAGE

(LE MANS CYCLING - 24 HRS.)

GEAR USE	RATIO	PERCENT OF TIME	HOURS
1ST GEAR DRIVE	2.32	4.8	1.15
1ST GEAR COAST		5.8	1.39
2ND GEAR DRIVE	1.54	10.3	2.47
2ND GEAR COAST		3.2	.77
3RD GEAR DRIVE	1.19	12.3	2.95
3RD GEAR COAST		8.4	2.02
4TH GEAR DRIVE	1.00	12.1	2.91
4TH GEAR COAST		12.1	2.91
4TH GEAR CRUISE		16.0	3.84
CHANGING GEARS		15.0	3.60

Table 1

The operation of the transmission when downshifting requires that the clutch discs must be capable of running at speeds of at least 10,000 rpm. Further, all transmission operation in gear is at 100% of available engine torques (except in first gear). This usage, with variable torque and speed, determines the load-carrying requirements of the transfer drive gears, bearings, differential locker, and ring and pinion gears.

Design Analysis

To establish quantitative values of torque, speed and usage for the design analysis, estimates of their respective averages were taken as 427 ft. lbs., 6000 rpm, and 3 hours in 1st gear, 6 hours in 2nd gear, 6 hours in 3rd gear and 9 hours in direct drive. While these estimates proved adequate for the initial design and development work, a verification of their accuracy and possible identification of areas having design improvement potential was needed. As a consequence, the engine-applied torque and speed data were integrated relative to time for each gear application. The results of these latter calculations are presented in this paper.

The transmission section of the transaxle provides for the gear ratio changes needed to utilize the engine horsepower effectively. There are four forward drive ratios, with values as shown in Table 1. As used in the race, their application was limited to acceleration by upshifting through each gear in sequence; holding in fourth gear at cruising speed for a short time; and then braking with the engine by downshifting through the gears in sequence. A typical shift pattern is shown in Figure 2; in this graph the engine speed is plotted against time. It should be noted that the engine speed versus time is nearly a straight line for each gear application; to simplify gear tooth fatigue stress and life analysis, the speed is approximated by a straight line.

The available engine torque plotted against the engine speed in rpm is shown in Figure 3. As in the graph of the engine speed, the torque data curve is approximated by straight-line segments; in this instance, three. Further, the engine torque applied in low gear is limited by the rear wheel tractive effort and is assumed to have a constant value near 400 ft. lbs. until the ratio of tractive effort to available engine torque becomes greater than the over-all gear reduction.

The bases for the speed and torque curves shown in Figures 2 and 3 are graphs run in the dynamometer from a simulated Le Mans test cycle. Four such cycles are equivalent to one lap over the Le Mans course at a competitive speed.

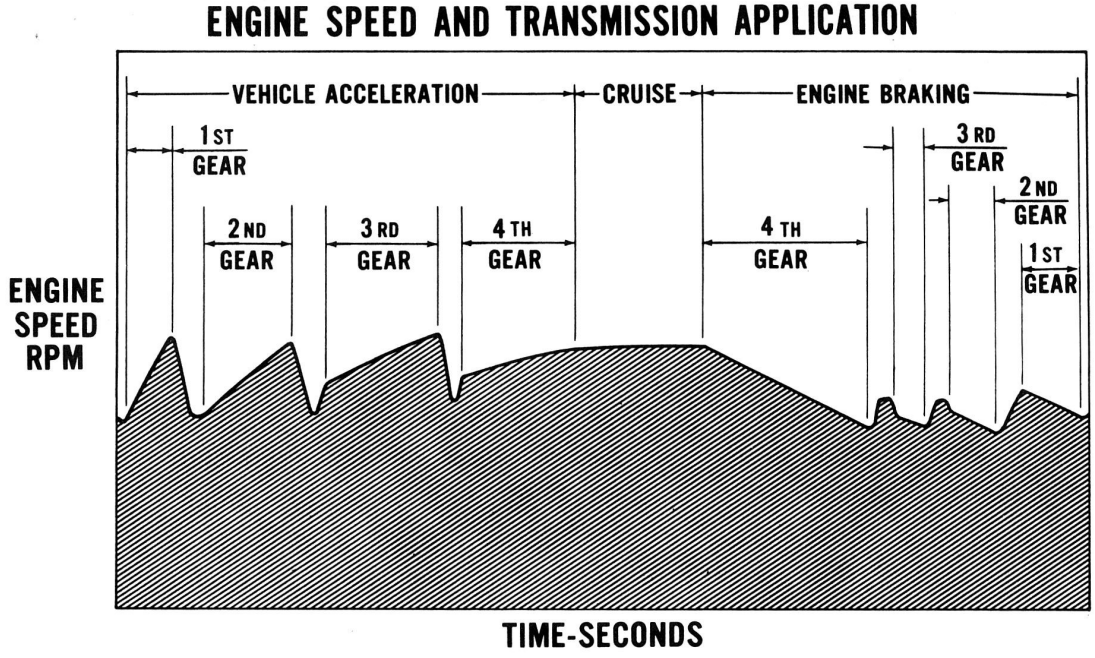

Figure 2

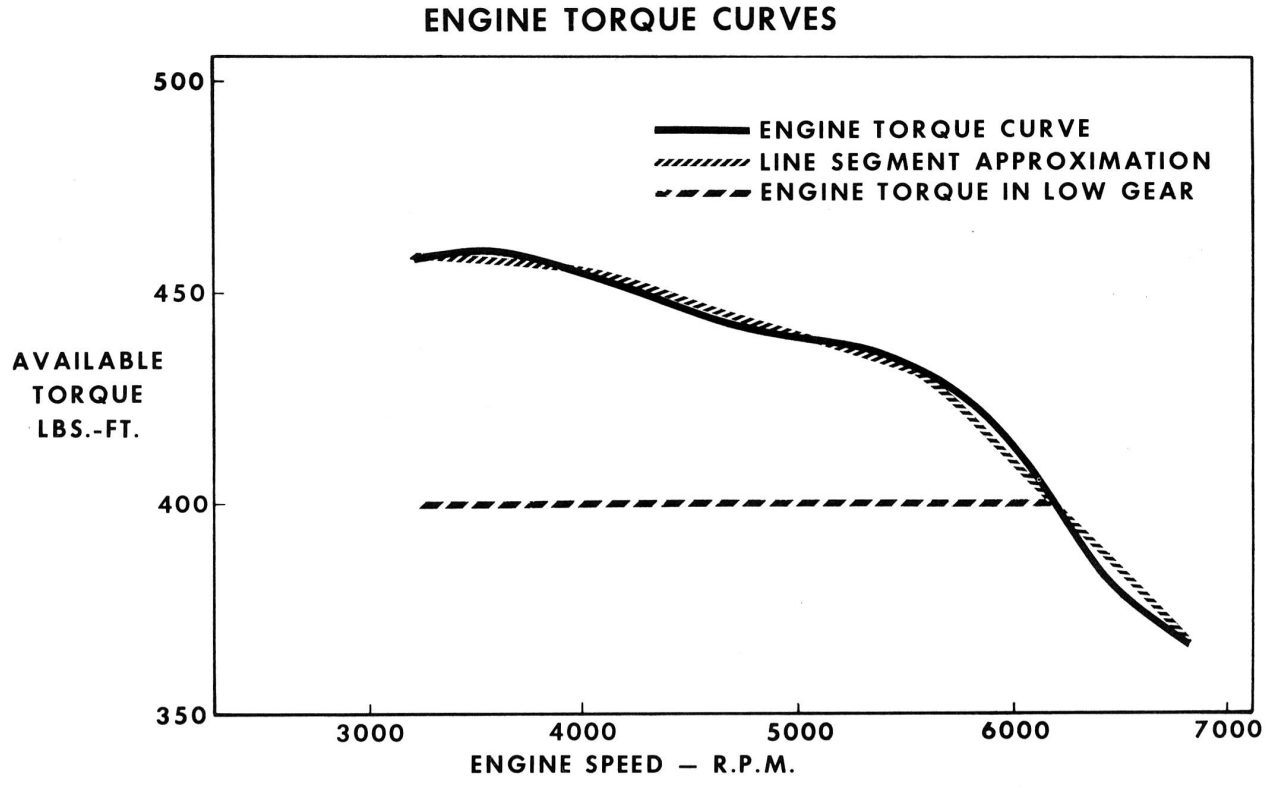

Figure 3

The formula for maximum gear tooth bending stress, as published in an AGMA report, [1]* is given as:

$$S = \frac{3\ \pi\ T_G}{fZN_GX} \tag{1}$$

where S = Maximum Stress, psi
T_G = Torque of Gear, Pounds Inches
f = Face Width of Gear, Inches
Z = Length of Contact, Inches
N_G = Number of Gear Teeth
X = Strength Factor, Inches

If the torque T_G is taken as $T_G = 12$, then the value for stress per ft. lb. of torque is

$$G = \frac{3\ \pi\ 12}{fZN_GX} \tag{2}$$

Also included in this report [1] is an S-N curve for carburized, hardened and shot-peened gears, which for our purpose is represented as:

$$\Gamma = 19 \times 10^{64}\ S^{-12} \tag{3}$$

where Γ = Expected fatigue life, number of cycles
S = Maximum working stress, psi

The engine speed graph with transmission gears under load, as shown in Figure 2, is readily approximated by a series of straight-line segments. All of the segments may be represented analytically by a function linear in time of the form.

$$n(t) = C + Dt \tag{4}$$

where t is restricted to the interval of time, $O \leq t \leq T$ and unless stated otherwise this range is to be assumed, and where

C = the initial engine speed, rpm
D = acceleration, rpm per sec.
t = time in seconds
T = interval of time a gear is in use, seconds.

For the engine torque graph in Figure 3, the line segment approximations can, of course, be represented by a function linear in engine rpm such as:

$$\tau(n) = E + Fn$$

where n has the range, $n(O) \leq n \leq n(T)$ and where

τ = engine torque, ft. lbs. (5)

---

* Numbers in parentheses designate references at the end of paper.

n = engine speed, rpm

E = initial torque, ft. lbs.

F = change in torque, ft. lbs. per rpm

Having developed the engine speed as linear to time and the engine torque linear to speed, it follows that the torque is also linear in time. Its expression as a function of time may be derived by substituting values for speed from equation (4) into equation (5); the result is represented by:

$$\tau\,(t) = A(B-t) \tag{6}$$

where A & B are constants determined by C, D, E and F in the above substitution.

Returning to equation (1) and making use of equations (2) and (6), we find that the maximum stress as a function of time is derived as:

$$S\,(t) = G\,\tau\,(t) = GA\,(B-t) \tag{7}$$

Introducing this expression for stress in equation (3) gives:

$$\Gamma\,(t) = 19 \times 10^{64} \left[GA\,(B-t)\right]^{-12} \tag{8}$$

Equation (8) gives the fatigue life in cycles as a function of time; this may be reduced to life in minutes by:

$$L\,(t) = \frac{\Gamma\,(t)\,R}{n\,(t)} \tag{9}$$

where R is the ratio of the engine speed to the speed of the particular gear.

To establish the expected fatigue life for the total service of a gear, the life function L (t) is integrated over one cycle which is representative of the gear's service. The integration is made through use of Miner's ratio for cumulative fatigue damage [2]; the composite life is expressed as:

$$L = \frac{T}{\int_0^T \frac{dt}{L\,(t)}} \tag{10}$$

where L is given in minutes of composite fatigue life.

Results of the transmission gear life calculations are shown in Table 2; the life in minutes for each gear has been converted to hours of Le Mans service life. The life for each gear as calculated reflects the drive loads only. With the engine braking torques being only 30 to 40%

of the drive torques, the S-N curve, as given by equation (3), is adequate to predict the fatigue life satisfactorily without further allowance for reverse bending stresses from the braking torques. Also, with the transmission in first or low gear, the rear wheel traction torque limits the use of available engine torque to approximately 400 ft. lbs.; this value of torque was assumed constant in calculating the fatigue life for low gear service.

In vehicle operation, rapid release of the clutch throw-out mechanism induces impact loading on the powertrain, which may be several times the normal engine torque. To prevent gear tooth damage from shock loads, extra strength above that required for normal fatigue life was provided as required. The gear tooth bending stresses obtained from equation (1) by using the impact torque value, in place of that for the nominal engine torque, should be under 250,000 psi to avoid premature gear tooth failures.

The fatigue life expectancy of the axle ring and pinion gears and the B_{10} life expectancy of the bearings is established by use of a more general expression. A generalized form is developed by writing equation (3) as:

$$\Gamma(t) = K \times 10^{X} \; (G \; \tau(t) \times R \times E)^{J} \tag{11}$$

where $\Gamma(t)$ = Expected fatigue life in number of cycles for prevailing conditions at time t.

$\tau(t)$ = Engine torque in ft. lbs.

R = Ratio of engine speed to component speed

E = Mechanical efficiency factor

G, J, K and X are constants for a particular consideration.

With n(t) and $\tau(t)$ as given by equations (4) and (6) respectively, the general expression for composite life becomes:

$$\text{Life} = \frac{T \times R \times K \times 10^{X}}{(G \times R \times E)^{J} \sum_{i} \Delta i} \tag{12}$$

where $\Delta i = A_i^J \int_{T_{i-1}}^{T_i} (C_i + D_i t)(B_i - t)^J \, dt$

$$= A_i^J \left\{ \frac{\left[(C_i + D_i T_{i-1})(B_i - T_{i-1})^{J+1} - (C_i + D_i T_i)(B_i - T_i)^{J+1} \right]}{J+1} + D_i \frac{\left[(B_i - T_{i-1})^{J+2} - (B_i - T_i)^{J+2} \right]}{(J+1)(J+2)} \right\} \tag{13}$$

and $T = \sum_{i} (T_i - T_{i-1})$ (14)

These expressions give the expected life in minutes and are applicable if the engine speed is constant or linear to time, and if the torque is not constant but otherwise linear in the interval of time. However, if the torque is constant with a value of A_k ft. lbs. on any interval of time, such as $(T_k - T_{k-1})$, then for this k^{th} interval of time the expression

$$\left[A_k^J \left[\frac{(C_k + D_k T_{k-1})^2 - (C_k + D_k T_k)^2}{2D_k} \right] \right] \quad (15)$$

must be substituted for the more general expression given in equation (13).

In case the speed also is constant at C_k rpm on this interval of time, the expression:

$$\left[A_k^J C_k (T_k - T_{k-1}) \right] \quad (16)$$

is then used in equation (13).

The formula for life as shown in (12) was applied to the transfer gears, as well as the axle pinion and ring gears to determine their Le Mans service life. The composite fatigue life values for these parts are also included in Table 2.

GEAR FATIGUE LIFE

LE MANS SERVICE

TRANSMISSION	NUMBER OF TEETH	USAGE – % TIME DRIVE	USAGE – % TIME BRAKE	LIFE HOURS
1ST GEAR	32	4.8	5.8	37
CLUSTER	15			53
2ND GEAR	27	10.3	3.2	96
CLUSTER	19			80
3RD GEAR	24	12.3	8.4	124
CLUSTER	22			99
MAINDRIVE	23	27.4	17.4	76
CLUSTER	25			61
TRANSFER DRIVE				
DRIVER	30	55.5	29.5	1240
DRIVEN	26			1370
AXLE				
PINION	11	55.5	29.5	470
RING	34			470

Table 2

For the bearing B_{10} life in hours of Le Mans service, the calculations generally follow manufacturers' recommended methods. One exception is for all ball bearing applications, the "equivalent radial load" is taken as being proportional to the radial load; i.e., the conventional Y_2 factor[3] remains constant. Also, in the pinion bearing load analysis, the gear thrust load moment reaction loads are taken at the pilot and rear tapered bearings. The bearing B_{10} life in hours of Le Mans service for each of the various ball and roller bearings, as determined by application of formula (12), are shown in Table 3.

BEARING B-10 LIFE
LE MANS CYCLE SERVICE

LOCATION	TYPE	USAGE — % TIME DRIVE	USAGE — % TIME BRAKE	B-10 LIFE HOURS
CLUTCH				
CRANKSHAFT POCKET	B	27.4	17.4	5000+
TRANSMISSION				
INPUT SHAFT	B	27.4	17.4	69
INPUT SHAFT POCKET	B	27.4	17.4	330
CLUSTER GEAR FRONT	N	27.4	17.4	263
CLUSTER GEAR REAR	N	27.4	17.4	91
OUTPUT SHAFT FRONT	B	55.5	29.5	72
TRANSFER DRIVE				
OUTPUT SHAFT REAR	B	55.5	29.5	88
COUNTERSHAFT FRONT	B	55.5	29.5	453
COUNTERSHAFT REAR	B	55.5	29.5	221
AXLE				
PINION GEAR PILOT	R	55.5	29.5	45
PINION GEAR SHAFT FRONT	TR	55.5	29.5	46
PINION GEAR SHAFT REAR	TR	55.5	29.5	3060
RING GEAR SIDE	TR	55.5	29.5	54
DIFFERENTIAL SIDE	TR	55.5	29.5	476

Table 3

The synchronizer work requirements are best defined by establishing a comparison with known test data on production-type four-speed transmission synchronizers. The number of shifts per synchronizer in Le Mans service is weighted by a work factor established as the energy transfer ratio between Le Mans cycle use and the established test data. The equivalent number of shift cycles for each synchronizer are shown in Table 4. These may be compared to a test average of over 7000 shifts per synchronizer for passenger car applications.

SYNCHRONIZER SHIFT CYCLE REQUIREMENTS

SYNCHRONIZER LOCATION	TYPE OF SHIFT	ENERGY TRANSFER PER SHIFT LBS-FT	WORK FACTOR	NUMBER OF SHIFTS	EQUIVALENT NUMBER OF SHIFTS
1ST GEAR	2-1	1265	3.0	1125	3375
	3-1	2625	4.1	375	1435
2ND GEAR	1-2	1987	4.6	1400	5040
	3-2	749	1.3	1125	1460
3RD GEAR	2-3	1345	3.0	1400	4200
	4-3	864	2.0	1400	2800
4TH GEAR	3-4	1050	2.4	1400	3360

Table 4

The frequent use of transmission gears imposes severe loading upon the synchronizer components, particularly on the gear cone surface and the mating blocker ring cone surface. Energy transfers of up to 2600 lbs. ft. (with over 70% of the shifts above 1000 lbs. ft.) without synchronizer malfunction require that the surfaces of both elements be correctly processed. In particular, the character of surface finish on the gear cone and the microstructure of the blocker ring need to be maintained near an optimum.

The differential drive is a proprietary* item. This locking device consists of two independent (except for the outer race) two-way roll clutches, each one splined to an output shaft. In operation, the unit is not subjected to an excessive number of cycle loads; therefore, analysis is limited to the static load stresses. Published formulae[4] for stresses of similar loadings are applicable and may be used to evaluate the maximum tensile, compressive and Hertz stresses. For a wheel torque of 1250 ft. lbs. (limited by the tractive effort), the tensile stress in the outer race has a range of 35,000 to 75,000 psi, depending upon the locking angle of engagement. Under the same conditions, the inner race Hertz stress ranges from 525,000 to 800,000 psi and maximum compressive stress ranges from 10,000 to 25,000 psi.

*Hi-Torque Engineering Company, Chicago, Illinois

Many of the components, such as the output shaft and the shifter mechanism, are not analyzed for the specific Le Mans loading, since their anticipated loading and usage does not greatly exceed those loadings applied in test to their production counterparts. PVT factors[5] for transmission gears, however, were computed and range from 4.4×10^5 to 2.6×10^6. With the use of an EP-type lubricant suitable for hypoid gearing, no scoring problems were encountered.

Aside from the use of magnesium cases to reduce weight of castings, and the use of bronze shifter forks to reduce wear, no materials, other than those used in production were considered.

Design Evaluation and Development

During the initial design evaluation phase, nearly all of the criteria for lubrication and cooling were established and then implemented from time to time as the program progressed. In addition, several design and process weaknesses were observed and corrected.

The lubrication system of the transaxle, as developed for competition, uses a common lubricant in the axle and transmission sections. A schematic of the system is shown in Figure 4; a single-lubricant pump is used to maintain flow to and from the external cooler.

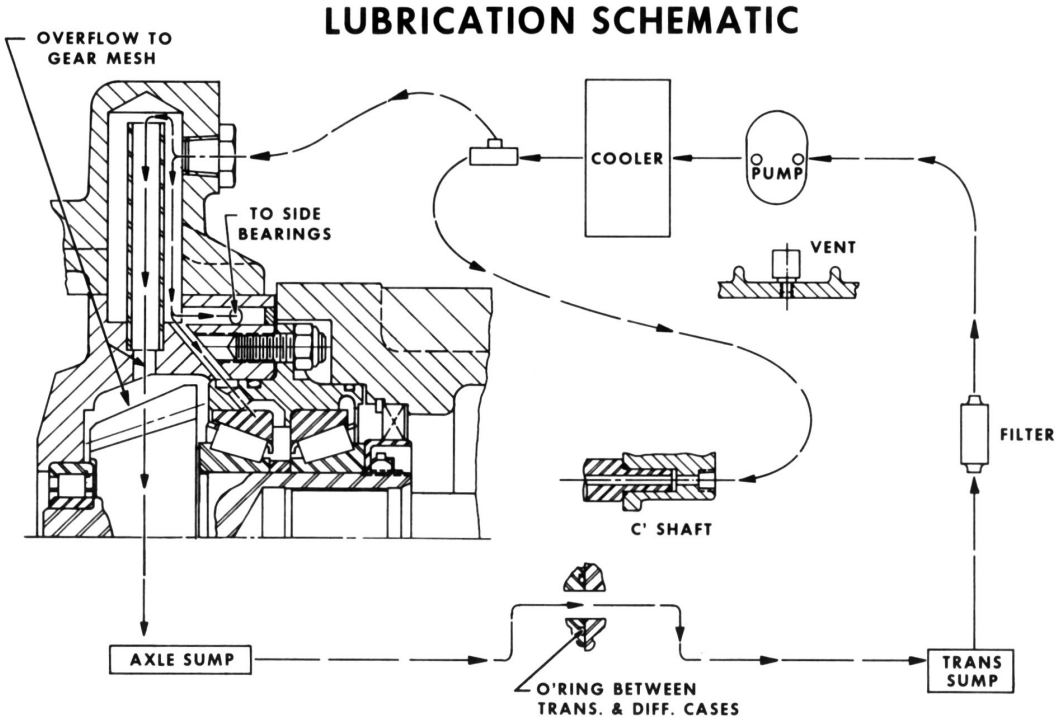

Figure 4

As indicated in this schematic, only the cluster gear needle bearings, pinion and differential tapered-roller bearings are pressure-lubricated. All oil not fed to the bearings is dumped on the pinion gear teeth as they emerge from ring gear engagement. The oil is pumped from a vented sump in the transmission section at a temperature of near $200^{o}F$ through a 40 micron oil filter to an external cooler, and returned at approximately $180^{o}F$ via bearing etc., to the axle sump. From the axle sump, the oil completes its circuit by flowing through mating port holes in each case wall to the transmission sump.

Prior to pressurizing the oil flow to the pinion bearings and also dumping oil on the pinion gear, the pinion gear and bearing supporting tapered bearings failed on test. Because of these failures and also because the bearing B_{10} life was low on the front tapered roller bearing, a larger size bearing (one with eight times longer rated life) was adopted. With the change to larger bearings, the oil flow to these bearings was pressurized, as well as, the oil flow to the differential side bearings. This latter modification not only provided ample lubrication and cooling for the side bearings but achieved satisfactory lubrication in the locking differential. Lack of adequate lubrication had been a problem in the differential. The side-tapered roller bearings splash-feed sufficient lubricant into the differential case through port holes in the end caps.

Deflection in the flywheel housing resulted in frictional heat being generated between the transmission input shaft and its tubular enclosure mounted in the axle case. This condition resulting in a failed clutch and throw-out bearing; it was remedied by increasing the stiffness of the flywheel housing and increasing the clearance between the two interfering components.

A further interference occurred between the transmission input shaft and transmission front ball bearing outer race. This specific problem was unique in that no functional deterioration was observed, and the fault was not found until teardown inspection; although, the bearing outer race had separated into several pieces. The problem was resolved by increasing the clearance between gear face and bearing race.

A third problem arising from deflection in the transmission occurred in the gear pump mounted on the face of the transmission rear cover and driven by a solid coupling to the transmission output shaft. Loading on the pump housing and gears, through the pump drive shaft, resulted in one pump failure and some other near failures. A special flex-coupling was designed and installed between the transmission output shaft and the pump shaft. This new arrangement proved satisfactory.

In vehicle tests, the outer race of one of the transfer drive rear bearings spun and damaged the housing cover. Although the inner race has only a finger-press fit, the spinning occurred at the outer race due to a differential in thermal expansion between the housing and bearing outer race. To avoid this problem occurring when competing in a race, a key was inserted in the cover with a flat ground on the outer race of the bearing.

A transmission gear failed in the 1964 Le Mans race; this particular input gear was one of the early prototypes, and was later found to be dimensionally incorrect in that the oil hole between clutch teeth and gear teeth was out of location. Another gear failure occurred in test at Sebring and was found to be due to faulty shot-peening after heat treat; this was a third-speed constant mesh gear.

The outer race of the locking differential became a problem early in the program. The outer race, in its original design, was too weak and split at the end opposite the ring gear mounting flange. This end of the race was reinforced by increasing its outer diameter to make the wall thickness comparable to that of the flanged end. Other problems, such as heat treat and finish grind, however, continued with this component throughout the program.

Initial set and wear of the drag springs in the locker assembly reduced its functional capability at high speeds. This condition was satisfactorily offset by reducing the amount of initial set in the spring, thus retaining more spring tension, and by controlling the character of the inner race surface on which the spring makes contact.

Static loading on the transaxle assembly to determine the maximum stresses in the housing components revealed the stresses to be well under their yield strength. Deflection studies[5] on the transaxle established the deflection in the axle section under full torque load at ring and pinion to be within acceptable limits.

Initial dynamometer experience paralleled the vehicle test failures closely; i.e., an outer race on the differential failed in dynamometer, and transfer gear bearing outer race damage to the cover was noted. On a subsequent dynamometer run after design changes, the transaxle completed the 48-hour test without incident.

In the clutch mechanism, a straight thrust-type throw-out bearing failed during the initial tests and was replaced by an angular contact bearing. The throw-out lever and fork, consisting of a welded and pinned assembly, encountered problems in obtaining a satisfactory weld; the condition was avoided by closer control of the welding technique.

Summary

The design analysis and test evaluations, after the incorporation of the development improvements, indicated the transaxles would be capable of meeting all operational requirements of the Le Mans race. The potential problem areas, which could never be fully covered, were quality of the components and their proper assembly. A degree of uncertainty, therefore, remained in the complete units throughout the race.

It is not expected that the present designs and stage of development will long retain superior competitive value; the weight and size of the unit are recognized handicaps and may soon require modifications to meet future requirements.

Acknowledgments

Individual contributions by personnel of the Ford Motor Company to the successful design, development and application of the Mark II GT transaxle have been significant, but are too numerous to list all of them individually. Messrs. E. I. Hull, R. D. Negstad and R. C. Lunn, Special Vehicle Activity, Ford Division, are acknowledged as the originators of the preliminary transaxle and clutch arrangements. The finalization of the design and build of the prototype transaxle was done by Standard Transmission Engineering, Experimental Engineering and Axle Engineering Departments, Product Engineering Office, Transmission & Chassis Division. Dynamometer tests were run by the Testing Department, Engine & Foundry Division; vehicle evaluation and track tests were coordinated by Special Vehicle Activity, Ford Division. The Timken Roller Bearing Company made the deflection tests on the ring and pinion axle gears. Thanks are again expressed to the many vendors who supplied component parts and assemblies, and generously supplied engineering data relative to their use in the subject application.

References

[1]H. Wohlers - Bending Stress of Spur and Helical Gearing - Progress Report AGMA 101.02, October, 1951, Section I, Pages 2 and 16.

[2]H. J. Grover, S. A. Gordon and L. R. Jackson - Fatigue of Metals and Structures - NAVAER 00-25-534, 1954, Page 45.

[3]Fafnir Bearing Catalogue No. 56 - Page 4.

[4]R. J. Roark - Formulas for Stress and Strain - Third Edition - McGraw-Hill, 1954, Pages 158 and 288.

[5]J. C. Straub, PVT Values for Gear Teeth Progress Report - AGMA 101.02, October, 1951, Section II.

Mark II-GT Sports Car Disc Brake System

Part I. Design & Development

Joseph J. Ihnacik, Jr.
Ford Motor Co.

Part II. Testing

Jerome F. Meek
Ford Motor Co.

ABSTRACT

The design and development of Mark II GT brake system within the parameters dictated by the Mark I chassis presented many problems. The Mark II GT with its larger 427 cubic inch engine had more weight and much higher performance than the Mark I. Space limitations of the carryover wheels and suspension imposed a severe handicap on individual brake component design. This was compounded by shortening the normal one year development time to a three month period.

Part I of this paper is devoted to the consideration of factors which control the design of a brake. The concept of kinetic energy and its effects on brake performance is reviewed briefly. Use of the ventilated rotor design is explained for applications where severe heat is a problem, as in the case of the Mark II GT.

The development of the brake system from the 24 hour Daytona endurance race to the Le Mans Grand Prix race is reviewed. And unique rotor problems resulting from the various energy loads experienced at Daytona, Sebring and Le Mans are analyzed.

In Part II the brake dynamometer, its automatic programmer and the logic of race simulation duty cycle are described.

Use of Ford's new Reliability Laboratory brake dynamometer for screening of potential rotor designs is explained. In the screening process, dynamometer results proved that significant brake development work can be performed in a laboratory where a race can be simulated under carefully controlled conditions.

INTRODUCTION

When the decision was made to build the first Ford GT sports car in 1964, many studies were conducted to select the ideal engine, drive-train and suspension designs. One chassis system concept selected with virtually no investigation was the brakes. This does not imply that the brake system was subordinated to other vehicle components. On the contrary, good brakes were considered of paramount importance. It was believed, however, that disc brakes were the only logical choice. Over the years, disc brakes have created a very favorable impression in the world of sports cars, and there was no doubt that pound for pound the disc brake was more efficient than the conventional drum brake. Therefore, if disc brakes were not selected, an entirely new braking concept would have been required. This idea was discarded as not feasible within the available time. The selection of disc brakes was justified during the past racing season, as in part the success of the Mark II GT can be attributed to the brake system.

Since the Daytona and Sebring victories were crowned with an impressive Grand Prix win at Le Mans, it is appropriate to reflect briefly on the events that led to the universal

adoption of disc brakes for Grand Prix cars. Disc brakes were introduced at Le Mans during the 1952, 24 hour Grand Prix race, and with each succeeding year more and more entries favored disc brakes. In June of 1953 the race was won by a Jaguar equipped with disc brakes. During the 2540 miles of the gruelling race both lining life and overall performance of the brake system were highly impressive. This practical demonstration of improved braking, coupled with satisfactory durability, contributed to the general acceptance of the disc brake for sports cars as the ten year trend shown in Figure 1 indicates.

Durability was by no means the only motivation for the acceptance of disc brakes. It must be agreed that disc brakes fitted with competition brake linings also have a high resistance to fade, which in part accounts for the linearity of the disc brake torque. The linear response of disc brakes with smooth progressive action permits drivers to go deeper into turns before braking, thus gaining vital seconds on every lap. These characteristics of linear response and resistance to fade under repeated brake applications must be considered as prime factors in the switch to disc brakes. By 1963, just ten years after the first successful demonstration of the disc brake at Le Mans, all entries were so equipped.

This optimistic picture does not imply that all GT sports car brake problems were solved with the adoption of disc brakes. It is interesting to note that after 13 years of disc brake development on the Grand Prix circuits — since the 1953 Jaguar victory — brake engineers are still faced with unresolved problems. Rotor failures, fluid boil and short lining life are just a few of the problems that must be coped with today. One possible explanation for this dilemma is that the 1953 race was won by the Jaguar at an average speed of 105 mph. The 1966 Ford Mark II GT Le Mans winner averaged 125 mph, an increase of 19 per cent. To achieve the average speed of 125 mph, the engine, drive-train and other chassis components of the Mark II were increased substantially in size and weight over the C-type Jaguar. The combination of high speed and weight of the Mark II GT imposed an unprecedented heat load on the disc brakes, and there is no indication that the trend to the use of higher horsepower engines on the GT sports cars is leveling off. It can be safely speculated that demands on brakes will be even greater in years to come. This will be especially true of the cars equipped with automatic transmissions.

How the original Mark I sports car brake system was up-graded to dissipate the higher Mark II heat loads with minimum changes to other vehicle components is described in Part I of this paper. Highlights of the Daytona, Sebring and Le Mans Grand Prix races as well as some of the unique problems encountered will be discussed. Part II of the paper describes the accelerated development work made possible with the aid of Ford's new brake dynamometer.

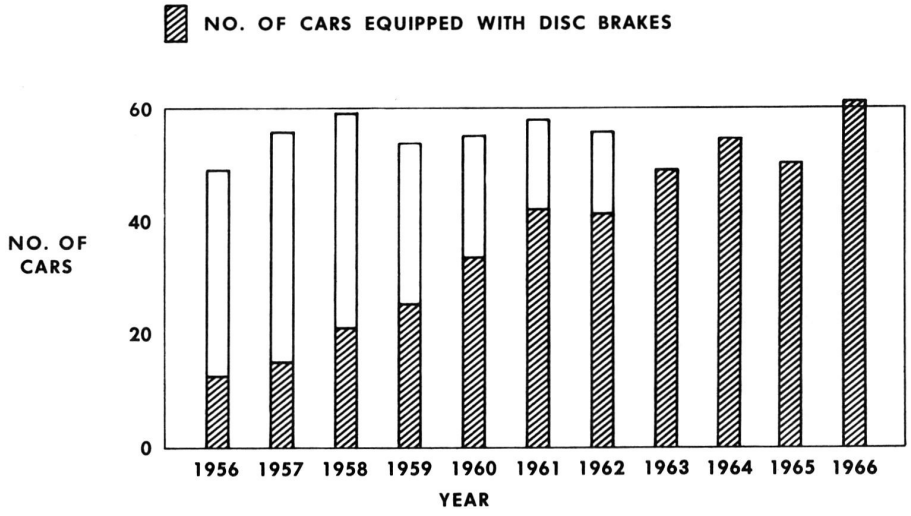

Figure 1 — Le Mans entries showing trend to disc brake usage

PART I
DESIGN AND DEVELOPMENT

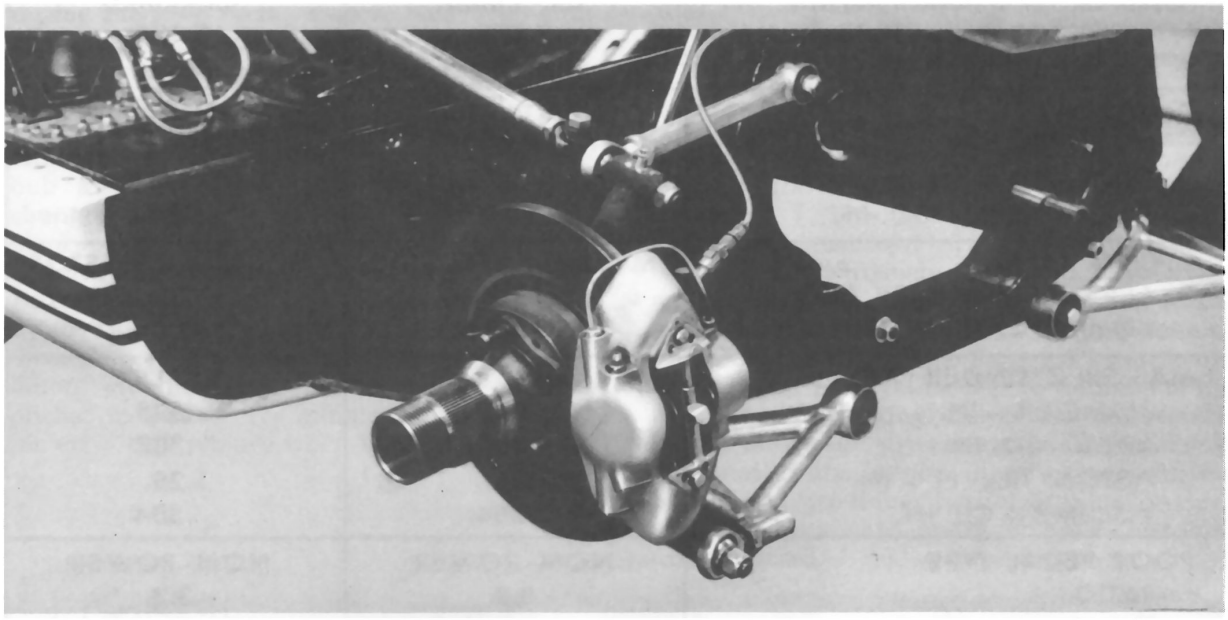

Figure 2 – Mark I GT brake assembly showing the original 1/2 inch solid rotor

BRAKE DESIGN FEATURES

The design of the Mark II disc brake system was governed to a great extent by the parameters established for the 289 cu. in. Mark I GT brake shown in Figure 2. As frequently happens in the racing business, a last minute decision was made to increase the performance of the car. To achieve this, a new 427 cu. in. engine was installed, with the necessary chassis modifications to support the new engine. These changes increased the car weight by approximately 500 pounds to a gross weight of 2860 pounds (Figure 3). The change produced an extremely heavy high performance vehicle with relatively low performance brakes originally designed for the lighter and slower car. Any plans to up-grade the brakes at this point were limited to these guide-posts:

WEIGHT (GROSS), LB.	2860
FRONT (38%)	1087
REAR (62%)	1773
WHEEL BASE, IN.	95
TRACK, IN.	
FRONT	57
REAR	56
TIRE SIZE	
FRONT	9.75-15
REAR	12.80-15

Figure 3 – Mark II GT general specifications

- Four wheel disc brakes
- Ventilated rotors
- Heat sink capacity of disc limited only by the available space
- Fixed calipers with floating pistons modified to accommodate new rotors
- Carryover wheels and suspension
- Minimum change to existing vehicle design

To meet these objectives in the relatively short space of time, we initiated a joint development program with the Kelsey-Hayes Co.

MARK II GT BRAKE SYSTEM SPECIFICATIONS

	FRONT	REAR
CALIPER TYPE (GIRLING/KH)	CR - FIXED	BR - FIXED
CYLINDER DIAMETER – IN.	2.375	2.125
CYLINDER AREA – SQ. IN.	4.43	3.55
ROTOR TYPE	VENTILATED	VENTILATED
DIAMETER – IN.	11.56	11.56
THICKNESS – IN.	.775	.775
SWEPT AREA – SQ. IN.	133	133
LINING TYPE	MOLDED ASBESTOS	MOLDED ASBESTOS
AREA – SQ. IN. PER SHOE	10.9	7.0
VOLUME – CU. IN. PER SHOE	6.5	2.8
MASTER CYLINDER TYPE	DUPLEX	DUPLEX
DIAMETER – IN.	.625	.625
AREA – SQ. IN.	.307	.307
PISTON TRAVEL – IN.	1.25	1.25
VOLUME – CU. IN.	.384	.384
FOOT PEDAL TYPE	NON-POWER	NON-POWER
RATIO	3.3	3.3
TRAVEL – IN.	4.1	4.1
BRAKING DISTRIBUTION (DESIGN)	55	45

The solid 1/2 in. rotors originally designed for the Ford GT-40 sports car were replaced with 3/4 in. ventilated rotors shown in Figure 4. Girling type CR front calipers with opposed 2.375 in. diameter pistons were modified in the bridge area to accommodate the vented rotor. Similarly, the type BR fixed rear calipers with opposed 2.125 in. pistons were also modified to accommodate a common 3/4 in. rotor.

Additional system changes incorporated were new integrally molded RM-4528-19M shoe and lining assemblies and EPT (Ethylene-Propylene-Terpolymer) brake cylinder seals to cope with the 300° F (plus) fluid temperatures. The intense heat generated at the interface of the lining pad and rotor is conducted to the fluid by the high metallic content of the friction material, through the steel pistons. Additional heat is picked up directly by the caliper housing through the process of radiation. The total effect of the transient heat resulted in occasional vaporization of brake fluid during the development stage. Periodic flushing of the hydraulic brake lines with Dow HD-50-4 brake fluid to purge the system of moisture, combined with improved ram air ducting, have virtually eliminated the fluid boil problem. Although other brake components have undergone changes to improve their performance,

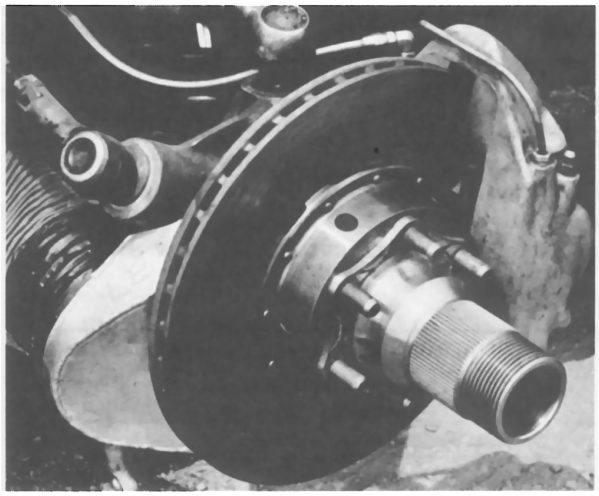

Figure 4 – Mark II GT sports car disc brake with 3/4 inch ventilated rotor

the lining, seal and fluid compounds continue to provide satisfactory service.

Two notable design improvements of a convenience nature prompted by the need for rotor and lining changes paid off handsomely during the 1966 racing season. Phil Remington of Shelby-American developed a quick-change brake pad retainer, shown in Figure 5, which facilitates removal and replacement of brake lining pads. During the same period John Holman of Holman-Moody redesigned the hub and rotor assembly to speed up rotor changes during the pit stops. The new design incorporates outboard mounting of the rotor and hat section assembly as shown in Figure 6. Retention of the rotor assembly is accomplished by the wheel; and braking torque is transmitted through the wheel drive lugs. New rotor installation with this arrangement can be accomplished in four to five minutes, while a skilled pit crew can replace worn lining pads in one to two minutes. Normally these changes are accomplished during a fueling stop to reduce pit time to a minimum. The merit of both components was amply demonstrated during the 1966 racing season. There is no doubt that the adoption of these features by other racing teams is imminent. The 1967 racing season will certainly see a greater use of quick-change brake components.

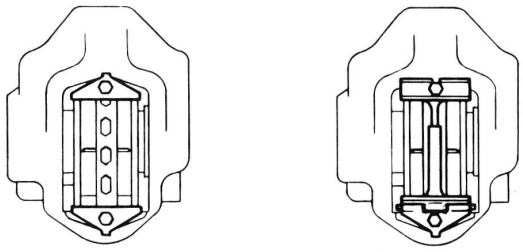

Figure 5 – GT brake lining pad retention brackets

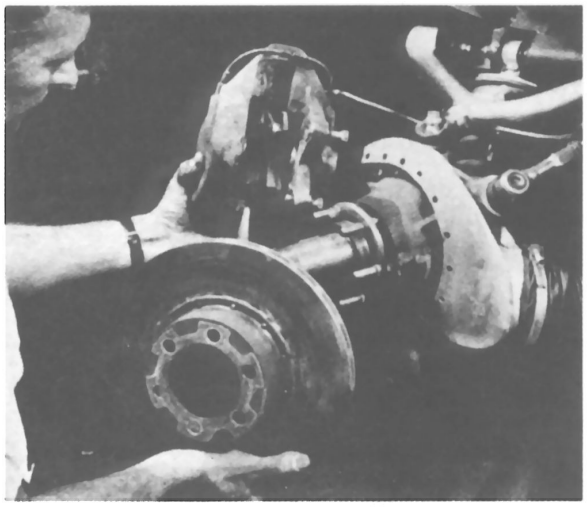

Figure 6 – Mark II GT brake assembly with quick-change rotor

The final brake design feature which merits a brief explanation is the whipple tree master cylinder and brake pedal arrangement shown in Figure 7. This balancing beam and push-rod arrangement carried over from the Mark I sports car is extremely functional. It provides a wide range of adjustment in braking forces at the front and rear wheels by simply shifting the fulcrum point on the threaded beam in the brake pedal pushrod sleeve. In addition to the flexibility in braking distribution adjustment to suit individual drivers and track conditions, the dual brake system has served a useful purpose in providing partial braking on several occasions when hydraulic brake line failures occurred.

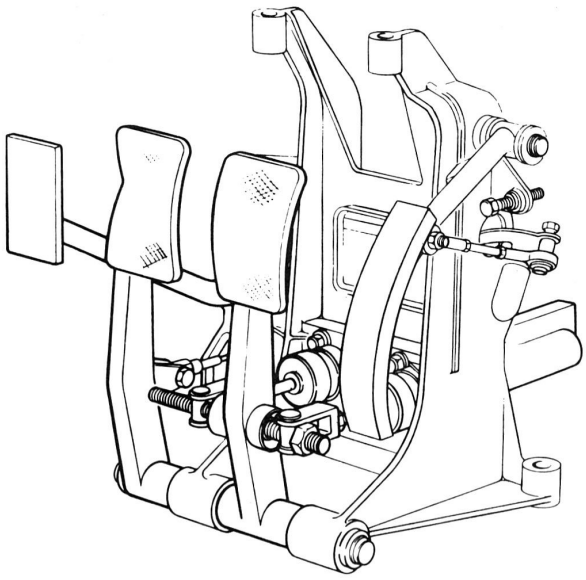

Figure 7 – Mark II pedal support bracket and brake master cylinder assembly

PERFORMANCE

Braking capacity, which determines the ability of a vehicle to slow down or stop, is without a doubt one of the principal factors that must be considered in the overall performance of a sports car. Unlike the Indianapolis

500 vehicles which use brakes primarily for pit stops, the sports cars rely heavily on the brakes to maneuver the hairpin turns of the Grand Prix circuits. Brakes are applied with punishing frequency for 12 to 24 hour periods.

While a detailed analysis of a braking vehicle is beyond the scope of this paper, a few significant factors affecting the vehicle's state of motion are pertinent and will be mentioned briefly.

The major forces affecting the deceleration of a vehicle are:

- Wheel braking force
- Engine braking
- Inertia of rotating parts
- Aerodynamic drag
- Rolling resistance

Influence of air resistance as a decelerating force is small at normal vehicle speeds, particularly for streamlined vehicles. For high speed vehicles the air resistance aids braking action and should be considered where accurate results of energy conversion rates are required.

In the case of a vehicle equipped with an automatic transmission, the rotating-mass effect of wheels and transmission must be added to the translatory mass of the vehicle. In the case of Mark II equipped with an automatic transmission it can be safely assumed that the effect of the aerodynamic drag cancels the inertia force of the wheels and transmission.

Braking potential of an engine can be utilized only with drive-trains that have a positive connection between engine and axle. This form of braking is particularly feasible for low values of deceleration. To achieve high rates of deceleration on hairpin turns, brakes are applied very suddenly, minimizing the engine braking effect. Frequently, in such cases of high deceleration the engine requires mechanical braking effort to synchronize the speeds of rotating parts for smooth shifting of gears. Depending on the inertia of the engine and the gear reduction ratio, a critical value of deceleration can be calculated above which the engine should be disengaged for optimum braking effect.

In stopping a moving vehicle, the brake performs an important function — that of converting energy of motion into heat. The temperature reached by the brake system during this process greatly affects the behavior of the rotor and the lining. Consequently, it is important to understand the concept of converting the kinetic energy of a moving vehicle into heat energy.

The prime factors to consider in determining the required braking performance are gross weight and the maximum speed of a vehicle. These factors are important because the kinetic energy of a moving vehicle varies as its weight and the square of its speed, or

$$E = \frac{Wv^2}{2g} \qquad (1)$$

where

E = Kinetic energy (ft-lbs)
W = Gross weight of the vehicle (lbs)
v = Maximum velocity of the vehicle (ft per sec)
g = Gravitational conversion factor (32.2 ft per sec^2)

Figure 8 shows graphically the effect of the velocity factor on the instantaneous energy of a Mark II vehicle. The concept of kinetic energy points out that a high speed vehicle requires brakes having a greater energy conversion and heat dissipation capacity.

If the rate of deceleration of a vehicle is known and if engine and aerodynamic braking forces are neglected, the rate of heat production at the surface of the brake rotor by the conversion of kinetic energy may be developed from the basic energy equation

$$E = 1/2\ mv^2 \qquad (2)$$

for

$$v = at \qquad (3)$$

$$E = 1/2\ ma^2t^2 \qquad (4)$$

where:

m = Mass in slugs
t = Time in seconds
a = Deceleration (ft/sec/sec)

taking the derivation of E with respect to time we obtain the rate of energy conversion to heat

$$\frac{dE}{dt} = 1/2\ ma^2 \times 2t \frac{dt}{dt}$$

$$\frac{dE}{dt} = ma^2t \qquad (5)$$

and since a = v/t the equation may be reduced to

$$\frac{dE}{dt} = \frac{ma\,(v)\,t}{(t)}$$

$$\frac{dE}{dt} = ma\,v \qquad (6)$$

It can be seen that the rate of heat production is proportional to the velocity. It is highest at the instant of brake application when the speed is maximum and gradually decreases until it reaches zero, when the wheel stops rotating.

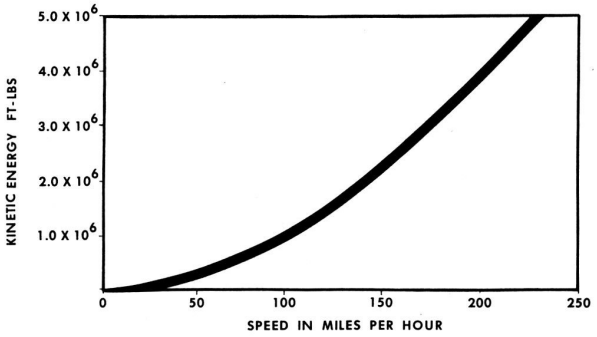

Figure 8 — Instantaneous kinetic energy curve of a Mark II GT plotted as a function of speed

THERMAL ASPECTS OF DISC BRAKE DESIGN

In the foregoing section, elementary equations of motion and relationships between forces acting on a vehicle in decelerating were discussed. However, braking performance limitations imposed by the energy conversion rate in the brake and the accompanying temperature rise in both the rotor and the lining were not considered. It is known that the brake performs an irreversible conversion of kinetic energy into heat. This conversion is a frictional process which takes place at the interface of the rotor and the lining. Heat created in the process raises the temperature of the friction surfaces. In the design of a brake system for a sports car severe brake applications of short duration are a rule rather than an exception. Under these conditions, equilibrium between the frictional heat generated in the brake and the heat dissipated by the brake to the surrounding air is of vital importance, as it affects the size and weight of the system. To provide a brake system capable of dissipating the heat generated during braking requires a knowledge of the thermal characteristics of disc brakes.

An investigation of the steady state heat characteristics of brake rotors conducted by Ford and Kelsey-Hayes engineers showed very graphically the advantage of a ventilated over a solid rotor of equal weight for energy conversion and heat dissipation under repeated brake applications. Figure 9 shows the results of a series of brake applications under controlled conditions for a solid and a ventilated rotor. For the steady state condition shown, the ventilated rotor reached a peak equilibrium temperature of 700°F after eight cycles. Equilibrium temperature is defined as the point at which the heat loss between brake applications

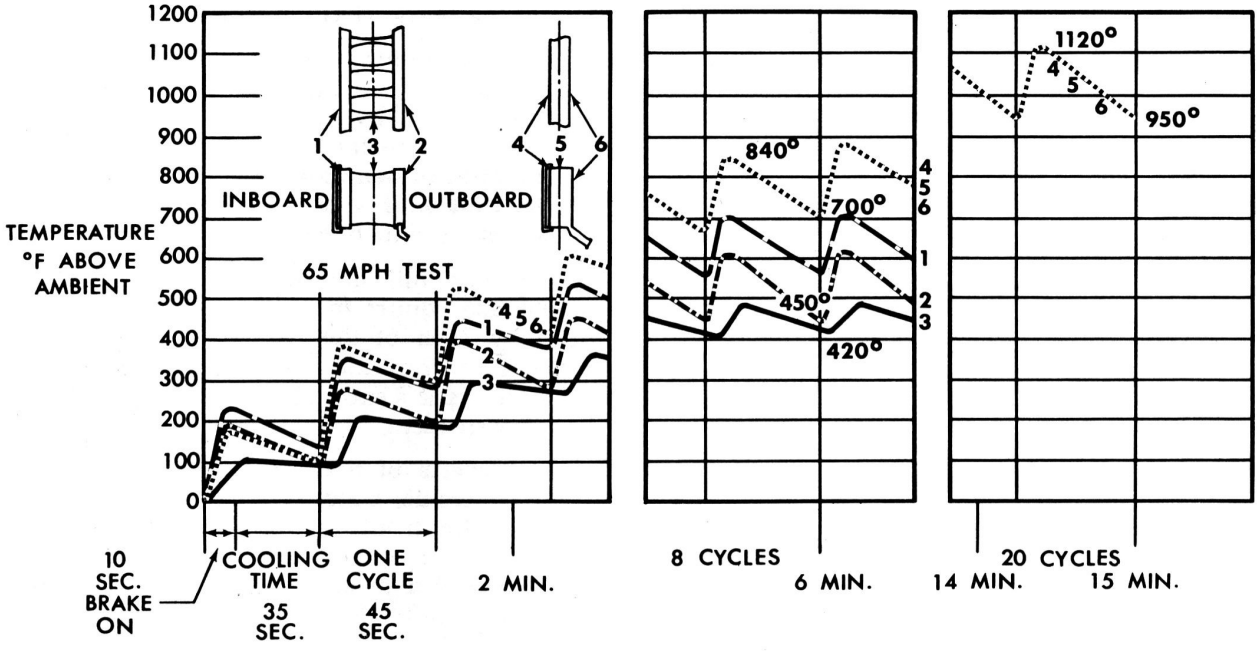

Figure 9 — Steady state temperature curves for solid and ventilated rotors of equal mass

is equal to the heat generated during braking. Eksergian (1)* Fazekas (2) and Petrof (3) have explored experimental and theoretical aspects of transient temperatures under these conditions. The solid rotor, because of its lower potential for dissipating heat attained a considerably higher peak equilibrium temperature of 1120°F. In the case of the solid rotor more of the kinetic energy converted to heat during each braking cycle is retained by the mass of the rotor due to less heat dissipation during each cooling cycle. As the curves in Figure 9 verify, subsequent brake applications drive the rotor to the higher equilibrium temperature.

When the brake is applied more heat is generated than dissipated, resulting in rotor temperature rise. This temperature rise during braking may be expressed in equation form as

$$T = \frac{E_h}{778\ wq} \qquad (7)$$

Where: E_h = Kinetic energy converted to heat (ft-lbs)

w = Weight of brake rotor (lbs)

q = Specific heat of the rotor material Btu per lb per degree F

Having established the temperature rise for a given brake stop, the measure of overall performance can be determined by equating the heat dissipation rate between brake application against the energy conversion rate.

HEAT LOSS

As we have stated earlier, in the case of the solid rotor, the rate of heat loss by radiation is relatively small in comparison to the rate of energy conversion to heat by the brake. However, radiation is one of two effective means for heat dissipation. The rate of heat loss by radiation can be determined as follows:

From Stefan-Boltzmann law of radiation

$$E_h = \sigma (T_2^4 - T_1^4) \qquad (8)$$

Where: T_1 = Ambient temperature (°R)

T_2 = Temperature of exposed rotor surface (°R)

σ = 0.174×10^{-8} Btu/Sq Ft/Hr/°R^4 (9)
Based on King's "Basic Laws and Data of Heat Transmission".

Combining Equation 8 and 9 a general equation for the rate of heat loss can be established

$$H = \frac{\sigma \xi A_s (T_2^4 - T_1^4)}{3600} \qquad (10)$$

Where: H = Rate of heat loss (Btu per sec.)

A_s = Area of exposed disc surface (sq. ft.)

ξ = Emissivity coefficient

Based on an emissivity coefficient ξ of .8 and a Stephan-Boltzmann constant of radiation of $.174(10^{-8})$ Btu per hour per square foot per degree Rankine to the fourth power the rate of heat loss becomes

$$H = .386\ (10^{-12})\ A_s\ (T_2^4 - T_1^4) \qquad (11)$$

In the case of the ventilated rotor there is still another effective way of heat transmission — that of forced convection made possible by the rapidly moving air stream directed into the vents of the rotor. Theoretical and experimental work by Petrof (3) Eksergian (4) Newcomb (5) and Koffman (6) support the generally accepted fact that ventilated rotors are superior to solid rotors for heat dissipation by convection. It was logical to conclude that a ventilated disc brake rotor offered the best short range solution for the Mark II GT brake design.

In the previous section it was stated that the largest part of the heat exchange in the brake is accomplished by radiation and convection from the rotor surface area to the ambient air. The amount of heat convected is a function of the size and quality of the contact surface and the velocity and turbulence of the air flow.

To take full advantage of the approximately 325 square inches of surface area provided by each of the ventilated rotors we installed air scoops and ducts as shown in Figure 10 to direct a steady stream of cooling air to the rotor surface.

The effects of the ram air were evaluated at the Riverside, California track with excellent results. The front brake rotor temperature, where the air stream has a relatively direct path, showed a drop in peak surface temperature from 1500° F. to 1250° F. Directing an

** Numbers in parentheses designate references at the end of the paper.*

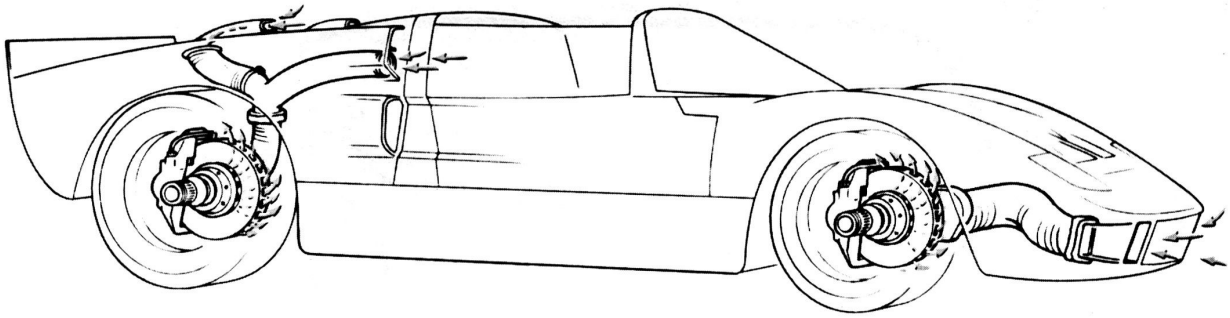

Figure 10 — Mark II GT ram-air brake cooling ducts

air stream to the rear brake presented a more serious problem. The air at the rear of the Mark II is generally at a lower pressure and is more turbulent than that at the front of the vehicle. But the most serious obstacle to an adequate air duct is the limitation imposed by the engine and transaxle package. One solution to this problem was used with some success at Sebring and Le Mans. A periscope-like air scoop mounted on the rear deck reached out into the high velocity air stream to supplement a weaker stream channeled from the rear quarter body scoop. The success of these air ducts can be measured in part by the reduction in rotor surface temperatures, but equally important is the side effect of lower brake fluid temperatures and improved lining life. Since the improved air ducts were incorporated, the problem of fluid vaporization has been virtually eliminated.

TWENTY-FOUR HOUR DAYTONA CONTINENTAL RACE

Because the sports car brakes must be capable of performing at high speeds under varying track and climate conditions, many factors must be taken into consideration in their design. The final brake design must be tested thoroughly under actual operating conditions to assure that the desired characteristics and performance have been obtained. This phase of development of the Mark II GT sports car brakes was spread over a three month period, culminating with a 72 hour "run in" at Daytona. Although all brake components were evaluated, the main purpose of the test was to develop a durable rotor.

After reviewing all considerations with respect to thermal shock, mechanical strength and resistance to wear, we specified a high grade of cast iron with randomly oriented graphite flakes. To provide assurance that the friction surface will not spall under the severe braking loads required to control the car on the Daytona circuit, we utilized a flame spraying technique to apply a thick coating of silicon carbide in a matrix of copper. The flame sprayed coating resists wear and has a high coefficient of friction and thermal conductivity. Test results obtained during the "run in" prior to the race confirmed the fact that the iron and spray coating specified were suitable materials.

The Daytona International Speedway shown in Figure 11 is a 3.81 mile course consisting of 2.5 miles of high banked speedway course and 1.31 miles of twisting infield roads. This course proved to be a formidable test for the Mark II brakes. In the skillful hands of drivers like Ken Miles, Lloyd Ruby and Bruce McLaren, the Mark II GT responded with speeds up to 196 mph on the banked speedway course. To enter the winding infield course, cars must decelerate violently to 45 or 50 mph at the No. 1 braking zone. The car is accelerated to 120 mph on the eastbound infield straight. Reaching the end of the straight, the car must decelerate to 45 mph at zone 2. Coming out of the southbound turn, the car accelerates to 125 mph and snubs down to 110 on the southbound leg. Once again the car is decelerated to 30 mph to navigate the hairpin turn. The final leg of the infield course is limited to approximately 107 mph before the 5th and final braking zone is reached.

In braking the car from the speeds just described, the brakes must convert the kinetic energy of a moving vehicle into heat energy. From Equation 1 the energy of a moving vehicle may be expressed as

$$E = \frac{WV^2}{2g} \frac{(88)^2}{(60)^2} \qquad (12)$$

Where: V = Instantaneous velocity (mph)

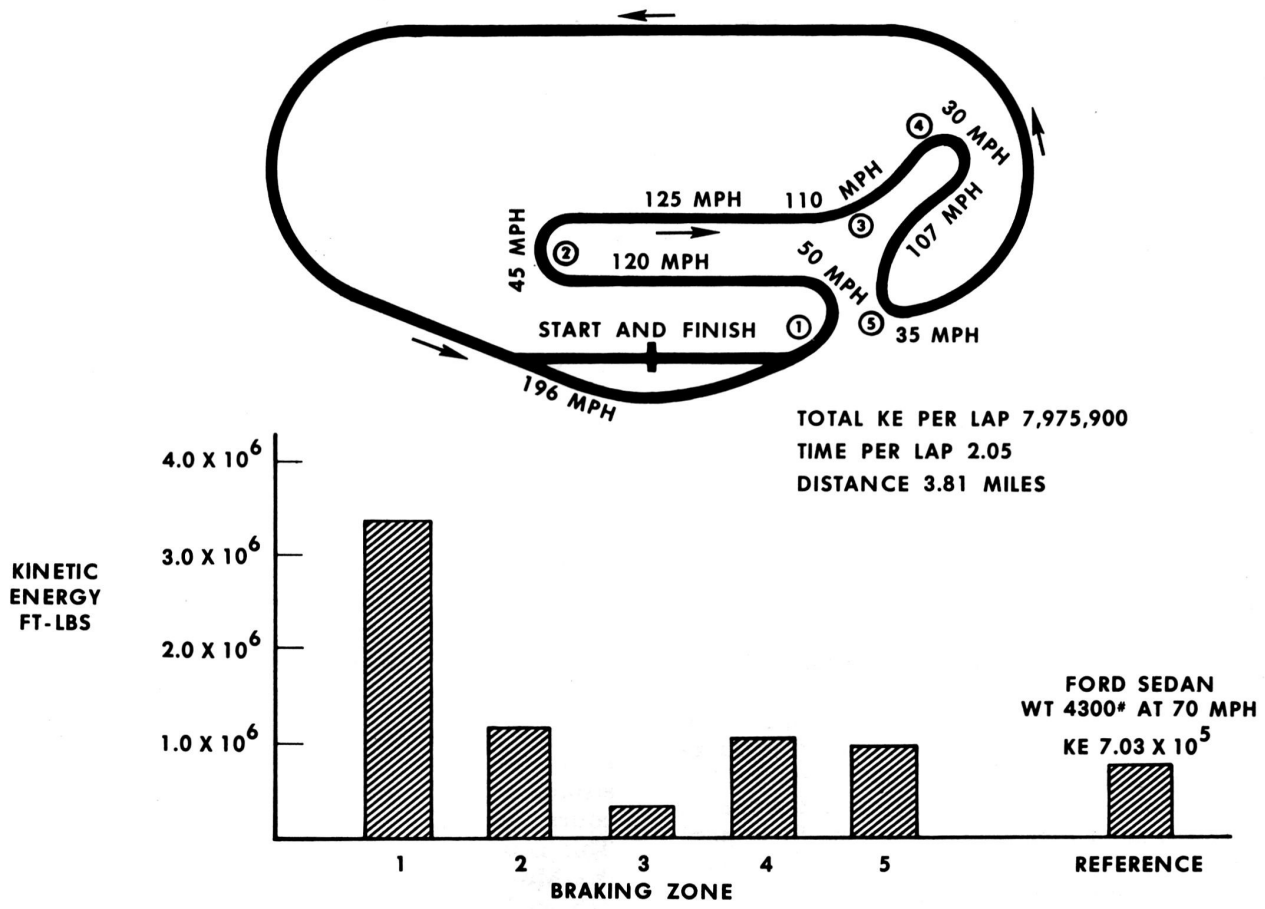

Figure 11 — Daytona International Speedway showing braking zones and the approximate energy converted to heat at each zone

But Equation 1 applies only to the case of a vehicle brought to rest. A vehicle decelerating from 196 mph to 50 mph at braking zone No. 1, the kinetic energy remaining at velocity V_2 is E_2 and the kinetic energy (E_h) converted to heat, if engine and aerodynamic braking forces are neglected, becomes

$$E_h = E_1 - E_2$$

$$= \frac{W(V_1^2 - V_2^2)}{2g} \qquad (13)$$

$$= \frac{2860\,(196^2 - 50^2)\,(88)^2}{2(32.2)\,(60)^2}$$

$$= 3{,}430{,}700 \text{ ft.-lbs.}$$

The values of the kinetic energy for stops 2, 3, 4 and 5 can be derived in the same manner. Plotting these values of the energy converted to heat against the braking zone produces a graphic profile of the heat energy that must be dissipated to the atmosphere on each lap of the course. Some appreciation of the amount of energy that is involved may be derived from Figure 11 by referring to the 703,000 ft-lbs of kinetic energy of a 4300 pound Ford sedan traveling at 70 mph (102.7 ft per sec). This energy is equivalent to 904 Btu of heat which must be dissipated in making a complete stop from 70 mph.

Neglecting the effect of aerodynamic drag, engine braking and rolling resistance, and assuming that the vehicle rate of deceleration was approximately 18 ft per sec^2 the time required to slow the Mark II GT from 196 mph to 50 mph is

$$t = \frac{(V_1 - V_2)\,(88)}{a\,(60)} \qquad (14)$$

$$= \frac{196 - 50\,(88)}{18\,(60)}$$

$$= 12 \text{ sec.}$$

And since power is defined at the time rate of doing work, the average power developed by the brakes in retarding the vehicle from 196 to 50 mph is

$$P_a \text{ (Average power)} = \frac{\text{work done}}{\text{time taken to do the work}}$$

$$= \frac{3{,}430{,}700}{550 \times 12} \qquad (15)$$

$$= 520 \text{ hp}$$

Some measure of the efficiency of the brake system may be derived from the fact that the 520 hp is dissipated by 60 pounds of rotor iron and 12 pounds of shoe and lining assemblies.

Frequently the load on a brake is judged by the power at initial application, that is, initial energy rate. This value is based on the fact that the brakes of a moving vehicle begin to convert kinetic energy to heat at the moment the brakes are applied. The rate of energy conversion is initially high, but decreases with speed until both speed and power are zero. The instantaneous power developed by the brakes in stopping from 196 mph may be expressed as follows:

$$P_i = \frac{WaV\,(88)}{550g\,(60)} \qquad (16)$$

$$= 8.29\ (10^{-5})\ WaV \qquad (17)$$

Where: P_i = Instantaneous power developed by brake (hp)

W = Weight of car (lbs).

a = Deceleration (ft/sec/sec)

V = Instantaneous velocity (mph)

Assuming the average rate of deceleration for the Mark II to be 18 ft/sec^2, the power developed by the brakes at zone No. 1 at initial velocity of 196 mph is

$$P_i = 8.29\ (10^{-5})\ (2860)\ (18)\ (196)$$

$$= 836 \text{ hp}$$

The ability of the brake to carry the power burden imposed upon it is related to the area of the brake surfaces. The ratio of the instantaneous power (P_i) and the effective area (A) of the friction contact surface in sq. in. is called the "power density". Thus, the Mark II with approximately 55 per cent of braking, at the front wheels generates a front brake power density of

$$P_i = .55\ (8.29)\ (10^{-5})\ \frac{WaV}{A} \qquad (18)$$

$$= \frac{.55\ (836)}{435}$$

$$= 10.7 \text{ hp per sq. in. of lining}$$

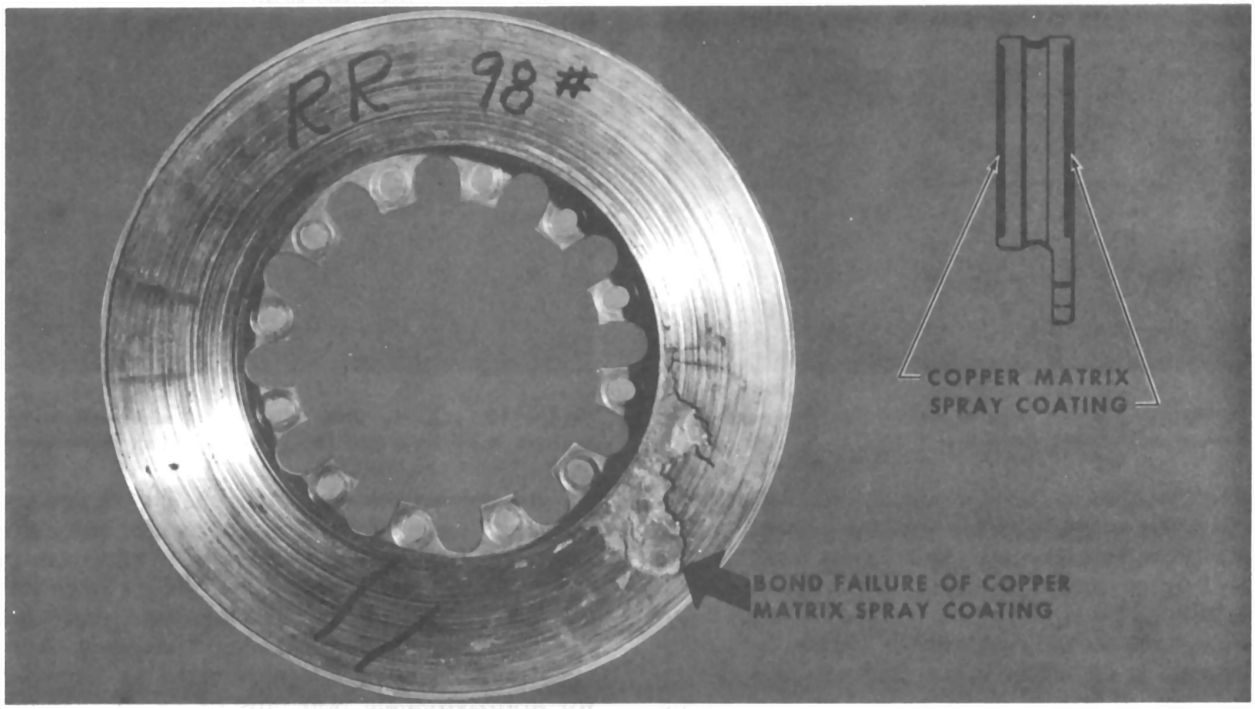

Figure 12 – Daytona Mark II GT brake rotor removed from car No. 98 after 18 hours

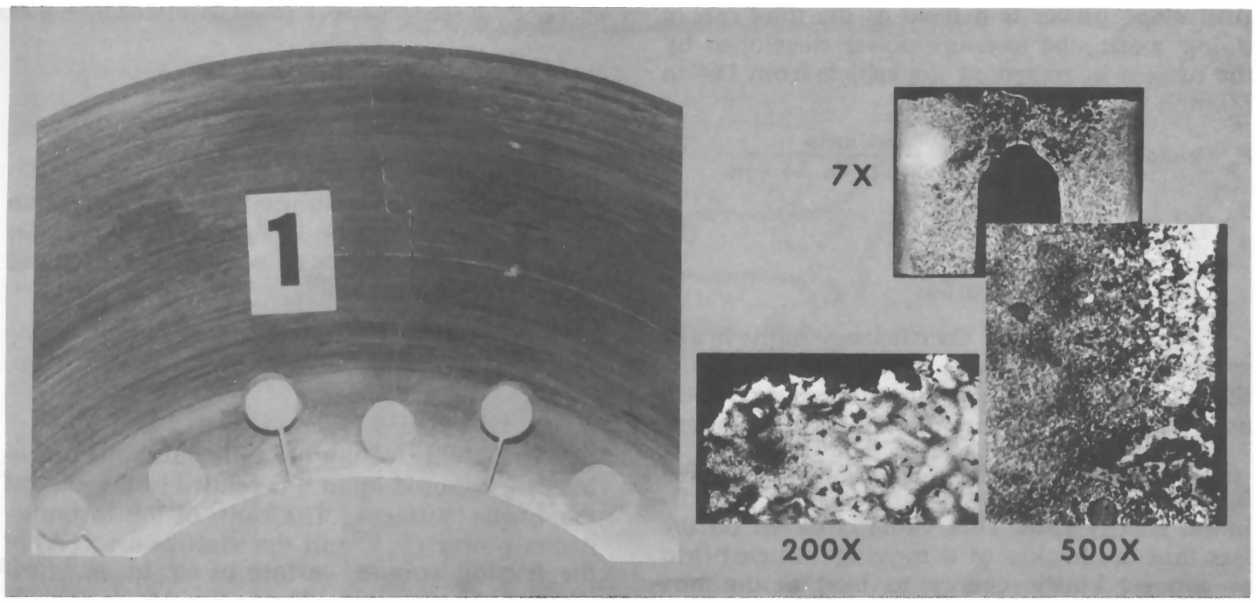

Figure 13 — Microstructural analysis of a development rotor showing heavy shrink and heat checks

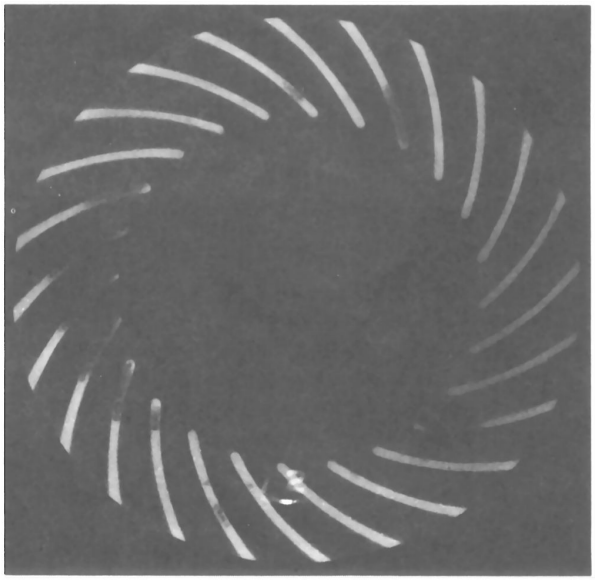

Figure 14 — X-ray view of a poor rotor casting showing dark areas of heavy shrinkage

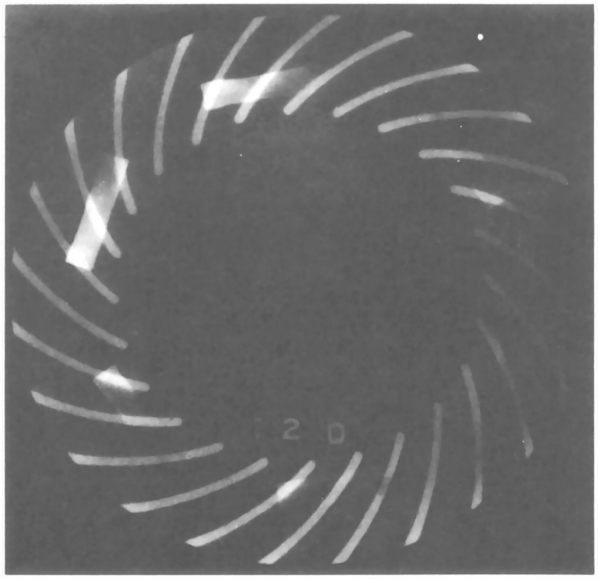

Figure 15 — X-ray view of a sound casting shown by uniform color tone and sharp definition of rib structure

The area of friction material in contact with the rotor varies according to the particular application. For normal applications a maximum of 6 hp per sq. in. is usually recommended, but values of 10 hp have been used for certain installations where pad wear is a secondary consideration or where space limitations preclude the use of larger pads as in the case of the Mark II GT.

As the results show, the Mark II brakes were not only efficient but durable. Since the Daytona 3.81 mile course was traversed in roughly two minutes and the brakes were applied five times per lap, the heat was generated and dissipated with punishing frequency. During the race the brakes performed as expected for approximately 500 laps or 18 hours of the 24 hour endurance race before the thermal

stresses weakened the base metal and caused some rotors to fail.

The failures in all cases were due to flaking of the flame sprayed coating, similar to the case shown in Figure 12. The failure was attributed to a combination of base metal breakdown due to heat checking and to heavy shrinking in the rib area, a condition which was encountered with a development rotor (Figure 13). To prevent failures of this nature in the future, we developed improved coring and casting techniques. In addition, as a final precaution, all castings were x-rayed prior to machining. Figure 14 shows a typical x-ray view of a poor casting with heavy shrinking, indicated by the dark area, in contrast a sound casting shown in Figure 15 presents a uniform color tone without the pockets of spongy metal. X-raying eliminated castings which otherwise may have caused structural brake failures.

SEBRING 12 HOUR GRAND PRIX

Long before the Daytona brake rotors had a chance to cool off, a new brake program was initiated to prepare the Mark II GT's for the next race — the Sebring 12 Hour Grand Prix. With less than two months remaining to complete system modification and to initiate procurement of hardware, the entire staff of the Manufacturing Research Cast Metals Section was assigned to the project. After weighing all alternatives, this group decided that the inability to check the soundness of spray metal coating ruled out the use of Daytona type rotors for Sebring. It was further decided that for the Sebring's twisting course nodular iron brake rotors could provide the necessary structural strength at the high temperatures recorded on a test run, provided the lower frictional characteristics of nodular iron could be tolerated. To determine this and other questionable

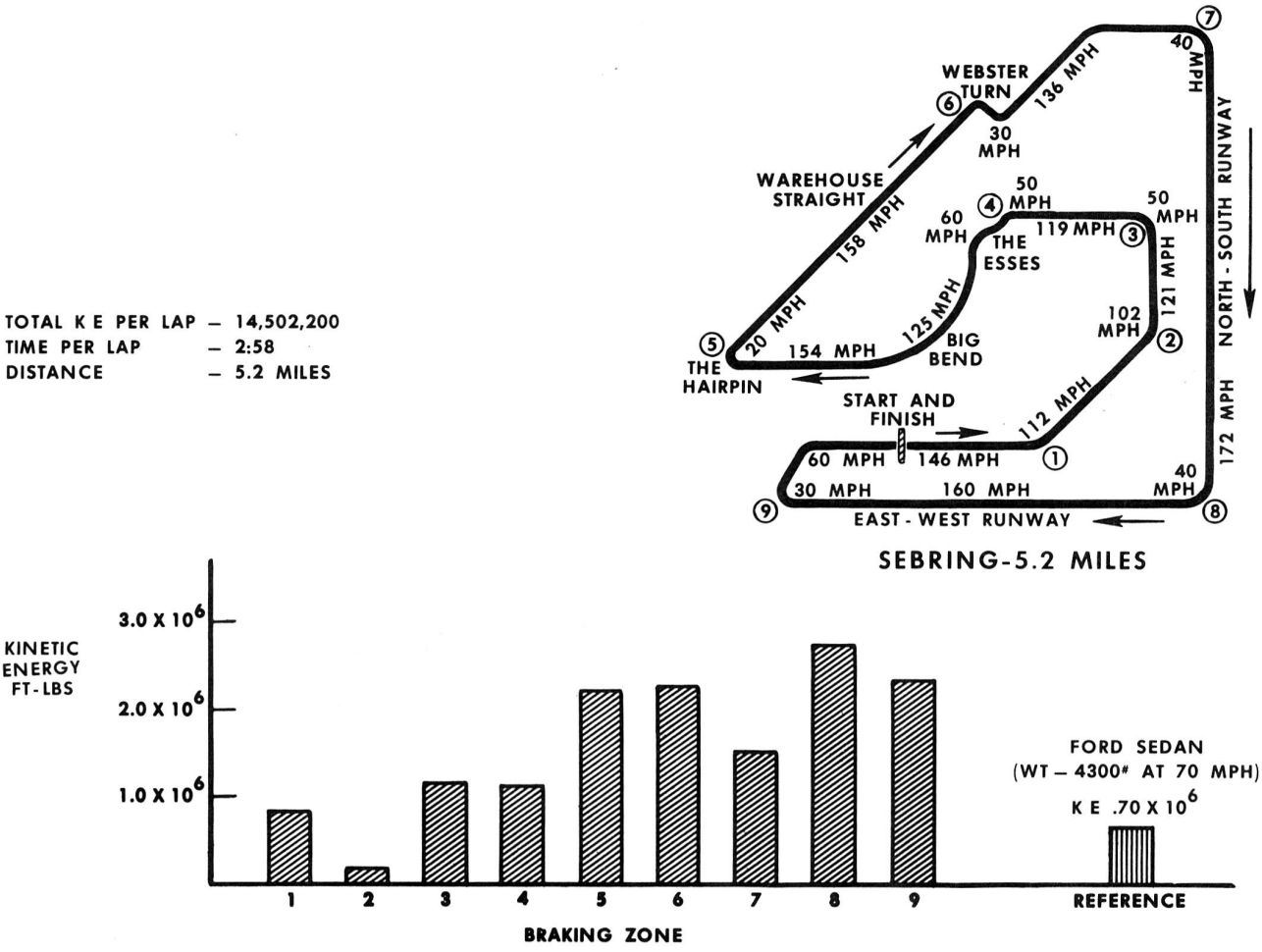

Figure 16 – Sebring 5.2 mile twisting course showing braking zones and energy loads

properties of the proposed high strength iron at elevated temperatures, we employed Ford's new brake dynamometer on a 24-hour basis. Nodular iron and other recommended rotor materials were evaluated on the basis of a race simulated from vehicle data recorded on the Sebring course. The dynamometer tests showed the nodular rotors were in fact superior to the Daytona type rotors. At this point, with only three weeks left before the race, a 24 hour durability test was conducted at the Riverside, California track. As expected, the pedal efforts for wheel lock-up were found to be high, but the lining and rotor combination survived the 24 hour test, correlating results with the dynamometer test. With the exception of a minor rotor dishing, .010 to .015 of an inch, which at this point was not recognized as a problem, the new brake package was considered ready for the Sebring Grand Prix.

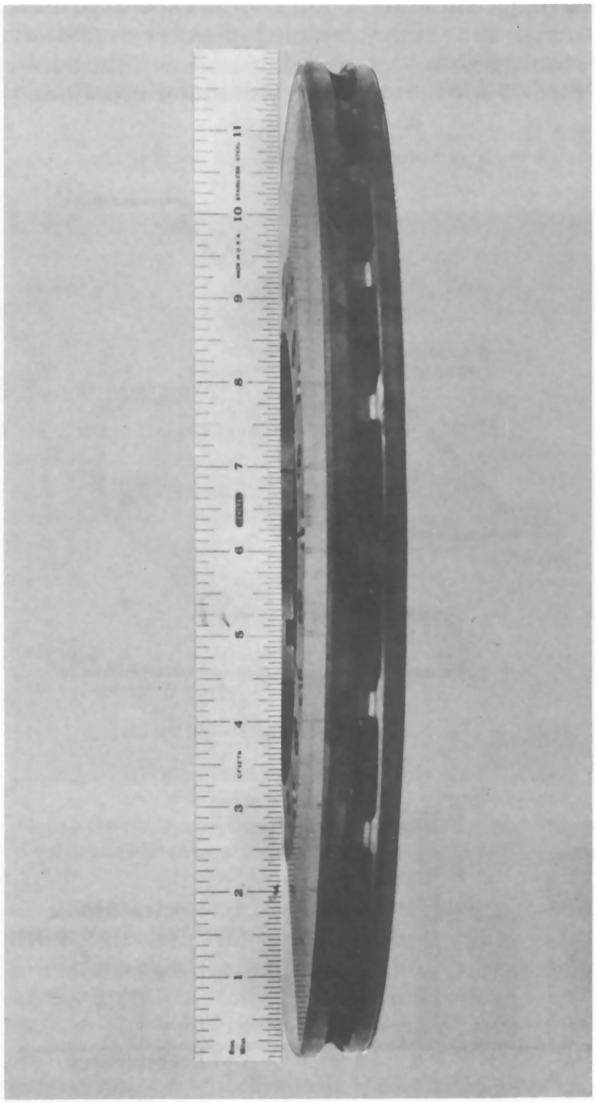

Figure 17 – Mark II Sebring rotor showing severe warping after 12 hours of racing

The 5.2 mile Sebring circuit shown in Figure 16 is unquestionably the most demanding in the country. The nine braking zones require a total of 14,502,200 ft.-lbs. of energy to be dissipated in a span of approximately 3 minutes. This punishing brake cycle was repeated 228 times in the 12-hour period.

The high rate of energy conversion once again took its toll of brake rotors. Although there were no structural failures, warped rotors such as the one shown in Figure 17 did present a problem. The saucer shaped friction face made lining pad replacement difficult, if not impossible. On several occasions new rotors were installed simply to facilitate pad replacement.

A post-mortem examination of microstructural evidence by the Ford Applied Research Laboratory showed that the rotor surface temperature exceeded 1500°F. Thermal stresses generated by alternately heating and cooling the iron produced some localized heat checking and general warping. This condition was duplicated by heating the brake rotor to 1480° for one hour followed by cooling in an air blast. It was not obtained when the rotor was heated to 1375°F and cooled in the same manner. This explains in part the discrepancies between the Riverside durability, where the rotor performed exceptionally well, and the Sebring race, where at the higher temperatures the rotors showed evidence of heat checking and warping.

LE MANS 24 HOUR GRAND PRIX

Sebring's twisting course is generally considered the most torturous test of brake performance encountered on the sports car circuits, and the amount of kinetic energy that is converted to heat energy by the brakes per lap certainly supports this claim. Figure 18 shows that there is, in addition to the total kinetic energy per lap, still another consideration in measuring brake requirements for a given circuit — the maximum instantaneous energy for any single brake application On the Le Mans circuit the Mulsanne corner after the high speed straight is the most challenging single brake retardation. It exceeds all of the Sebring or Daytona high speed stops.

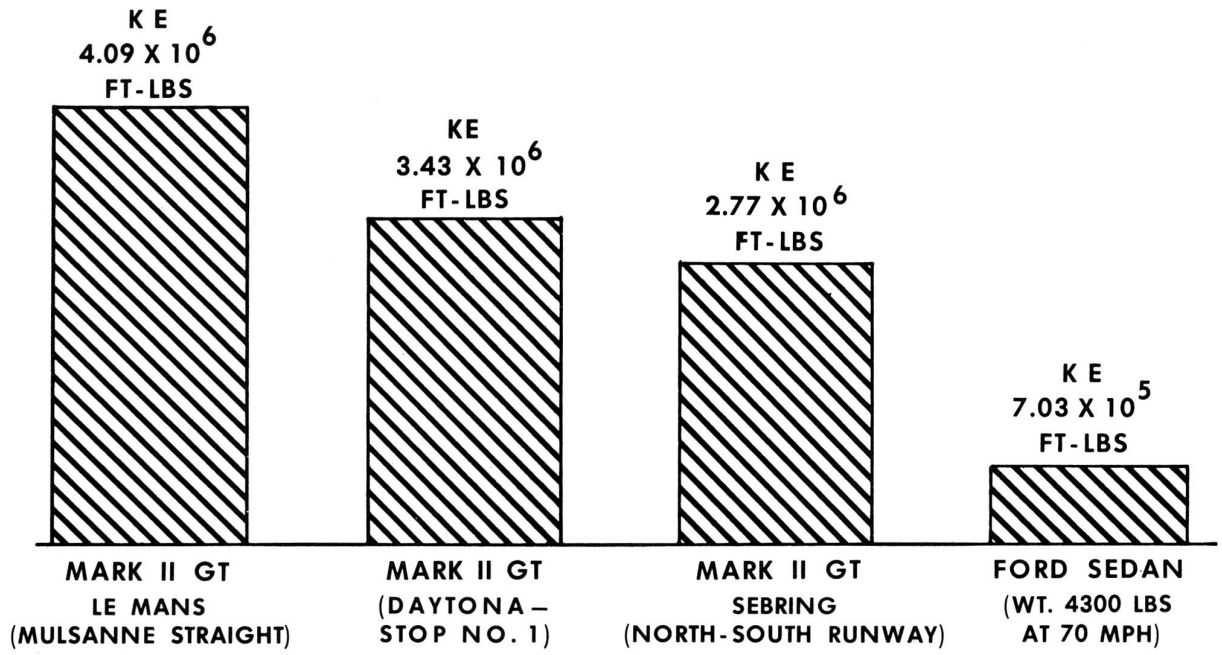

Figure 18 – Maximum energy converted to heat by the Mark II brakes during a single vehicle retardation

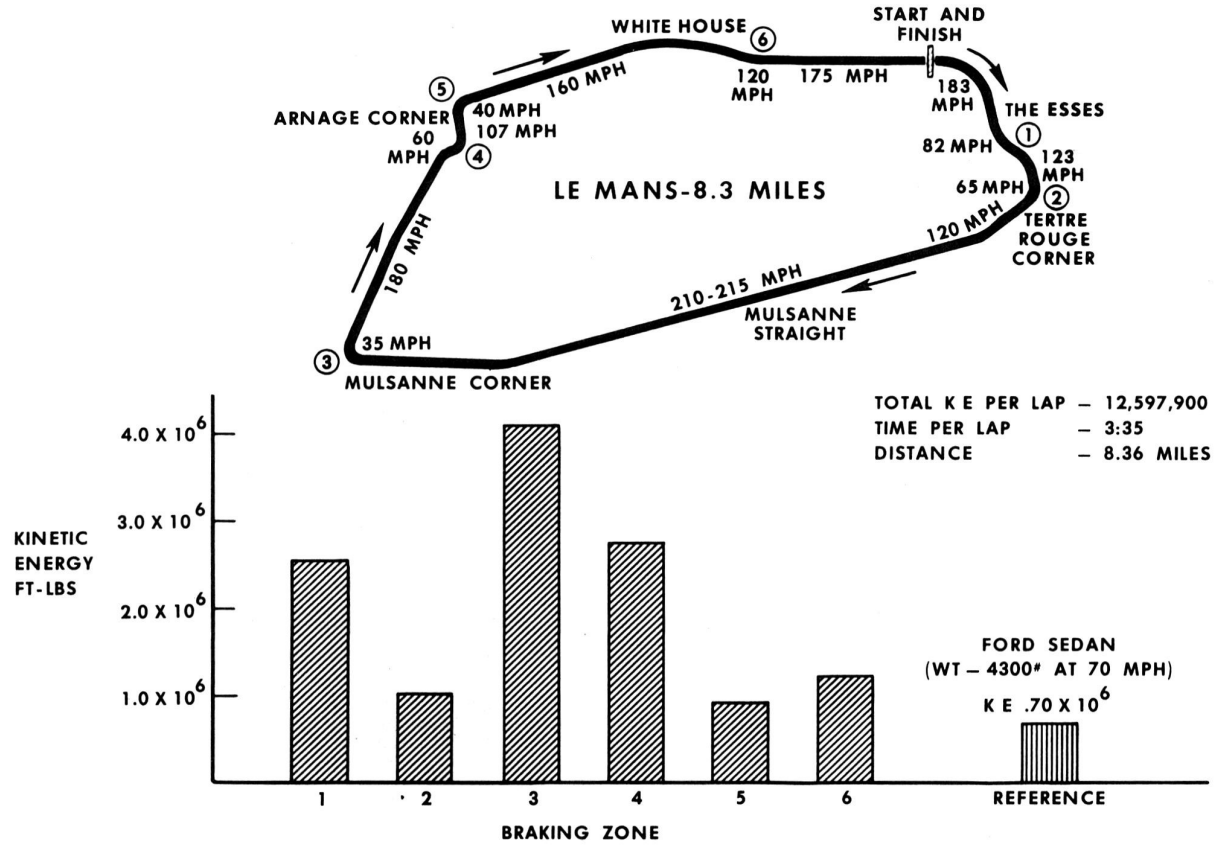

Figure 19 – Le Mans circuit showing the high speed Mulsanne straight and braking zones with related brake energy loads

After the experience at Sebring it was self evident that the energy conversion and cooling rates at Le Mans would require a material with considerably more thermal stability than the nodular iron offered. Once again a search for a suitable material was initiated. Experimental rotors were made from several cast iron compositions modified with alloy elements of chromium and molybdenum, primarily to harden the cast iron matrix but also to increase the thermal stability of iron carbide. These rotors were thoroughly evaluated on the dynamometer for susceptibility to cracking under thermal shock. Final test of the selected iron-moly rotor material was conducted on a vehicle at the Riverside circuit at a record braking pace with only slight surface heat checking.

The Le Mans course shown in Figure 19 is considered one of the fastest of the Grand Prix circuits. The 3.6 Mulsanne straight provides the Mark II with an opportunity to take advantage of its power as it reaches, with relative ease, speeds of 210 to 215 mph.

To negotiate the Mulsanne corner, the driver must reduce car speed to approximately 35 mph. In the process, 4,095,600 ft.-lbs. of kinetic energy are converted to heat. The instantaneous power developed by the brakes in com-

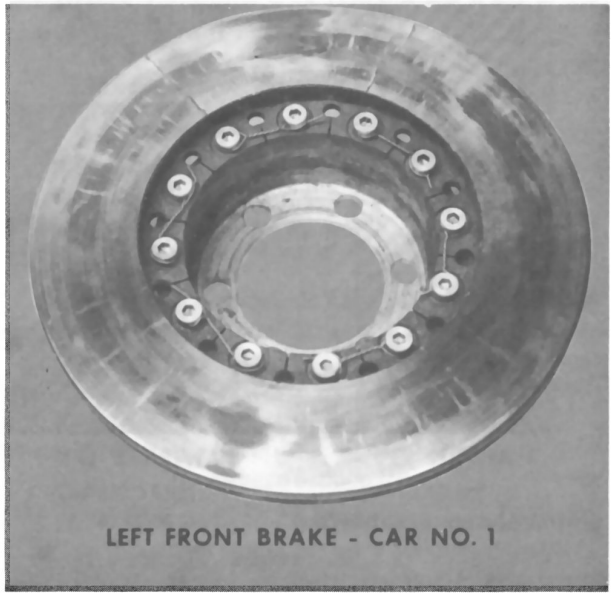

Figure 20 — Le Mans rotor showing extensive radial cracks after 65 laps

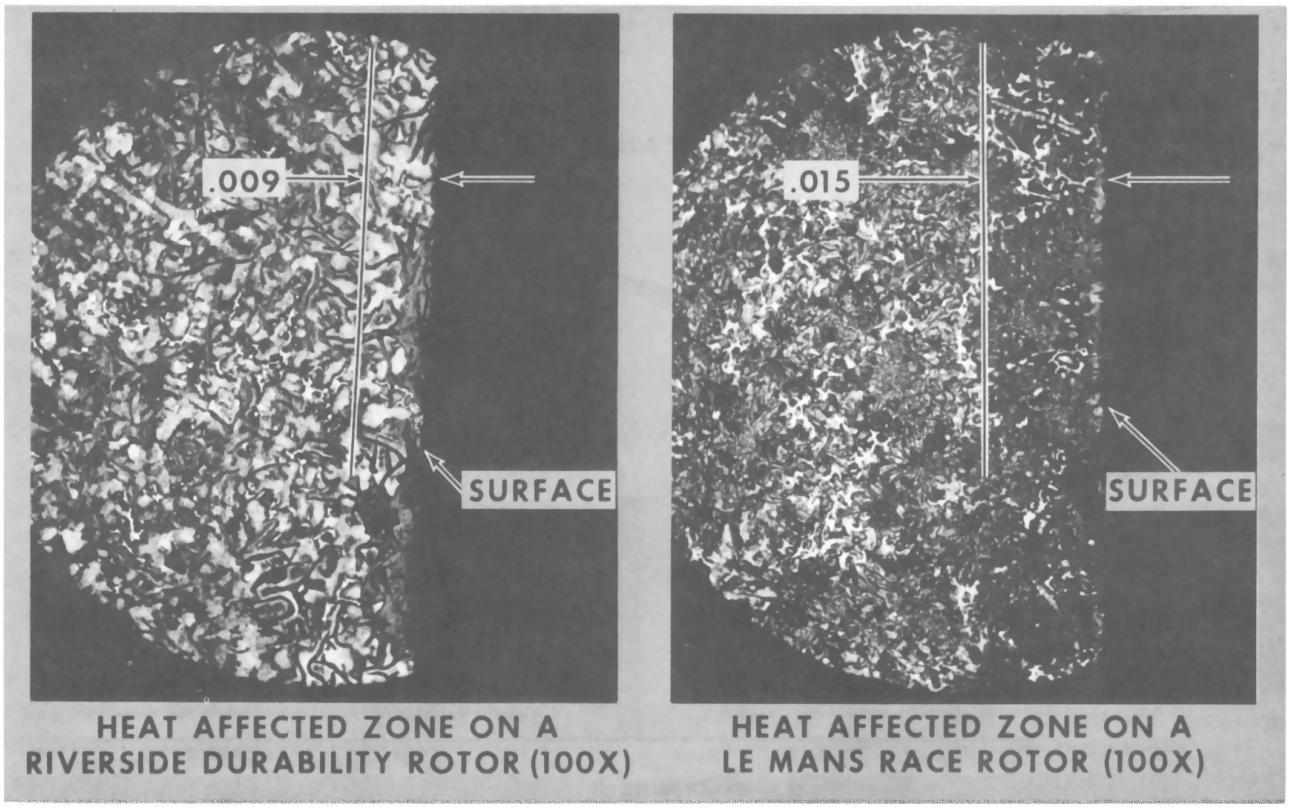

Figure 21 — Photomicrographs of (a) Riverside rotor showing .009 in. heat affected area (b) Le Mans rotor heat affected zone of .015 in. shows effects of more severe brake usage

pleting this retardation can be determined from Equation 17, derived earlier in the paper. Assuming an initial speed of 210 mph, we can compute the instantaneous power developed by the brakes as follows

$$P_i = 8.29\ (10^{-5})\ (2860)\ (210)\ a$$

and for a deceleration rate of 18 ft/sec^2

$$P_i = 8.29\ (10^{-5})\ (2860)\ (210)\ (18)$$

$$= 896 \text{ hp}$$

The effects of this energy conversion were manifest on the rotors removed from the racing vehicles. One such rotor (Figure 20) removed from car No. 1 after only 5-1/2 hours of racing showed extensive radial cracks. A later metallographic examination by the Ford Manufacturing Development Office indicated that the heat affected zone at the braking surface shown in Figure 21 was approximately .015 in. deep while the 24 hour Riverside durability rotor shows a much lower heat penetration of .009 in. The microstructure in the heat affected zone of both rotors experienced temperatures in excess of 1500°F. With knowledge of the rotor soak temperature derived from the Riverside test data, an isochronic temperature gradient (Figure 22) was constructed to show the extreme temperature conditions experienced by the metal through the rotor cross section. This gradient explains in part the volume change at the surface as it goes through the transformation point at the critical temperature of the metal. Since the base metal is at a temperature substantially below the critical temperature, thermal stresses are developed at the interface. Thermal stresses generated by alternately heating and cooling the material in time produce localized heat checking, which if sustained generally produces radial cracks. Investigations of this phenomenon are discussed in detail by Fazekas (2) and Crosby (7).

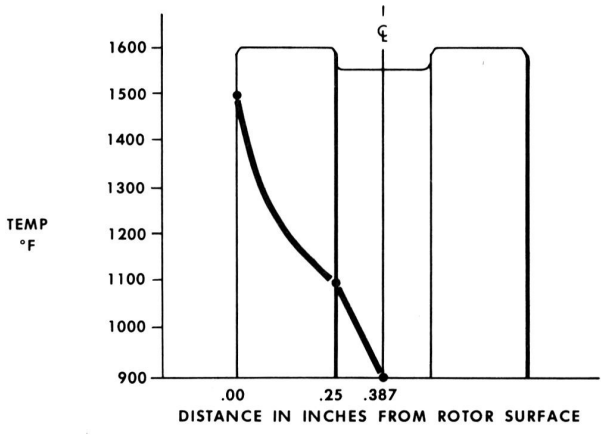

Figure 22 — Isocronic temperature gradient in a 3/4 in. ventilated rotor

Although the main part of this discussion appears to be preoccupied with the problems under racing conditions, there were other interesting observations recorded during the Le Mans race which should be mentioned. In the course of the 24 hour event, Car No. 2 driven by Bruce McLaren completed 360 laps of the circuit at an average speed of approximately 125 mph — including pit stops. In the process, the car required one change of rear lining pads and two changes of front brake lining pads. The general pattern for rotor changes indicates that the early pace of 135 to 140 mph resulted in a Mark II rotor life of 5-1/2 to 6-1/2 hours. After the competitors' vehicles were eliminated and the Mark II cars settled down to a cruising speed of 125 mph, no additional rotor changes were required. Both the No. 1 and No. 2 cars completed the race with the original rear brake rotors.

CONCLUSION

There is no doubt that as long as brakes are used for stopping from high speed, thermal stresses will occur. It is believed, however, that while these stresses experienced under racing conditions at Daytona, Le Mans and Sebring cannot be eliminated completely within the space limitations imposed by the Mark II package, they can be minimized by using an austenitic form of ductile iron. When properly heat treated, the ductile iron should provide greater dimensional stability, improved resistance to heat checking and better oxidation resistance. Certainly, these highly desirable thermal characteristics of ductile iron warrant a thorough investigation of the material for future high performance brake application.

Throughout the discussion a great deal of emphasis has been directed at the metallurgical aspects of the brake rotor design. Experience shows, however, that metallurgy alone cannot solve the problem. For a successful solution to the high performance brake problem, additional knowledge is needed in the area of the

mechanics of heat transfer. Determining the proper wall thickness and the optimum amount of cooling air for ventilated rotors is of great importance. Rotor wall plays an important role in the braking cycle. It must store the energy of heat for dissipation to atmosphere at the completion of the braking cycle and must conduct the heat away from the lining interface to the vented surface area. A balance of these functions must be established to reduce thermal stresses by maintaining relatively low temperature gradients. Only with a working knowledge of these functions can the engineer make a notable contribution to future brake design.

While much of this work was aimed at sports cars, there is no doubt that the brake systems on all Ford Motor Company products will benefit from the experience. The design of efficient brake systems based on economy of space and weight is of paramount importance to the manufacturer. It is equally important to the customer who receives a superior product for his money.

REFERENCES

1. C. L. Eksergian, "Steady State Thermal Capacity of Ventilated Rotors", Kelsey-Hayes Company Report, July, 1962, Romulus, Michigan
2. G. A. G. Fazekas, "Temperature Gradients and Heat Stress In Brake Drums", paper presented at S.A.E. Summer Meeting, Atlantic City, New Jersey, June 6, 1952.
3. R. C. Petrof, "Transient Temperatures in Brakes", Ford Motor Company Report No. AR 65-14, May, 1965, Dearborn, Michigan
4. C. L. Eksergian, "Design Approach to the Automotive Disc Brake", Paper Presented at S.A.E. Meeting, Detroit, Michigan, March, 1956
5. T. P. Newcomb, "Temperatures Reached In Disc Brakes", Journal Mechanical Engineering Science, Vol. 2, No. 3 (1960), p. 167
6. J. L. Koffman,"Ventilated Disc Brakes", Automotive Egnineer, July, 1956, p. 277
7. V. A. Crosby, "Metallurgical Development In Brake Drums", paper presented at S.A.E. Meeting, Detroit, Michigan, January, 1959

PART II

TESTING

INTRODUCTION

Although the brake system had experienced rotor durability problems, it was not until after the 1966 Daytona Continental 24-hour race that the magnitude of these problems was recognized. It was obvious that the brake system would require major improvements to be competitive at Sebring or Le Mans. Furthermore, timing was critical. Only three weeks were available for rotor development for the Sebring race and eight weeks to the ultimate goal at Le Mans.

TEST EQUIPMENT SELECTION

Due to the critical timing, the test equipment and procedure selections were of primary concern. A test program that normally takes several months had to be compressed into three weeks. The key to fast, accurate rotor development proved to be the new brake dynamometer in the Ford Reliability Laboratory. The brake dynamometer was chosen for development testing for the following reasons.

1. The brake dynamometer would operate an equivalent to 10,000 miles of Sebring racing or eight Sebring races without wearing out a single vehicle. It would be very difficult to do this with an actual Mark II GT without major vehicle component replacements, which would delay the test program.
2. Brake dynamometer testing eliminated the need for skilled racing drivers and mechanics. A complete team of personnel, much the same for an actual race, is needed to conduct 10,000 miles of racing durability.
3. Testing with the brake dynamometer eliminated the variable of weather. When track tests are conducted, it is often difficult to tell whether changes in performance are due to weather or due to a design change.
4. The brake testing could be conducted using only one brake assembly, rather than a complete set of four prototype brakes which are required for a track test. The dynamometer can test a complete vehicle system of four brakes which is useful in brake distribution studies or in brake "pull" studies, but the Mark II GT had neither of these problems.

DETERMINING TEST REQUIREMENTS

To duplicate the conditions that a brake experiences, it was necessary to measure these conditions on a car at racing speeds. Since the initial goal was to develop a brake that would meet the grueling requirements of Sebring, accurate data for this track was required.

Although the brake dynamometer eliminated the need for a test car and a skilled driver, their use was required for a few hours to measure the brake operating conditions to set up the laboratory test. A Ford Mark II GT was instrumented and driven around the Sebring race course, recording the conditions the brakes were experiencing. The car was driven at average lap times of 2:58 minutes by several experienced drivers who would be driving the Ford Mark II GT's during the race. We utilized the instrumentation that had been used to obtain engine data to obtain the brake data. The compact test instrumentation in the car continuously recorded engine speed, throttle position, and brake rotor surface temperature. The oscillograph records obtained were analyzed to determine the following:

1. Car speed at brake application and brake release.
2. Car deceleration during brake application.
3. Maximum brake rotor surface temperature during brake application.

The car speed was calculated from engine speed, transmission gear ratios, rear axle ratio, and tire size. The brakes were assumed to be applied when the driver closed the throttle and assumed to be released when the driver opened the throttle. The vehicle deceleration was cal-

culated from brake "on" time and the car speed change during this time. The resulting calculated deceleration was 18 ft/sec^2 for all brake applications.

The brake operating temperatures were measured by a radiation-type transducer which sensed surface temperature by the color of the glowing brake rotors. With this type of transducer, the brake had to be "red-hot" before the transducer would function. A thermocouple in the disc rotor would have been more desirable since temperatures over the complete operating range could be recorded. The radiation transducer installation, however, was relatively simple, while a thermocouple installation would have required a more complicated slip-ring assembly installation.

THE FORD BRAKE DYNAMOMETER

When the actual braking requirements for Sebring were known, the dynamometer phase of the testing program began. To better understand these tests, and how the brake development was accomplished so quickly, a description of the Ford brake dynamometer would be helpful.

The dynamometer consists of the following basic sections:

- Rotating inertia flywheels which simulate the translational inertia of the vehicle.
- Drive motor to bring rotating inertia flywheels to test speed.
- Test stations where brakes are mounted.
- Dynamometer controls and instrumentation.

As shown in Figure 23, the dynamometer can simultaneously test a complete set of brakes for a four-wheel vehicle. The dynamometer installation in the laboratory is shown in a photograph in Figure 24.

Dynamometer Inertia Section

The dynamometer inertia section, which simulates vehicle weight, is shown in Figure 25. Inertia loads can be varied between 15 and 453 slug-ft^2 by means of removable inertia flywheels piloted on the dynamometer shaft and bolted to an inertia mounting flange. The dynamometer inertia consists of:

- 15 slug-ft^2 of motor and dynamometer shaft inertia
- 21 — twenty slug-ft^2 flywheels
- 12 — one and one-half slug-ft^2 flywheels

The small and large inertia flywheels are stored in groups on either side of the inertia mounting flange. The flywheels in storage are moved over and bolted to the flange as required for a test. The inertia loading on the dynamometer is calculated as follows:

$$I = \frac{Wr^2}{4637}$$

Where: I = Dynamometer inertia, slug-ft^2

W = Vehicle weight, lb

r = Vehicle tire rolling radius, in.

The complete 453 slug-ft^2 of inertia represents the inertia imposed upon the four brakes of a 10,000 GVW truck, or one front brake of some of the largest Ford trucks. The Mark II GT tests were conducted with one front brake on the dynamometer. This one brake handled 870 lbs. of vehicle weight which is equivalent to 30 slug-ft^2 of dynamometer inertia.

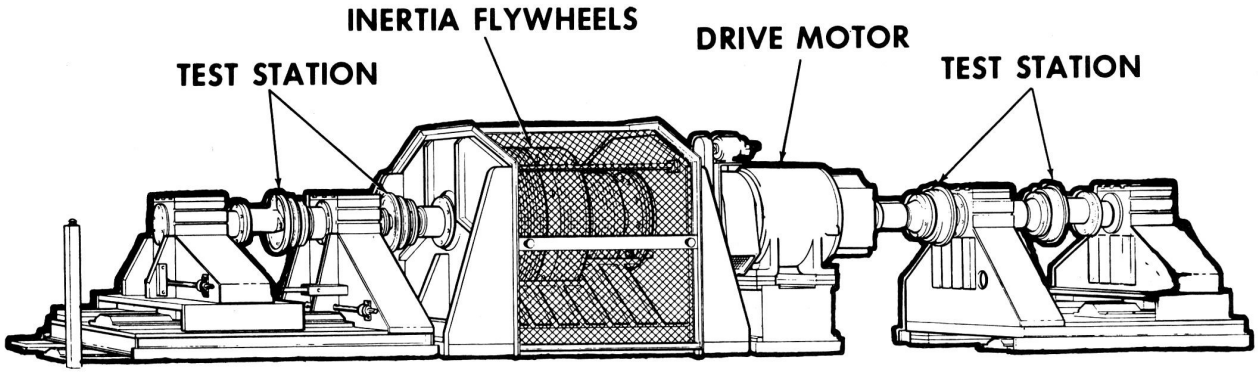

Figure 23 — Ford Reliability Laboratory Brake Dynamometer

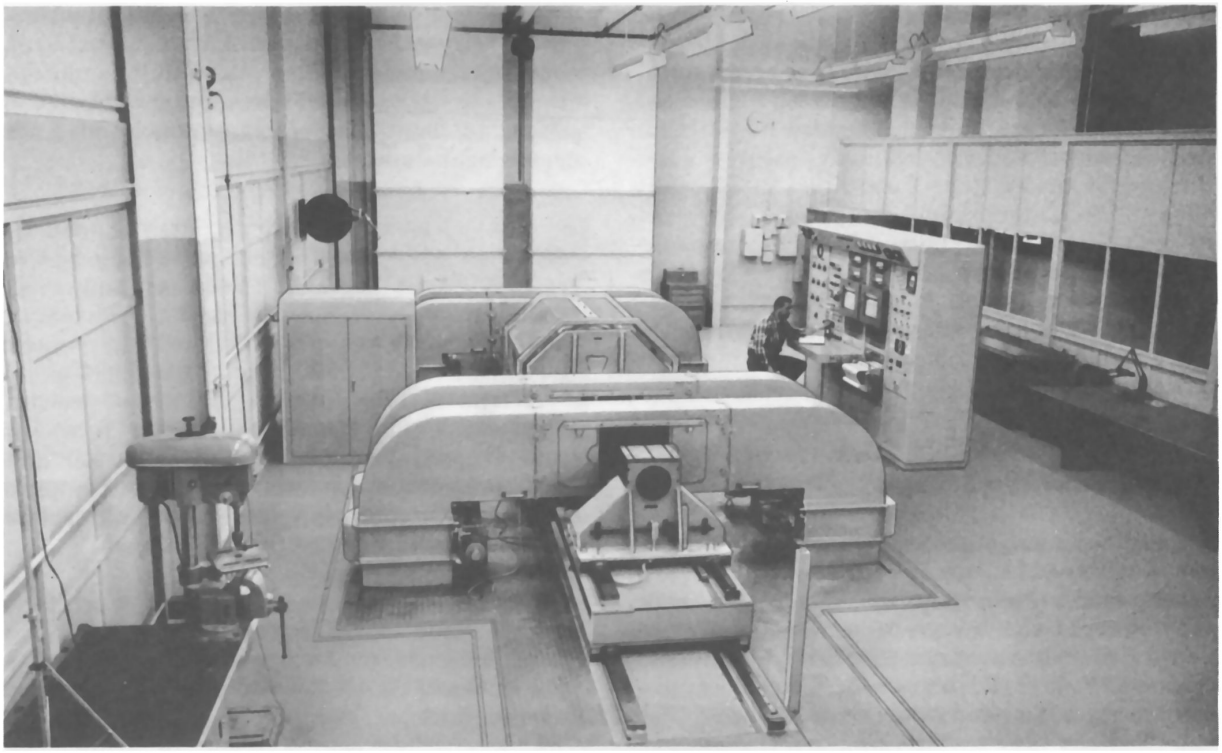

Figure 24 — Reliability Laboratory Brake Dynamometer

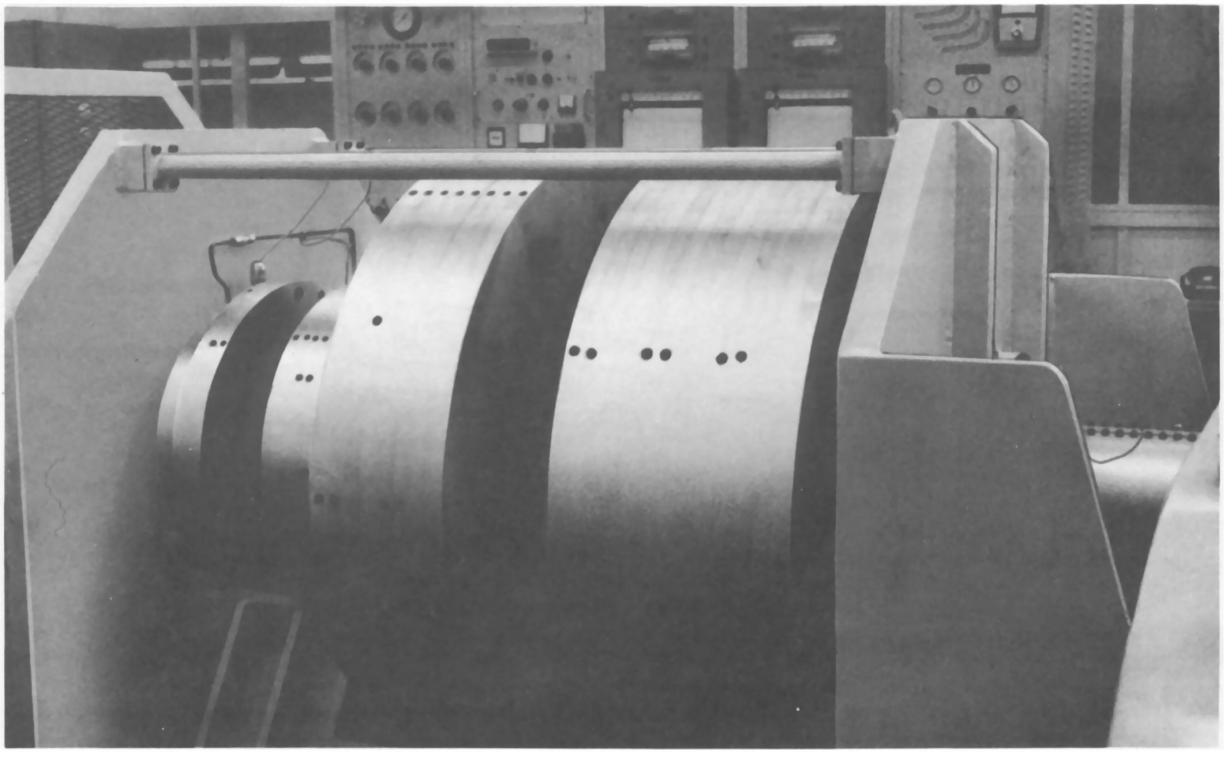

Figure 25 — Dynamometer Inertia Section

Dynamometer Drive Motor

A DC electric motor drives the dynamometer up to test speed. As the test brakes are applied, the drive motor is normally electrically disconnected, immediately prior to and during the brake stop. For steady speed brake "drag" tests, the drive motor can be programmed to operate during the brake application. The motor can produce 125 hp from its 650 rpm base speed to the 2400 rpm maximum speed. Below the base speed, the motor can produce 1000 lb-ft torque on a continuous basis and up to 1500 lb-ft intermittently.

Dynamometer Test Stations

The four test stations on the dynamometer are positioned in an inboard and outboard arrangement. Normally, vehicle front brakes are tested at the outboard test stations while vehicle rear brakes are tested at the inboard stations. Figure 26 shows the test station arrangement at the end of the dynamometer. The front vehicle brake at the outboard test station is driven by the dynamometer shaft system which passes through the open center of the rear brake assembly at the inboard test station. Figure 27 shows the coupling required to drive a test brake drum or rotor at any test station. The coupling is normally fabricated from an automobile wheel "spider" welded inside a heavy circumferential steel ring. The test brake backing plate or caliper assembly is attached to the test station with an adapter. Figure 28 shows a front disc brake adapter and a rear drum brake adapter.

The brake backing plate adapter is mounted on a shaft which is restrained from rotation by a load cell. Each test station has a torque capacity up to 5000 ft-lb. The torque capacity of the two inboard test stations may be extended to 7500 ft-lb by relocating the load cells farther out on the torque reaction lever arms. The signal from each of these load cells is used to control the dynamometer and also is recorded as test data. More complete details of the controlling and recording aspects of the dynamometer are described later.

Each test station on the dynamometer is mounted on ways so that it can be moved back for easy removal and installation of the test brakes. Figure 29 shows both test stations moved back at one end of the dynamometer. The inboard test station moves on the machine base, and the outboard station moves on the base of the inboard station. This arrangement allows moving any individual station for access to a test brake without disturbing the adjacent station. Figure 30 shows both test stations in the normal running position.

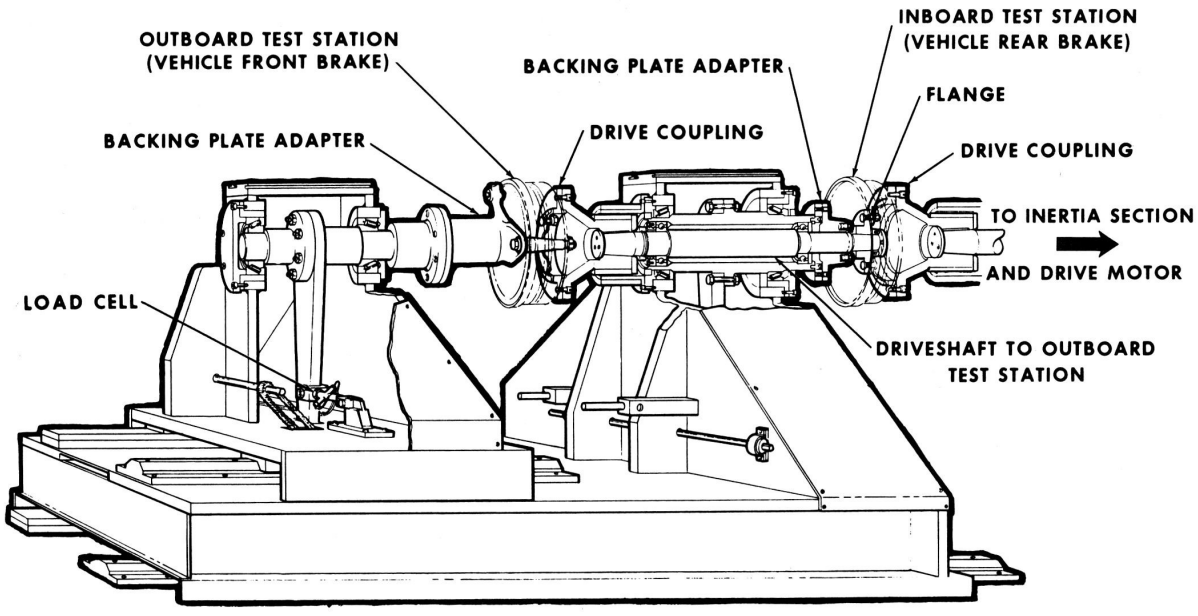

Figure 26 - Test Station Arrangement

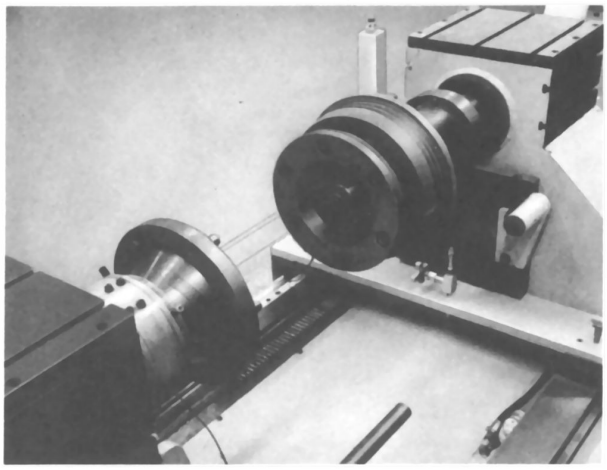

Figure 27 — Coupling connecting test brake drum to dynamometer drive

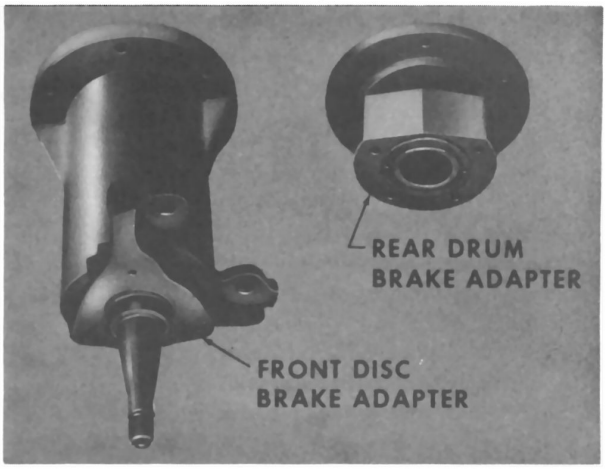

Figure 28 — Backing plate and disc brake caliper mounting adapter

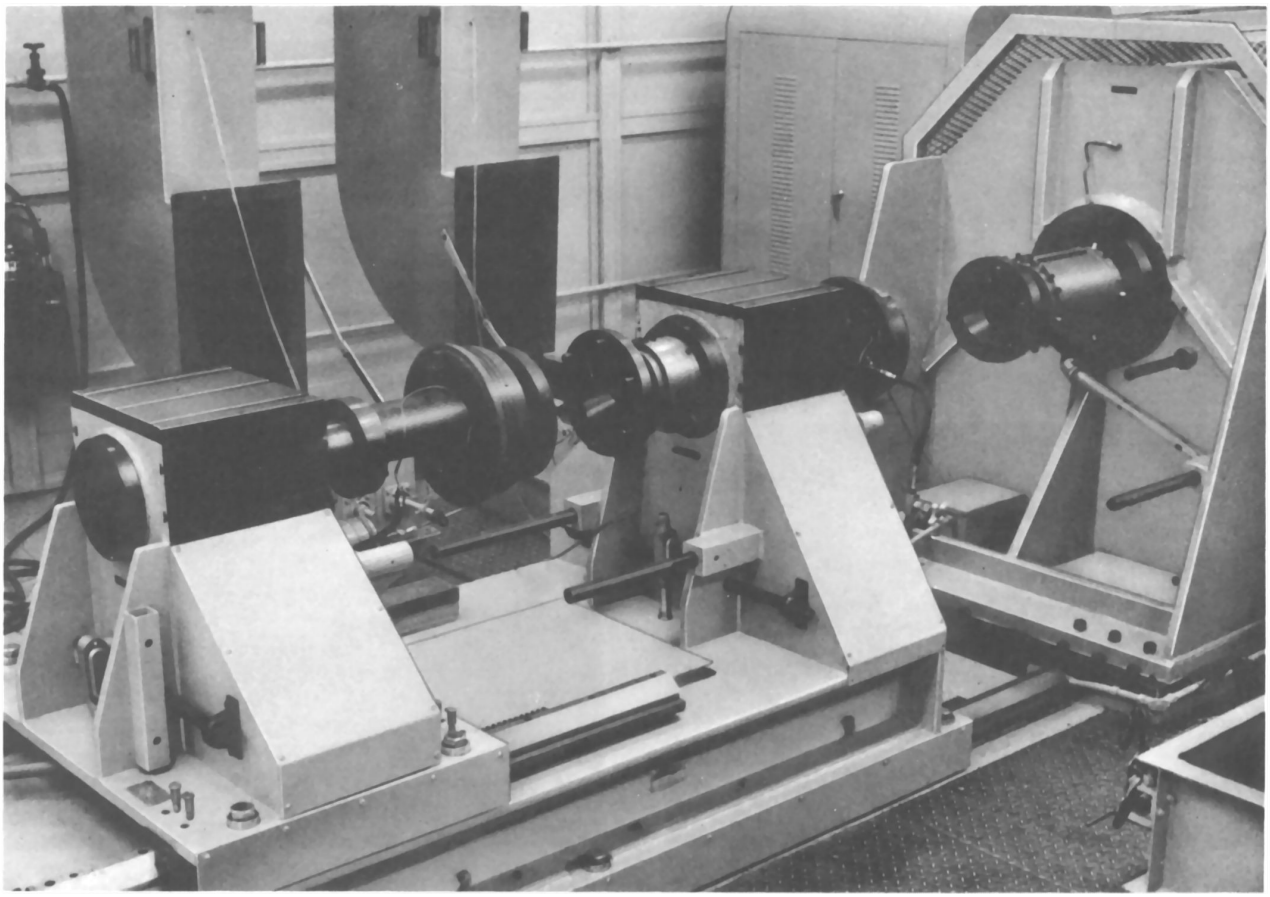

Figure 29 — Test stations on dynamometer moved to provide access to test brakes

Installing the Mark II GT Brake

As was shown in Figure 28, a passenger car front brake adapter is normally fabricated from a front suspension spindle. Adapting a Mark II GT disc brake to the dynamometer presented problems not present in testing current passenger car and truck brake systems. The Mark II GT suspension components and wheels are made from thin-wall magnesium-aluminum alloy forgings which are difficult to attach solidly to the dynamometer. Also, the

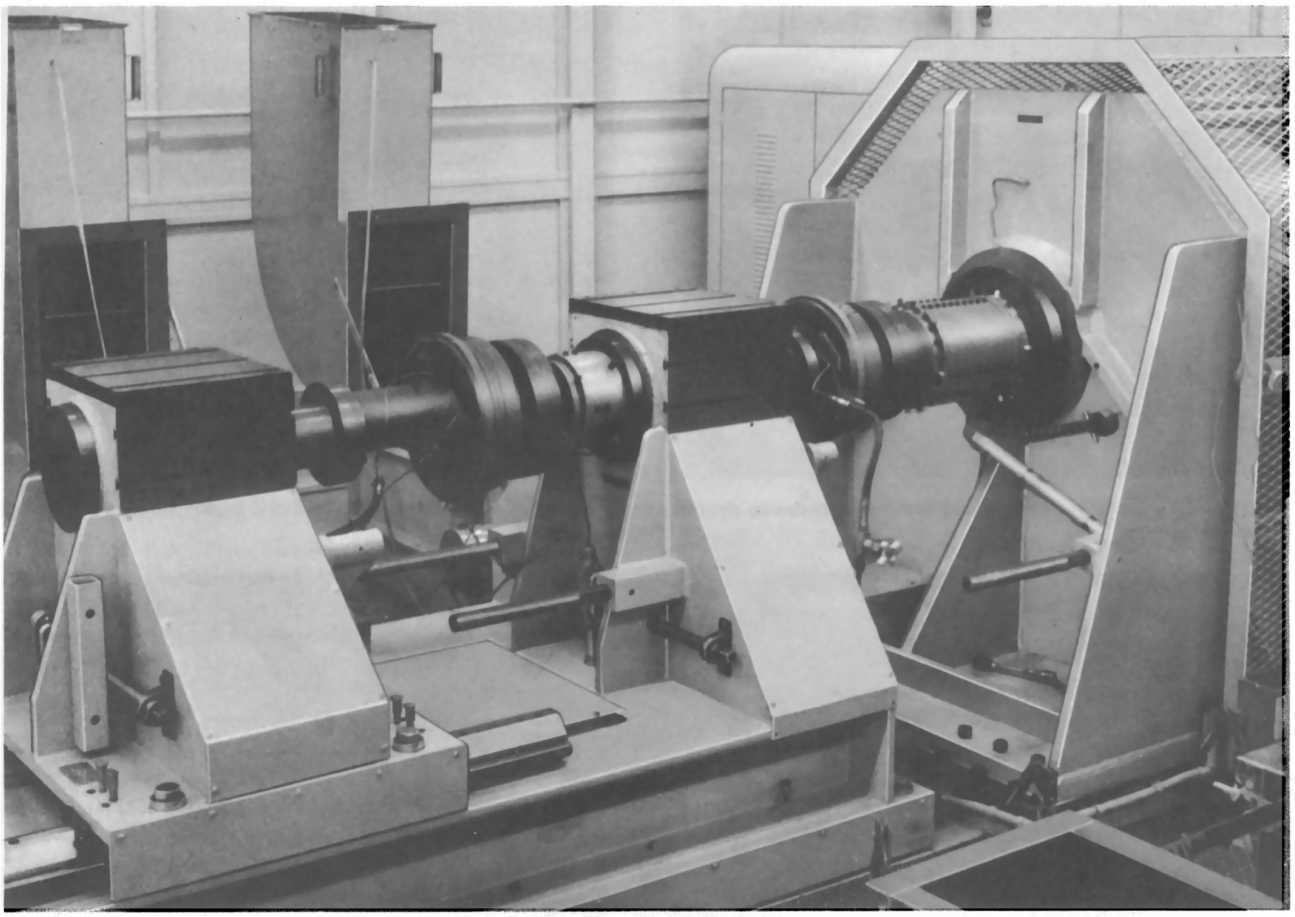

Figure 30 — Test stations on dynamometer in test position

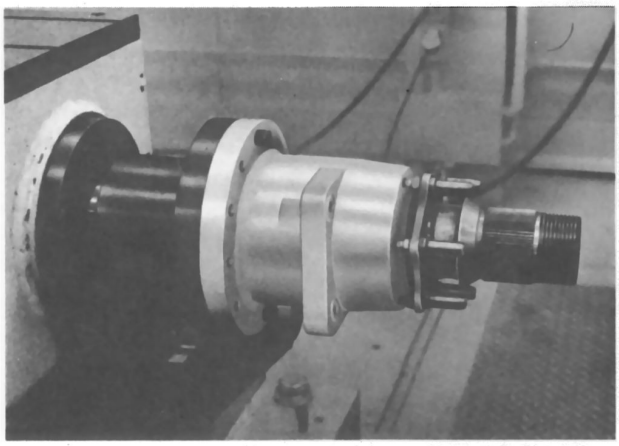

Figure 31 — Ford Mark II GT brake caliper mounting adapter on brake dynamometer

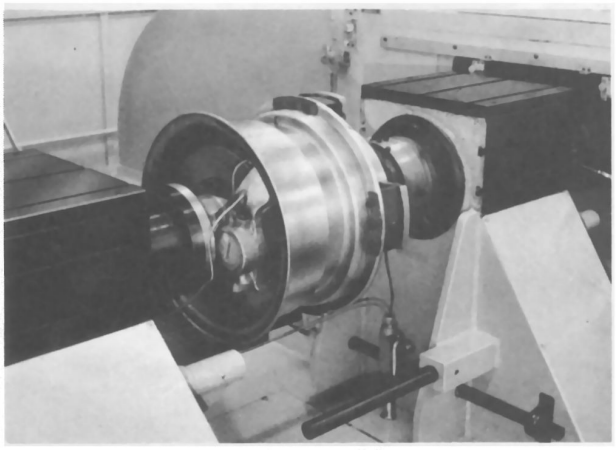

Figure 32 — Complete Ford Mark II GT brake and wheel mounted on brake dynamometer

critical time limitation forced all adapter and coupling construction to be of the utmost simplicity. The fabrication problem was solved by designing the adapter and coupling using aluminum. This permitted fast machining, and adequate strength was obtained without excessive size. Figure 31 shows the aluminum adapter, and Figure 32 shows the complete Mark II GT brake mounted on the dynamometer.

Test Brake Cooling

Brake cooling air is supplied to each test station on the dynamometer through 12 x 24 inch ducts. Air velocities up to 30 mph can be supplied to all four stations, and even higher air velocities can be provided for tests involving only one or two test stations. Figure 33 shows the air duct at one test station with the top half of the duct removed and the air return duct pivoted out of the way for access to the test brake. The cooling air is supplied from an under-floor plenum chamber, and exhausted to another under-floor plenum chamber on the opposite side of the dynamometer. The brake air cooling system has two variable speed fans. One fan pressurizes the supply plenum while the other evacuates the exhaust plenum. The air duct at the test station is maintained at slightly below atmospheric pressure so that no smoke or brake lining odor will escape into the laboratory.

The air velocity at each test station is controlled by varying the fan speeds and the individual test station damper position. During most tests, the brake cooling air velocity in the cooling duct is held constant to expedite the test cycle rather than duplicate the exact air velocity changes during braking. Heating coils are provided in the air system so that the cooling temperature can be controlled to any temperature between the outside ambient air temperature and 100°F.

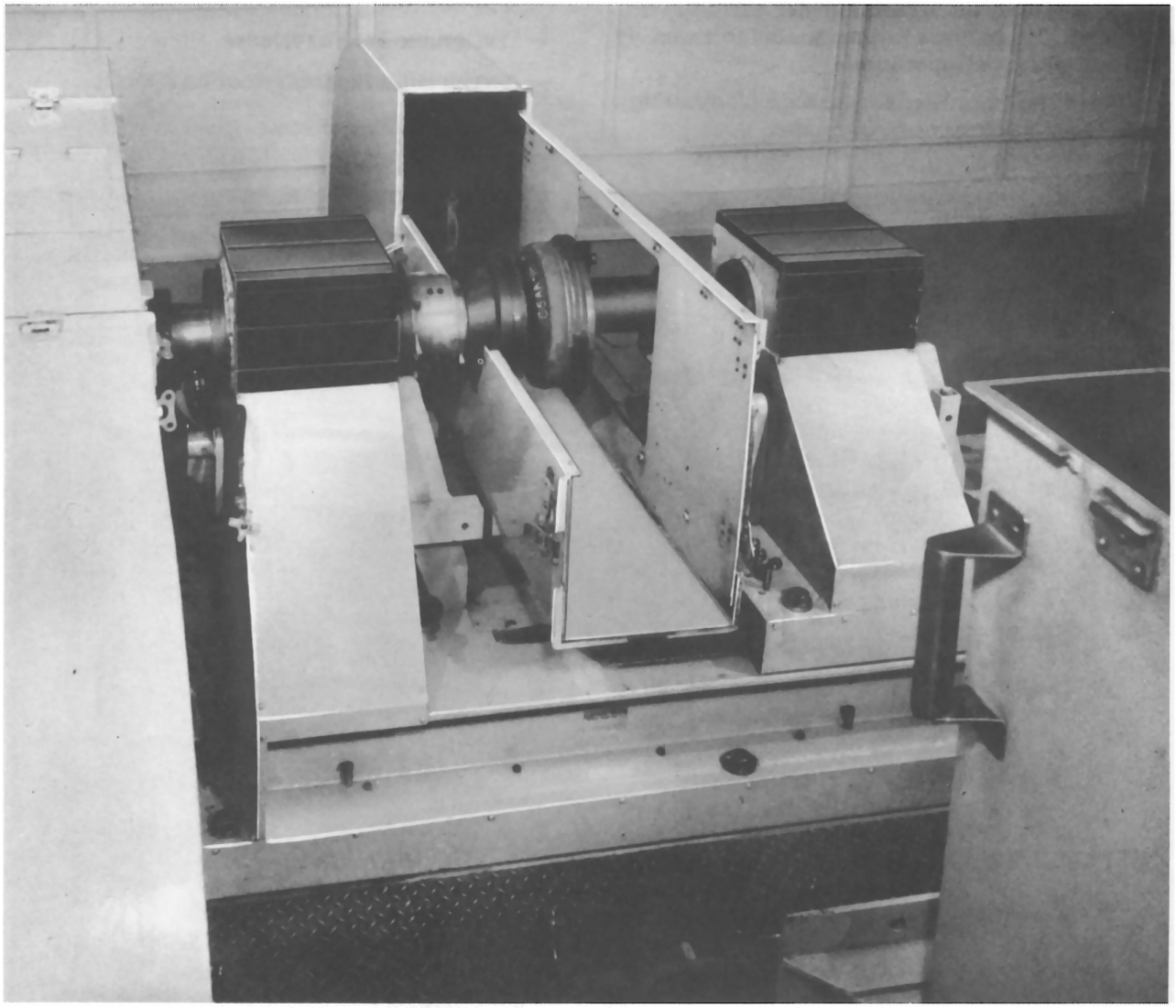

Figure 33 — Dynamometer brake cooling ducts partially removed for access to test brakes

The Mark II GT tests were conducted with a complete vehicle wheel in place, causing the brake cooling air to flow through the ventilated rotor in the same manner as it would on the car. A nominal 50 mph cooling air velocity at 70°F. was used for all tests. Although this did not duplicate the variances in brake cooling during a lap at racing speeds, it did approximate the average cooling conditions.

Dynamometer Controls and Test Cycles

All brake tests are controlled and data recorded at the brake dynamometer operator's control console (Figure 34). The control system can be highly automatic and brake tests, such as completed on the Ford Mark II GT, can be conducted with the dynamometer virtually unattended. This allows test personnel to carefully observe all brake operations.

The dynamometer is capable of operating under four different control modes.

- Manual operation by the dynamometer operator.
- Constant speed operation with the brakes applied and released automatically at preset time intervals.
- A programmed test cycle that is automatically repeated up to 9999 times.
- A programmed brake test whereby up to sixty different test cycles follow each other automatically.

All programmed brake tests are based on a standard test cycle illustrated in Figure 35. The brake cycle consists of:

- Acceleration to stabilized braking speed.
- Brake application with deceleration to dwell speed.
- Dwell after brake release.
- Acceleration to brake cooling speed.
- Brake cooling period.

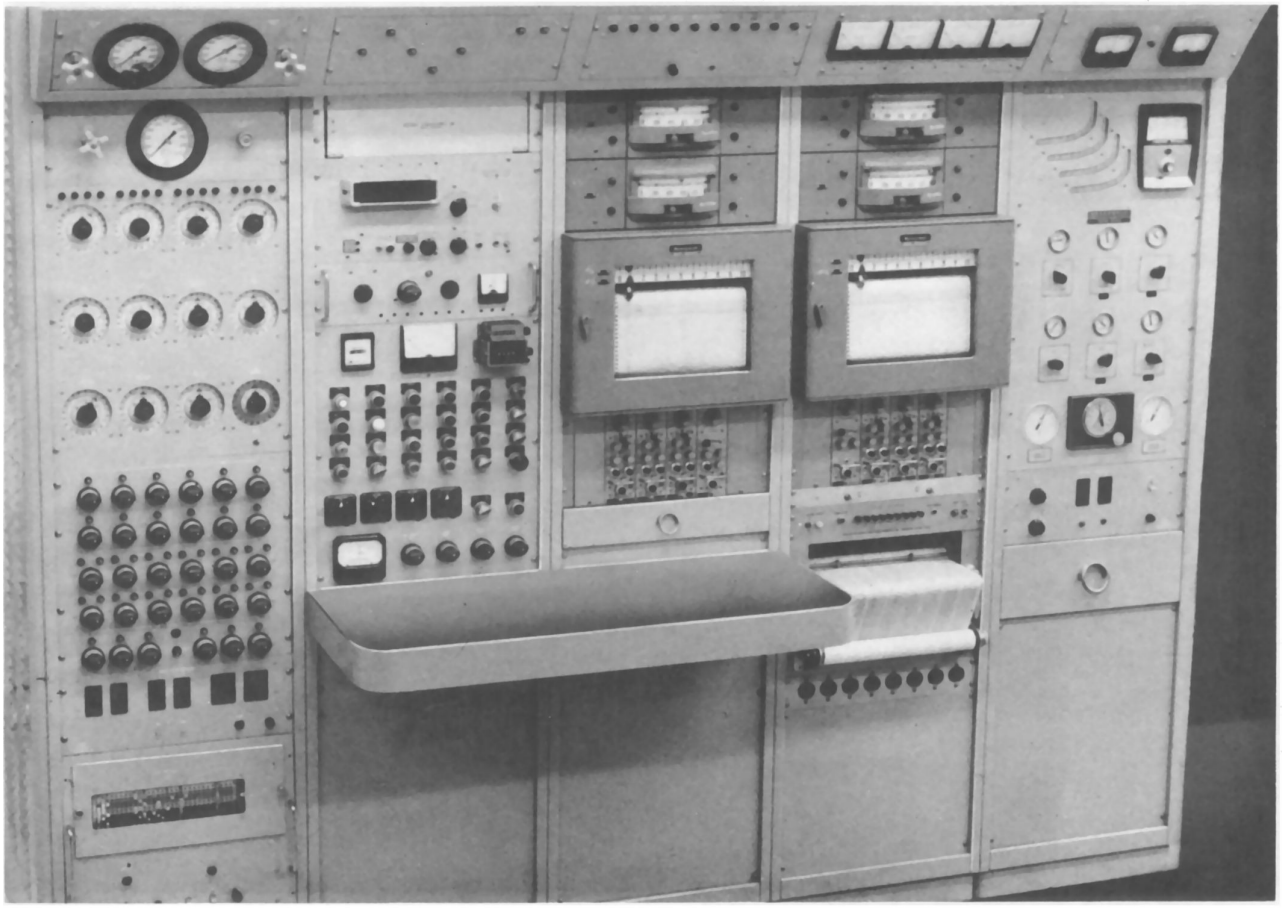

Figure 34 – Brake Dynamometer Operator's Control Console

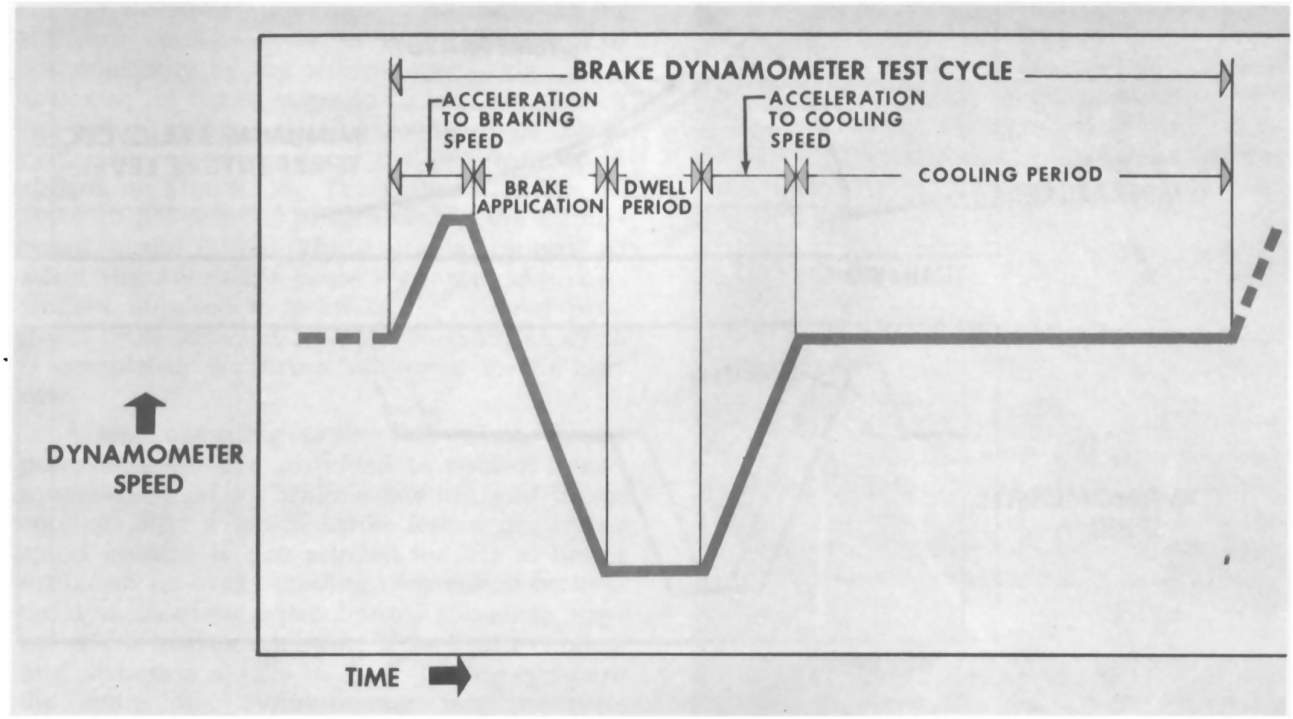

Figure 35 — Typical Brake Dynamometer Test Cycle

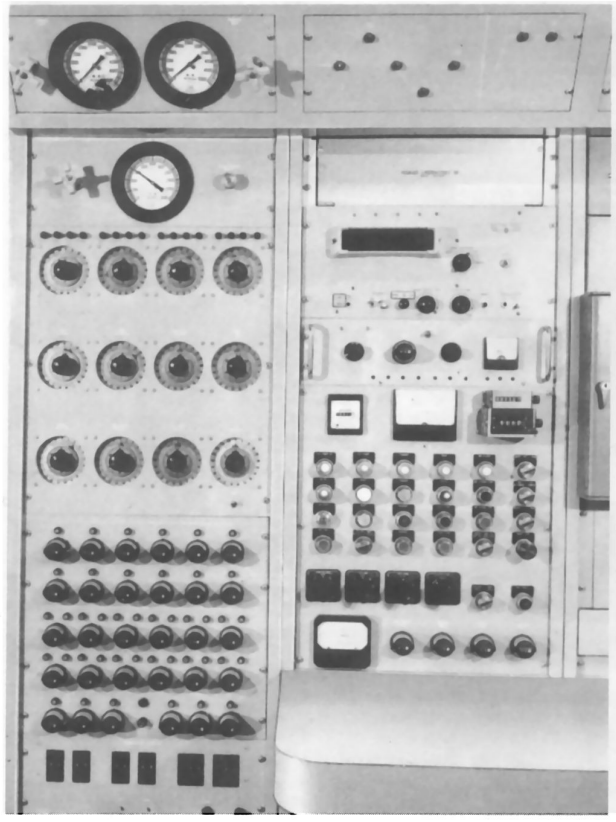

Figure 36 — Brake Dynamometer Programmer

To control the various parts of a programmed test cycle, a series of timers and potentiometers are used. The panel for the programmer controls is shown in Figure 36.

The timers normally program the time intervals for the different phases of the test cycle, while the potentiometers control dynamometer speed. For a repetitive programmed test cycle, only a limited number of the potentiometers and timers are used. For a typical brake cycle, the dynamometer speed at brake application, brake release, and brake cooling are preset on the potentiometer controls. Additional potentiometers are preset so a brake deceleration can be programmed at a constant brake line pressure or at a constant value of the sum of the brake torques. To perform these two functions, brake line pressures up to 2000 psi are supplied to the test brakes by a servo-controlled hydraulic power supply.

Additional capabilities of the dynamometer permit the length on one brake cycle to be controlled by either time or minimum brake temperature. Typical brake cycles with these two control methods are shown in Figure 37. A time-controlled cycle can be preset up to 1200 seconds. A brake temperature-controlled cycle can be preset for minimum brake temperatures up to 1000°F.

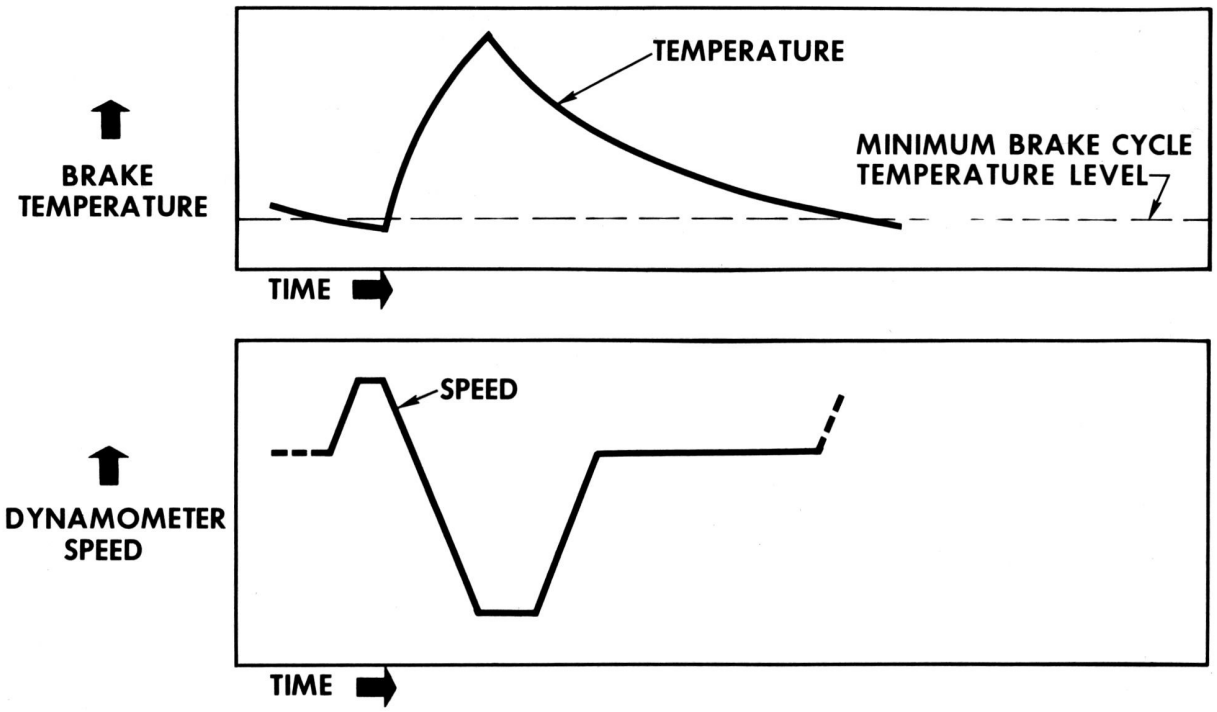

Figure 37 — Time or Temperature Controlled Brake Cycle

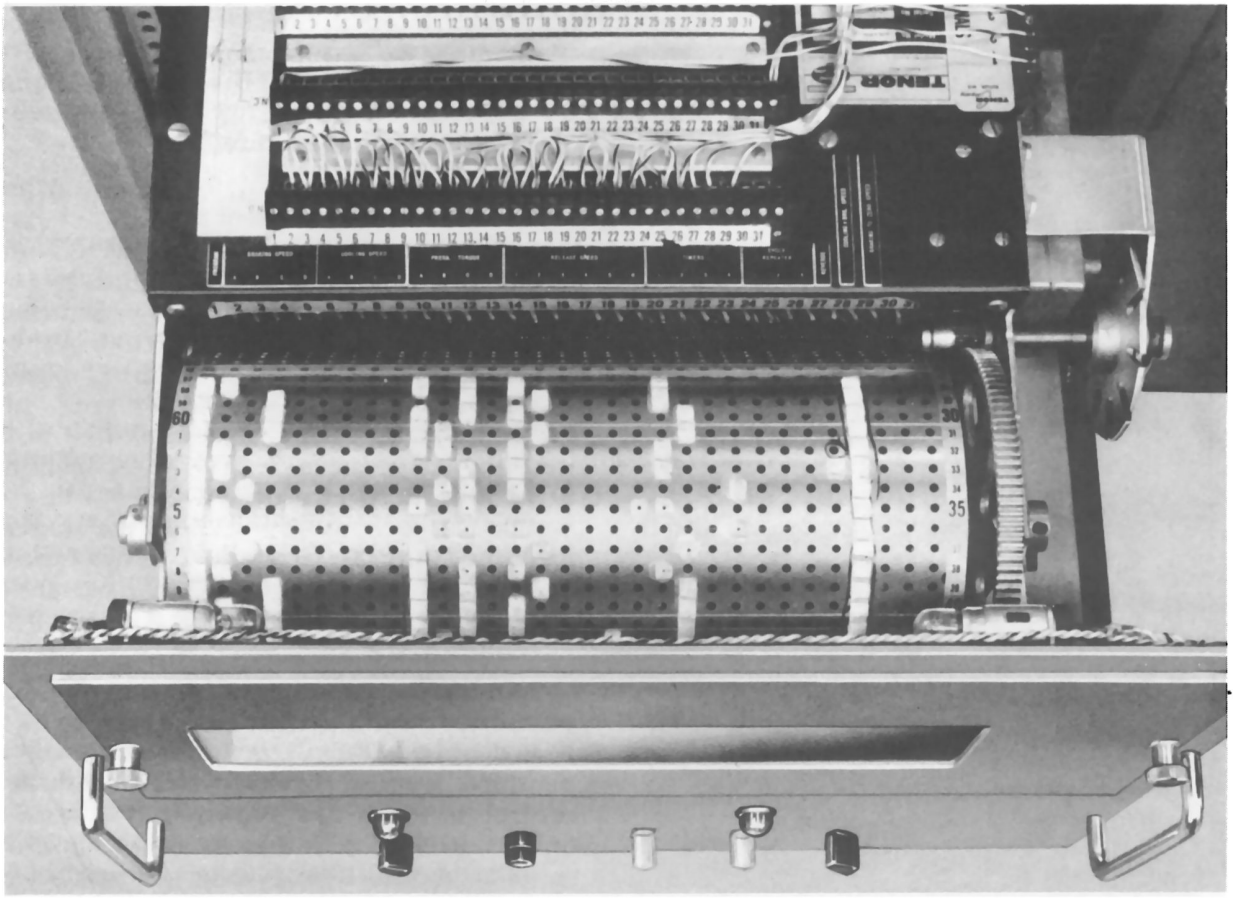

Figure 38 — Program Drum

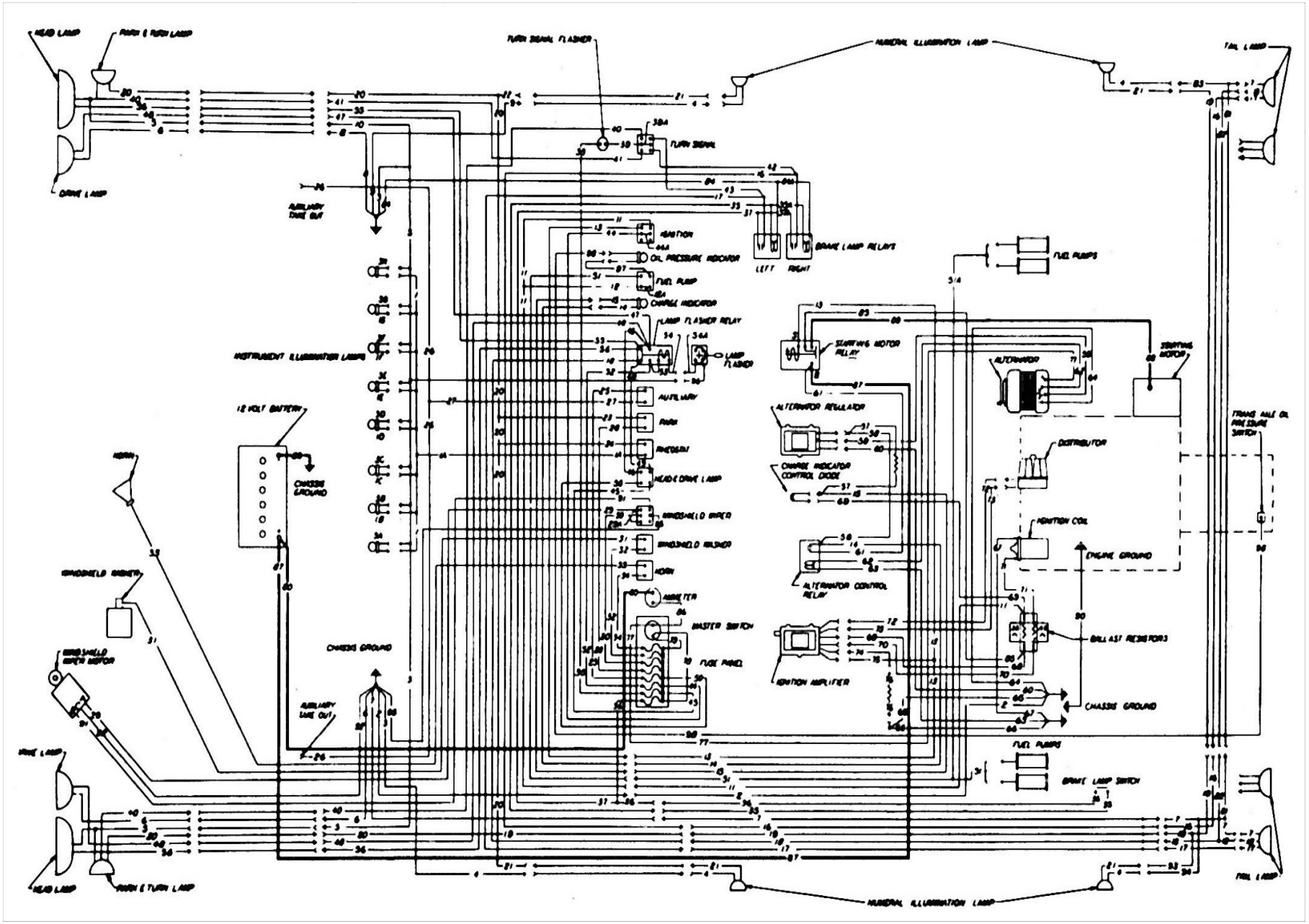
HEAD LAMP
PARK & TURN LAMP
TURN SIGNAL FLASHER
NUMERAL ILLUMINATION LAMP
TAIL LAMP
TURN SIGNAL
AUXILIARY FUSE BLK
IGNITION
OIL PRESSURE INDICATOR
FUEL PUMP
CHARGE INDICATOR
LAMP FLASHER RELAY
LAMP FLASHER
BRAKE LAMP RELAY
LEFT
RIGHT
FUEL PUMPS
INSTRUMENT ILLUMINATION LAMP
AUTO LAMP
PARK
RHEOSTAT
HEAD & DRIVE LAMP
WINDSHIELD WIPER
WINDSHIELD WASHER
HORN
AMMETER
MASTER SWITCH
FUSE PANEL
STARTING MOTOR RELAY
ALTERNATOR
STARTING MOTOR
ALTERNATOR REGULATOR
CHARGE INDICATOR CONTROL DIODE
DISTRIBUTOR
IGNITION COIL
ENGINE GROUND
ALTERNATOR CONTROL RELAY
IGNITION AMPLIFIER
BALLAST RESISTORS
CHASSIS GROUND
FUEL PUMPS
BRAKE LAMP SWITCH
TRANS AXLE OIL PRESSURE SWITCH
12 VOLT BATTERY
CHASSIS GROUND
HORN
WINDSHIELD WASHER
WINDSHIELD WIPER MOTOR
AUXILIARY FUSE BLK
TAIL LAMP
HEAD LAMP
PARK & TURN LAMP
NUMERAL ILLUMINATION LAMP